EJA
European Journal of Anatomy
Volume 26 - Number 2 March 2022

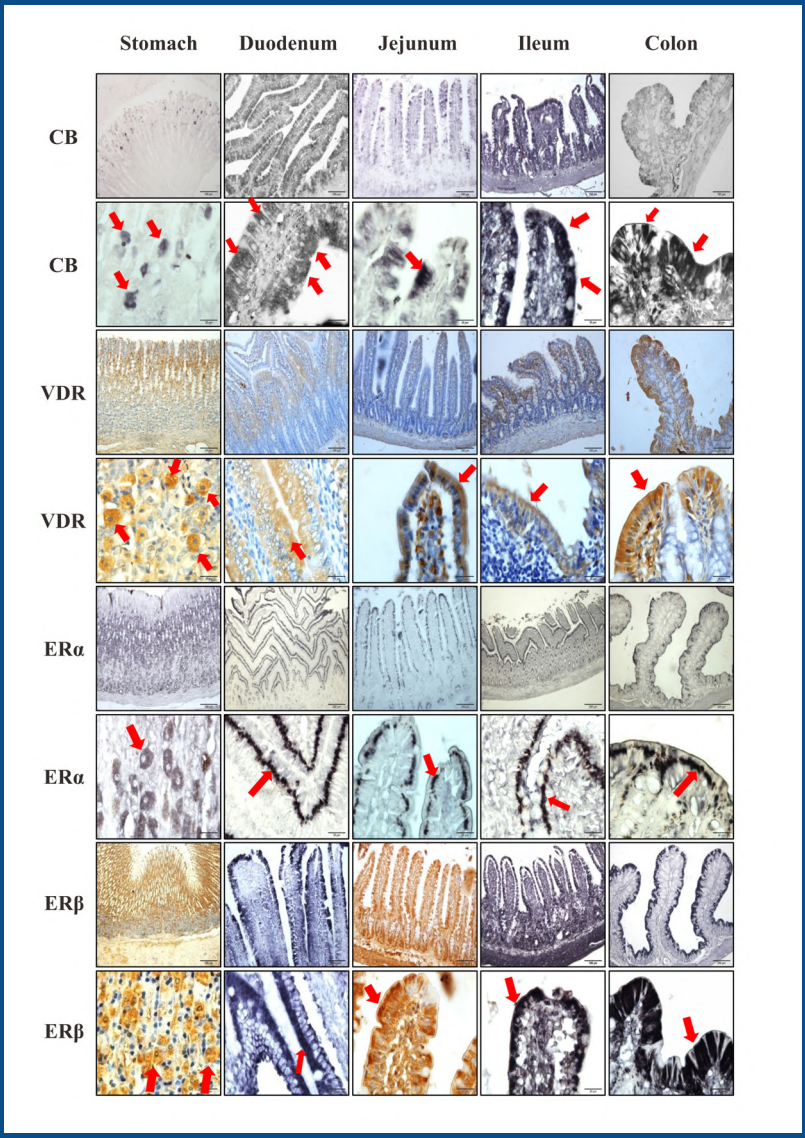

Indexed in:

CLARIVATE
• JCR:2020
• Q4 (21/23)
• I.F. J.C.I.: 0.19
DIALNET
EMBASE / Excerpta Medica

SCOPUS
• SJCR: 2020
• Q4 (31/39)
• I.F.: 0.162
Emerging Sources Citation Index
LATINDEX. Catálogo v1.0 (2002-2017)

Official Journal of the Spanish Society of Anatomy

www.eurjanat.com

EJA
European Journal of Anatomy
Volume 26 - Number 2 March 2022

From theory to practice: what did the students learn in an anatomy pedagogy course?

Joy Y. Balta[1], Gerard W. O'Keeffe[2,3], Briony Supple[3]

[1] Division of Anatomy, Department of Biomedical Education & Anatomy, College of Medicine, The Ohio State University, Columbus, Ohio

[2] Department of Anatomy and Neuroscience & Cork Neuroscience Centre, University College Cork, Cork, Ireland

[3] Centre for the Integration of Research, Teaching and Learning (CIRTL), University College Cork, Cork, Ireland

SUMMARY

There is an increasing interest in understanding the educational background of anatomy teachers arising from the reported shortage of such staff. This has led to the development of several anatomy graduate training programs, which provide courses on theoretical and practical teaching training as part of their curricula, to prepare graduates for a career in anatomy education. A recent study has reported the design of such a course as part of a Master's program in Human Anatomy at University College Cork, Ireland. The aim of this study was to investigate the ability of students who were enrolled in this course, to apply conceptual knowledge of teaching and learning, to the practical design and delivery of anatomy teaching, and what challenges this posed. Consent was obtained from the students to analyze their reflective teaching portfolios. Analysis showed that students varied from those who demonstrated superficial understanding of core concepts in the teaching and learning, to those who were able to adapt and apply these concepts to their teaching. Moreover, they reported that a lack of experience in educational theory, and the brevity of their exposure to it, was a challenge. This highlights that it is important to equip future anatomy teachers with the necessary skills to build their identity as teachers, in parallel to developing their content knowledge. This highlights the need to develop their intrinsic motivational factors that will help them balance the dual identity both as teachers of, and researchers in, the discipline of anatomy.

Key words: Anatomy – Education – Evaluation – Curriculum Design – Identity

INTRODUCTION

The definition of the term "anatomy" is to cut into pieces to display or examine the structure and use of parts. The noun "anatomist" describes a dissector of dead bodies and a person skilled in anatomy (Jones, 1997). Anatomy as a discipline is taught to different cohorts of students ranging from the health and life sciences, through to the arts and humanities. With anatomy being an integral part of several professions, the question of who teaches anatomy is an important one.

Corresponding author:
Dr. Joy Y. Balta. Division of Anatomy, Department of Biomedical Education & Anatomy, College of Medicine, The Ohio State University, Columbus, Ohio. E-mail: Joy.Balta@gmail.com

Submitted: September 5, 2021. **Accepted:** December 12, 2021

https://doi.org/10.52083/LOAJ8673

In this context, there has been significant interest in recent years in the question of who teaches anatomy (Balta et al., 2016). This is an important consideration, given that educators shape the identity of scholars in the field. While once most anatomy educators were medically qualified, a recent study has highlighted the diversity that now exists by reporting that of 125 anatomy teachers in Ireland and the UK, 26.4% had a medical degree, while 25.6% had a PhD in non-anatomical sciences, with 19.2% having a PhD in anatomical sciences (Balta et al., 2016). Furthermore, work in the USA has shown that approximately 60% of anatomists teaching at undergraduate level lack any graduate level experience in neuroanatomy, embryology, and histology, regardless of whether they earned a master's or terminal degree (Schaefer et al., 2019). This highlights the issues arising from the changing landscape following the retirement of classically trained anatomists, and the need for them to be replaced with well-trained early-career anatomists (Schaefer et al., 2019).

Both studies show that arguably the discipline of anatomy lacks scholars trained in anatomy that can teach the varied aspects of the anatomical sciences. This lack of anatomy teachers may have a significant impact on the training of medical doctors and allied health professionals, which needed to be addressed. These shortages of qualified anatomy teachers have led to the development of several graduate education programs in Anatomy. Many of these programs are developed in the United Kingdom (UK) and the United States of America (USA) (Schaefer et al., 2019).

In 2016, the first author was appointed as the program development coordinator of a new taught master's program in human anatomy, which was developed to fulfill the need for anatomy educators with a training in human anatomy and pedagogy. One of the courses that was designed as part of this program was an anatomy pedagogy course, the design of which has previously been reported (Balta et al., in 2019). The goal of the anatomy pedagogy course is to help develop two identities: first, the individual's identity as a practitioner *of* the discipline, and second, as an educator/teacher *within* the discipline (Aydeniz and Hodge, 2011). Despite the dual nature of this professional identity, there is often the assumption that once an individual has the required training in disciplinary knowledge, this is sufficient preparation for them to be effective educators of the discipline. This is coupled with the fact that there is a lack of a formal training of disciplinarians establishing their identity as a teacher. Faculty are often hired on the basis of their research track record, with teaching often being an afterthought; leading to a situation described by Randy Bass, where "*we merely have to pray that this young scholar can teach*" (Bass, 1999). However, with the development of formal anatomy training programs, some anatomy education students are now required to deliver different types of teaching sessions as part of their graduate training program, while others do not face this requirement (Svyantek et al., 2015). Developing an identity as an educator is essential to equip aspiring anatomy teachers with the skills required to optimize student learning later in their career. Furthermore, it is important that students gain practical teaching skills as part of their training, which helps in grounding their practice in theoretical knowledge to allow for a responsive and reflective approach to student learning. However, there is often a gap in this informed practice or *praxis* (Korthagen and Kessels, 1999).

It is naive to simply say that we need to help the students apply the theory into practice, as research has indicated that several factors influence an individual's teaching. While theoretical knowledge could be used to inform conscious teaching, several 'immediate teaching situations' are informed by feelings, former similar experiences, values, needs, routines, and role conceptions (Korthagen and Kessels, 1999). Several distinctions have been made to define knowledge. The two that will be the focus for this paper are knowledge as *phronesis* and knowledge as *episteme*.

Knowledge as episteme consists of a set of assertions that can be investigated, explained, and transmitted; here it is defined as educational theoretical knowledge. Meanwhile, knowledge of phronesis is not abstract or theoretical, it is practical knowledge of concrete particulars; here it is defined as practical teaching knowledge.

While the knowledge as episteme is conceptual, the knowledge as phronesis is perceptual (Kessels and Korthagen, 1996). This is illustrated in Figure 1 below, where knowledge is divided into theoretical and practical elements, with influencing factors playing a role in putting the theoretical knowledge into practice in the teaching of anatomy.

Within this context, helping anatomy trainee teachers develop their identity as educators requires investigating the challenges that they will face in phronesis and episteme. To do this, in this study a Scholarship of Teaching and Learning framework was used to investigate the following three questions by capturing data from this multi-faceted, interdisciplinary, student experience in the anatomy pedagogy course from students who are enrolled in the MSc in Human Anatomy at University College Cork, Ireland.

The three research questions that were investigated are:

1. To what extent did students engage with the material taught in this course by applying the concepts learned about teaching and learning to the discipline of anatomy?
2. To what extent were the students able to use the educational theories learned, on this course, in their teaching practice?
3. What are the challenges that students faced as they engage with Teaching and Learning?

MATERIALS AND METHODS

Anatomy Pedagogy Course

The anatomy pedagogy course is a 5-credit course (towards a total of 60 credits) that is taught over the first 2 semesters of the MSc in Human Anatomy and University College Cork in Ireland. The course is divided into 3 elements which are delivered over the first (September to December) and second semesters (January to April). The first element is faculty-led, where students took 16 h of lectures from September to December on foundational topics in the scholarship of teaching and learning. During the faculty-led sessions, students were introduced to the principles of multiple intelligences (MI), mind mapping, assessment for learning and reflective practice

The second element is student-led and the students are asked to deliver a 50-minute interactive teaching session using an anatomical teaching method of their choice. The third element is practical, and the students shadow an anatomy faculty member in delivering a small-group tutorial in anatomy using cadaveric specimens. Students then deliver one of these small-group

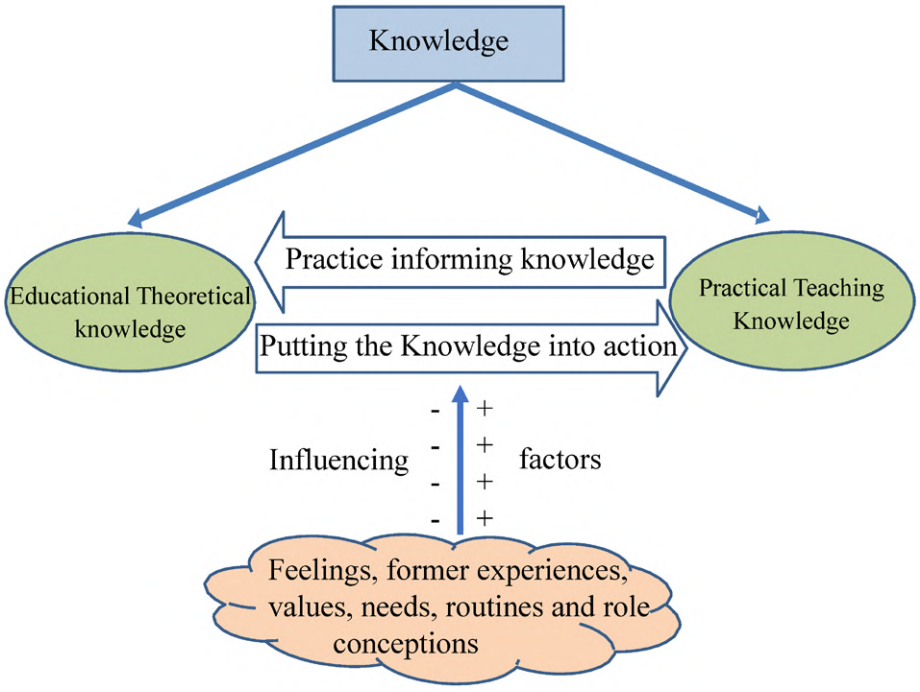

Fig. 1.- The interaction between two different types of knowledge and the influencing factors that affects putting the knowledge into action.

tutorials sessions at a later stage in the course. Students are provided with clear rubrics on how their student-led learning session, teaching portfolio and teaching practice are assessed.

As part of the assessment method on this course, students are required to write a reflective portfolio comprised of four different sections. The first section is a lesson plan that they learned how to prepare in one of the sessions. The second section relates to a teaching or learning incident they experienced, where they were asked to analyze it with reference to the different principles of the Scholarship of Teaching and Learning. Meanwhile, sections three and four are their reflections and analysis of their shadowing and teaching experiences.

Reflective Portfolio

The main aim of this course is to teach the students effective strategies to teach human anatomy. This learning outcome does not fall entirely within the cognitive domain where the students are expected to memorize facts and information. For this reason, reflective portfolios were used to assess two main aspects of learning: 1) whether the students can achieve deeper levels of learning when engaging with a subject (theories of teaching, learning and assessment) which is not directly discipline-specific, and 2) whether students develop their ability to apply the knowledge regarding teaching, learning and assessment, into their practice.

Details pertaining to the portfolio assessment can be seen below:

"Teaching Portfolio: The teaching portfolio will include 4 different parts with total of 30 marks towards the overall course grade. The first part will include the lesson plan for the Student-Led Learning session and is worth 15 pts. The second part will be a 1000-1500 words reflective essay, worth 35 pts. In this section, students will try to identify a clear question of challenge you have found either in your teaching, your students' learning or your own learning. Discuss it in the light of one or more theories which you have encountered over the course. The third and fourth sections are short essays reflecting upon the shadowing and teaching experience, each contributing 25 pts. to the overall mark."

To address the research questions, data were collected from the reflective portfolios of six students who were registered on the MSc in Human Anatomy during the academic year 2017/2018. Ethical approval was granted by the Social Research Ethics Committee of the University on the 20th of November 2018.

Thematic Analysis

To analyze the reflective portfolios, a thematic analysis approach was used to review the data to allow for flexibility in data interpretation. Each portfolio was read multiple times by the primary investigator to search for different viewpoints in the data. Multiple readings included searching for the student experience and how the students demonstrated their understanding of learning theories evidenced using relevant terminology.

A Likert scale was developed to rank the extent to which the students' portfolios reflected the learning theories, with 0= not at all, 1= to a small extent, 2= to some extent, 3= to a moderate extent, 4= to a great extent and 5= to a very great extent. This scale was used to assess the following statements:

- Demonstrated knowledge of teaching and learning theories
- Demonstrated knowledge of teaching and learning terminology
- Was able to use teaching and learning terminology effectively
- Was able to analyze learning experiences using teaching and learning principles
- Was able to use knowledge learned to access literature
- Was able to use knowledge learned to improve on teaching
- Demonstrated passion for teaching

RESULTS

Data Analysis

After reviewing the portfolios several times, some clear observations were made. One of the observations was that there was a wide spectrum in understanding and engaging with the teaching and learning terminology and literature. Below are the different theories that were discussed by students that appeared in their portfolios.

Multiple Intelligences (MI): All 6 students mentioned

MI theory. However, the portfolios could be divided into 3 distinct groups with 2 students in each group who demonstrated a different level of understanding of this theory. For the purpose of analysis, these three groups will be discussed individually.

Group 1 did not name the theory, but they described some of the intelligences in an ambiguous way. One of these two students describes the kinesthetic and the visual intelligences as can be seen in the following comments.

"When the tangible objects were used in the bodily-kinesthetic teaching method, the approach was successful in teaching the subject to the kids."

"So, the real challenge was how to take the control over my mood during learning, I tried to apply the visual-spatial learning style"

Meanwhile, group 2 named the theory and referred to it in their reflections.

"Therefore, as a teacher or lecturer, it is vital to understand the multiple intelligence theory and implement it and utilize it in the classroom."

"From a multiple intelligence point of view, allowing the students to view these video clips, guaranteed that kinesthetic and visual learners got the opportunity to achieve the best education possible on the region of interest."

Group 3 named the MI theory, referred to it in their reflection and were also able to relate it to the discipline. We evidence this by showing in Table 1 part of one of the students' lesson plan that demonstrates an in-depth understanding of the MI theory.

Table 1. Part of a student lesson plan demonstrating an in depth understanding of the MI theory by a student in group 3.

Content	Methodology
Development 4: Nature& Activity **13 minutes**	• I will explain what is meant by Nature in MI. • I will offer an image of the trees and ask the class how this could be used in an anatomy lesson. • I will then show the image that links trees to the lungs and further discuss this. • I will ask somebody to read out extract about lungs/nature. • I will draw an image on the whiteboard like the one in the workbook and ask the students to draw in the flow of blood between the lungs and heart. • This will display how other learning styles can used in collaboration.
Development 5: Linguistic **4 Minutes**	• I will discuss how students studied word roots in their learning of anatomy. • I will compare this to the Latin we see in our learning of anatomy. • I will mention the merits of this shown in the slides. • I will provide examples of this in reference to the lungs. • I will show the image with the origin of the word lungs.
Development 6: Concept Cartoons Interpersonal Visual Literacy Further discussion **5 Minutes**	• I will show the class an image of the cartoon and ask them to review it in their own time. • I will mention the MI that is included in this style. • I will discuss the merits of using this and the literature on this. • We will discuss how this can offer further potential for higher level discussion. • I will ask the class about the merits of this.
Development 7: Interpersonal Donor Program **12 minutes**	• I will elaborate off James Stephens quote • I will ask one of my classmates to read out quote. • I will go through the points about the donor program and the conflict of respecting and dehumanasing the donor. • I will explain the initiative in University of Oklahoma of Medicine. • I will explain the term dethatched concern.
Quote from book **3 Minutes**	• I will ask the audience the talk about how dissection relates to interpersonal skills and what other styles it promotes. • I will refer the audience to the quote in the workbook and have a discussion on this. • I will present the idea about angor animi to show why doctors need interpersonal skills and how this can differ from clinical skills.
Development 8: Intrapersonal **3 Minutes**	• I will define what intrapersonal n anatomy education means. • I will read out the quote from Henry Marsh. • I will explain how this book is prescribed and the quote from a reader who was a doctor.

Learning styles:

The concept of learning styles is contentious and was not taught as part of this program. Despite there being no focus on learning styles in this program, an interesting observation was that students from all 3 groups mentioned learning styles.

Students in Group 1 used the term style interchangeably with intelligence, as demonstrated in the earlier statements, even though learning styles was not a focus of any of the taught teaching and learning theories. Meanwhile, students in Group 3 were able to show some differentiation between the MI theory and the concept of learning styles. A clear demonstration of that is the student having the below methodology as part of his lesson plan:

"I will briefly show the audience the VARK questionnaire and discuss why questions are asked in the style that they are and note why these don't ask students straight out what learning style they prefer"

Other terminology: Students used a mix of other teaching and learning terminology. Some of these were theories, tools and other concepts that are used in educational literature. While some of these were taught in the different sessions within the faculty-led learning section, others were from the literature that the students decided to include in their portfolio. Table 2 summarizes a terminology list and the number of students that used it, if used by more than one student.

Table 2. A list of different terminology used by students along with the number of students that used them.

Terminology	Number of students
Multiple intelligences	6
Learning style	6
Mind mapping	3
Reflective Practice	2
Assessment for learning	2

Some other terminology used by individual students included: theory of constructivism, single/double loop learning, organizational learning, Bloom's taxonomy, differential instructions and Socrative teaching.

Table 3 summarizes the scores that were given to the students for each statement. In the tables, the students are given a letter for convenience of description and divided into 3 groups that were described earlier. It also includes a mean score for each statement. Some of the statements describing the student's passion for teaching include:

"To my surprise, I found the teaching sessions to be a very enjoyable experience"

"Once it started, I felt I was confident and overall, I was delighted with how it went. I was actually disappointed when the final rotation ended, finding myself looking forward to my next teaching session."

"Overall, I found the teaching sessions to be very enjoyable and pleasant experiences. I think they will help and benefit me not only in my own studies and but also in my career in the future."

"My aim was to make the sessions educational, memorable and meaningful and I hope that the students have benefitted from the lab sessions. I will continue to teach with enthusiasm and inspire my students. I hope that I have allowed my students to "find their voice" by allowing them to articulate and activity take part in the discussions."

Table 3. A summary of the score given to each student for the above listed statements with a mean for each statement with (0) being the lost score and (5) being the highest.

	Students						Mean
	Group 1		Group 2		Group 3		
Statements	**A**	**B**	**C**	**D**	**E**	**F**	
Demonstrate knowledge of Teaching and learning theories	0	3	4	2	5	5	3.17
Demonstrate knowledge of Teaching and learning terminology	0	1	3	3	5	4	2.67
Ability to use Teaching and learning terminology effectively	0	1	2	3	4	5	2.50
Ability to analyze learning experiences using Teaching and learning principles	1	1	2	2	4	4	2.33
Ability to use knowledge learned to access literature	0	0	1	2	3	5	1.83
Ability to use knowledge learned to improve on teaching	1	0	2	2	5	4	2.33
Demonstrated passion for teaching	2	0	4	3	4	5	3.00
Overall score per group	0.71		2.5		4.43		

"Overall, I found the teaching to be a very rewarding and enjoyable experience."

Each student portfolio (A, B, C, D, E & F) was scored based on the statements in Table 3 with 0 being the lowest score and 5 being the highest.

DISCUSSION

In relation to the first two research questions *(1) To what extent did students engage with the material taught in this course by applying the concepts learned about teaching and learning to the discipline of anatomy?*; and *(2) To what extent were the students able to use the educational theories learned, on this course, in their teaching practice?,* while it is clear that all students were able to engage with the teaching and learning theories to a certain extent, a few were not able to connect these theories to the discipline of Anatomy. In relation to the third research question –*What are the challenges that science students face as they engage with teaching and learning?*– only a small number of students were able to apply this theory to their teaching practice. This leads to the conclusion that this course was able to provide an introductory-level engagement to students with no specific training in education or approach to teaching and learning, while providing a deeper level of learning for students with previous teaching/educational exposure. Hence the challenges that our students face is the lack of previous experience with educational theory, and the short period of exposure that they have on this course.

Reconnect Teaching to the Discipline

Equipping the next generation of anatomists with enough knowledge of the scholarship of teaching and learning along with the practical training in teaching will help in addressing Lee Shulman's first strategy aimed at reconnecting teaching to the discipline which was to improve the recognition and reward attached to teaching (Shulman, 1993). On the Anatomy Pedagogy course, we are trying to connect and embed foundational educational principles with the discipline of anatomy. Several studies have highlighted the vast differences among disciplines across the humanities, social science and science disciplines. These differences fall into different areas such as the nature of teaching, teaching practices, teaching outcome, assessment and student learning (Neumann, 2001). The teaching staff on this course come from non-anatomical backgrounds. This raises the question whether students attending these sessions can connect these teaching principles to the discipline of anatomy, from the theoretical principles such as signature pedagogies (Shulman, 2005) to the application of practical concepts such as entry points to learning (Gardner, 1999).

Skill and Will

While reading the portfolios, links and trends were made between them which led to the creation of 3 Groups.

Group 1, consisting of 2 students, neither showed an interest in teaching and learning nor demonstrated their ability to understand the topic throughout their reflections. This theme was tagged as 'skill and will' and was very clear in some of the statements made in the portfolio, as one of the students started her teaching portfolio with *"Teaching is not my passion"* and then follows with *"In the class day, I tried to focus more on my strengths and tried to ignore that I don't like teaching".* The other student in the group meanwhile was not able to establish meaningful connections by linking the learned teaching and learning theories to her reflective writing. The portfolios written by students in this group did not express their skill or will to achieve the set of learning outcomes

Meanwhile, Group 2 demonstrated a strong will for learning and expressed a passion for teaching. This group of students just completed a Bachelor's degree before joining this program, and did not have any previous teaching experience. Having said that, both students in this group expressed their interest in teaching and were able to comprehend the educational theories taught, as demonstrated in section 2 of their portfolio. When only considering their portfolios, the group of students were not able to demonstrate deeper level of learning. Perhaps this is because students in this group do not have any previous teaching experience, which meant they possibly found it more difficult to connect the learning theories to the discipline of anatomy.

The third group of students achieved the highest scores in their assessment, which is also arguably an indication that they have also achieved the highest level of learning among their peers. There are several reasons that may have given them an advantage over their colleagues. One of the reasons is the age of the students and their previous experiences that they have accumulated before joining the program. Both students have completed several degrees, which gives them a better understanding of teaching and learning in general and their own learning. Moreover, both have had some experience in teaching, which gives them a better understanding of the process and the challenges faced. Students in group 3 demonstrated a high level of understanding of the educational theories taught, connected the theories taught to the discipline of anatomy and used these theories to improve their teaching. Both students were also able to use what they learned on this course to expand their knowledge by engaging with the teaching and learning literature. This could be an indication that students that have the will and the necessary skills are able to achieve higher scores and hence a higher level of learning.

While analyzing student portfolios was able to reveal some of their understanding of the topic, this methodology does not fully reflect the students' own skill or will as individuals, or their respective potential to be anatomy educators. Developing students' will and skill is our responsibility as educators. As this was a 5-credit course, there is a certain assumption regarding students' pre-acquired knowledge and experience. This is below ideal as this does not allow for equal opportunities for students who do not have those pre-acquired skills for teaching and learning.

It is worth acknowledging that there are several limitations that could limit the findings of this study. While the use of the student portfolios is an effective tool to gather information, the students were not provided with guiding questions that could better address the research question. It would have also been beneficial to use an anonymous questionnaire with open ended questions to ask the students about their own experiences when taking this course.

Now What?

Looking at the three groups enabled an understanding regarding whether the students might achieve the set learning outcomes. Group 3 of students were able to achieve the set learning outcomes and we were able to identify that through the assessment methods devised. This is an indication that there is no need to completely redesign the course, but there is room for improvement.

Helping Group 1 change their attitude towards teaching is one of the major things that could be done to motivate them for learning. This could be done by emphasizing the need for teaching or training in any career. The main motivational issue with a student in Group 1 was that they chose a career in medicine and not teaching. Highlighting the need for teaching skills in medicine, whether it was training new clinicians or engaging with other scholars, would provide an element of motivation (Smesny et al., 2007). While this would promote a better will for learning, improving their skill could be shared with group 2.

The majority of students were able to understand the educational theories taught throughout this course, but the major challenge was connecting it to the discipline. This has also led to their inability to use these theories in their teaching. To help the students in bridging this gap, it is important to schedule an interactive session by an anatomist that enables an integration of theory into the disciplinary context. This will assist the students in connecting the knowledge learned about educational theory to the discipline of anatomy. Students will then learn those skills or way of thinking and will lead to a better application process. It would also be helpful to collect longitudinal data and feedback from different cohorts of students to have more robust conclusions.

CONCLUSION

With the potential shortage of science, technology, engineering, and mathematics (STEM) professionals, it is important to foster the growth of faculty to prepare the upcoming generation of STEM educators. Both identities in this upcoming

generation, as scientists and educators, need to be cultivated to improve teaching and learning. Future studies need to address those challenges faced by STEM educators as they engage with teaching and learning techniques. As the third class of the MSc in Human Anatomy is getting ready for graduation, future research will gather data for the coming three cohorts to provide more robust feedback. While using a reflective portfolio, which was written while the students are immersed in the experience, was extremely beneficial, it would also be helpful to guide those reflection with more specific questions. It would also be beneficial to collect feedback through questionnaires where the students are asked about their opinions and feedback.

REFERENCES

BALTA JY, CRONIN M, CRYAN JF, O'MAHONY SM (2016) The utility of cadaver-based approaches for the teaching of human anatomy: A survey of British and Irish anatomy teachers. *Anat Sci Educ*, 10(2): 137-143.

BALTA JY, O'KEEFFE GW, SUPPLE B (2019) Utilizing the scholarship of teaching and learning to design an Anatomy Pedagogy Couse. *Eur J Anat*, 23(3): 233-240.

BASS R (1999) The scholarship of teaching: What's the problem. *Inventio: Creative thinking about learning and teaching*, 1(1): 1-10.

BRAUN V, CLARKE V (2006) Using thematic analysis in psychology. *Qual Res Psychol*, 3(2): 77-101.

BROWN S (2005) Assessment for learning. *Learn Teach High Educ,* 1: 81-89.

D'ANTONI AV, ZIPP GP, OLSON VG, CAHILL TF (2010) Does the mind map learning strategy facilitate information retrieval and critical thinking in medical students? *BMC Med Educ*, 10: 61-72.

DEELEY SJ (2018) Using technology to facilitate effective assessment for learning and feedback in higher education. *Assess Eval High Educ*, 43(3): 439-448.

DEWEY J (1938) *Experience and education* (6th ed.). MacMillan, New York.

FARRAND P, HUSSAIN F, HENNESSY E (2002) The efficacy of the 'mind map' study technique. *Med Educ*, 36: 426-431.

FARRELL TS (2012) Reflecting on reflective practice: (Re) Visiting Dewey and Schon. *Tesol J*, 3(1): 7-16.

GARDNER HE (1983) Frames of mind: The theory of multiple intelligences. Hachette, UK.

GARDNER H (1999) *Intelligence reframed: Multiple intelligences for the 21st Century*. Basic Books, New York, US.

GARDNER H, HATCH T (1989) Educational implications of the theory of multiple intelligences. *Educ Res J,* 18(8): 4-10.

JONES DG (1997) Anatomy departments and anatomy education: Reflections and Myths. *Clin Anat,* 10(1): 34-40.

KESSELS JP, KORTHAGEN FA (1996) The relationship between theory and practice: Back to the classics. *Educ Res J,* 25(3): 17-22.

KORTHAGEN FAJ, KESSELS JPAM (1999) Linking theory and practice: changing the pedagogy of teacher education. *Educ Res J*, 28(4): 4-17.

NEUMANN R (2001) Disciplinary differences and university teaching. *Stud High Educ*, 26(2): 135-146.

NOVAK JD, CANAS AJ (2006) The theory underlying concept maps and how to construct them. Technical Report IHMC Cmap Tools 2006-01.

SCHAEFER AF, WILSON AB, BARGER JB, AZIM HM, BROKAW JJ, BROOKS WS (2019) What does a modern anatomist look like? Current trends in the training of anatomy educators. *Anat Sci Educ*, 12(3): 225-235.

SCHÖN DA (1987) *Educating the Reflective Practitioner. Toward a New Design for Teaching and Learning in the Professions. The Jossey-Bass Higher Education Series*: ERIC.

SHULMAN LS (1993) Teaching as community property: Putting an end to pedagogical solitude. *Change*, 25(6): 6-7.

SHULMAN LS (2005) Signature pedagogies in the professions. *Daedalus*, 134(3): 52-59.

SMESNY AL, WILLIAMS JS, BRAZEAU GA, WEBER RJ, MATTHEWS HW, DAS S (2007) Barriers to scholarship in dentistry, medicine, nursing, and pharmacy practice faculty. *Am J Pharm Educ*, 71(5): 91.

SVYANTEK MV, KAJFEZ RL, MCNAIR LD (2015) Teaching vs. Research: An approach to understanding graduate students' roles through eportfolio reflection. *Int J ePortfolio*, 5(2): 135-154.

ZIPP G, MAHER C, D'ANTONI A (2015) Mind mapping: Teaching and learning strategy for physical therapy curricula. *J Phys Ther Educ*, 29(1): 43-48.

Human portal system morphometry based on 3D computer aided modelling

Andrey N. Russkikh

Department of Operative Surgery and Topographic Anatomy, Krasnoyarsk State Medical University named after Prof. V.F. Voino-Yasenetsky, Krasnoyarsk, Russia

SUMMARY

There is no discussion about human portal system variability. Features of interposition, veins branching included in this system, stereometric and lineal characteristics define its development, stream and ways of operation interference for several surgery diseases, which all in all decides the end of surgery pathology. Morphometry study of portal system using computer-aided modelling and methods of computational anatomy has been performed. DICOM data segmentation was performed using Dragonfly software (Object Research Systems, Canada) at the Innovation Technology Management Resources of the Reaviz University. Using series with arterial and vein contrast, we performed the segmentation of contrasting vessels, obtained three-dimensional data topology in .obj format. Then we processed the obtained models using scripts prepared for the pythonOCC framework. We built the central lines of the vessels and formed the branching tree. Methods of computational hemodynamics were implemented using the Visual-CFD application for OpenFOAM environment (ESI, France). Veins forming the portal vein are presented by three systems; in every one of them there are scapi and affluxes, which are different in branching types and other morphological characteristics. The superior mesenteric vein, for instance, is characterized by interjacent branching type, has one scapus 93,5 (78,5; 119,5) mm in length and diameter 9,5 (6,5; 12,0) mm, going to portal vein under the corner 170,0 (160,0; 175,0)^0, and formed by venous inflows of majority unpaired organs of upper and down floors in abdominal cavity. Affluxes of the superior mesenteric vein have almost the same diameter from 3,5 to 12 mm but the length. The shortest affluxes are jejunal ones (40,0 (38,5; 46,5) mm) and right gastroepiploic vein (45,0 (38,5; 53,5) mm), then iliac (50,0 (48,5; 53,5) mm), middle colonic (60,0 (58,5; 63,5) mm) and iliac colonic (70,0 (68,5; 78,5) mm) veins. The system of inferior mesenteric vein contains a lower number of veins going to its bed in comparison with vessels net of superior mesenteric vein. Magistral type of branching of inferior mesenteric vein is found in 23% of cases and in 77% of cases it has interjacent type of branching. In case of interjacent type of branching mesenteric vein goes to superior mesenteric vein between right colonic and jejuna veins. Inferior mesenteric vein of magistral type goes to splenic vein in most cases (as it is shown on picture 1) or it is independent afflux of portal vein. Its diameter is significantly less than diameter of superior

Corresponding author:
Andrey Nikolayevich Russkikh. Department of Operative Surgery and Topographic Anatomy, Krasnoyarsk State Medical University named after Prof. V.F. Voino-Yasenetsky, 1, Partizana Zheleznyaka St., Krasnoyarsk, Russia, 660022. Phone: 8-962-070-36-36. E-mail: tat_yak@mail.ru

Submitted: August 1, 2020. **Accepted:** December 15, 2021

https://doi.org/10.52083/OUWB2921

mesenteric vein and makes 4,5 (2,0; 6,5) mm. The current research gives quantitative orienting points for main vein structures of portal vein system. The research results have allowed adding science materials about types of branching and morphological patterns of portal vein and its branching. Variations common for every system are preferably being used for regulation of the discussed subject in terms of tactic patients' curing with syndrome of portal hypertension or at the step of pre surgical preparation.

Key words: Portal system – Morphometry – 3D modelling – Computational anatomy – Computational fluid dynamics

INTRODUCTION

There is no discussion about human portal system variability (Khamanarong et al., 2016; Sharma et al., 2017; Cheluvashetty and Rachapalli., 2017; Guerra et al., 2017). Features of interposition, veins branching included in this system, stereometric and lineal characteristics define its development, stream and ways of operation interference for several surgery diseases what all in all decides the end of surgery pathology (Gayvoronskiy et al., 2018; Iqbal et al., 2017). According to main abdominal surgeons, diagnostics development of portal system features building gives answers for many questions about curing and diagnostic tactics in pre-surgical (Nakamura et al., 2002; Schmidt et al., 2008; Sakamoto et al., 2017).

Medical imaging of vessels, organs and whole systems research in different areas of medical practice shows good diagnostic results (Akagi et al., 2019; Karunakaravel, 2016). The research made by a standing X-ray instrument in order to find out features of portal-system rectal vessels has shown a high informative capacity of the method, and allowed to find out characteristics postmortem –morphometry, location and vein branching (Silant'eva, 2009; Gibson et al., 2018; Ghesu et al., 2019).

The variant anatomy of magistral vessels of the portal vein was learnt by a number of authors (Lang et al., 2019; Durand et al., 2020). Gaivoronskiy and his coauthors presented main results in 2018, which were characteristic of formation variants of the portal vein scapus, quantity measurements of vein length and diameter and its roots, showing a wide range of morphometric characteristics. The results obtained by MSCT of abdominal cavity were defined as markers allowing to plan an optimal surgery tactic, and to reduce, after operation, difficulties from the side of the mesoportal system, taking into account terebrant major thrombosis of the portal vein or the superior mesenteric vein (Gayvoronskiy et al., 2018). However, the results might be implemented only in case of operation of abdominal organs where magistral vessels of the portal system work. According to Kolsanov (2017), for a full research of the portal system living people, it is eligible and competent to use computer tomography with bolus contrasting, which is one of the most precise methods to estimate morphometric features of vessel formations. Such research is the best to learn variant angioanatomy with a visualization of vessels of 1 mm diameter and more, as it allows to use this method not only in choosing the tactic of surgery curing of portal hypertension, but also in all types of liver and pancreas resection, liver transplantation, etc. (Kolsanov et al., 2017).

A new branch of human morphology is computational anatomy. Computational anatomy is now understood to be a new discipline at the junction of human morphology and information and computing technology. Despite the fact that the object of its study is the human body, computational anatomy offers a new, synthetic approach to cognition, in which organs and tissues are studied by layers of data, in their movement and function, and the visual approach is supplemented by a superficial one, using artificial intelligence technologies.

MATERIALS AND METHODS

Our aim was to perform morphometric study of portal system using computer aided modelling and methods of computational anatomy.

Contrast research was done among 53 men who were patients in surgery departments at Krasnoyarsk regional hospital #1, Russia (KRH). Criteria for taking part in this research were

patients with surgery diseases of abdominal organs without blood interference. The average age of the patients was 54.9 ± 1.7, from 36 to 71 years old. Estimations were made using 3D models of portal system (working stations GE Advantage Workstation, Siemens singo.via), based on multi-slices computed tomography of abdominal cavity with bolus contrasting with help of medication "Ultravist-370". The volume of the used contrasting stuff made 100 ml, the speed of infiltration was 4 ml per second, and the average radial strain was 11,3 m3v. DICOM data segmentation was performed using Dragonfly software (Object Research Systems, Canada) at the Innovation Technology Management Resources of the Reaviz University. Using series with arterial and vein contrast, we performed the segmentation of contrasting vessels, and obtained three-dimensional data topology in .obj format. Then we processed the obtained models using scripts prepared for the pythonOCC framework. We built the central lines of the vessels and formed the branching tree. Methods of computational hemodynamics were implemented using the Visual-CFD application for OpenFOAM environment (ESI, France).

X-ray research was made in order to learn formation variants of portal system and morphometric patterns, and types of vessel branching at different levels of structure organization.

To define types of portal vein division and its branching formation, the Nakamura et al. (2002) classification was used to define types of branching, and Shevkunenko classification was used (magistral, interjacent and loose types) (Shevkunenko, 1949; Gadzijev and Eldar, 1996).

The length, diameter, and corner of formation of portal vein towards the middle line of the human body were estimated, as well as corners of vessel formation creating the portal vein in the frontal plane. Measurements were made by building a central vessel line with further measure of lineal patterns (Kolesnikov, 2003; Covey et al., 2004).

Statistics processing was made by using analysis SPSS Statistics 17,0. Normality of dividing was defined based on Shapiro-Wilk criteria. Characteristics of variant rows for quantity features with non-parametric dividing and data with parametric dividing taking into account their small number were presented with help of measures of central tendency —middle (M), median (Me), mode (Mo) and dispersion measures– mean square departure, swing, interquartile interval (P25; P75). Comparing two independent selections of nonparametric data and nonparametric criteria Mann-Whitney (U-test) was used.

Ethic rules and normal ranges were obeyed in full during the research (extract from meeting report of local ethic committee №84/2018 dated 06.06.2018).

RESULTS

3D models of computed tomographic images of the portal system among all examined men are characterized by stability of portal vein existence, its right branch (with front and back branching), left branch (with diametrical and omphalic parts) as well as splenic, superior and inferior mesenteric veins and veins of a higher row creating main afflux. According to X-ray, the portal vein is a cylinder with diameter of 14.5 mm (13.0; 14.5). Length is in the range from 58 mm and to 71 mm and the average length is about 63 mm. The portal vein is created under the corner of 68° degrees towards man's body middle line corner what proves earlier published data about frequency of the corner (Gayvoronskiy et al., 2018).

Morphometric measures of portal vein branching are shown in Table 1.

Creation corners of the main branching of the portal vein are statistically different ($p<0.05$); the creation corner of the right main branching makes 135.0 (130.0; 141.0)°, so the left branching towards the portal vein makes 53.0 (49.5; 60.0)°. In most cases, both branchings are created according to a classical type of branching (T. Nakamura), and in a few cases there have been trifurcations and intrahepatic departure of front branching. The left branching of the portal vein is longer than the right one (82.0 (79.5; 89.0) mm and 46.0 (39.5; 47.5) mm) but the diameter

is almost the same at 13.0 (10.5; 14.5) mm and 11.0 (10.5; 12.0) mm). The right branching of the portal vein is divided dichotomically for front and back branching; the length of the front branching (75.5 (73.0; 77.5) mm) and back one (80.5 (75.5; 81.0) mm) and their diameters (8.0 (7.0; 8.5) mm and 7.0 (6.5; 8.5) mm) are statistically the same with the exception of formation corners. The front branching is a kind of continuation of the right branching and goes under the corner of 160.0 (145.0; 170.0)°, the back branching forms almost a straight angle with the right branching (115.0 (100.0; 125.0)°). Parts of the left branching of the portal vein have peculiarities in length. The diametrical part (53.0 (48.0; 61.0) mm) is always longer than the omphalic one (31.0 (28.0; 39.0) mm), their diameters are statistically the same.

As a result, variants of morphometric patterns of portal vein intrahepatic vessels are obvious, although branching variants are not various and lead to one type.

Veins forming the portal vein are presented by three systems. In all of them there are scapi and affluxes that are different in branching types and other morphological characteristics. The superior mesenteric vein (Fig. 1), for instance, is characterized by interjacent branching type (23), has one scapus 93.5 (78.5; 119.5) mm in length and diameter 9.5 (6.5; 12.0) mm, going to the portal vein under the corner 170.0 (160.0; 175.0)°, and formed by venous inflows of majority unpaired organs of upper and down floors in the abdominal cavity. Affluxes of the superior mesenteric vein have almost the same diameter from 3.5 to 12

Table 1. Morphometric measures of portal vein branches found by X-ray.

Pattern	**Length** Me [P_{25}; P_{75}] mm	**Diameter** Me [P_{25}; P_{75}] mm	**Formation corner**, degree*
1	2	3	4
Portal vein	63.0 [58.0; 71.0]	14.5 [13.0; 14.5]	68.0 [46.0; 72.0]
Right branch of portal vein - anterior branch - posterior branch	46.0 [39.5; 47.5] 75.5 [73.0; 77.5] 80.5 [75.5; 81.0]	11.0 [10.5; 12.0] 8.0 [7.0; 8.5] 7.0 [6.5; 8.5]	135.0 [130.0; 141.0] 160.0 [145.0; 170.0] 115.0 [100.0; 125.0]
Left branch of portal vein - diametrical part - omphalic part	82.0 [79.5; 89.0] 53.0 [48.0; 61.0] 31.0 [28.0; 39.0]	13.0 [10.5; 14.5]	53.0 [49.5; 60.0]

*Formation corner of portal vein towards middle line of a man's body

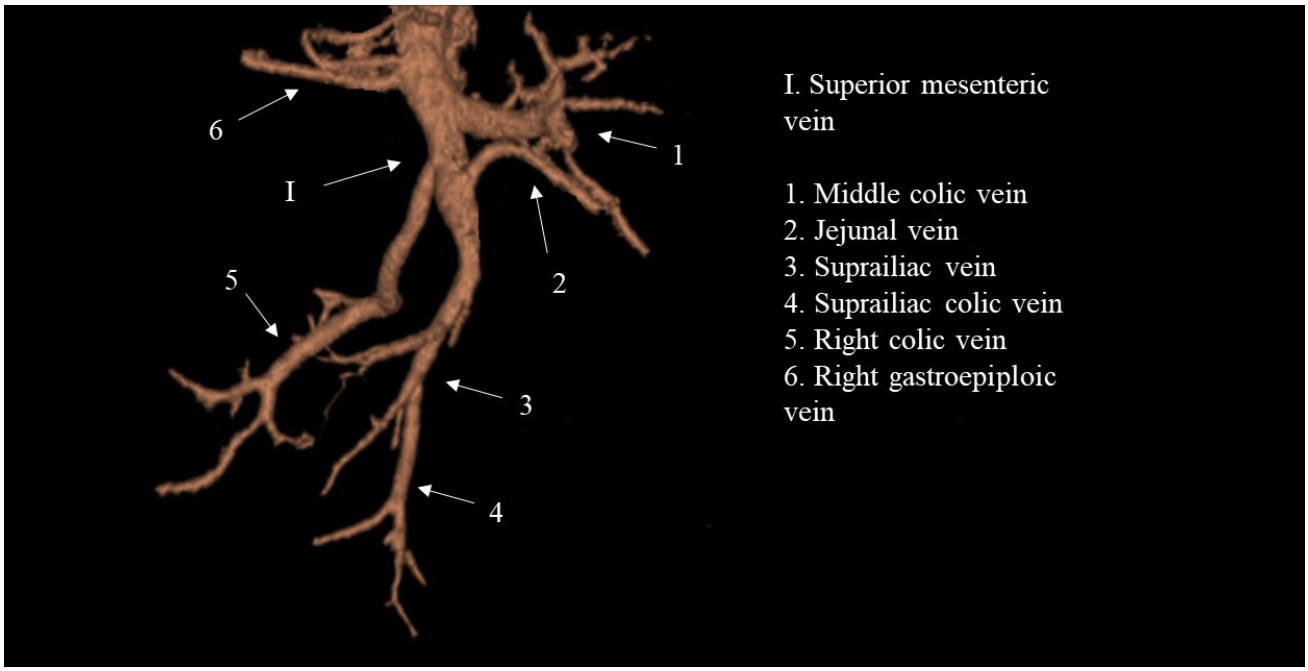

Fig. 1.- 3D model of human superior mesenteric vein.

mm but the length. The shortest affluxes are the jejunal ones (40.0 (38.5; 46.5) mm) and the right gastroepiploic vein (45.0 (38.5; 53.5) mm), then the iliac (50.0 (48.5; 53.5) mm), the middle colonic (60.0 (58.5; 63.5) mm) and the iliac colonic (70.0 (68.5; 78.5) mm) veins. The maximum length is defined in the right colonic vein (115.0 (108.5; 120.5) mm), draining ascending and diametrical colonic parts of the colon. Angles of convergence of every afflux of the superior mesenteric vein are defined by internals from which venous drainage is made. As long as iliac and iliac colonic veins are caudal branches, so their corners measures lead to large scale and make 160° (155.0; 171.0) and 160.0° (150.0; 171.0). The given measure is statistically maximum towards angles of convergence of other veins of this system. The average measure is for the middle (120.0° (110.0; 131.0) and right (140.0° (130.0; 145.0) colonic veins. Minimal measures are common for jejunal and right gastroepiploic veins (70.0° (60.0; 81.0) and 85.0° (80.0; 91.0), respectively.

The system of the inferior mesenteric vein (Fig. 2) contains a lower number of veins going to its bed in comparison with vessels net of superior mesenteric vein. Magistral type of branching of inferior mesenteric vein is found in 23% of cases and in 77% of cases it has interjacent type of branching (23). In case of interjacent type of branching mesenteric vein goes to superior mesenteric vein between right colonic and jejuna veins. The inferior mesenteric vein of the magistral type goes to the splenic vein in most cases (as it is shown on Fig. 3), or it is independent afflux of portal vein. Its diameter is significantly shorter than the diameter of the superior mesenteric vein, and makes 4.5 (2.0; 6.5) mm. Length measures are still variant depending on branching features, but statistically they are not different from the analogous measure of the superior mesenteric vein. The formation corner in the case of influx to upper or splenic vein is in a range from 135 to 151°. Lineal patterns and formation corners of affluxes of the inferior mesenteric vein do not have statistically significant differences (Table 2).

In comparison with systems of superior and inferior mesenteric veins, the splenic vein (Fig. 4) always has magistral type of branching. The vena lienalis has an intermediary diameter of 7.5 (5.5; 8.5) mm, a maximum length of 125.0 (97.5; 129.5) mm, and goes to the portal vein under a less corner (100.0° (95.0; 111.0) towards the analogous measures of the superior and inferior mesenteric veins. Affluxes of splenic vein are numerous; measures of lineal patterns are statistically not different. Average measures of length, diameter and angle of convergence of the left gastroepiploic vein make 20.0 (13.5; 29.5)

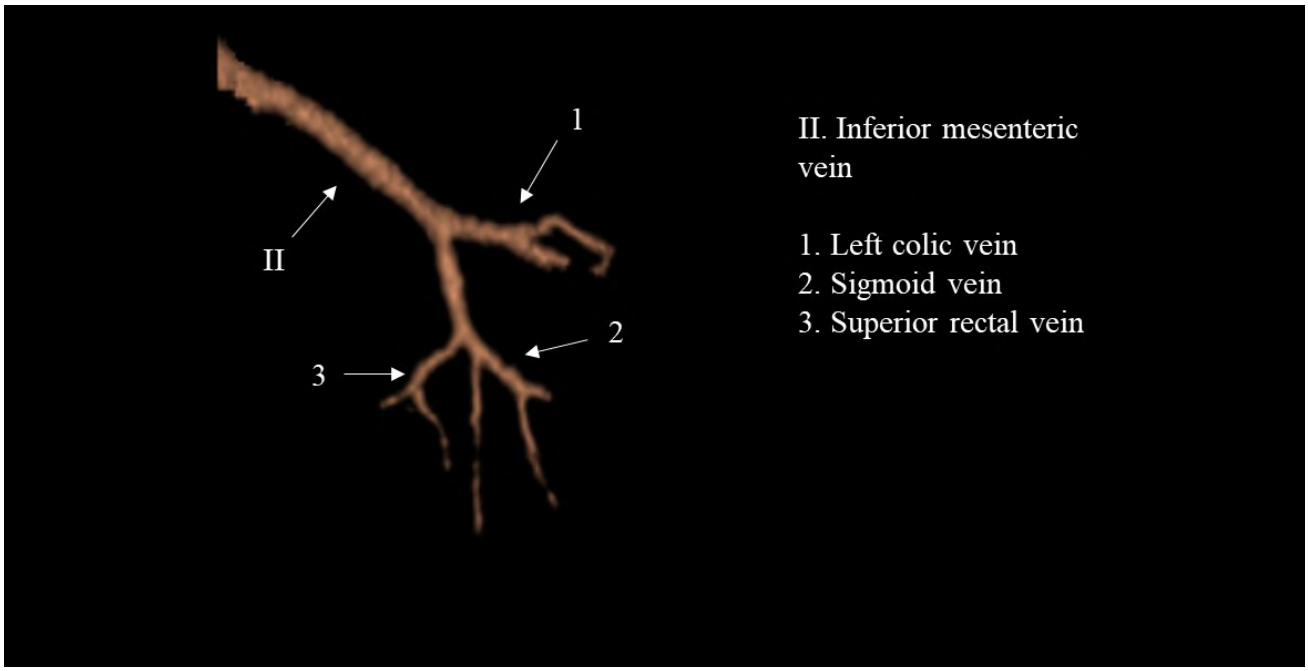

Fig. 2.- 3D model of human inferior mesenteric vein.

mm; 5.0 (4.0; 6.0) mm and 130.0° (120.0; 135.0). The short veins of the gaster go to splenic vein under the straight corner (90.0° (90.0; 95.0), and average measures of length and diameter make 12.0 (7.0; 18.5) mm and 4.0 (3.0; 4.5) mm.

Estimating the length, diameter and formation corners of the portal vein and its affluent vessels, we have come to a conclusion that in order to study the system of the portal vein at different levels of its structure organization, it is needed to use modern methods of X-ray diagnostics with help of contrast stuff and what is more important with bolus contrasting.

With the use of created three-dimensional computer model, the blood flow in the portal vein at various variants of its structure was simulated. It was obtained that, in the presence of the main type of structure with predominance of blood flow along the splenic vein, the blood flow turbulence and risk of thrombosis development are higher. At the same time, with virtual thrombosis of the portal vein trunk, the pressure gradient is 1.4 times higher than with the bulk type, which is more favorable for the proposed reconstruction. Thus, these data can be used for preoperative planning in surgical treatment of portal vein thrombosis in liver transplantation (Fig. 5).

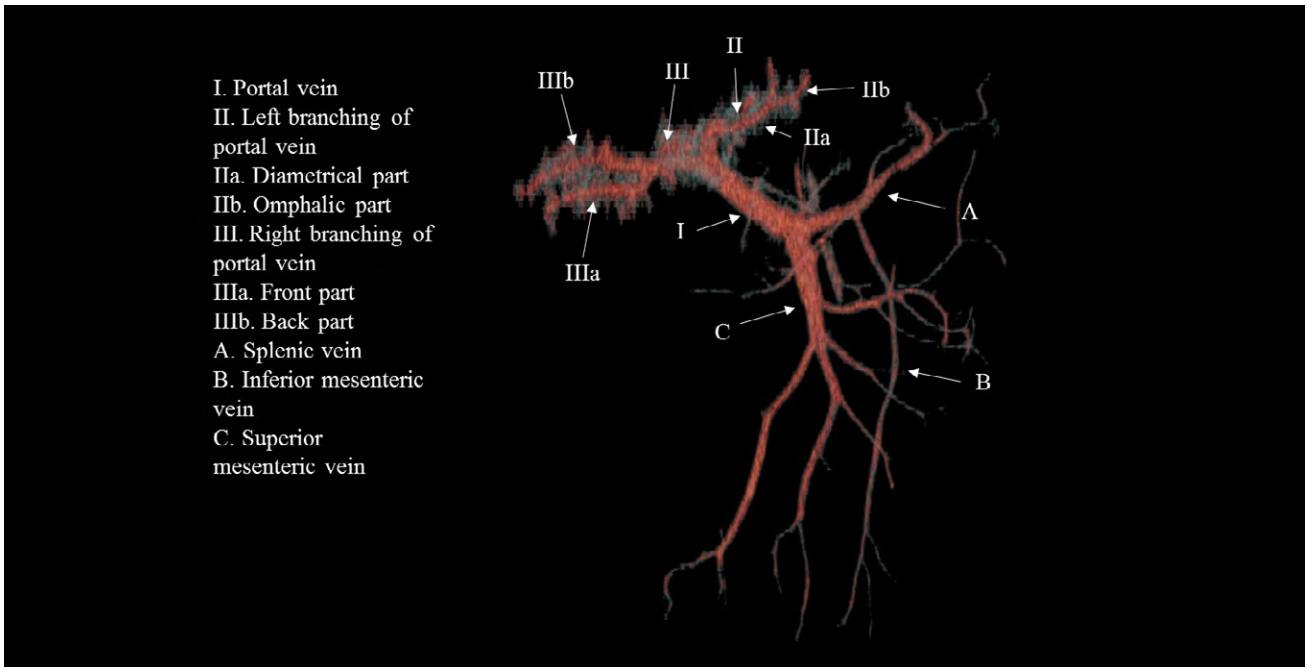

Fig. 3.- 3D model of human portal vein system.

Table 2. Morphometric measures of portal vein roots found by X-ray.

Pattern	**Length** Me [P_{25}; P_{75}] mm	**Diameter** Me [P_{25}; P_{75}] mm	**Formation corner**, degree
1	2	3	4
Superior mesenteric vein - middle colonic vein - jejunal vein - suprailiac vein - suprailiac – jejunal vein - right colonic vein - right gastroepiploic vein	93.5 [78.5; 119.5] 60.0 [58.5; 63.5] 40.0 [38.5; 46.5] 50.0 [48.5; 53.5] 70.0 [68.5; 78.5] 115.0 [108.5; 120.5] 45.0 [38.5; 53.5]	9.5 [6.5; 12.0] 9.0 [6.0; 11.0] 4.0 [3.5; 6.0] 5.5 [5.0; 7.0] 5.0 [3.5; 6.5] 6.0 [6.5; 9.0] 4.0 [3.5; 6.0]	170.0 [160.0; 175.0] 120.0 [110.0; 131.0] 70.0 [60.0; 81.0] 160.0 [155.0; 171.0] 160.0 [150.0; 171.0] 140.0 [130.0; 145.0] 85.0 [80.0; 91.0]
Low mesenteric vein - left colonic vein - vein of sigmoid bowel - upper rectal vein	108.5 [104.0; 111.5] 40.0 [33.5; 49.5] 50.0 [27.0; 53.5] 30.0 [20.0; 50.0]	4.5 [2.0; 6.5] 3.5 [2.0; 4.5] 3.0 [2.0; 3.5] 3.0 [2.0; 4.0]	140.0 [135.0; 151.0] 175.0 [170.0; 179.0] 165.0 [160.0; 170.0] 160.0 [155.0; 165.0]
Splenic vein - left gastroepiploic vein - short gaster veins (n=6-12)	125.0 [97.5; 129.5] 20.0 [13.5; 29.5] 12.0 [7.0; 18.5]	7.5 [5.5; 8.5] 5.0 [4.0; 6.0] 4.0 [3.0; 4.5]	100.0 [95.0; 111.0] 130.0 [120.0; 135.0] 90.0 [90.0; 95.0]

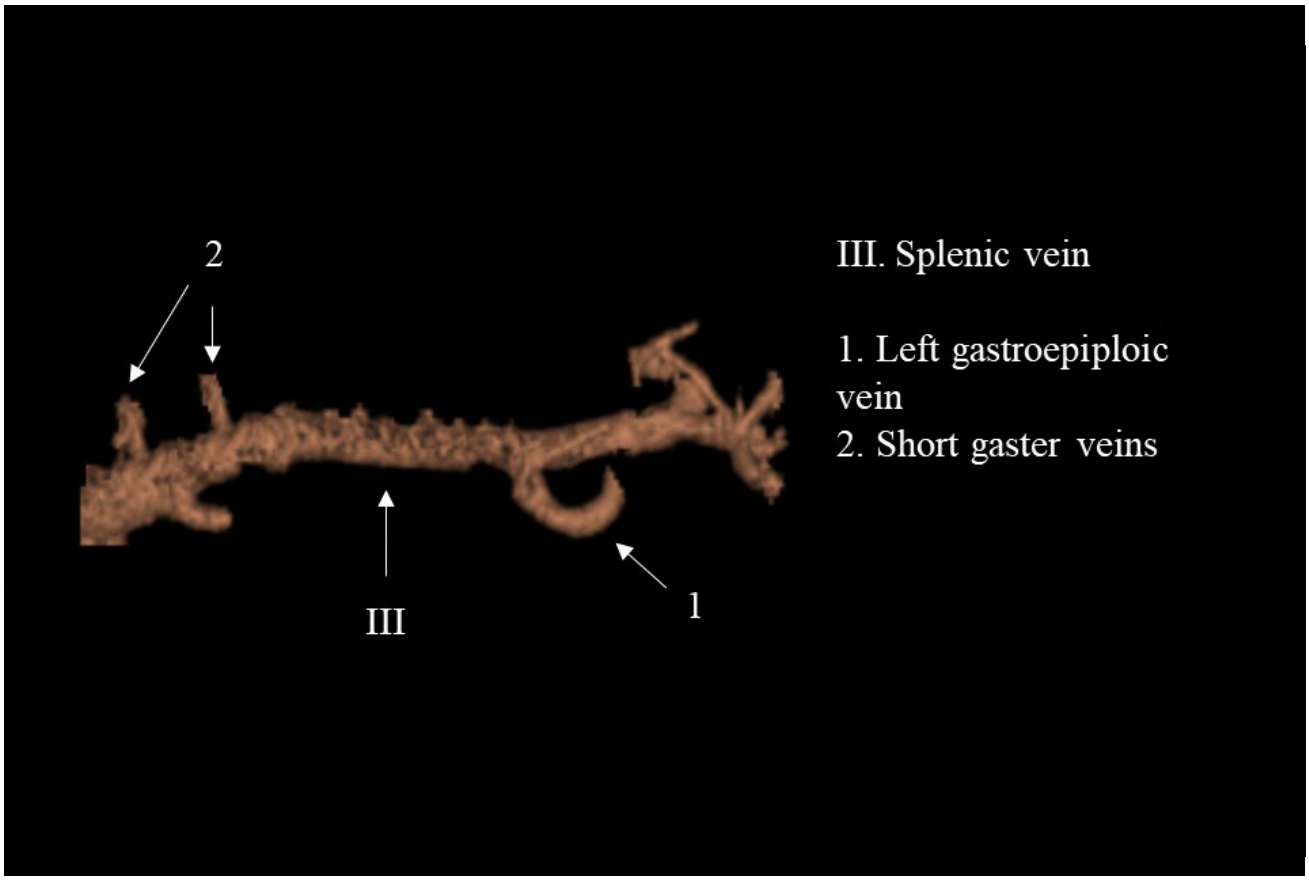

Fig. 4.- 3D model of human splenic vein.

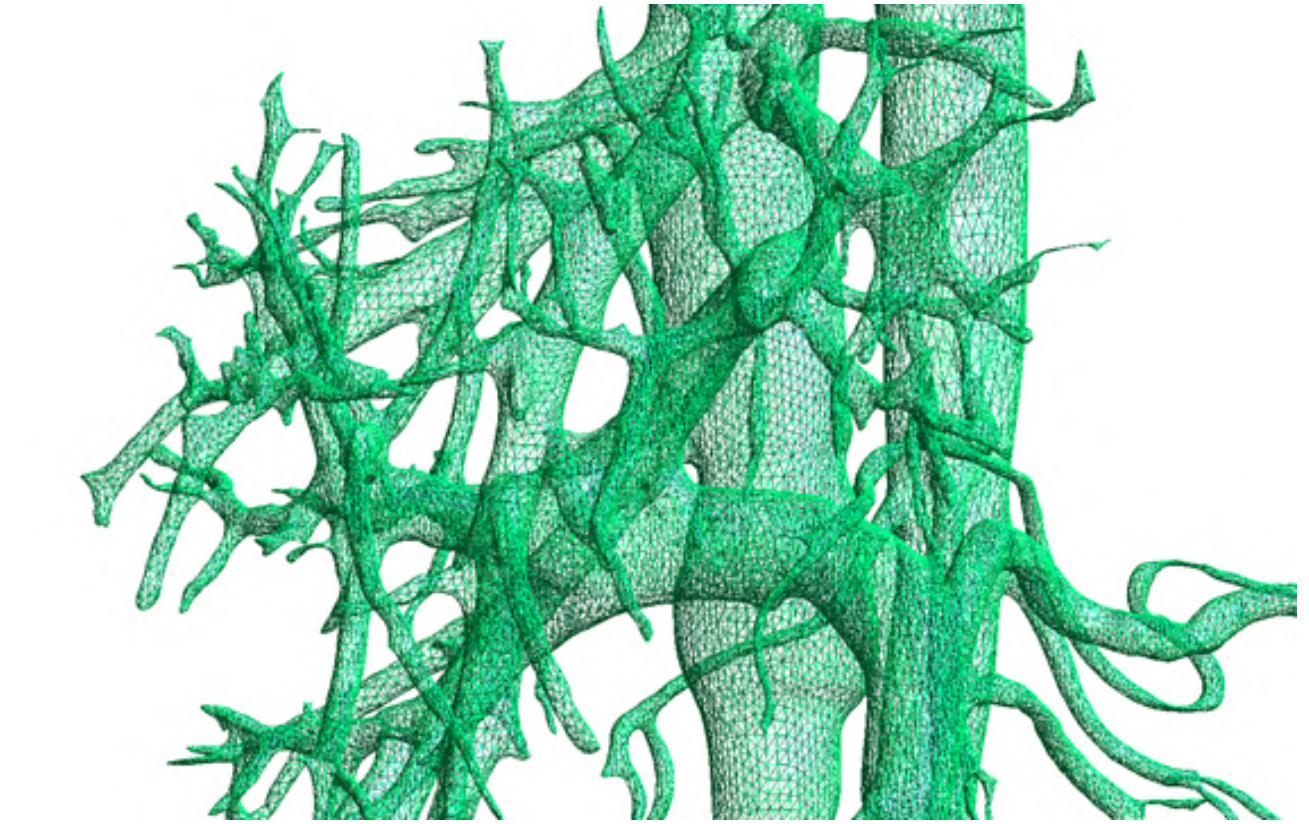

Fig. 5.- 3-dimensional model of portal system (mesh model).

DISCUSSION

The current research gives quantitative orienting points for main vein structures of portal vein system. The research results have allowed adding science materials about types of branching and morphological patterns of the portal vein and its branching. The results of the current research reflecting morphometric characteristics of superior, inferior mesenteric vein and splenic vein prove the variability of veins system v. portae, wide range of its structure anatomy, and can be used for solving questions of surgery interference for abdominal organs. Variations common for every system are preferably being used for regulation of the discussed subject in terms of tactic patients' curing with syndrome of portal hypertension or at the step of pre surgical preparation.

REFERENCES

AKAGI M, NAKAMURA YU, HIGAKI T, NARITA K, HONDA YU, ZHOU J, YU Z, AKINO N, AWAI K (2019) Deep learning reconstruction improves image quality of abdominal ultra-high-resolution CT. *Eur Radiol*, 29(11): 6163-6171.

CARNEIRO C, BRITO JO, BILREIRO C, BARROS M, BAHIA C, SANTIAGO I, CASEIRO-ALVES F (2019) All about portal vein: a pictorial display to anatomy, variants and physiopathology. *Insights into Imaging*, 10(1): 1-18.

CHELUVASHETTY SB, RACHAPALLI V Unusual (2017) Branching pattern of the portal vein: its importance. *J Clin Diagn Res*, 11(8): TD01-TD02.

COVEY AM, BRODY LA, GETRAJDMAN GI, SOFOCLEOUS CT, BROWN KT (2004) Incidence, patterns, and clinical relevance of variant portal vein anatomy. *Am J Roentgenol*, 183: 1055-1064.

DURAND CAL, RÁZURI CB, VALDERRAMA MW, ARREDONDO GM, RAMOS DS (2020) The Human Liver: Vascular Anatomy to Determine its Segments and Divisions. *Int J Morphol*, 38(1): 226-229.

GADZIJEV, ELDAR M (1996) Atlas of applied internal liver anatomy. Foreword by Stig Bengmark. Springer, Wien, New York, pp 204.

GAYVORONSKIY IV, KOTIV BN, KOVALENKO NA, LAZARENKO VA (2018) Variant anatomy of magistral vessels of portal vein system and its applied significance. *Kursk scientific and practical bulletin "Man and his health"*, 2: 70-75.

GHESU F-C, GEORGESCU B, ZHENG YE, GRBIC S, MAIER A, HORNEGGER JO, COMANICIU D (2019) Multi-scale deep reinforcement learning for real-time 3D-landmark detection in CT scans. *IEEE Trans Pattern Anal Mach Intell*, 41(1): 176-189.

GIBSON E, GIGANTI F, HU YI, BONMATI E, BANDULA S, GURUSAMY K, DAVIDSON B, PEREIRA SP, CLARKSON MJ, BARRATT DC (2018) Automatic multi-organ segmentation on abdominal CT with dense V-networks. *IEEE Trans Pattern Anal Mach Intell*, 37(8): 1822-1834.

GUERRA A, DE GAETANO AM, INFANTE A, MELE C, MARINI MG, RINNINELLA E, INCHINGOLO R, BONOMO L (2017) Imaging assessment of portal venous system: pictorial essay of normal anatomy, anatomic variants and congenital anomalies. *Eur Rev Med Pharmacol Sci*, 21(20): 4477-4486.

IQBAL S, IQBAL R, IQBAL F (2017) Surgical implications of portal vein variations and liver segmentations: a recent update. *J Clin Diagn Res*, 11(2): AE1-AE5.

KARUNAKARAVEL K (2016) Utility of cone-beam computed tomography in the assessment of the porto-spleno-mesenteric venous system. *Cardiovasc Diagn Therapy*, 6(6): 544-556.

KHAMANARONG K, WORAPUTTAPORN W, AMARTTAYAKONG P, AHOOJA A, KHUNTIKEO N (2016) Classification of portal vein tributaries in Thai cadavers including a new type V. *Surg Radiol Anat*, 38(6): 735-739.

KOLESNIKOV LL (2003) International anatomical terminology. Moscow: Medicine, p 424 (in Russian).

KOLSANOV AV, ZEL'TER PM, MANUKYAN AA, CHAPLYGIN SS, IVANOVA VD (2017) Studying the anatomy of the portal vein using the preoperative planning system. *Operative Surg Clin Anat*, 2: 3-6.

KOVALENKO NA, GAIVORONSKIY IV, KOTIV BN, TYAGUN VS, NOVITSKAYA NY (2018) Variant anatomy of portal vein and its applied significance in surgery. *Surgery*, 19(14): 182-208.

LANG H, DE SANTIBAÑES E, SCHLITT HJ, MALAGÓ M, VAN GULIK T, MACHADO MA, JOVINE E, HEINRICH S, ETTORRE GM, CHAN A, HERNANDEZ-ALEJANDRO R, CAMPOS RR, SANDSTRÖM P, LINECKER M, CLAVIEN P-A (2019) 10th Anniversary of ALPPS-Lessons learned and quo Vadis. *Ann Surg*, 269(1): 114-119.

NAKAMURA T, TANAKA K, KIUCHI T, KASAHARA M, OIKE F, UEDA M, KAIHARA S, EGAWA H, OZDEN I, KOBAYASHI N, UEMOTO S (2002) Anatomical variations and surgical strategies in right lobe living donor liver transplantation: lessons from 120 cases. *Transplantation*, 73(12): 1896-1903.

RUSSKIKH AN, SHABOKHA AD (2019) The method of x-ray examination of morphometric parameters of the vessels of the portocaval system of the rectum of male corpses. *Byulleten' sibirskoy meditsiny - Bulletin of Siberian Medicine*, 18 (2): 146-156 (in Russian).

RUSSKIKH AN, SHABOKHA AD, GORBUNOV NS, DEREVTSOVA SN (2013) Features of the local constitution in the structure of the veins of the human rectum. *Vestnik novykh meditsinskikh tekhnologiy - Bulletin of new Medical Technologies*, 2: 53-57.

SAKAMOTO YO, KOKUDO N, KAWAGUCHI YO, AKITA K (2017) Clinical Anatomy of the Liver: Review of the 19th Meeting of the Japanese Research Society of Clinical Anatomy. *Liver Cancer*, 6(2): 146-160.

SCHMIDT S, DEMARTINES N, SOLER L, SCHNYDER P, DENYS A (2008) Portal vein normal anatomy and variants: Implication for liver surgery and portal vein embolization. *Semin Intervent Radiol*, 25: 86-91.

SHARMA V, CHAUHAN RS, SOOD RG, MAKHAIK S, NEGI K, CHAWLA K, DIWAN Y, PARTAP A, RANA S, GUPTA A (2017) Study of the normal anatomy and variations of portal vein in North Indian population: a MDCT study. *Eur J Anat*, 21(1): 13-18.

SHEVKUNENKO VN (1949) Atlas of peripheral nervous and venous systems. Moscow: MEDGIZ, pp 345 (in Russian).

SILANT'EVA NK (2009) The importance of computed tomography in the study of x-ray anatomy of the pelvis after combined treatment of patients with rectal cancer. *Sibirskiy onkologicheskiy zhurnal - Siberian Oncology Journal*, 5: 17-23 (in Russian).

SINGH HR, RYMBAI ML, JOHN R, EAPEN A, RABI S (2019) Branching pattern of the portal vein in Indian population. *Eur J Anat*, 23(6): 425-433.

The neuroglia of the rat optic nerve. Part I. Golgi-Hortega and Golgi-EM studies

Pedro Mestres-Ventura[1], Gilberto del Rosario Hernández[2]

[1] Department of Anatomy and Cell Biology, Faculty of Medicine, Saarland University, 66421 Homburg Saar (Germany)
[2] Laboratory of Electron Microscopy, Centre for Technical Support (CAT), University Rey Juan Carlos, 28933 Mostoles, Madrid (Spain)

SUMMARY

In the present study, one describes the morphology of the macroglia (astrocytes and oligodendrocytes) of the optic nerve of the albino rat, having been stained according to the modification of del Rio-Hortega of Golgi-Kopsch's method. This cytology has been studied in the intra-orbital optic nerve, in the intracranial portion of the same, in the optic chiasm and in a first segment of the optic tract.

Astrocytes show small differences between those located in the marginal zone of the nerve and those located in the center, being all of them classified as belonging to the fibrous type of astrocytes. With their extensions, these cells establish contact with the external limiting membrane, blood vessels and myelinic nerve fibers. On the level of the limiting membrane, their terminal feet form a kind of cellular barrier similar to that of the cerebral cortex in contact with the pia mater. With the nervous fibers, they establish close relationships at Ranvier's nodes level, being arranged around them forming small rings.

The oligodendrocytes show their main branches impregnated up to where they reach the myelin sheath, but the protoplasmic compartment of this one is not impregnated, giving a different image to the one seen after microinjections with markers.

Morphometric studies using fractal dimension and related parameters are presented next in part II of this work.

Keywords: Optic nerve – Astrocytes – Neuroglia – Golgi-method – Golgi-EM

INTRODUCTION

The main virtue of the method described by Golgi (1873) is to reveal the complete shape, the silhouette, of nerve and glia cells of the central nervous system. The number of cells that may be impregnated according the "*reazzione nera*" is very small, around 5% of them, which, far from being a disadvantage, allows the visualization of the cells stained in their entirety without important superposition of cellular structures.

The performance of this method has been improved by the introduction of numerous variants and modifications, of which the Cajal ones should be highlighted, which made it much more productive and ultimately reliable (Cajal and de Castro, 1933; Valverde, 1965).

Corresponding author:
Pedro Mestres-Ventura, PhD, MD, Prof. Emeritus. Department of Anatomy and Cell Biology, Bld. 61, Faculty of Medicine, Saarland University, D-66421 Homburg Saar, Germany. Phone: +34 644217127. E-Mail: pedro.mestres@uks.eu

Submitted: December 20, 2021. **Accepted:** January 7, 2022

https://doi.org/10.52083/BIBN7983

However, impregnation of neuroglia cells with the Golgi method is somewhat more difficult, and that is the reason why variants have been devised in which different chemical components have been introduced, such as mercury salts (Cox, 1891), formalin (Kopsch, 1896), and, in more recent times, glutaraldehyde (Colonnier, 1964; Braitenberg et al., 1967).

Regarding neuroglia, undoubtedly an effective modification of the Golgi method was described by del Rio Hortega (1928) and collected in the methods book of Cajal and de Castro (1933), a variation in which, together with the potassium chromium salt and formaldehyde, the chloral hydrate interacts with the tissue, being the technique used by us in this study.

In order to analyze the relationships of the astrocyte prolongations with the neighboring nerve fibers, as well as with the superficial limiting membrane of the nerve, the one which is in contact with the meninges involving the optic nerve, the gold-toning technique for electron microscopy was applied to selected sections stained according the Golgi-Hortega method, an approach not used till now for neuroglia cells (Fairen et al.,1977; Mestres and Schneider, 1997).

In a second part of this paper, the cell shape of the astrocytes of the optic nerve has been investigated, determining their fractal characteristics and related parameters.

MATERIAL AND METHODS

Golgi method. Light microscopy

In the 1980s, series of rat brains treated according to the Golgi-Cajal method (Valverde, 1965), as well as the Cox method (1891) and Hortega's modification of Kopsch's method (1828), were prepared in our laboratory in Homburg Saar and stored in our institute archive, which has been consulted for the present investigation.

The mentioned collections were prepared along several years (1984-1989) using approximately 150 adult Sprague-Dawley rats (200-230 g BW) of both sexes, which were sacrificed by decapitation with the aim to avoid the use of anesthetic agents (with permission of the Animal Welfare Commission of Saarland).

The brain was removed very quickly and, after washing in a buffered saline solution, they were segmented by cutting them in horizontal and coronal directions (slabs of 3-4 mm. thick) and immersed in the Rio-Hortega's solution (dichromate potassium 3 g, chloral hydrate 3 g, 10% formaldehyde 50 ml).

The solution became intensely cloudy within a few hours, so it was replaced by a fresh solution every 10-12 hours, working in total for about 60 hours at room temperature and protected from light. The tissue specimens were placed in a vessel with a porous porcelain basket hanging to prevent the tissue to come in contact with the precipitates of the Golgi-Hortega solution, which accumulated at the bottom of the vessel (Romeis, 1968). At the end of this step, the hardened pieces were washed in a 1.5% aqueous solution of silver nitrate, giving time to the solution to act on the surface of the tissue blocks, where soon silver chromate crystals appeared that were partly removed by brushing the surface gently. The tissue blocks were then transferred to a 1.5% silver nitrate aqueous solution, changing it every 24 hours and working for a total time of 3 days.

After impregnation, the blocks were embedded in celloidin following the protocol described by Ramon-Moliner (1970), and sectioned with a thickness of 50 to 70 microns in a sliding microtome (Jung, Heidelberg). The histological sections were dehydrated in an ascending series of alcohols, passed through xylol or toluol, and mounted on slides covered with Eukitt (Sigma-Aldrich) and a very thin coverslip, and examined and photographed in a light-microscope Vanox (Olympus).

The Golgi-Hortega protocol rendered surprising good results in the optic nerve, optic chiasma and optic tract, obtaining impregnations of astrocytes both in the periphery and in the central nerve area, as well as of the oligodendroglia cells (preliminary communication by Mestres, 1988).

Electron Microscopy - Golgi-EM method

Sections of rat brain and optic nerve stained according to the del Rio-Hortega method were

selected for further processing in electron microscopy. For this purpose, the gold-toning procedure was applied, which allows a considerable reduction in size of the silver chromate crystals, greatly facilitating a good ultra-structural examination of the sample (Fairén et al., 1977; Mestres and Schneider, 1997). After submitting the sections to gold-toning, they were post-fixed with osmium and dehydrated in an ascending series of alcohols, transferred anhydrous acetone or propylene oxide (Sigma-Aldrich) and infiltrated into Epon (Polyscience) and polymerized at 60ºC for 48 hours. Ultrathin sections of approximately 80 nm thick were obtained with a diamond knife (Diatome) on an ultramicrotome Leica-Ultracut S. The thin sections were stained with uranyl acetate and lead citrate, and examined and documented under a transmission electron microscope Zeiss EM CR.

RESULTS

In the three locations studied, intra-orbital optic nerve, optic chiasm and optic tract, a remarkable number of impregnated neuroglia cells was found. The range of impregnated cells observed was approximately 8% of the cells existing in each location (Cavalloti et al., 2000). These estimates were made taking as reference the average number of cell nuclei (234± 8) counted in cross sections of rat optic nerve with H&E stained (not shown).

Astrocytes

In the intra-orbital optic nerve, astrocytes in two different locations can be distinguished, some located in the marginal zone of the nerve close to the meningeal envelop, and others located in the central part of the nerve.

Marginal located astrocytes show processes that radiate towards the meningeal sheath, having others that go inwards and insinuate themselves between the nerve fibers of this nerve. In general, the prolongations of these so-called marginal astrocytes are quite robust and run in a transversal plane of the nerve, but some others are longitudinally oriented (Figs. 1, 2).

The central astrocytes give the impression that they have many more extensions, but these, unlike those of the marginal ones, are thinner and more delicate and in some cases are exhausted before they reach the surface of the nerve, however, many of them reach the limiting membrane (Figs. 1, 3). Relevant to typify the cell type is the fact that the processes and ramifications of these cells have a smooth surface, which allows us to classify them as fibrous astrocytes.

In the intracranial itinerary of the optic nerve, astrocytes maintain these morphological characteristics (Figs. 1, 2). In the chiasm and optic tract, the astrocytes become adapted to the cracks and slots between the nerve fiber bundles, and giving the impression that the extensions are arranged in planes determined by the nerve fascicles (Fig. 1).

For ultrastructural observations, the Golgi-EM method was used revealing the cell nucleus and the cytoplasm of the impregnated astrocytes, which present a thin layer of metallic deposits just below the plasma membrane. The cell nucleus shows a homogeneous distributed chromatin with only few condensations. The nuclear membrane is perfectly perceptible and, in the cytoplasm, there are few organelles, as well as gliofibril-bundles (Fig. 2). These structures, corresponding to the system of intermediary filaments, i.e., the cytoskeleton, were evident in the astrocytes of the marginal zone, particularly at the end foots of those glial processes in contact with the limiting membrane (Fig. 5).

Relationships between astrocytes and nerve fibers

In longitudinal sections of the optic nerve, it can be seen how longitudinal processes of the astrocytes appeared arranged following a parallel course closely associated with the nerve fibers. In the transverse sections, these longitudinal running processes can be seen as black points scattered between the nerve fibers (Fig. 3).

One thing that caught our attention was the presence of small incomplete rings that are part of these longitudinal cell processes and that are well to see in cross sections of the nerve. They seem to surround some fine cylindrical structure whose diameter correspond to that of the optic nerve axons, i.e., without myelin sheath, as is the case in the Ranvier nodes (Fig. 3). Although these

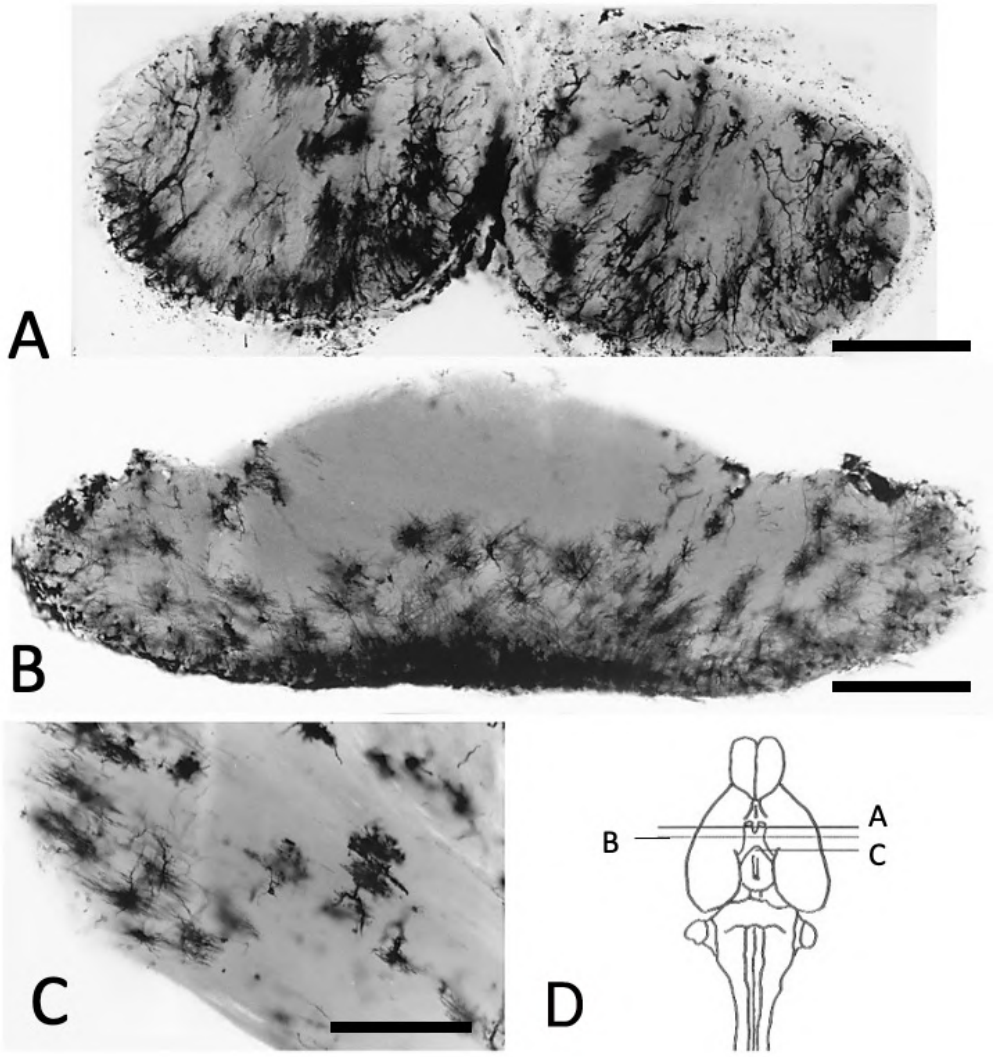

Fig. 1.- Cross sections of the optical paths at different levels (see diagram). **A)** both optical nerves shortly before forming the optic chiasm. Intensely stained astrocytes can be seen both in the margins and in the central part of the nerve (arrows). Bar= 100 µm. **B)** Cross section of the chiasm. Glial cells appear stained in the ventral part and lateral margins. Astrocytes are seen with great profusion of extensions (arrows). Bar= 100 µm. **C)** Cut through the optical tract. In the marginal zone astrocytes show great abundance of prolongations that insinuate along the nerve fiber fascicles (arrow). Bar= 100 µm. **D)** Diagram indicating the location of images A, B and C. At all path level's astrocytes stand out in black, with more impregnated cells in the periphery of the nerve, while in the tract the impregnation is more even.

rings are more frequently found associated to central astrocytes, the marginal astrocytes also have them in their prolongations.

These rings have been examined with Golgi-EM, and it has been confirmed that they are indeed extensions of astrocytes, and they coil around the axon at the Ranvier node level, establishing direct contact between astrocyte and axon membranes (Fig. 4). This description is valid for all the rings examined.

The astrocytes and their relationship with the limiting membrane

In the marginal zone, astrocytes project a good part of their radial running processes to the external limiting membrane, a basement membrane between pia mater and glial cells, where they end up forming terminal feet (Fig. 5).

In these processes, and just before the terminal foot, these processes have several small protuberances that inter-digitate with those of the neighboring astrocytic processes (Fig. 5A, insert). These protuberances appear interlaced in a close and compact way, which suggests a kind of cellular barrier attached to the external limiting membrane.

With the electron microscope, in these robust astrocytic extensions abundant gliofibrils were observed (Fig. 5).

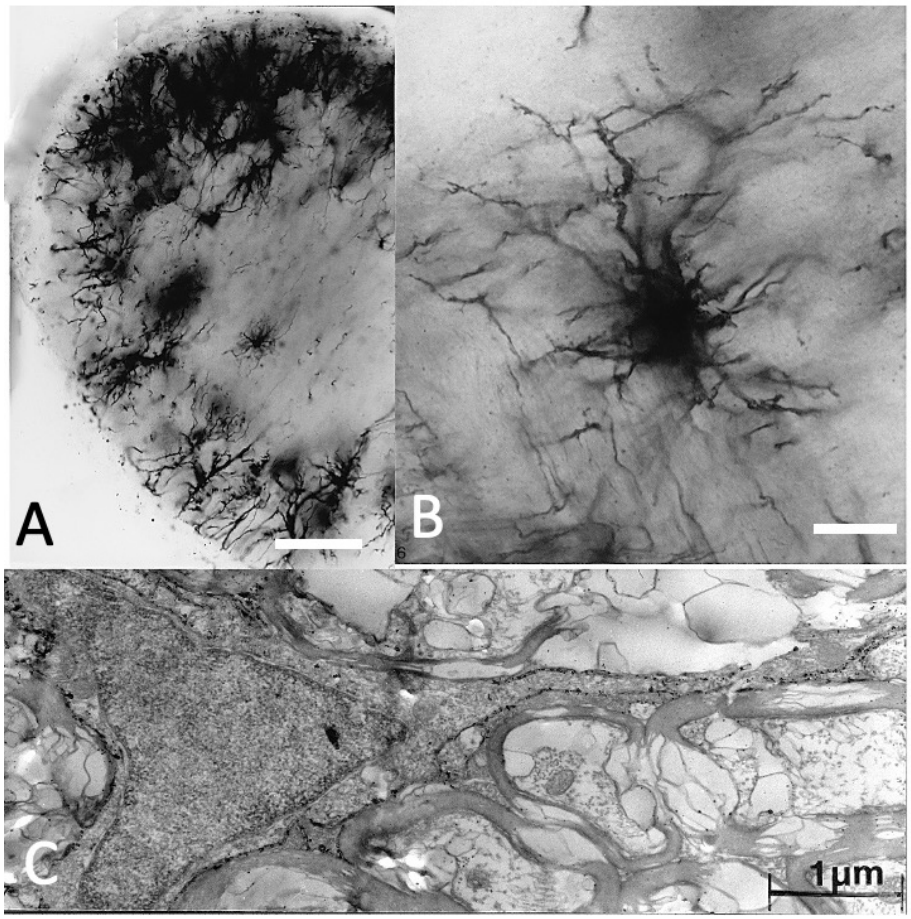

Fig. 2.- A) Cross section showing astrocytes in the marginal zone and in the center of the nerve. Bar= 100 µm. **B)** Astrocyte located in the center of the nerve with abundant ramifications of different orders. Bar= 10 µm. **C)** Golgi-EM gold-toning method. Note the fine deposit of metallic particles immediately below the plasma membrane. The cell nucleus (N) presents a homogeneous chromatin distribution, with soft condensations associated to the nuclear membrane.

Between the small protuberances of the glial processes, numerous gap junctions and direct apposition of cell membranes exist (Fig. 5).

Oligodendrocytes

These cells, following the Golgi procedure modified by the Rio-Hortega, appear very well stained and show a typical shape already described by this author (Rio-Hortega, 1928) with few processes, at least if compared to astrocytes, a fact that justifies its name.

In our samples, they appear sometimes isolated or one found many of them in relatively small areas. They were most frequently found in the intracranial portion of the optic nerve, in the chiasm itself, as well as some in the optical tract.

The soma of these cells is spherical or slightly oblong in shape, from which three or more main processes emerge, emitting several thinner branches that in the vicinity of the myelin sheaths of the nerve fibers can no longer be followed, as they are not impregnated, so that the relationship of oligodendrocytes with myelinated fibers of the optic nerve cannot be shown with Hortega's method (Fig. 6). Unlike astrocytes, in oligodendrocytes the soma impregnation is such that it allows to distinguish the cell nucleus as a clear or translucent field into the cell (Fig. 6).

The main processes are rather thin, and run on a plane more or less transversal to that of the nerve fibers, and as already mentioned, the secondary processes are unstained and practically undetectable close to the myelin sheath. In the most external part of the myelin sheath to which the cellular process is associated, there is still a certain amount of cytoplasm, so that the cell membrane there could be detected in thin sections with a TEM. However, such structural

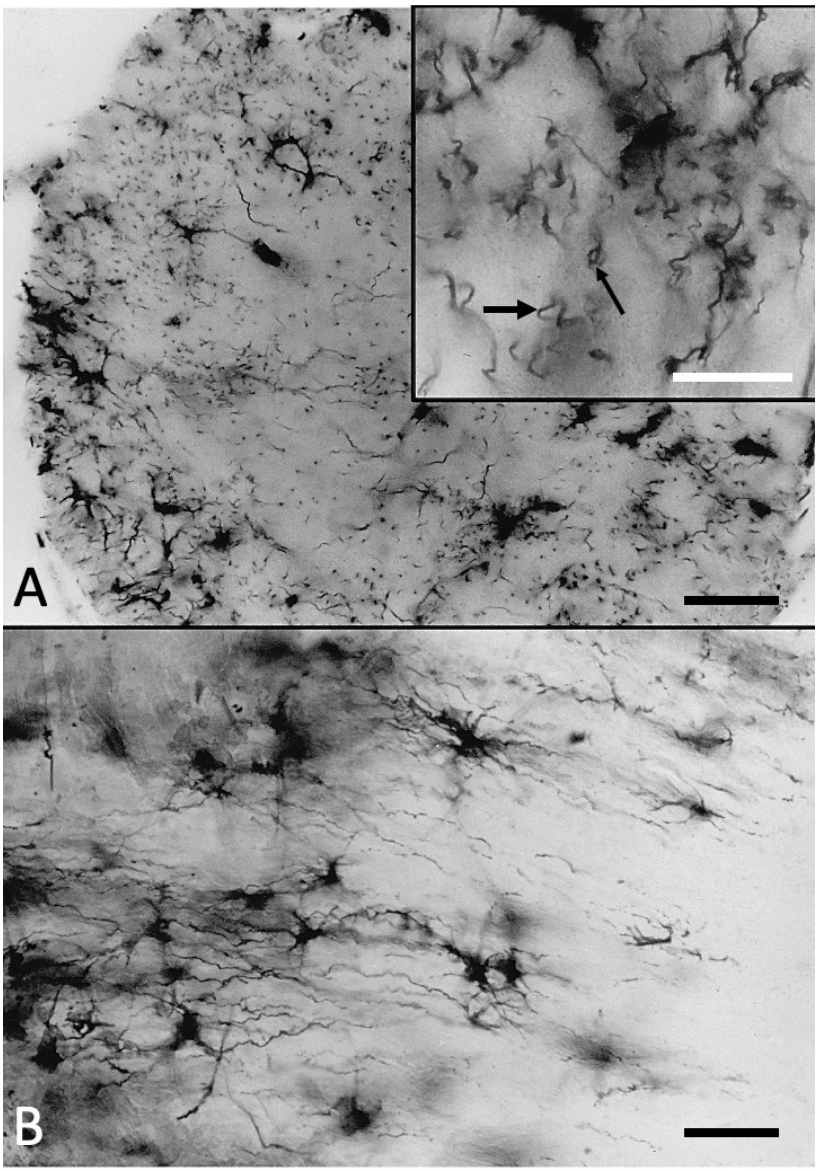

Fig. 3.- Cross section **(A)** and longitudinal section **(B)** of the optic nerve. In A there are abundant black points corresponding to transversely cut astrocyte processes. Bar = 50 µm. In the insert of A, small complete and incomplete ring formations can be distinguished from the astrocyte extensions (arrows). Bar= 20 µm. In B we can see processes of astrocytes oriented longitudinally and with a parallel course to the optic nerve fibers. Bar= 50 µm.

details could not be visualized in impregnated material.

In our specimens we have not observed specific relationships of the oligodendrocytes with the vessels, also not with the external limiting lamina of the optic nerve.

DISCUSSION

In the first decades of the past century, probably the first author who has shown images of the astrocytes of the optic nerve in its intracranial portion has been Ramon y Cajal, in the context of his retina investigations (1909). More recently, images of astrocytes of the optic nerve have been published, but applying variants of the Golgi method different from ours (Miller et al., 1989; Reichenbach et al, 1992). With the variant of the Golgi method described by Rio-Hortega (1928), high quality impregnations of the macroglia cells of the albino rat optic nerve have been achieved, showing the preparations a very clean background and without contaminating precipitates (Mestres, 1988).

The astrocytes described in the present study exhibit a morphology known of classical fibrous astrocytes, cells existent in all locations of the white matter of the central nervous system (Montgomery, 1994; Lundgaard et al. 2014; Li et al., 2016). The distinction made here between central and marginal astrocytes is simply a

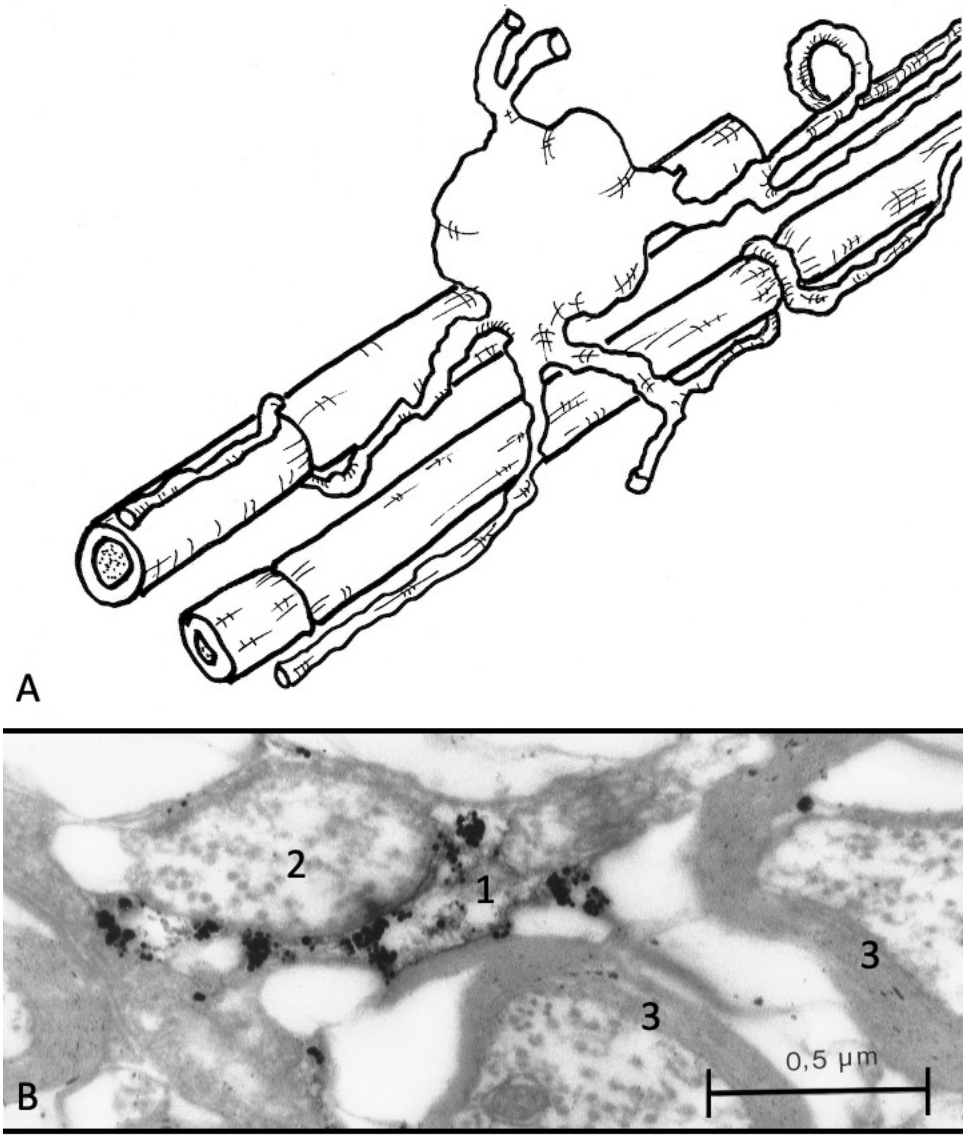

Fig. 4.- A) Diagram showing the relationship between the ring formations and the Ranvier nodes of the optic nerve fibers. **B)** Golgi-EM with gold toning of an astrocyte process (1) in contact with the axon in the Ranvier node (2). Note the lack of myelin sheath at that level and compare with (3).

subterfuge for the presentation of our results in a understandable manner, but it should be noted that the morphological differences between one and the other are really slight if at all, and may merely reflect the spatial adaptation of the cells to anatomical features of the area.

A technique that has made possible to obtain completely labeled astrocytes in the optic nerve is the intracellular micro-injection of markers such as HRP or fluorescents such as Lucifer Yellow (Butt et al., 1994). For example, HRP labeling produces images with high contrast, and in them the cell processes can be distinguished accurately without overlapping with those of the neighboring cells, and the overhang of the processes can be appreciated in their entirety (Butt and Ransom, 1989). Such a situation also occurs in the Golgi preparations, although less frequently and in principle without being able to directly influence the result, unless the protocol of the method is fortunately modified.

In our preparations we have found astrocytes, whose processes establish contact with blood vessels, are approaching to the fibers of the optic nerve and with their terminal feet contact the subpial basement membrane, which separates the parenchyma of the nerve from the pial sheath that surrounds it. This description agrees with those based on HRP microinjections and also with fluorescent tracers, techniques with which the

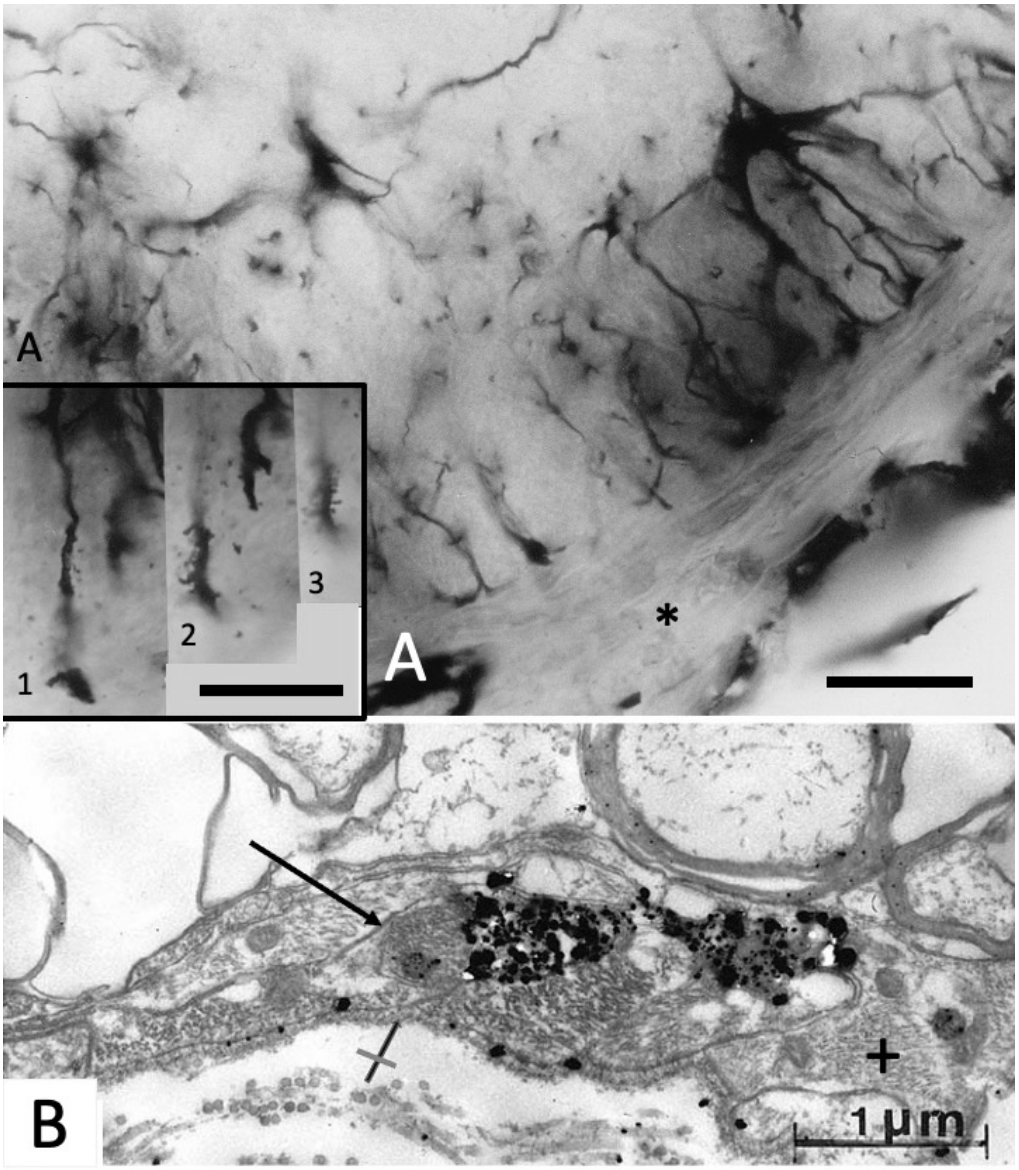

Fig. 5.- Marginal zone of the optic nerve. **A)** Astrocytes with feet in contact with the limiting membrane and the meningeal envelope (*). Bar= 40 µm. Insert: Three focusing planes (1, 2, 3) of an astrocyte end foot showing fine spines or protrusions that articulate with neighboring similar formations. Bar= 20 µm. **B)** Feet of astrocytes in contact with the limiting membrane (cross arrow) with gliofilaments (+) and gap junctions between them (arrow). Collagen from the meningeal layers is visible at the bottom.

known uncertainty in terms of results of the Golgi method can be faced with great advantage (Butt and Ransom, 1989, 1993).

Studies by Butt's group state that astrocytes from any location within the nerve establish the contacts mentioned above, but do not confirm the differences in the contact patterns proposed by other authors, who postulate the existence of two different types of astrocytes in the optic nerve, which would be distinguished by their relationship with other structures such as blood vessels and pial surface, a hypothesis that in view of the results of other authors and of our own does not seem sustainable at all (Miller et al., 1989; Butt et al., 1994).

On the other hand, the optic nerve is nothing more than a special compartment of the white matter of the brain, in which there are only astrocytes of the fibrous type and oligodendrocytes, later forming the myelin sheaths around the corresponding axons (Peters et al., 1976). However, studies with specific antibodies such as A2B5, which binds to surface markers such as certain gangliosides, have revealed the existence of astrocytes with positive marking and others that are negative (Raff, 1989). Based mostly on immunocytochemical studies with A2B5 and investigations on the cell linage, the existence of two different astrocytes, type- 1, related with the classical protoplasmic astrocyte, and type-2 related with the

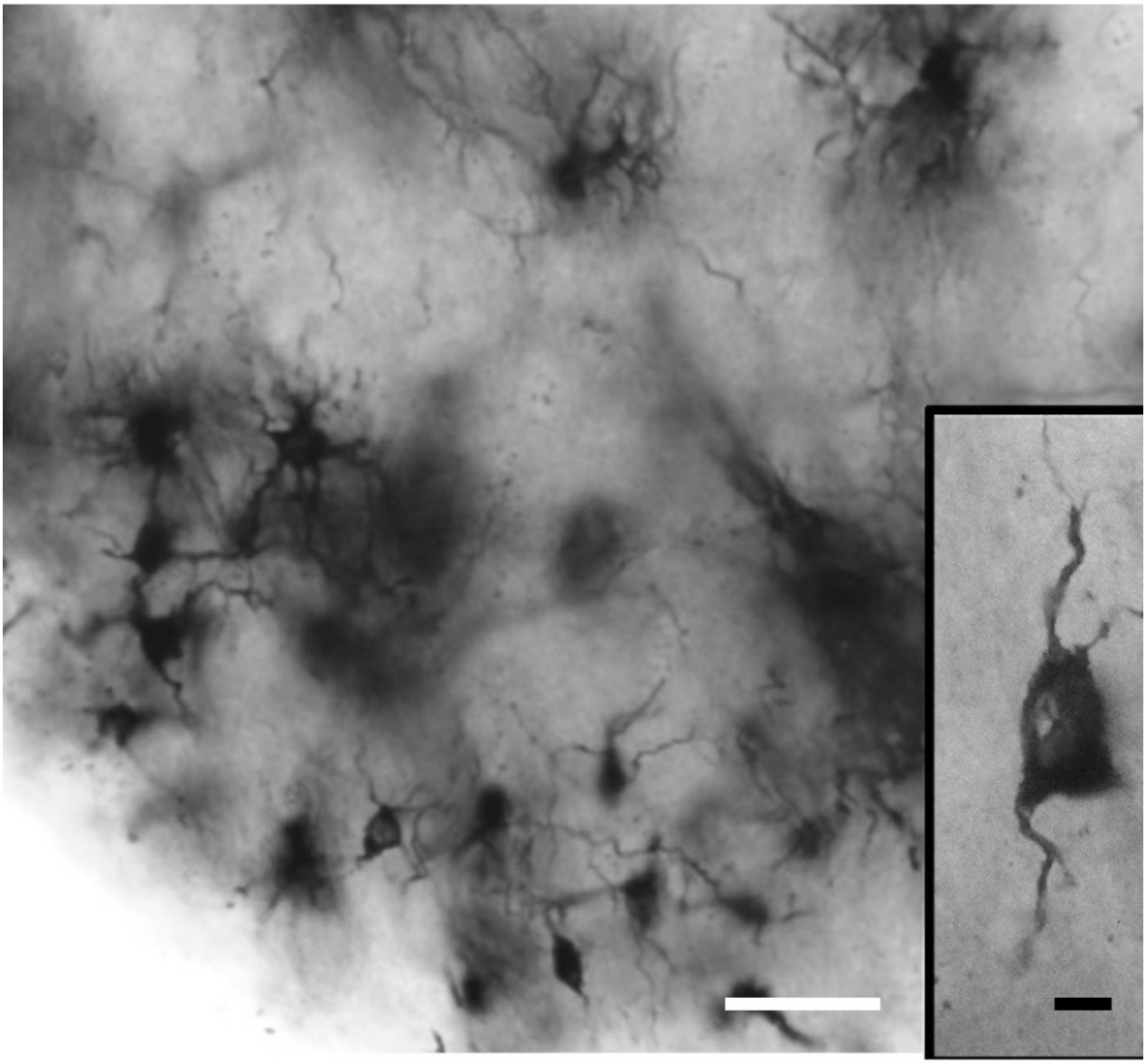

Fig. 6.- Field of the optic nerve showing astrocytes (upper part) and oligodendrocytes (lower part). Bar= 50 µm. Insert: Detail of an oligodendrocyte. Bar= 20 µm.

classical fibrous astrocyte, in the optic nerve has been postulated, which, without a doubt, would be a very unique fact, considering the general cell composition of the white matter (Scolding et al., 1999). On the one hand, the A2B5 antibody binds to gangliosides that are expressed in glial precursor cells and also in various cancers, and in some cases the expression is transient, particularly under in vitro conditions and at certain moments of development (Haas et al., 2012). At this point, the question of the reliability of this labeling seems at least justified. As has already been said, a histological classification of the astrocytes of the optic nerve in terms of anatomical relationship, at has been postulated by others, does not seem to hold up in light of Golgi studies, and especially of investigations with the tracer microinjections technique (Butt and Ransom, 1989, 1993).

Certainly, the astrocytes located near the surface of the nerve present well visible radial extensions that end in the subpial basement membrane; but also the astrocytes located more deeply within the nerve present such contacts, which agrees with what has been observed in our preparations and by other authors (Butt and Ransom, 1989; Butt et al., 1994).

In the present study, it has been seen how astrocytes form a glial foot zone next to the subpial basement membrane, where such feet are closely intertwining and forming something

reminiscent of the outer glial zone of the cerebral cortex (Braak, 1975). Similar to the cortex, in the optic nerve the outer glial feet contains abundant intermediate filaments, 10 nm thick filaments surely GFAP positive (Sun et al., 2009), the glial end feet appearing interconnected by numerous gap junctions (Braak, 1975). In the optic nerve, there exist gap junctions between astrocytes, and also between astrocytes and oligodendrocytes, but not between oligodendrocytes (Orthmann-Murphy et al. 2008). Astrocytes located rather to the center of the nerve generally have thin and long processes, which end by means of glial feet on several anatomical structures, such vessels and pial surface.

Our description of the astrocytic processes and their relationship with Ranvier's nodes is in direct agreement with the previous investigations dealing with the optic nerve and the spinal cord (Hildebrand, 1971; Raine, 1984; Sims et al., 1985). The gold-toning technique (Fairén et al., 1974; Mestres and Schneider, 1997), applied for the first time to visualize in TEM glial cells of the optic nerve stained according with the del Rio-Hortega method, allows the observation of intracellular details of the astrocytes, as well as the relationship of their processes with the Ranvier node. These observations are in agreement with those obtained in transmission electron microscopy with or without combination with tracer techniques (Butt et al., 1994). What could be designated as a new observation fact are the rings that form the astrocyte processes around the Ranvier node, which in this way had not been visualized until now (see interpretation diagram in Fig. 5).

The oligodendrocytes have been also well impregnated applying the Golgi-Hortega method. In these cells, only the main processes have been stained, getting lost or finishing in the proximity to the myelin sheaths. However, studies with micro-injection techniques show in injected oligodendrocytes numerous extensions of longitudinal course and therefore parallel to the nerve fibers (Hildebrand, 1971; Butt and Ransom, 1989). It is likely that these tracers label compartments due to an intracellular diffusion of the same in the inner and outer cytoplasmic border of the myeline sheath after wrapping around the axon, hence their appearance as if they were processes of oligodendrocytes running alongside the myelinic sheaths, as if they were cellular extensions, which they are not in fact. The Golgi method fails to impregnate these cytoplasmic zones of the myelin sheath, and only the rather short portions of the oligodendrocyte processes connecting cell body and myelin sheath appear stained.

ACKNOWLEDGEMENTS

This work is dedicated to Dr. med. Karl Meller, Professor of Anatomy and Head of the Laboratory for Experimental Cytology at the Ruhr-Universität in Bochum (Germany) on the occasion of his 85th anniversary.

The authors indebted to Mrs. Ann Soether for linguistic revision of the manuscript. We thank Dr. Laura Lopez Gomez (Department of Human Histology and Pathology, University Rey Juan Carlos, Madrid, Spain) for her help in various matters related to this work.

Founding: This study has been generously supported by the University of Saarland (Germany) and the Technological Support Center, University of Rey Juan Carlos, Madrid.

REFERENCES

BRAAK E (1975) On the fine structure of the external glial layer in the isocortex of man. *Cell Tissue Res*, 157: 367-390.

BRAITENBERG V, GUGLIELMOTTI V, SADA E (1967) Correlation of crystal growth with the staining of the axons by the Golgi procedure. *Stain Technol*, 42: 277-283.

BUTT AM, COLQUHOUN K, TUTTON M, BERRY M (1994) Three-dimensional morphology of astrocytes and oligodendrocytes in the intact mouse optic nerve. *J Neurocytol,* 23: 469-485.

BUTT AM, RANSOM BR (1989) Visualization of oligodendrocytes and astrocytes in then intact rat optic nerve by intracellular injection of Lucifer yellow and horseradish peroxidase. *Glia*, 2: 470-475.

BUTT AM, RANSOM BR (1993) Morphology of astrocytes and oligodendrocytes during development in the intact rat optic nerve. *J Comp Neurol*, 338: 141-158.

CAVALLOTI D, CAVALLOTTI C. PESCOSOLIDO N, IANNETTI GD, PACELLA E (2001) A morphometric study of age changes in the rat optic nerve. *Ophthalmologica*, 215: 366-371.

COLONNIER M, GUILLERY RW (1964) Synaptic organization in the lateral geniculate nucleus of the monkey. *Z Zellforsch*, 62: 333-355.

COX WH (1891) Impregnation des Centralen Nervensystems mit Quecksilbersalzen. *Arch Mikr Anat*, 37: 16-22.

DEL RIO HORTEGA P (1928) Tercera aportación al conocimiento morfológico e interpretación funcional de la oligodendroglía. *Mem Real Soc Esp Hist Nat,* 14: 5-122.

FAIRÉN A, PETERS A, SALDANHA J (1977) A new procedure for examining Golgi impregnated neurons by light and electron microscopy. *J Neurocytol*, 6 (3): 311-337.

GOLGI C (1873) Sulla struttura de la sostanza grigia del cervello. *Gazetta Medica Italiana: Lombardia*, 33: 244-246.

HASS CH, NEUHUBER B, YAMAGAMI T, RAO M, FISCHER I (2012) Phenotypic analysis of astrocytes derived from glial restricted precursors and their impact on axon regeneration. *Exp Neurol*, 233(2): 712-732.

HILDEBRAND C (1971a) Ultrastructural and light-microscopic studies of the nodal region in parge myelinated fibers of the adult feline spinal cord white matter. *Acta Physiol Scand Suppl.* 364: 43-79.

HILDEBRAND C (1971b) Ultrastructural and light-microscopic studies of the developing feline spinal cord white matter. I. The nodes of Ranvier. *Acta Physiol Scand Suppl,* 364: 364-381.

KOPSCH F (1896) Erfahrungen über die Verwendung des Formaldehyds bei der Chromsilber-Imprägnation. *Anat Anz,* 11: 727-729.

LI J, I ZHANG L, CHU Y, NAMAKA M, DENG B, KONG J, BI X (2016) Astrocytes in oligodendrocyte linage development and white matter pathology. *Front Cell Neurosci,* 10: 119 (pp. 1-13).

LUNDGAARD I, OSÓRIO MJ, KRESS B, SANGGAARD S, NEDERGAARD M (2014) White matter astrocytes in health and disease. *Neuroscience*, 12: 161-173.

MESTRES P (1988) The neuroglial cells of the optic nerve. A morphological characterization with the Golgi-Method. In: Suppl. European Journal of Neuroscience. 11th annual ENA Meeting, Zurich 4-8 September.

MESTRES P, SCHNEIDER LF (1997) The Golgi-method for electron microscopy. An X-Ray microprobe study. *Eur J Anat*, 1: 53-65.

MILLER RH, FULTON BP, RAFF MC (1989) A novel type of glial cell associated with nodes of Ranvier in rat optic nerve. *Eur J Neurosci*, 1(2): 172-180.

MONTGOMERY DL (1994) Astrocytes: form, functions, and roles in disease. *Vet Pathol*, 31: 145-167.

ORTHMANN-MURPHY JL, ABRAMS ChK, SCHERER SS (2008) Gap junctions couple astrocytes and oligodendrocytes. *J Mol Neurosci*, 35(1): 101-116.

PETERS A, PALAY SL, WEBSTER HDF (1976) The Neuroglia Cells. In: Peters A, Palay SL, Webster HDF (eds). *The Fine Structure of the Nervous System: The Neurons and supporting Cells*. Saunders, Philadelphia.

RAFF MC (1989) Glial cell diversification in the rat optic nerve. *Science*, 243: 1450-1455.

RAINE CS (1984) On the association between perinodal astrocytic processes and the node of Ranvier in the C.N.S. *J Neurocytol*, 13: 21-27.

RAMON MOLINER E (1970) The Golgi-Cox Technique. In: Nauta WJH, Ebbesson SOE (eds). *Contemporary Research Methods in Neuroanatomy*. Springer Verlag Berlin, Heidelberg, New York.

RAMON y CAJAL S (1955) *Histologie du System Nerveux de l'Homme et des Vertebres.* Edition francaise traduit par L. Azoulay. Re-edited by Consejo Superior de Investigaciones Cientificas. Madrid. Vol. II, p 302.

REICHENBACH A, SIEGEL A, SENITZ D, SMITH JR TG (1992) A comparative fractal analysis of various mammalian astroglial cell types. *Neuroimage*, 1: 69-77.

ROMEIS B (1948) *Mikroskopische Technik*. R Oldenburg Verlag. München.

SCOLDING NJ, RAYNER PJ, COMPSTON DAS (1999) Identification of A2B5-positive putative oligodendrocytes progenitor cells and A2B5-positive astrocytes in adult human white matter. *Neuroscience*, 89(1): 1-4.

SIMS TJ, WAXMAN SG, BLACK JA, GILMORE SA (1985) Perinodal astrocytic processes at nodes of Ranvier in developing normal and glial deficient rat spinal cord. *Brain Res*, 337(2): 321-331.

SUN D, LYE-BARTHEL M, MASLAND RH, JAKOBS TC (2009) The morphology and spatial arrangement of astrocytes in the optic nerve head of the mouse. *J Comp Neurol,* 516(1): 1-19.

VALVERDE F (1965) *Studies on the Piriform Lobe*. Harvard University Press. Cambridge, Massachusetts. See pp 4-7.

The neuroglia of the optic nerve. Part II. Fractal morphometry of astrocytes

Gilberto del Rosario Hernández[1], Pedro Mestres Ventura[2]

[1] *Laboratory of Electron Microscopy, Centre for Technical Support (CAT), University Rey Juan Carlos, 28933 Mostoles, Madrid, Spain*
[2] *Department of Anatomy and Cell Biology, Faculty of Medicine, Saarland University, 66421 Homburg Saar, Germany*

SUMMARY

The astrocytes of the optic nerve form a network of cells around the nerve fibers and - in particular - establish contacts with the meningeal envelope of the nerve. The morphology of these cells has been analyzed by applying fractal methods (FracLac software) to camera lucida (two-dimensional) drawings of astrocytes, taking the following three parameters into consideration: fractal dimension (D_B), lacunarity (lambda) and density. These parameters provide information on the morphological complexity, heterogeneity and size of the cells respectively.

All three parameters demonstrate that differences exist between astrocytes located in the central region of the optic nerve and those in a marginal position. The former are larger than the latter, which are closely associated with the meningeal envelope of the nerve.

Our results suggest that peculiarities in the morphology of astrocytes are related to the anatomical region in which they are located, where they adapt to the gaps that remain between other neural elements, as is the case of the myelinated nerve fibers of the white matter. This theory is supported by the results of a study in which the morphology of the astrocytes of the corpus callosum were analyzed by applying the same fractal geometry methods.

Keywords: Optic nerve – Astrocytes – Fractal dimension – Lacunarity – Density

INTRODUCTION

The morphology of rat optic nerve astrocytes has been described in analogue microscopy in part I of this study (Mestres and del Rosario, 2022). This second part focuses on examination of these cells by applying fractal geometry analysis.

Fractal geometric analysis is a relatively new tool available to the microscopist interested in quantitatively measuring the dimensions of objects of irregular and complex shape, such as cells, which, as experience shows, are less accessible to analytical scrutiny, such as Euclidean geometry (Cross, 1994). The application of fractal geometric analysis requires digital imaging of the cells to be analyzed (Cross, 1994).

This approach has received much attention in the field of neuroscience. The shapes of neurons are both complex and highly variable (cell body, dendrites and axon), even within one and the same type of neuron, such as, for example, in the case of retinal ganglion cells. With fractal geometry, subtle differences can be defined

Corresponding author:
Pedro Mestres-Ventura, PhD, MD, Prof. Emeritus. Department of Anatomy and Cell Biology, Bld. 61 Faculty of Medicine, Saarland University, D-66421 Homburg Saar, Germany. Phone: +34 644217127. E-mail: pmestresv@gmail.com

Submitted: January 18, 2022. **Accepted:** January 27, 2022

https://doi.org/10.52083/URGQ2358

within that group of cells, for example with regard to activity or to functional and pathological reactions (Fernandez and Jelinek, 2001). Studies have been carried out on astroglial cells which display a variety of different shapes in the same species, depending on their anatomical location in the brain. However, morphological differences have also been detected when comparing astroglial types from a different animal species. Fractal geometry enabled the quantification of such differences (Reichenbach et al., 1992).

Another interesting case are the microglia cells, which constitute the autochthonous macrophage population of the central nervous system. Inherent to their nature as macrophages is the fact that they react quickly to external attacks (infections, wounds...) or internal ones (necrosis of the nervous tissue, degeneration, inflammations, etc.), with considerable changes in shape. The application of methods based on fractal geometry has made it possible to document the changes and responses of these cells in a precise and elegant way (Karperien et al., 2013; Young and Morrison, 2018).

As already noted in Part I of this study (Mestres and del Rosario, 2022), hypotheses have been presented which postulate the existence of different types of astrocytes —fibrous and protoplasmic— in the optic nerve (Raff, 1989). However, it remained unclear as to whether these differences in the morphology of this singular population of neuroglial cells are due to their location in the optic nerve. In view of the fact that the Golgi method provides complete impregnations of the astrocytes of the rat optic nerve, we surmised that the application of fractal geometry methods could provide an answer to the question as to whether there are two different morphological types of astrocytes in this anatomical location.

MATERIALS AND METHODS

Tissue preparation and staining of astrocytes

As already described in part I, the animals were sacrificed and processed according to the Golgi-Hortega method, which selectively stained the astrocytes.

Image acquisition

The optic nerve was examined under an M20 WILD optical microscope (Heerbrugg, Switzerland), equipped with a WILD drawing tube and a 50X LWD (long working distance) Olympus objective. For more panoramic examinations, a 20X LWD Olympus objective was used. A fine-tipped (0.2 mm) pigment liner (black water-resistant ink) was used and a total of 60 astrocytes of the optic nerve were traced.

Scale invariance analysis and selection of lenses and magnification

This analysis was performed in order to verify that the selected conditions enabled the definition of a linear relationship between the magnification of the images and the fractal dimension (Sandau, 1996).

Image processing prior to fractal analysis

The determination of the invariance of the scale was a basic step towards understanding the behaviour of the fractal morphology of our cells. Three different magnifications were used (10X, 20X and 50 X), and the linear relationship between fractal dimension and magnification was monitored. Subsequently, the images of the cells obtained from different regions of the optic nerve were digitally processed prior to performing fractal analysis.

This pre-treatment includes the following steps:

1. Digitalization of each cell drawing in black and white with high resolution. The 8-bit grayscale digital image thus obtained was then converted into a binary one using ImageJ's Binary function. This method of generating images is carried out in order to minimize loss and distortion of information during pre-processing. Finally, the background was converted to black pixels, while the lines corresponding to the outline of the cell and its interior were changed into white pixels.
2. All of the images analysed were adjusted to 1000 x 1000 pixels. This was done in order to ensure that neither the cell size nor the length of the drawing traces influences the fractal analysis.

Fractal analysis

The software used for fractal analysis was *FracLac for Image J* (Karperien and Jelinek, 2015). The parameters of interest were: fractal dimension (D_B), lacunarity (λ) and density.

The fractal dimension supplies information on the complexity of a morphological pattern; the higher the value, the higher the complexity.

Lacunarity is associated with changes in the cell body and its extensions, and this parameter measures the heterogeneity of the cell shape (Karperien et al., 2011). A low value of lacunarity indicates homogeneity. Conversely, high values of this parameter imply heterogeneity.

The lacunarity calculated with the FracLac box counting software is nothing other than the pixel mass distribution of the measured astrocytes. The value of lambda obtained is a coefficient of variation expressed as pixel density per box and as a function of box size (Karperien et al., 2011).

The calculation of density involves parameters such as the area of the measured cell (total number of pixels filling the image of the cell under examination, which, if desired can be transformed into square microns) and the so-called convex hull area (CHA), in which the convex hull is the smallest polygon in which the cell is completely included in it (Karperien et al., 2011; Young and Morrison, 2018). The density parameter gives us a measurement of the cell size, understood not only as the cell soma but also including the field occupied by the cell extensions.

Analysis of data

The data were numerically analyzed (polynomic adjustments) and a descriptive statistical analysis was also performed. All algorithms are included in the FracLac software package (Sandau, 1996).

RESULTS

Figure 1 shows examples of optic nerve astrocytes stained according to the Golgi-Hortega method and drawn with the aid of a camera lucida.

Astrocytes located in the central part of the optic nerve exhibit numerous quite thin processes with a smooth surface. Additionally, in some cases cell bodies –somewhat tuberous in shape– have been observed, as well as more robust processes than usual (Fig. 1A).

The cells located in the marginal zone of the nerve have prolongations that are directed towards the surface and enter into a proximity relationship with the meningeal sheaths (Fig. 1B). The astrocytes located in the central part of the nerve display processes in contact with blood vessels and Ranvier nodes, as well as the pial surface.

On the whole, these cells repeat the same morphological pattern in both zones. They do, however, show subtle differences which have been quantified by fractal morphometry methods.

Fractal dimension (D_B)

On average, the fractal dimension of astrocytes in the central zone of the nerve was 1.45303 (SD=0.01822), the minimum value measured in

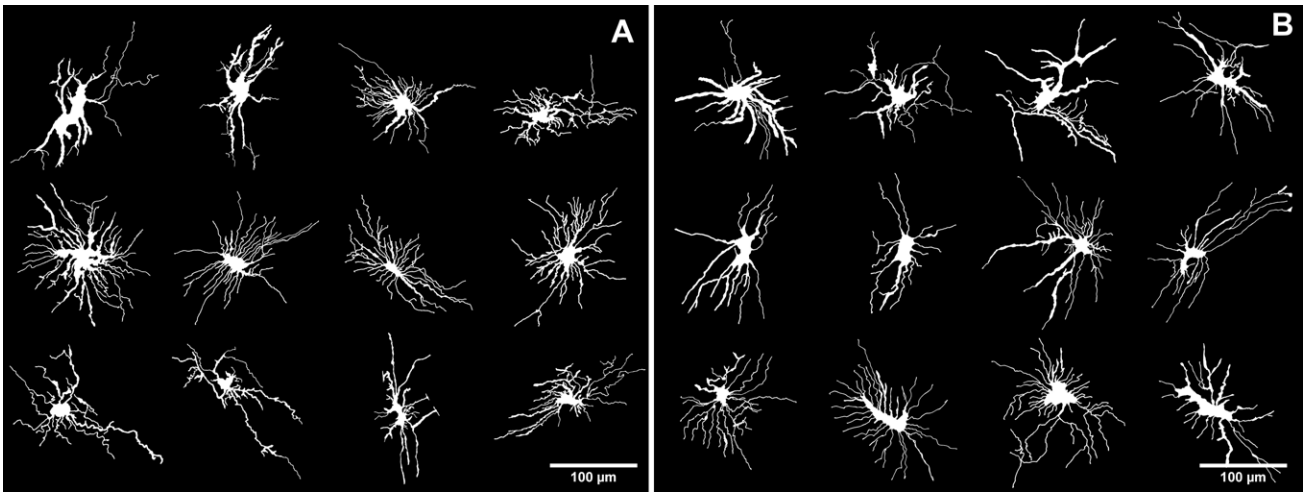

Fig. 1.- Digital images in binary format optimized for the analysis of the fractal dimension, contours and branched structures belonging to astrocytes of the intra-orbital portion of the optic nerve. **A:** Central location. **B:** Marginal location.

our material being 1.3079 (SD=0.0057), while the maximum value is 1.5946 (SD=0.0369). See Fig. 2A.

The morphological complexity of the cells was defined according to the following formula: $(D_{B\,max} - D_{Bmin})/ D_{Bmin}$. This formula expresses the growth rate, or rate of variation, which is a positive change of a variable, and in general terms is defined as: [(final value - initial value) / initial value] x 100 %.

Applying this formula to our data, we obtained a growth rate of 0.22 for the group of central

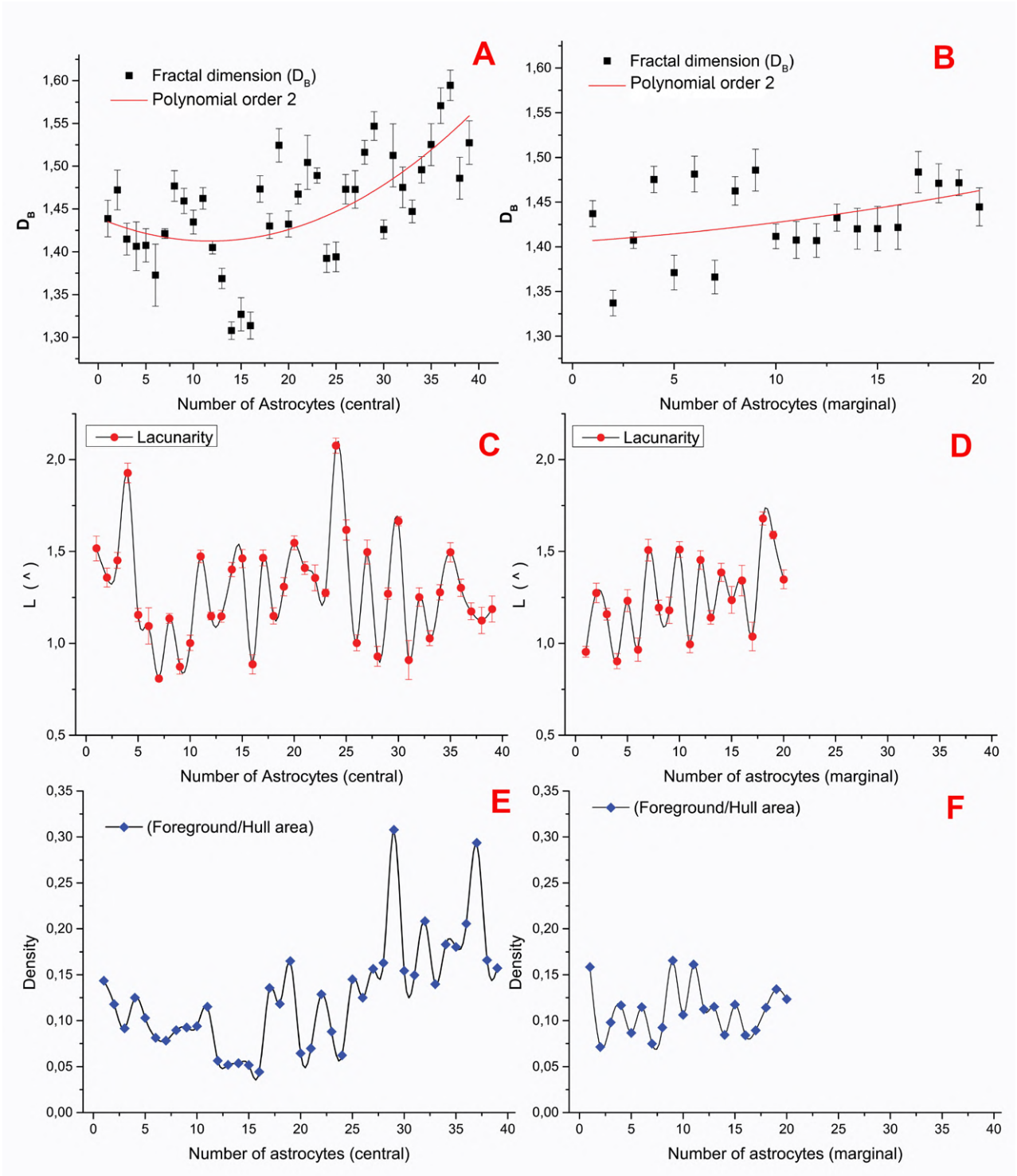

Fig. 2.- Fractal analysis of the complexity of the astrocytes of the optic nerve.

1. Graphic representation of the calculation of the fractal dimension (D_B) of astrocytes of central and marginal location, graph **2A** and **2B**. Polynomial fitting describes details of a similar trend complexity pattern.
2. The lacunarity obtained from the standard box counting calculation is presented in graphs **2C** and **2D**. On the left, lacunarity is shown for central astrocytes that show greater variation and gaps than those obtained from the marginal astrocytes on the right. Consequently, the heterogeneity and complexity registered on the left is higher.
3. The density of pixels in the foreground as an indicator of the degree of occupancy of astrocytes in the optic nerve presents a higher mean value for the central location in comparison with the marginal one, graphs **2E** and **2F**.

astrocytes, which indicates that, within this group, there are variations of the fractal dimension in the order of 22%.

In the population of astrocytes of the marginal zone of the optic nerve, the mean fractal dimension was 1.4308 (SD= 0.0186), while the minimum value measured in this population was 1.3370 (SD=0.0093) and the maximum value 1.4858 (SD=0.0249). See Fig. 2B.

The morphological complexity of this population, which was calculated with the above-defined expression, shows a value of 0.11, which indicates that the variations of the fractal dimension in this group is in the order of 11%.

The values of D_B in each of the populations are represented graphically in Figs. 2A and 2B. Through the application of the polynomial fitting function, we can recognize a clear difference in the behavior of the two populations.

As can be seen from a comparison of the distribution of the measured values with the polynomial fitting curve, D_B is lower in the marginal population than in the central population. In the marginal group, the curve is almost rectilinear, but the central population shows a very marked curve (Fig. 1A, B).

Lacunarity (λ)

The astrocyte population of the central zone of the nerve displays mean values of this parameter of 1.2861(SD = 0.2763), with a coefficient of variation (CV) of 0.0473 (Figure 2C). In this cell population, minimum values of 0.8084 (CV= 0.0152) were measured, while the maximum values were 2.0762 (CV= 0.1060). It is noteworthy that there is a considerable variance between the minimum and maximum values in lacunarity in this region of the nerve.

In the marginal zone, there is less variation in the value of the lacunarity parameter of the cells than in the central zone, which would seem to indicate reduced heterogeneity in comparison with the central part. In this zone, the mean value of lacunarity is λ =1.2544 (CV= 0.0509), while the minimum value measured was λ = 0.9032 (CV=0.0210), with a maximum value of 1.6790 (CV=0.0831). See Fig. 2D.

Density

The measurements of this fractal parameter are based on the convex of Hull and bounding circle, as well as on the pixel density of the image.

In the central region of the nerve, the density shows stochastic values. The mean value was 0.1271 (SD= 0.0605), while the lowest value was 0.0442 and the maximum one was 0.3078 (Fig. 2E).

In the marginal region, variations in this parameter were more discrete with a mean value of 0.1111 (SD= 0.0276). The minimum and maximum values of density were 0.0713 and 0.1655 respectively (Fig. 2F). Accordingly, the variation of density was 1.32 times higher than the minimum value measured for this parameter.

Data Normalization

In order to compare the three parameters measured in the two cell populations, the data were normalized (normalize [0,1]) by applying the following mathematical formula: Y=(Y-Ymin)/(Ymax-Ymin) [source: Origin 9.0 analysis program (64 bit)]

The alignment of the values to a normal distribution enables comparison of the normalized values with those of data sets in a way that eliminates external influences. The results of this operation are shown in Fig. 3.

The normalized distribution of points belonging to the fractal dimension D_B of the central astrocyte population fitted with a Gaussian function is symmetric with respect to a value identified in Figure 3 A as Xc, which coincides with the mean of the D_B values calculated in this population (mean D_B = 1.45303). Similarly, the fitting of the normalized point distribution of the marginal astrocyte population shows a smaller variance and deviates to the right of the mean obtained in the central population (Fig. 3A).

Fig. 3B shows the behavior of the lacunarity parameter in both astrocyte populations. The two curves appear a little shifted to the left, but the marginal astrocyte population still appears to the right of the central astrocyte curve.

This shift of the two curves to the left is even more marked in the density data (Fig. 3C).

DISCUSSION

The optic nerve is a unique tract of cerebral white matter composed of myelinated nerve fibers and neuroglia cells (Sandell and Peters,

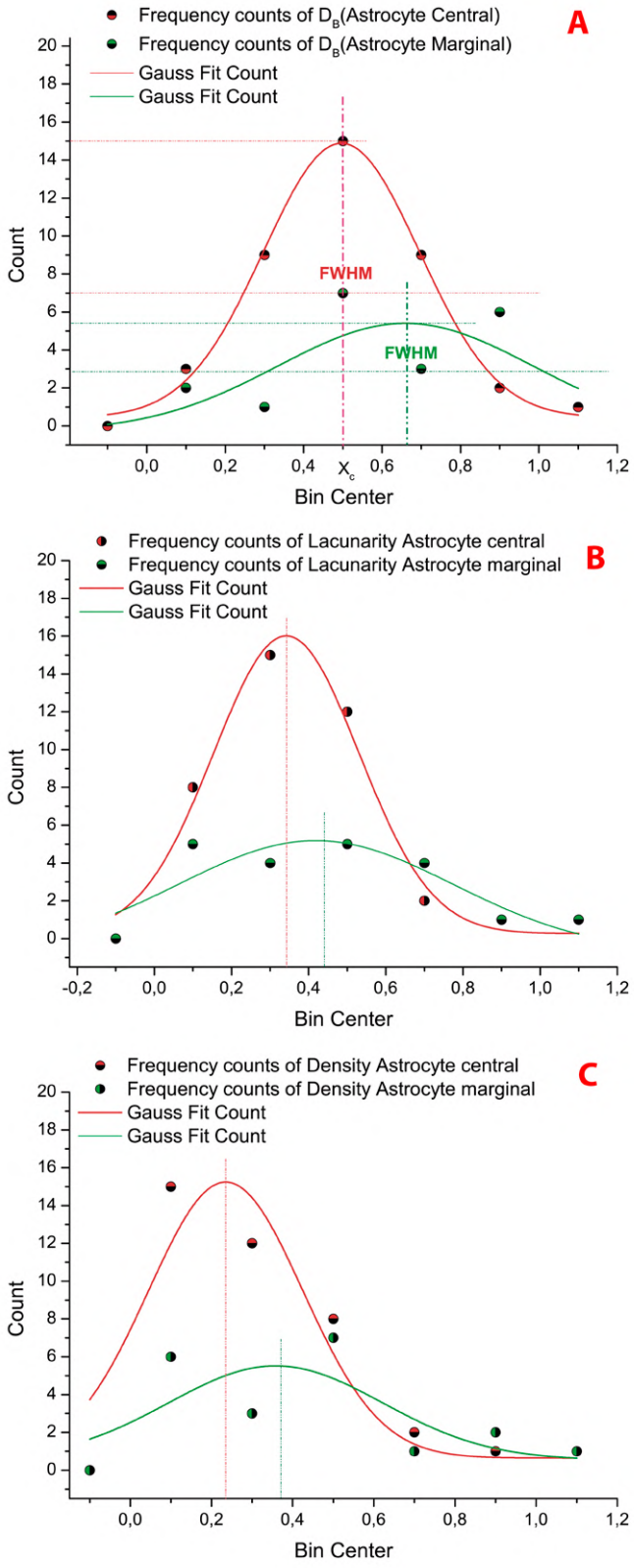

Fig. 3.- Comparative analysis of the normalized data of three calculated fractal parameters (D_B, λ, Density) for both populations of astrocytes, central and marginal. The fitting of the values measured on different scales represented on a common dimensionless index scale. The adjustment using a Gaussian distribution function for both populations allowed us to describe the general behavior of the morphological patterns displayed by the central astrocytes in contract to the singular patterns described by the marginal astrocytes.

2002). Astrocytes, which, in the optic nerve are of the fibrous type, are neuroglia cells that form a braid that embraces the nerve fibers of the optic nerve in bundles or fascicles. However, a part of them maintains a close relationship with the pial sheath of the nerve through terminations of their prolongations.

In this study, we addressed the question as to whether these neuroglia cells –the astrocytes– in the optic nerve of the rat display differences according to their location within the nerve. This is an eminently morphological question and fractal geometry is a very useful tool as it enables us to quantify the morphology of the astrocytes (Jelinek and Fernandez, 1998).

According to Jelinek and Fernandez (1998) "the Euclidean dimension describes objects in space as an integer". Thus, a straight line has a dimension of one (DE=1), a plane a dimension of two (DE=2), and a volume a dimension of three (DE=3). Df, as a dimension, is simply a number that reflects a particular aspect of a geometric form. The dimension value is called fractal because it is a fraction and not a whole number. It is called dimension because it provides a means of measuring how completely an object fills a space. Since a cell represented in two dimensions is not a straight line and does not completely cover a two-dimensional area, it cannot be adequately characterized by Euclidean geometry.

These considerations justify the use of fractal geometry to determine as exactly as possible whether cells with irregular shapes, such as the astrocytes of the optic nerve, show differences in shape.

Fractal geometry is based on several parameters, three of which we have considered in our study: fractal dimension (D_B), lacunarity (λ), and density (Karperian et al., 2013).

The fractal dimension (D_B) summarizes the complexity of the cell, while the lacunarity (lambda) describes its heterogeneity of the cell, such that the higher the value of the lacunarity the greater the heterogeneity. Conversely, lower values of this parameter indicate that the population in question is more homogeneous in morphological terms (Young and Morrison, 2018). The density parameter gives an idea of the size of the cell; this value corresponds to the field occupied by a cell with its soma and all its extensions within the confines of this field (Young and Morrison, 2018).

Fractal geometry has been applied to various types of glial cells such as, for example, Bergmann cells in the cerebellum, also known as Golgi epithelial cells. Using fractal geometry, it was determined that, in terms of fractal geometry, there are differences between these cells, depending on the vertebrate species from which they originate (Siegel et al., 1991). The differences described are very subtle, and generally escape simple examination with an optical microscope. After having studied the fibrous astrocytes of the cat optic nerve (Reichenbach et al., 1992), Professor Reichenbach's group examined in a later study the differences between astrocytes from different locations within the cat brain. This was a comparative study determining the D_B of protoplasmic astrocytes and that of fibrous astrocytes. It especially highlighted that the marginal astrocytes of the cerebral cortex are in contact with the pial envelope, a situation that also occurs in the optic nerve.

Fractal dimension (D_B)

Our results indicate that there is a difference in terms of fractal dimension between the astrocytes in a central position within the optic nerve and the marginal ones, with the D_B being higher in the former. Normalization of the data further supports this interpretation.

Lacunarity (λ)

This parameter also shows differences between central and marginal astrocytes, the former being more heterogeneous than the latter. This further supports the hypothesis that there are two populations of astrocytes in the optic nerve according to their anatomical localization.

Density

Finally, density indicates that the size of the field in the tissue occupied by central astrocytes is significantly larger than that of marginal astrocytes.

On the normalization of the data

The parameter known as "full width at half maximum" (FWHM) is defined as a variance and explains why the three curves of the central population shown in Fig. 3 A, B, C present a more uniform (homogeneous) behavior than those of the marginal one.

This means that the marginal population in the three parameters (Fractal dimension, Lacunarity and Density) presents a higher FWHM than the one corresponding to the central population. However, the fact that the marginal population maintains its maximum (maximum height of the curve) within the representation of the function belonging to the central population indisputably relates them, since it can be affirmed that there are variables which both populations share, to the order of 55 to 70 %. Nevertheless, that differences do exist between them can be deducted from the curves shown in Fig. 3.

Final considerations

The data presented show that, morphologically, central and marginal astrocytes differ to a high degree. They are not distinct cell types, since the morphology of their prolongations in particular corresponds to that of fibrous astrocytes, with

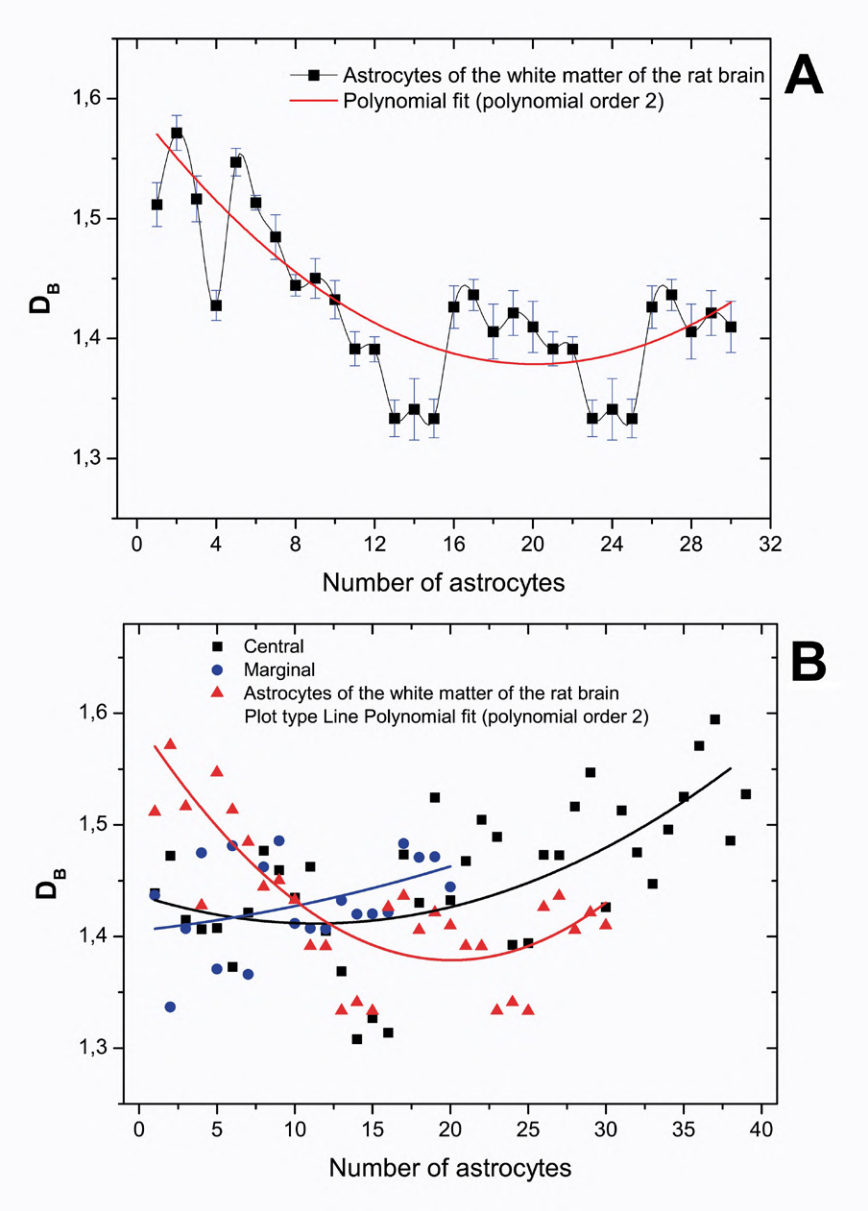

Fig. 4.- Graphical representation of the calculated values of fractal dimension of astrocytes of the white substance **(A)**. The polynomial line of fitting describes a trend contrary to that observed in central and marginal astrocytes of the optic nerve. The behavior described by the three populations is described by polynomial regression methods. This is a procedure of applying the optimal degree to a quadratic model, which provides an explanation of the relationship between both types of interconnected cell populations **(B)**.

their typical thinness and smooth surface. They thus differ from protoplasmic astrocytes, which have shorter prolongations and exhibit a very rough surface (Siegel et al., 1991). The shape changes exhibited by optic nerve astrocytes when cultured in vitro is a sign of great plasticity in that they adopt other shapes as they adapt to the geometric conditions of the culture surfaces (Smith and Behar, 1994). Following this line of thought, it seems plausible to contend that optic nerve astrocytes adapt to the anatomical conditions of the nerve. This also correlates with the differences that can be observed in the cells presented in the work of Reichenbach et al. (1992).

In a parallel study of owr own (unpublished) using the brains of the same animals from which the optic nerves were extracted, it has been shown that the fibrous astrocytes of the corpus callosum (Atlas of König and Klippel, 1963), approximate level A 7470 microns show fractal dimension values different from those measured in the optic nerve, although their cell characteristics (microscopical images) are analogous, if not identical. These differences in D_B after polynomial fitting can be clearly seen in the graph below (Fig. 4).

These findings, although based on a smaller set of cells (30), speak in favor of the interpretation that fibrous astrocytes display morphological differences in the optic nerve in relation to their anatomical environment, i.e., in relation to their location. This seems to be a general pattern of behavior in such cells in the central nervous system.

ACKNOWLEDGEMENTS

This study has been generously supported by the Technological Support Center, University of Rey Juan Carlos to GRH and the University of Saarland (Germany) to PMV.

REFERENCES

CROSS SS (1994) The application of fractal geometric analysis to microscopic images. *Micron*, 25(1): 101-113.

FERNANDEZ E, JELINEK HF (2001) Use of fractal theory in neuroscience: methods, advantages, and potential problems. *Methods*, 24: 309-321.

JELINEK HF, FERNANDEZ E (1998) Neurons and fractals: how reliable and useful are calculations of fractal dimensions? *J Neurosci Methods*, 81: 9-18.

KARPERIEN AL, AHAMMER H, JELINEK HF (2013) Quantitating the subtleties of microglial morphology with fractal analysis. *Front Cell Neurosci*, 7(3): 1-18.

KARPERIEN AL, JELINEK HF (2015) Fractal, multifractal, and lacunarity analysis of microglia in tissue engineering. *Front Bioeng Biotechnol (Biomaterials)*, 3(51): 1-4.

KARPERIEN AL, JELINEK HF, MILOSEVIC NT (2011) Reviewing lacunarity analysis and classification of microglia in neuroscience. Proceedings of the 8th European Conference on Mathematical and Theoretical Biology. European Society for Mathematical and Theoretical Biology (ESMTB) 2011 MS#88.

KÖNIG JFR, KLIPPEL RA (1963) *The rat brain. A stereotaxic atlas of the forebrain and lower parts pf the brain stem*. The Williams and Wilkins Company. Baltimore.

MESTRES VENTURA P, DEL ROSARIO HERNANDEZ G (2022) The neuroglia of the rat optic nerve. Part I. Golgi-Hortega and Golgi-EM studies. *Eur J Anat,* 26(2):167-177.

RAFF MC (1989) Glial cell diversification in the rat optic nerve. *Science*, 243: 1450-1455.

REICHENBACH A, SIEGEL A, SENITZ D, SMITH Jr TG (1992) A comparative fractal analysis of various mammalian astroglial cell types. *Neuroimage*, 1: 69-77.

SANDAU K (1996) A note on fractal sets and the measurement of fractal Dimension. *Physica A,* 233: 1-18.

SANDELL JH, PETERS A (2002) Effects of age on the glial cells in the Rhesus Monkey optic nerve. *J Comp Neurol*, 445: 13-28.

SIEGEL A, REICHENBACH A, HANKE S, SENITZ D, BRAUER K, SMITH Jr TG (1991) Comparative morphometry of Bergmann glial Golgi epithelial) cells. A Golgi study. *Anat Embryol*, 183: 605-612.

SMITH JR TG, BEHAR TN (1994) Comparative fractal analysis of cultured glia derived from optic nerve and brain demonstrate different rates of morphological differentiation. *Brain Res,* 634: 183-190.

YOUNG K, MORRISON H (2018) Quantifying microglia morphology from photomicrographs of immunohistochemistry prepared tissue using Image J. *J Vis Exp,* (136): e57648. doi:10.3791/57648 (2018).

Bone marrow quality in chemically prepared dogs

Thiago A.S.S. Rocha, Andréa B.P.S. Queiroz, Raphael C. Zero, Fabrício S. Oliveira

Department of Animal Morphology and Physiology, School of Agrarian and Veterinary Science, São Paulo State University (UNESP), Via de Acesso Paulo Donato Castelane, s/n, CEP 14884-900, Jaboticabal-SP, Brasil

SUMMARY

Besides preventing deterioration, conservation also prevents the proliferation of pathogens that cause diseases in those who work in laboratories. This research aimed to evaluate the color of the bone marrow of chemically prepared dog corpses, seeking to determine whether long-term preservation maintains their original morphological aspect. Fifty cadavers of adult dogs were used. The control group (G0) consisted of fresh corpses; the others were fixed in curing salt solution (20% sodium chloride, 1% nitrite, and 1% sodium nitrate) (120 ml/Kg) and ethanol with 5% glycerin (120 ml/Kg). Cadavers were assessed at 30 days (G30), 60 days (G60), 90 days(G90), and 120 days (G120). In addition, two veterinary observers evaluated the long bones' bone marrow during a biomechanical compression test after a fracture. Qualitative bone marrow color variables were transformed into scores, in which 0=excellent (more vivid than fresh cadaver), 1=good (similar to G0), 2=poor (darker than G0), and 3=bad (rotten appearance, brownish). By Dunn's test, the bone marrow of the bones was better at 30 days when compared to G0 (G0>G30), G0≅G60 and G0<90, and G0<G120. This conservation technique was promising in orthopedic training in dogs, and provided a better bone marrow aspect between 30 to 60 days after fixation.

Key words: Anatomy – Conservation – Orthopedics – Surgery

INTRODUCTION

Anatomical specimens are fixed so that tissues do not deteriorate, so tissues remain firm, insoluble, and protected (Rodrigues, 2010). Besides preventing deterioration, exemplary conservation also avoids the proliferation of pathogens that can cause diseases in those who live daily in laboratories (Corrêa, 2003).

For conservation, the most common substances used to avoid microorganisms' proliferation are formaldehyde, glycerin, ethanol, and phenol (Rodrigues, 2010).

Formaldehyde is the most widely used fixer and preservative, commonly in a 10% aqueous solution. Because it is not expensive and penetrates rapidly into tissues (six millimeters in twelve hours), it is widely used in anatomy laboratories (Rodrigues, 2010). In addition, several types of fixative solutions can preserve cadavers for surgical use, as Thiel's solution (Groscurth et

Corresponding author:
Andréa Barros Piazzon de Souza Queiroz. Department of Animal Morphology and Physiology, São Paulo State University (UNESP), School of Agrarian and Veterinary Science, Via de Acesso Paulo Donato Castelane, s/n., 14884-900 Jaboticabal, Brasil. Phone: +5519971026700; Fax: +551932516237. E-mail: andrea.queiroz@unesp.br Orcid: 0000-0003-0199-6105

Submitted: January 7, 2021. **Accepted:** January 8, 2022

https://doi.org/10.52083/JHHV2096

al., 2001), Jores' solution (Rodrigues, 1998), and Larssen's modified solution (Silva et al., 2004), Laskowski solution (Silva et al., 2007), all of them presenting formaldehyde.

In a research using curing salt (CSS) as an alternative to formaldehyde in veterinary anatomy teaching in Germany, the solution successfully preserved dogs' corpses without environmental and health risks at a low cost (Janczyk et al., 2011). In Japan, using a salt-saturated solution in preserving human cadavers aiming for surgical education was successfully evaluated (Hayashi et al., 2016). In Hungary, a 16% curing salt solution was used as an alternative to formaldehyde for long-term preservation of anatomical specimens of dogs subjected to dissection at the University of SzentIstván Sciences (Werdelmann and Gerics, 2016).

The current model that best approaches the fresh corpse presents several problems: freezing, limited practising time due to fast putrefaction, and risk of infections. On the other hand, saturated salt solutions are a simple method with a low risk of infection and cost (Hayashi et al., 2016).

For five years, a 30% sodium chloride aqueous solution (30% SCAS) was used to conserve anatomical specimens previously fixed by formaldehyde; no visual contamination, putrefaction odors, or alteration of color and softness were noticed (Oliveira, 2014). The use of the sodium chloride hypersaturated solution on the pericardium (Brun et al., 2002) and phrenic center of dogs (Brun et al., 2004), both for surgical purposes, has also been successfully described.

The curing of meat products is a traditional practice in the food industry. The process consists of applying nitrite, nitrate, sodium chloride, and sugar to meat. By combined action, these components have a pronounced effect on the characteristics and stability of those products. For example, sodium nitrite causes stabilization of the typical red color, improves the organoleptic characteristics, and inhibits the growth of *C. botulinum* (Leitão, 1978).

Both nitrites and nitrates are curing salts widely used as additives by the food industry, mainly the meat industry. They are classified as conservative substances. They are added to foods to prevent or delay microbial or enzymatic actions, thus protecting the food from deterioration. They are also color fixers (Iamarino et al., 2015).

Recent studies present biomechanical analyses of tissues of dogs and cats during conservation (Cerqueira et al., 2017; Pelogia et al., 2018; Rocha et al., 2018; Fração et al., 2019; Zero et al., 2020), as well as microbiological analyses of fixative/conservative solutions (Pereira et al., 2019) and evaluation of students on surgical practice (Rocha et al., 2019).

This paper's objective was to evaluate bone-marrow aspect (staining), using glycerinated ethyl alcohol (GEA) as a fixative and curing salt as preservative solutions in dogs, with the aim of teaching veterinary orthopedics.

MATERIALS AND METHODS

Twenty-one male and twenty-nine female adult dogs whose death did not involve evident morphological alterations, such as large tumor masses, extensive lacerations, or bone fractures, were used. They came from the Zoonosis Center Control at Ribeirão Preto, São Paulo, Brazil (process 02.2014/000027-1 approved by the Municipal Legal Department and the University Ethical Committee (process 4593/19).

Shortly after death, the corpses were frozen (freezer at -18°C) and transported to the Laboratory of Animal Anatomy at UNESP (São Paulo State University), Jaboticabal, São Paulo, Brazil, located 50km away.

In this research, corpses weighing 9.46±2.80 Kg and body score 4 or 5 (on a scale from 1 to 9) were used (Laflamme, 1997). The control group consisted of fresh cadavers; all the others were fixed. The fixation was performed with a CSS (20% sodium chloride, 1% nitrite, and 1% sodium nitrate) injected via the common carotid artery (120 ml/Kg). Subsequently, 120 ml/Kg of ethyl alcohol associated with 5% glycerin (GEA) was infused. Dogs were randomly divided into four groups and remained at different times, except the control group, in a horizontal refrigerator at 4-6°C after fixation:

- Group 1: refrigerated for 30 days;

- Group 2: refrigerated for 60 days;
- Group 3: refrigerated for 90 days;
- Group 4: refrigerated for 120 days.

The long bones of the control group were collected and subjected to biomechanical tests immediately after thawing. After the final refrigeration time, each group was exposed to room temperature (24°C). The bones were collected using surgical instrumentation (scalpel, Mayo and Metzenbaum scissors, and rat tooth forceps) for biomechanical assay (humerus, radius, ulna, femur, and tibia).

The bones were measured to determine the midline of the diaphysis, where the fracture was performed using a compression test by the EMIC® Universal Testing Machine – (model DL-2000). The load cell was 20 kN, and the speed was 500 mm/min., the free range of 25 mm from the shear and 60 mm between the columns. The equipment belongs to the Laboratory of Surgical Anatomy of the Department of Animal Morphology and Physiology at São Paulo State University in Jaboticabal, Brazil.

Two veterinarians with at least 15 years of experience in anatomy and surgery, and who already had training in bone marrow observation in biomechanical assays, were chosen as the project performers and evaluators. Observers evaluated 100 analyses of the bone marrow (BM) staining during each group samples mechanical. All samples were placed in 0.9% saline solution at room temperature (24°C) to avoid tissue dehydration. To prevent more than one group from being analyzed on the same day, there was no way to carry out a blind test due to the extensive work in each collection. However, the same trained professionals performed all the analyses to minimize errors. The same professional made all the analyses. As the control group was the first

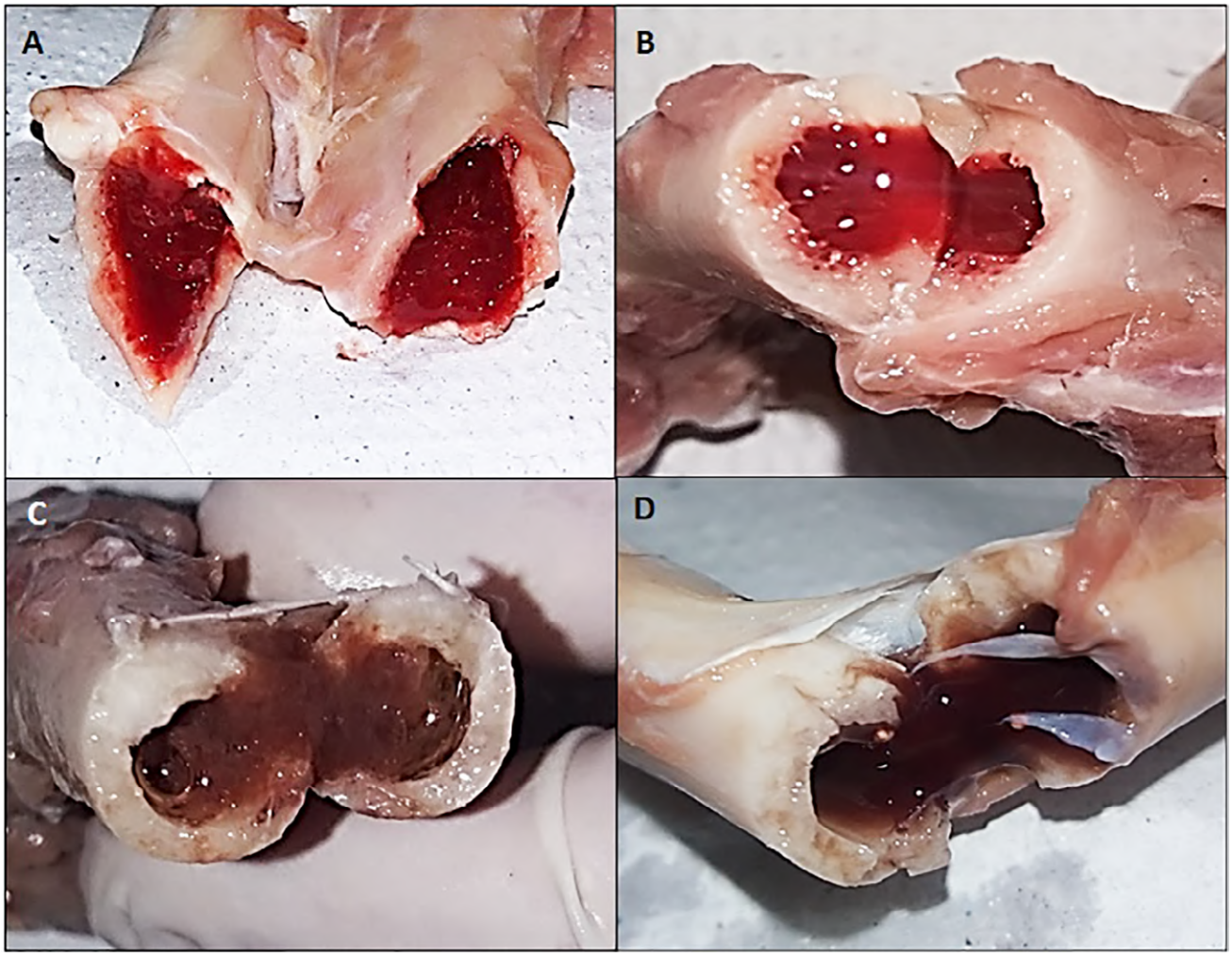

Fig. 1.- Photographic image of bone marrow stains from cadavers of dogs submitted to the fixation process with glycerinated ethyl alcohol and preserved with curing salt. **A:** excellent (more vivid coloring than fresh corpse); **B:** good (fresh corpse-like color); **C:** poor (darkened color about fresh corpse); **D:** bad (brown, putrid color).

to be evaluated (fresh corpses), the marrow's observation of its long bones is considered a parameter for the classification. Thus, the BM staining of the fresh animal was considered a reference and classified as "good." After the fracture of bone samples, they were classified as excellent (color considered more vivid than fresh bone), good (color similar to the fresh bone), poor (color darker than the fresh bone), or bad (brown color, rotten appearance) (Fig. 1).

Qualitative variables of the BM were transformed into scores, in which 0 = excellent (BM staining more vivid than in the one in fresh cadaver), 1 = good (similar to the one from the fresh carcass), 2 = poor (darker than the one from a fresh corpse) and 3 = bad (rotten appearance, brownish), the lower the value, the better the appearance (Table 1).

After the BM scores, the genders were analyzed to search if there were differences.

The significance analysis (p-value) of the BM aspect regarding the right and left antimers was used to search for differences. There was no statistical difference between the right and left antimeres in relation to length and craniocaudal and lateral lateral diameters (Table 2). The measurements are shown in table 3. In addition, Dunn's test was performed to determine when the BM presented the best visual aspect.

Table 1. Analysis of the qualitative variables of the aspect of the bone marrow staining, generated by the analysis of two observers subjected to Dunn's test to determine the moment related to the aspect of the conservation time of dog corpses fixed with glycerinated ethyl alcohol and preserved with curing salt, subjected to biomechanical testing.

	G0		G30		G60		G90		G120		
BM	**Median**	**AQI**	**Median**	**AQI**	**Median**	**AQI**	**Median**	**AQI**	**Median**	**AQI**	**P Value**
HUMERUS AD	1,00	0	0,00	0	1,00	1	1,00	2	2,00	0	0,0019
Dunn	b		a		ab		b		c		
HUMERUS AE	1,00	0,00	0,00	0,00	0,50	1,00	2,00	1,00	2,00	0,75	<0,0001
Dunn	bc		a		ab		c		d		
RADIUS AD	1,00	0,00	0,50	1,00	1,00	0,75	2,00	1,00	2,00	0,00	<0,0001
Dunn	ab		a		b		c		c		
RADIUS AE	1,00	0,00	0,50	1,00	1,00	0,75	1,00	1,00	2,00	0,00	<0,0001
Dunn	b		a		b		b		c		
ULNA AD	1,00	0,00	0,50	1,00	1,00	0,00	1,00	1,00	2,00	0,00	<0,0001
Dunn	b		a		b		b		c		
ULNA AE	1,00	0,00	0,00	0,75	1,00	0,00	1,00	0,00	2,00	0,00	<0,0001
Dunn	b		a		b		b		c		
FEMUR AD	1,00	0,00	0,00	0,00	1,00	1,75	1,00	1,00	2,00	1,50	<0,0001
Dunn	b		a		b		b		c		
FEMUR AE	1,00	0,75	0,00	0,00	0,50	1,75	1,00	2,00	1,50	1,00	0,0009
Dunn	bc		a		b		bc		c		
TIBIA AD	1,00	0,00	0,00	0,75	1,00	0,75	1,00	1,00	2,00	0,75	0,0002
Dunn	b		a		b		bc		c		
TIBIA AE	1,00	0,00	0,50	1,00	1,00	1,75	1,00	1,00	2,00	0,75	0,0011
Dunn	ab		a		ab		b		c		

* The bone marrow aspect, qualitative variables, were transformed into scores where 0 = excellent, 1 = good, 2 = poor, and 3 = very bad; so the lower the value, the better the appearance. AQI: interquartile range. AD: right antimere, AE: left antimere.

Table 2. ANOVA (p<0.05) between right (RA) and left (LA) antimeres regarding bone midline measurements of dog cadavers subjected to chemical preparation with ethyl alcohol and curing salt.

Comparison between antimeres	
Variables	**P value**
UMERUS RA Length	0.92
UMERUS LA Length	
UMERUS RA Diam CCd	0.88
UMERUS LA Diam CCd	
UMERUS RA Diam LL	0.66
UMERUS LA Diam LL	
RADIUS RA Length	0.89
RADIUS LA Length	
RADIUS RA Diam CCd	0.42
RADIUS LA Diam CCd	
RADIUS RA Diam LL	0.76
RADIUS LA Diam LL	
ULNA RA Length	0.84
ULNA LA Length	
ULNA RA Diam CCd	0.97
ULNA LA Diam CCd	
ULNA RA Diam LL	0.81
ULNA LA Diam LL	
FEMUR RA Length	0.67
FEMUR LA Length	
FEMUR RA Diam CCd	0.90
FEMUR LA Diam CCd	
FEMUR RA Diam LL	0.94
FEMUR LA Diam LL	
TIBIA RA Length	0.62
TIBIA LA Length	
TIBIA RA Diam CCd	0.62
TIBIA LA Diam CCd	
TIBIA RA Diam LL	0.98
TIBIA LA Diam LL	

*Length: length em milimeters, Diam: diameter em milimeters, CCd: cranio-caudal, LL: laterolateral.

RESULTS

There were no significant differences between cadaver genders and BM appearance for all measured variables.

The p-value analysis of the BM aspect regarding the right and left antimers presented no significant differences, which increased the number of samples (n) by summing the values related to antimers. The confidence interval was 5%.

After running the Dunn's test, it showed that the humerus bone marrow aspect was better at 30 days of conservation when compared to the control group (G0>G30), similar at 60 days (G0≅G60), and worse at 120 days (G0<G120). The radius presented a better appearance of BM at 30 days when compared to the control group (G0>G30), similar at 60 days (G0≅G60), and worse appearance at 90 (G0<90) and 120 days (G0<G120). The ulna presented the best aspect of BM at 30 days (G0>G30),

Table 3. Means of the long bones measurements in dog cadavers subjected to chemical preparation with ethylic alcohol and curing salt.

	G0 Control	G30	G60	G90	G120	MEAN (mm)
UMERUS Length	123.35	118	107.10	117.72	98.55	**113.00**
UMERUS Diam CCd	13.76	12.49	11.21	11.5	11.87	**12.10**
UMERUS Diam LL	10.18	9.28	9.21	9.33	9.96	**9.60**
RADIUS Length	118.95	113.05	99.15	114.83	92.20	**107.60**
RADIUS Diam CCd	6.41	6.22	7.03	6.43	6.90	**6.60**
RADIUS Diam LL	9.85	9.52	9.95	9.6	10.77	**9.90**
ULNA Length	140.60	134.50	118	139.27	111.30	**108.70**
ULNA Diam CCd	8.20	6.72	7.31	7.41	7.89	**7.50**
ULNA Diam LL	7.27	7.68	7.86	6.03	8.68	**7.50**
FEMUR Length	133.15	126.95	114	125.83	107.20	**121.40**
FEMUR Diam CCd	10.50	9.75	10.13	9.81	10.53	**10.10**
FEMUR Diam LL	10.82	10.12	9.86	10.03	10.75	**10.30**
TIBIA Length	132.95	128.50	108.26	129.38	105.30	**121**
TIBIA Diam CCd	10.66	9.94	9.32	9.61	10.01	**9.9**
TIBIA Diam LL	10.71	10.08	10.24	10.04	10.78	**10.30**

* Length: length em milimeters, Diam: diameter em milimeters, CCd: cranio-caudal, LL: latero-lateral. G0: fresh samples; G30: 30 days of conservation; G60: 60 days of conservation; G90: 90 days of conservation; G120: 120 days of conservation.

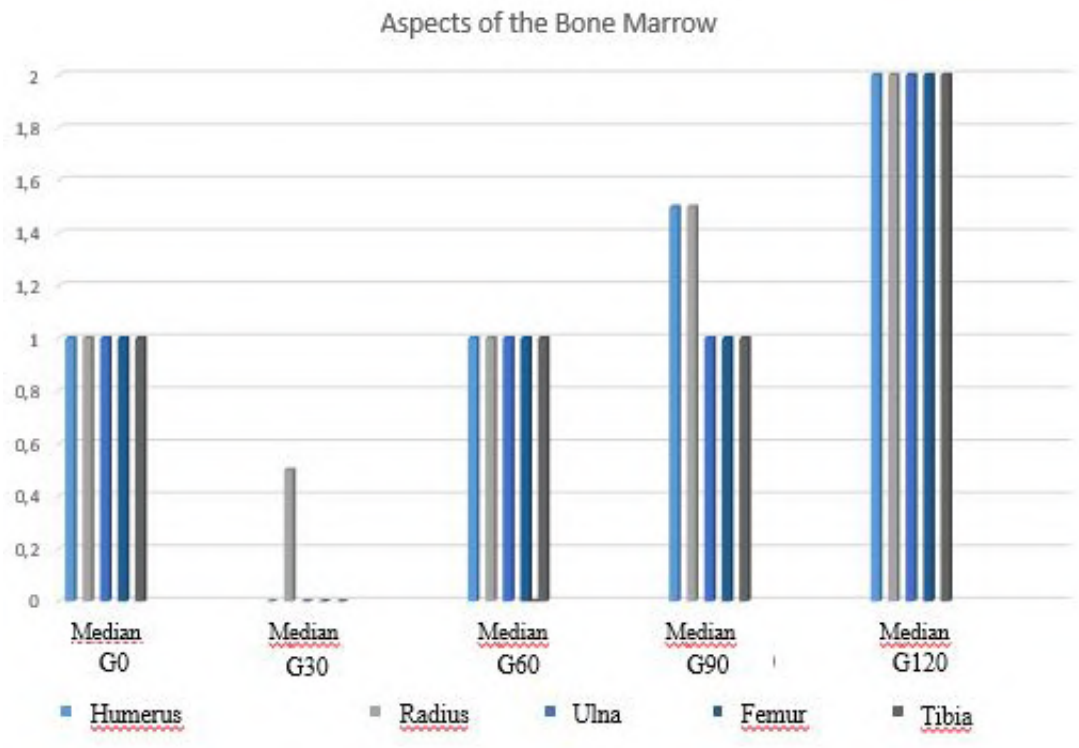

Fig. 2.- Illustrative image of the bone marrow's qualitative aspects fixed with glycerin ethyl alcohol and curing salt. Note that the medians in the 30-day conservation group (G30) are lower than those in the control group (G0) and that the medians in the 60-day conservation group are similar to G0. The other medians (G90 and G120) greater than G0.

similar at 60 days (G0≅G60), and worse aspect at 90 and 120 days (G0<90 and G120). The femur presented a better aspect of BM at 30 days when compared to the control group (G0>30), similar at 60 days (G0≅G60), and worse aspect at 90 (G0 <90) and 120 days (G0<G120). The tibia presented a better aspect of BM at 30 days when compared to the control group (G0>G30), similar to 60 days (G0≅G60) and worse aspect at 90 (G0<90) and 120 days (G0<G120) as seen on Fig. 2.

DISCUSSION

The GEA was efficient as a fixative, with CSS as a preservative solution, allowing good conservation and avoiding deterioration, maintaining the characteristics and the color of the dogs' corpses, similar to corpses fixed with GEA and preserved 30% SCAS (Cerqueira et al., 2017; Pelógia et al., 2018; Rocha et al., 2018). The CSS also presented similar aspects in cats fixed with GEA, with no skin hardening or color change during the conservation (Fração et al., 2019; Zero et al., 2020).

The excellent results on BM of corpses fixed with GEA and CSS are promising as for their use in orthopedic surgery, as it occurred in surgery training in chemically prepared dogs, with more than 81% (Rocha et al., 2018) or 93% (Silva et al., 2003) of students' approval in Brazil. Also, there were no differences among groups through different times, similar to the scores of incision or suture in chemically prepared cats (with GEA and CSS) compared to fresh corpses (Fração et al., 2019).

Conventional procedures for fixation of corpses using formaldehyde for conservation are limited in surgical practice due to the significant change of color, resistance, and fragility of organs and tissues (Groscurth et al., 2001). In addition, this substance also causes stiffness of corpses, coagulation of blood and presents an unpleasant odor (Hayashi et al., 2014).

Differently, the conservation solution applied in this research demonstrated that the color of the long bones' BM was markable after 30 days, with a more vivid appearance than a fresh corpse, and similar to the color of a fresh cadaver in 60 days. However, after 90 days of conservation, the BM began to decay, and the color became progressively worse until 120 days. The better color of the BM on the 30 and 60 days of conservation could be explained using the curing salt solution, which is widely utilized in food factory industries to fix the meat's color (Iamarino et al., 2015).

Toxic preservative solutions generate contaminated effluents (Who, 1991) and dangerous vapors, such as those released by formaldehyde (Cury et al., 2013). In addition, these harmful products increase the institution's financial and environmental costs making it necessary to look for lower risky alternatives (Janczyk et al., 2011), such as the GEA and CSS solutions applied in this research.

The use of embalmed corpses in veterinary surgery practice is an alternative to using live animals. It reduces costs and increases exercise repeatability (Oliveira, 2008), and it is a trend in universities worldwide to avoid euthanasia of thousands of specimens for this purpose (Balcombe, 2000). In this research, the BM was conserved for 120 days without bad odor or visual contamination, like soft tissues fixed with the same anatomical technique (Fração et al., 2019; Pereira et al., 2019; Zero et al., 2020).

The CSS is effective for the preparation of anatomical species in Veterinary and Human Medicine in several countries (Janczyk et al., 2011; Hayashi et al., 2016; Fração et al., 2019) and provided, together with the GEA, the maintenance of corpses without visual contamination for 120 days in refrigeration temperature only.

The high concentration of sodium chloride in the CSS complicates microorganisms' survival because it requires an enormous capacity for osmoregulation, similar to what occurs in the oceans (Munro et al., 1989) and the Dead Sea (Nissenbaum, 1975). In addition, several concentrations of fixative substances in the preservation of anatomical specimens have already been evaluated and, the use of sodium chloride solution in a concentration below 20% fail to preserve specimens for tissue dissection (Friker et al., 2007), differently from what was observed in our study, in which 20% sodium chloride, associated with 1% nitrite and sodium

nitrate, is effective for the preservation of dog corpses for four months, in addition to providing good malleability to tissue handling.

Teaching models using human and animal corpses are a historical part of the surgery. Their use is secular and remains the most respected training method due to exposure to real anatomy and allowing the surgeon in training to appreciate the dissection and practice the actual handling of tissues (Silva et al., 2007; Stirling et al., 2014).

ACKNOWLEDGEMENTS

Fundação de Amparo à Pesquisa do Estado de São Paulo, FAPESP (process 2018/18567-0) and Conselho Nacional de Desenvolvimento Científico e Tecnológico, CNPq (proc. 483443/2013-1) for the finantial support and Usina São Martinho, Pradópolis, SP, Brazil.

REFERENCES

BALCOMBE J (2000) The use of animals in higher education: problems, alternatives and recommendations. Washington, DC: The Humane Society Press.

BRUN MV, PIPPI NL, DREIMEIER D, CONTESINI EA, BECK CAC, CUNHA O, PINTO FILHO SL, ROEHSIG C, STEDILE R (2002) Solução hipersaturada de sal como conservante de pericárdio canino utilizado na reparação do músculo reto abdominal de ratos Wistar. *Ciência Rural*, 32: 1019-1025.

BRUN MV, PIPPI NL, DRIEMEIER D, CONTESINI EA, BECK CAC, CUNHA O, PINTO FILHO SL, ROEHSIG C, STEDILE R, SILVA TF (2004) Solução hipersaturada de sal ou de glicerina a 98% como conservantes de centros frênicos caninos utilizados na reparação de defeitos musculares em ratos Wistar. *Ciência Rural*, 34: 147-153.

CERQUEIRA ESF, PELOGIA MES, SILVEIRA CPB, FECHIS ADS, ROCHA TASS, LAUS JL, OLIVEIRA FS (2017) Suture analysis and arterial traction test in dogs fixed on alcohol and preserved on saline solution aiming surgical practice. *Global Adv Res J Med Medical Sci*, 6: 292-295.

CORRÊA WR (2003) Isolation and identification of filamentous fungi found in anatomical pieces preserved in 10% formalin solution. Dissertation (Biological Sciences). Institute of Research and Development, University of the Valley of Paraíba. 59 p.

CURY FS, CENSONI JB, AMBRÓSIO CE (2013) Técnicas anatômicas no ensino da prática de anatomia animal. *Pesq Vet Bra*, n. 33, v. 5, pp 688-696.

FRAÇÃO VC, ZERO RC, RODRIGUES A, FERREIRA BN, FECHIS ADS, ROCHA TASS, IOZZI MT, OLIVEIRA FS (2019) Analysis of the skin of cats' corpses chemically prepared with ethylic alcohol and curing salt aiming veterinary surgical practice - Chronic effect on biomechanics and students' evaluation. *CPQ Medicine*, 6: 01-08.

FRIKER J, ZEILER E, MCDANIEL BJ (2007) From formalin to salt. Development and introduction on a salt-based preserving solution for macroscopic anatomic specimens. *Tierärztl Praxis*, 35: 243-248.

GROSCURTH P, EGGLI P, KAPFHAMMER J, RAGER GJ, HORNUNG P, FASEL JDH (2001) Gross anatomy in the surgical curriculum in Switzerland: Improved cadaver preservation, anatomical models, and course development. *Anat Rec*, 265: 254-256.

HAYASHI S, HOMMA H, NAITO M, ODA J, NISHIYAMA T, KAWAMOTO A, KAWATA S, SATO N, FUKUHARA T, TAGUCHI H, MASHIKO A, AZUHATA T, ITO M, KAWAI K, SUZUKI T, NISHIZAWA Y, ARAKI J, MATSUNO N, SHIRAI T, QU N, HATAYAMA N, HIRAI S, FUKUI H, OHSETO K, YUKIOKA T, ITOH M (2014) Saturated salt solution method: a useful cadaver embalming for surgical skills training. *Med J*, 93: 1-10.

HAYASHI S, NAITO M, KAWATA S, QU N, HATAYAMA N, HIRAI S, ITOH M (2016) History and future of human cadaver preservation for surgical training: from formalin to saturated salt solution method. *Anat Sci Int*, 91: 1-7.

IAMARINO LZ, OLIVEIRA MC, ANTUNES MM, OLIVEIRA M, RODRIGUES RO, ZANIN CICB, SCHIMILE M, LIMA AA (2015) Nitritos e Nitratos em produtos cárneos enlatados e/ou embutidos. *Gestão em Foco*, 7: 246-251.

JANCZYK P, WEIGNERA P, LUEBKE-BECKERB A, KAESSMEYERA S, PLENDLA J (2011) Nitrite pickling salt as an alternative to formaldehyde for embalming in veterinary anatomy - A study based on histo- and microbiological analyses. *Annals Anat*, 193: 71-75.

LAFLAMME D (1997) Development and validation of a body condition score system for cats: a clinical tool. *Feline Pract*, 25: 13-18.

LEITÃO MFF (1978) Microrganismos patogênicos na carne e derivados. *Boletim ITAL Campinas*, 59: 15-48.

MUNRO PM, GAUTHIER MJ, BREITTMAYER VA (1989) Influence of osmoregulation processes on starvation survival of Escherichia coli in seawater. *Appl Environ Microbiol*, 55: 2017-2024.

NISSENBAUM A (1975) The microbiology and biogeochemistry of the Dead Sea. *Microbial Ecology*, 2: 139-161.

OLIVEIRA HP (2008) Situação atual do ensino da técnica cirúrgica e da clínica cirúrgica. *Ciênc vet tróp*, 11: 93-94.

OLIVEIRA FS (2014) Assessing the effectiveness of 30% sodium chloride aqueous solution for the preservation of fixed anatomical specimens: a 5-year follow-up study. *J Anat*, 225: 118-121.

PELOGIA MES, CERQUEIRA ESF, SILVEIRA CPB, ROLIM GS, FECHIS ADS, ROCHA TASS, LAUS JL, OLIVEIRA FS (2018) Suture and venous traction test analysis in dogs fixed in alcohol and preserved in saline solution. *Pesq Vet Bra*, 38: 1834-1837.

PEREIRA N, CARDOZO MV, ROCHA TASS, ÁVILA FA, MACHADO MRF, OLIVEIRA FS (2019) Microbiological analysis of a new anatomical specimen preparation technique for use in veterinary surgery. *Semina Ciências Agrárias*, 40: 3099-3106.

ROCHA TASS, SANTOS CCC, IOZZI MT, DIAS RS, ZERO RC, CARDOZO MV, OLIVEIRA FS (2019) Chemically prepared dog cadavers in teaching of surgical technique - evaluation by students of a veterinary medicine course. *Acta Sci Anat*, 1: 136-140.

ROCHA TASS, YANAGIHARA GR, SHIMANO AC, ROLIM GS, SANTOS CCC, FECHIS ADS, OLIVEIRA FS (2018) Biomechanical analysis of the skin and jejunum of dog cadavers subjected to a new anatomical preservation technique for surgical teaching. *J Plastination*, 30: 16-23.

RODRIGUES H (2010) Técnicas Anatômicas. 3 ed. Arte Visual, Vitória, ES, p 269.

SILVA RMG, MATERA JM, RIBEIRO AACM (2003) Avaliação de ensino da técnica cirúrgica utilizando cadáveres quimicamente preservados. *Revista de Educação Continuada do CRMV-SP*, 6: 1-3.

SILVA RMG, MATERA JM, RIBEIRO AACM (2004) Preservation of cadavers for surgical technique training. *Vet Surg*, 33: 606-608.

SILVA RMG, MATERA JM, RIBEIRO AACM (2007) New alternative methods to teach surgical techniques for veterinary medicine students despite the absence of living animals. Is that an Academic Paradox? *Anat Histol Embryol,* 36: 220-224.

STIRLING ERB, LEWIS TL, FERRAN NA (2014) Surgical skills simulation in trauma and orthopaedic training. *JOSR*, 9: 126.

WERDELMANN R, GERICS B (2016) Preservation of specimens for students – formaldehyde vs. salt based fixative. XXXI Congress of the European Association of Veterinary Anatomists. University of Veterinary Medicine, Vienna, Austria.

WHO – WORLD HEALTH ORGANIZATION (1991) IPCS International Programme on Chemical Safety Formaldehyde - Health and Safety Guide 57: 5-44.

ZERO RC, SHIMANO AC, CARDOZO MV, SANTOS CCC, FECHIS ADS, ROCHA TASS, OLIVEIRA FS (2020) Cadáveres de gatos preparados químicamente para la enseñanza de técnicas quirúrgicas: análisis biomecánico de piel y yeyuno. *Rev investig vet Perú,* 31: e1617.

Young coconut juice increased number of calbindin and vitamin D receptor cells via estrogen receptors in gastrointestinal tract of orchidectomized rats

Mareeyae Hayeelateh[1], Albert M. Hutapea[2], Nisaudah Radenahmad[1]

[1] Division of Health and Applied Sciences, Faculty of Science, Prince of Songkla University, Hat Yai, Songkhla, Thailand
[2] Department of Pharmacy, Faculty of Science, Universitas Advent Indonesia, Bandung Barat, Indonesia

SUMMARY

Adult male rats were orchidectomized, and their gastrointestinal tract was stained immunohistochemically with specific antibodies against calbindin (CB), a calcium-binding protein and vitamin D receptor (VDR), two essential factors in calcium absorption and bone formation. Compared to normal rats, the number of CB-immunoreactive and VDR-immunoreactive cells in the gastrointestinal tract were significantly reduced in orchidectomized rats, but was restored to normal by injecting these rats with estradiol benzoate or by feeding with young coconut juice (YCJ), which was found to be not dose-related. In an attempt to find out if the osteoporosis-protective effects of YCJ were due to the binding of the YCJ active component(s) with estrogen receptors, ERα and ERβ, anti-ERα and ERβ were detected immunohistochemically, and a significant correlation was detected between CB-/VDR-reactive cells vs. ERα-/ERβ-reactive cells. Immunohistochemical profiles showed significant correlations between CB-/VDR-immunoreactive cells vs. ERα-/ERβ-immunoreactive cells. The results suggest that YCJ may be as effective as estradiol benzoate in reducing osteoporosis, probably as a selective estrogen receptor moderator.

Key words: *Cocos nucifera* L – *Arecaceae* – Calbindin – Vitamin D receptor – Osteoporosis – Orchidectomy

ABBREVIATIONS

CB	Calbindin
EB	Estradiol benzoate
ERα	Estrogen receptor-α
ERβ	Estrogen receptor-β
GI tract	Gastrointestinal tract
-ir	-immunoreactive
ORx	Orchidectomized
SERM	Selective estrogen receptor modulator
VDR	Vitamin D receptor
YCJ	Young coconut juice

INTRODUCTION

Osteoporosis is considered a harmful condition. Estrogen replacement therapy has been proposed to prevent bone loss in both females and males (Tu et al., 2018; Rochira et al., 2008). However, this therapy has been implicated with an increased

Corresponding author:
Dr. Nisaudah Radenahmad. Division of Health and Applied Sciences, Faculty of Science, Prince of Songkla University, Hat Yai, Songkhla, Thailand. E-mail: nisaudah@gmail.com

Submitted: August 20, 2021. **Accepted:** January 10, 2022

https://doi.org/10.52083/PIFI7968

risk of breast cancer in women and prostate cancer in men (Bitzer et al., 2008; Chen et al.,2015).

The gastrointestinal (GI) tract is responsible for many functions, e.g., nutrient, electrolyte and fluid, including calcium absorption. Calcium homeostasis is regulated by parathyroid hormone and vitamin D, and calcium plays a vital role in many crucial mechanisms, including cell differentiation, intracellular signaling, and bone formation (Kirchhoff and Geibel, 2006). Our previous study used Grimelius stain, a broad endocrine cell marker especially in the GI tract, to quantify the argyrophilic endocrine cells and, when applicable, to reflex GI functions, e.g., calcium absorption, GI motility, which might have an influence on osteoporosis in male rats. We have previously reported a decrease of GI argyrophilic endocrine cells in both male and female osteoporotic rat models, and young coconut juice (YCJ) feeding reversed this phenomenon (Sayoh et al., 2008; Radenahmad et al., 2014). Two preliminary studies were also conducted using the same model on the effects of YCJ on increasing the condylar cartilage thickness and mandibular cancellous bone in orchidectomized (ORx) rats by our group (Yusuh et al., 2010; Suwanpal et al., 2011). Later, we found that YCJ has estrogenic effects to prevent bone loss in ovariectomized rats (Yooprasert et al., 2015).

Calbindin-D9k (CaBP-9k), hereafter will be referred to as calbindin (CB), is a cytosolic vitamin D-dependent calcium-binding protein that strongly binds calcium, and is expressed in various tissues, such as the pituitary gland, uterus, placenta, intestines, kidneys, and bones (Choi and Jeung, 2008). It regulates cytoplasmic calcium concentration by facilitating calcium uptake to maintain intracellular Ca^{2+} concentrations below 10^{-7} mol/L. This regulatory role is essential to prevent cell death from free calcium toxicity (Hong and Jeung, 2013) and premature apoptotic cell death (Barboza et al., 2015).

Vitamin D plays an essential function in calcium homeostasis, and, in its active form of 1,25-dihydroxy, vitamin D3 is a potent stimulator of active intestinal calcium absorption through the active transcellular pathway, one of the essential pathways that carry out intestinal calcium uptake and the passive paracellular pathways through tight junctions, through the enterocytes, then to the body (Christakos et al., 2011).

Since calcium is an essential mineral in bones, intestinal calcium absorption through vitamin D and calbindin (Lee et al., 2003) plays a significant role in calcium uptake through the alimentary canal. Altogether, with this background, the aim of the present study was, therefore, to find out if YCJ could prevent osteoporosis in orchidectomized male rats by detecting calbindin and vitamin D receptor (VDR) cells in the GI tract, in addition to their effect on the ovariectomized rats (Jiangsakul et al.,2015). The number of ERα- and ERβ-immunoreactive cells were also investigated to determine if YCJ could act through these receptors.

Thus far, the active ingredient(s) of YCJ has not been identified, although it was suspected to be β-sitosterol (Rattanaburee et al., 2014) and probably to be isoflavone group due to its wound healing property. It was found that YCJ at 100 mL/kg BW/day caused unfavorable glycogen deposition in the liver in ovariectomized rats (Radenahmad et al., 2012 unpublished data). Therefore, in the present study, three lower doses (10, 20, and 40 mL/kg BW/day) were designed to investigate whether it effectively prevents osteoporosis via preventing relevant cells in the GI tract of orchidectomized rats.

MATERIALS AND METHODS

YCJ preparation

A large volume of YCJ was collected from Khlong Hoi Khong district, Hat Yai, Songkhla, Thailand. It was then dried, and the powder formed was kept at -30°C until used. The powder was freshly reconstituted and prepared daily for oral intake. A complete description of YCJ, including its preparation and administration, is provided in our previous publication (Radenahmad et al., 2006).

Animals

Adult male Wistar rats (8-month-old and 250-300 g) were purchased from Mahidol University, Salaya campus. The animals were maintained on standard food pellet housed in a room free from any source of chemical contamination, artificially illuminated (12h dark/light cycle), and under

controlled thermal (25 ± 1°C) and humidity (50 ± 5%) conditions, at the Animal House Laboratory, Faculty of Science, Prince of Songkla University, Hat Yai, Songkhla, Thailand. All animals were received humane care in compliance with the guidelines of the Animal Care and Use Committee of Prince of Songkla University and the National Institutes of Health (NIH publication 86-23 revised 1985. The protocol was approved under the license number 01/59).

Experimental design

After an acclimatization period of 1 week, the animals were divided into seven groups (10 rats/ group) and treated for ten weeks as follows: group 1, normal baseline control (NC) animals, were sacrificed on the first day of the experiment without any treatment; group 2, sham-operated rats (SC), received reverse-osmosis water; groups 3, orchidectomized rats, received reverse-osmosis water (OC); group 4, ORx rats, intraperitoneally injected three days a week with 2.5 µg/ kg BW estradiol benzoate, EB (OE). The dose of EB given was the same as in our previous studies (Radenahmad et al., 2009; 2012); groups 5, 6, and 7, ORx rats orally treated with YCJ at 10, 20, and 40 mL/kg BW/day (OJ10, OJ20, and OJ40), respectively (Table 1a). At the end of the treatment period, all animals were sacrificed, and the stomach (body and fundus), small intestines (duodenum, jejunum, ileum), and colon of each

Table 1. Animal grouping, antibodies, concentration, and manufacturer used for GI sections of each rats.

a. Animal grouping (10 rats per group).

Group	Treatment
NC	Normal (normal control)
SC	Sham-operated, received reverse-osmosis water (sham control)
OC	Orchidectomized, received reverse-osmosis water (ochidectomized control)
OE	Orchidectomized, and injected with estradiol benzoate (EB, 2.5 µg/kg BW) 3 days a week, for 10 wks
OJ10	Orchidectomized, received YCJ at 10 mL/kg BW/d for 10 wks
OJ20	Orchidectomized, received YCJ at 20mL/kg BW/d for 10 wks
OJ40	Orchidectomized, received YCJ at 40mL/kg BW/d for 10 wks

b. Description of slides for immunostaining for each rat GI regions.

Section No.	Staining
1-2	H & E staining, for histological orientation
3-4	Anti-calbindin antibody (N0142, Sigma-Aldrich, USA)
5-6	Anti-VDR antibody (P3088, Sigma-Aldrich, USA)
7-10	For sections 7 and 8, mouse anti-estrogen receptor α (aa-120-170) antibody (MAB447, Chemicon international, USA) and for sections 9 and 10, estrogen receptor β antibody (PA1-310B, Thermo Fisher Scientific, USA)
11-12	Immunostaining, omitting primary antibodies (negative control), one for each antibody

c. Dilutions of each antibody for each organ of GI tract (body and fundus of stomach; duodenum, jejunum, and ileum of small intestine; colon).

	Antibodies			
Organs	**VDR**	**Calbindin (CB)**	**ER-alpha**	**ER-beta**
Body	1:500	1:500	1:100	1:50
Fundus	1:500	1:500	1:100	1:50
Duodenum	1:500	1:100	1:500	1:100
Jejunum	1:500	1:100	1:500	1:75
Ileum	1:500	1:50	1:800	1:75
Colon	1:500	1:100	1:500	1:200

animal were removed, fixed with 10% neutral formalin, paraffin processing, sectioning, and immunohistochemical staining.

Immunohistochemistry

Twelve 5 µm-thick sections from each block were prepared for Hematoxylin and Eosin (H&E) stain and immunostaining (Table 1b and 1c). For immunostaining, the glass slides were coated with the poly-L-lysine solution. Sections of uterus and ovary from normal female rats were used as positive controls for ERα, and ERβ immunostaining, respectively, and the staining process was performed according to the method previously described (Radenahmad et al., 2009; 2012). Details of all antibodies, concentrations, and manufacturers used for GI sections of each rat can be consulted in Tables 1b and 1c.

Quantitative analysis of immunoreactive cells

The total number of immunoreactive cells from the stomach, small intestines, and colon were counted under light microscopy with 40x magnification power. Two blinded observers performed the counting on ten random fields of each slide using an image analysis system (Samba microscopic image processor; Samba Technologies, Meylan, France). Readings from 3 sections pertaining to each antibody were averaged and expressed as the mean number of immunoreactive cells/mm^2.

Statistical analysis

Shapiro-Wilk test was applied to test the normal distribution. Statistical analysis was performed using the One-way ANOVA, followed by the LSD test available in the statistical program SPSS version 16.0 (SPSS, Inc., Chicago, IL, USA). Altman's nomogram was used for calculations of sample size. Random selection of the microscopic fields was achieved using a computer-generated list of random numbers (Excel version 5.0). Results were expressed as mean ± SEM. A $p<0.05$ value was considered significant.

RESULTS

Figs. 1 and 2 depict examples of immunoreactive cells for CB, VDR, ERα, and ERβ in the GI specimens of the control groups. The most colorful staining for each antibody, the highest and the lowest

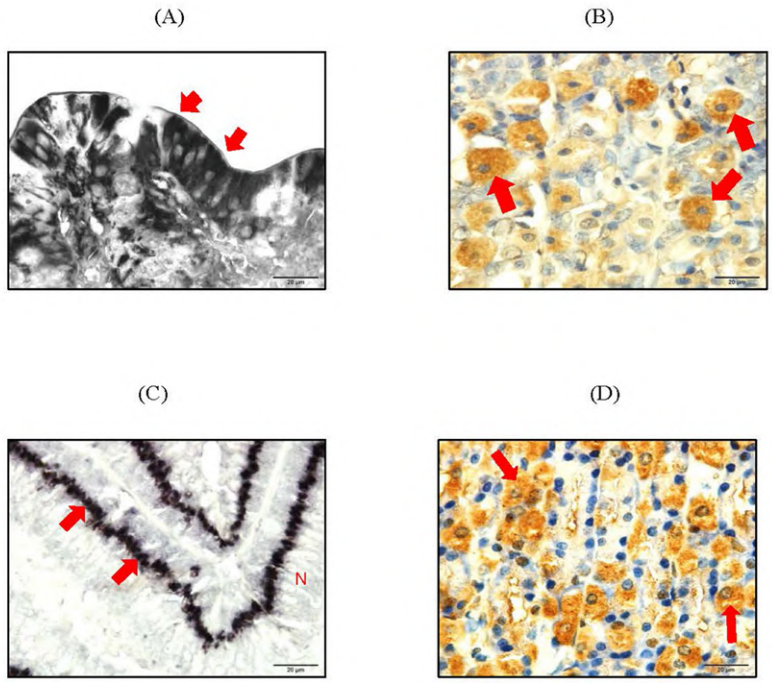

Fig. 1.- Examples of cells that were CB- (A), VDR-(B), ERα-(C) and ERβ-(D) immunoreactive cells in different parts of the gastrointestinal tract of the control groups (N = nucleus). **A)** CB-immunoreactive cells in the cytoplasm of the colon epithelium. **B)** VDR-immunoreactive cells in the cytoplasm of parietal cells of the stomach. **C)** ERα-immunoreactive cells in the villi of enterocyte of duodenum. **D)** ERβ-immunoreactive cells in the cytoplasm of parietal cells of the stomach. Scale bars: 20 µm.

number of immunoreactive cells of each organ, is shown in Table 2a. The CB and VDR were localized in parietal cells of the fundus and the body of the stomach. A positive reaction was observed in the cytoplasm, but not in the nucleus of stomach parietal cells, in enterocytes of the small intestine villi, and colonocytes of the colon. The ERα and ERβ were observed in the cytoplasm, not in the nucleus of the stomach's parietal cells. Surprisingly, a positive reaction was located in the perinuclear cytoplasm of enterocytes of villi throughout the small intestines and colon. In

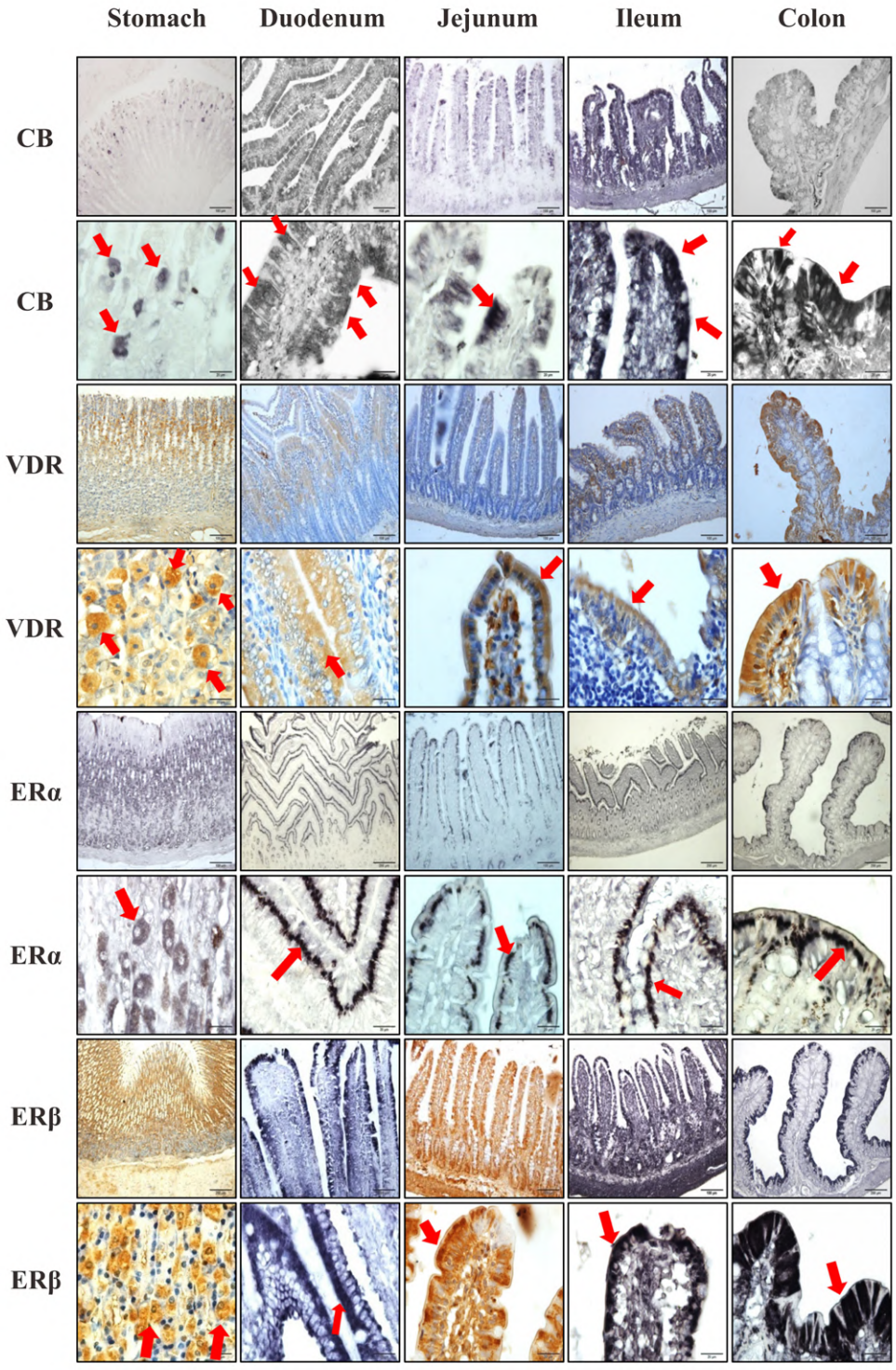

Fig. 2.- Photographs showing immuno-histochemistry of CB-, VDR-, ERα- and ERβ- immunoreactive cells from the stomach, duodenum, jejunum, ileum and colon of the control groups. CB-, VDR-, ERα- and ERβ-immunoreactivity was observed in the cytoplasm of parietal cells of stomach, cytoplasm of enterocytes of small intestines and colon. The same scale is used for all pictures of each row. The first row of each antibody is at 20x magnification, while the next row of the same antibody is at 100x magnification. Red arrows indicate immunoreactive cells for each antibody. Scale bars: 100 µm, 20 µm respectively.

addition, ERα immunoreactivity was found at the nucleus of the intestinal gland of the jejunum and the ileum. The ERα immunoreactivity was highest in the cytoplasm of the colonocytes. In contrast, The ERβ immunoreactivity was highest in the cytoplasm of parietal cells of the stomach.

In addition, ERα-ir cells were found at the nucleus of intestinal gland of the jejunum and the ileum. The intensity of ERα immunoreactivity was the strongest in the cytoplasm of the colonocytes. In contrast, The ERβ-ir cells were detected strongest in the cytoplasm of the parietal cells of the stomach.

Fig. 3A depicts the number of immunoreactive CB (CB-ir) cells in various regions of the GI tract. In the NC and SC groups, the immunoreactive cells were observed at high frequency in all regions. Following orchidectomy, the numbers of CB-ir cells significantly dropped in almost all regions except that in the duodenum. The values increased to normal when the ORx rats were treated with EB, except in the ileum. With YCJ treatments, the number of immunoreactive cells increased but was not dose-related. The number of CB-ir cells of all three OJ groups were not significantly different when compared to each other, nor when compared with the control groups, except in the ileum, where all three OJ groups were significantly lower than that of the NC and SC groups. The number of CB-ir cells in the OJ10 group (fundus) was, nevertheless, significantly higher than that of the NC, SC, OC, and OE groups.

In summary, the total number of CB-ir cells per mm^2 of seven groups examined was found highest in the duodenum (189.95±41.59), and the lowest in the fundus of the stomach (3.07±1.20) (Table 2b).

Table 2a. Description of each antibody for the most beautiful staining, the highest and the least number of positive staining of 6 regions of GI tract examined.

Antibodies	The most colorful staining	The highest number of positive staining	The least number of positive staining
CB	Colon	Duodenum	Stomach (Fundus)
VDR	Stomach	Colon	Stomach (Fundus)
ERα	Duodenum	Ileum	Stomach (Fundus)
ERβ	Colon	Stomach (Fundus)	Duodenum

Table 2b. Total number of immunoreactive cells of each antibody in 6 regions of gastrointestinal (GI) tract.

Antibodies	Organs Regions	Total number of Immunoreactive Cells (per mm^2) in 7 groups examined
CB	Fundus of Stomach Body of Stomach Duodenum Jejunum Ileum Colon	3.07 ± 1.20 3.96 ± 1.02 189.95 ± 41.59 56.47 ± 18.38 65.65 ± 17.47 91.14 ± 16.87
VDR	Fundus of Stomach Body of Stomach Duodenum Jejunum Ileum Colon	66.90 ± 12.71 81.77 ± 10.98 292.83 ± 72.31 249.84 ± 54.21 150.60 ± 34.97 340.97 ± 32.02
ERα	Fundus of Stomach Body of Stomach Duodenum Jejunum Ileum Colon	166.73 ± 23.08 235.77 ± 37.41 724.15 ± 126.27 580.43 ±93.02 760.92 ± 133.64 417.38 ±69.77
ERβ	Fundus of Stomach Body of Stomach Duodenum Jejunum Ileum Colon	542.58 ±46.54 718.89 ± 70.65 239.26 ± 34.84 378.68 ± 58.44 495.46 ± 73.47 242.19 ± 35.20

In contrast, the number of VDR-ir cells, compared with CB-ir cells region by region, increased in all six regions of the GI tract. In the NC and SC groups, VDR-ir cells were observed at a high number in all regions. Following orchidectomy, the numbers of VDR-ir significantly dropped in all six regions examined, then was reversed when treated with EB or YCJ treatments. With YCJ treatments, the increase of the immunoreactive cells was not dose-related (Fig. 3B).

Among the three doses of YCJ treatments, the numbers of VDR-ir in the OJ20 group were highest in the fundus and body of stomach, duodenum and jejunum, while VDR-ir cell numbers in the OJ10 group were highest in the colon. The number of VDR-ir cells in the OJ20 and OJ40 groups were comparable to those of the control (NC and SC groups). Surprisingly, there was no significant difference in the duodenum when the OJ groups were compared with the control

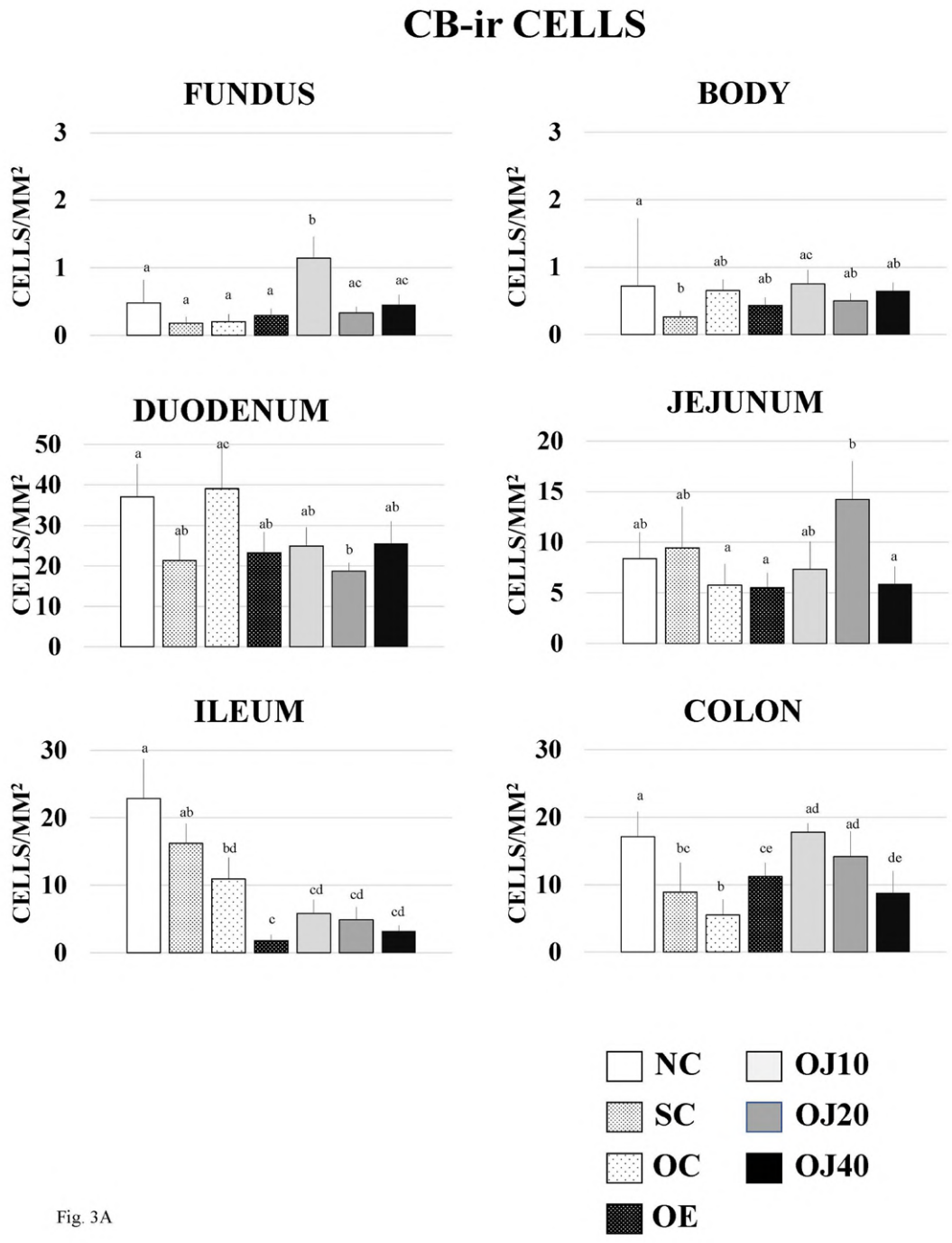

Fig. 3A

Fig. 3.- 3A) Number of CB-immunoreactive cells from the fundus, body, duodenum, jejunum, ileum, and colon. Columns superscript with different letters are significantly different at $p < 0.05$.

groups, neither when each group was compared (Figure 3B). In summary, Table 2b shows the total number of immunoreactive cells per mm^2 in the six regions. The highest was found in the colon (340.97±32.02), and the lowest in the fundus of the stomach (66.90±12.71).

Fig. 3C shows that, unlike VDR-ir cells, ERα-ir cells were found in more significant numbers in all six regions of the GI tract examined in this study. Nevertheless, the number of immunoreactive cells in the control and the YCJ treatment groups were like that of VDR-ir cells. In the NC and SC groups, like VDR-ir, the positive cells were observed at high frequency in all regions. Following orchidectomy, the numbers of ER-ir cells significantly dropped in all six regions. The number increased when the ORx rats were treated with EB or YCJ treatments. With YCJ treatments, the numbers of the immunoreactive cells did not increase in a

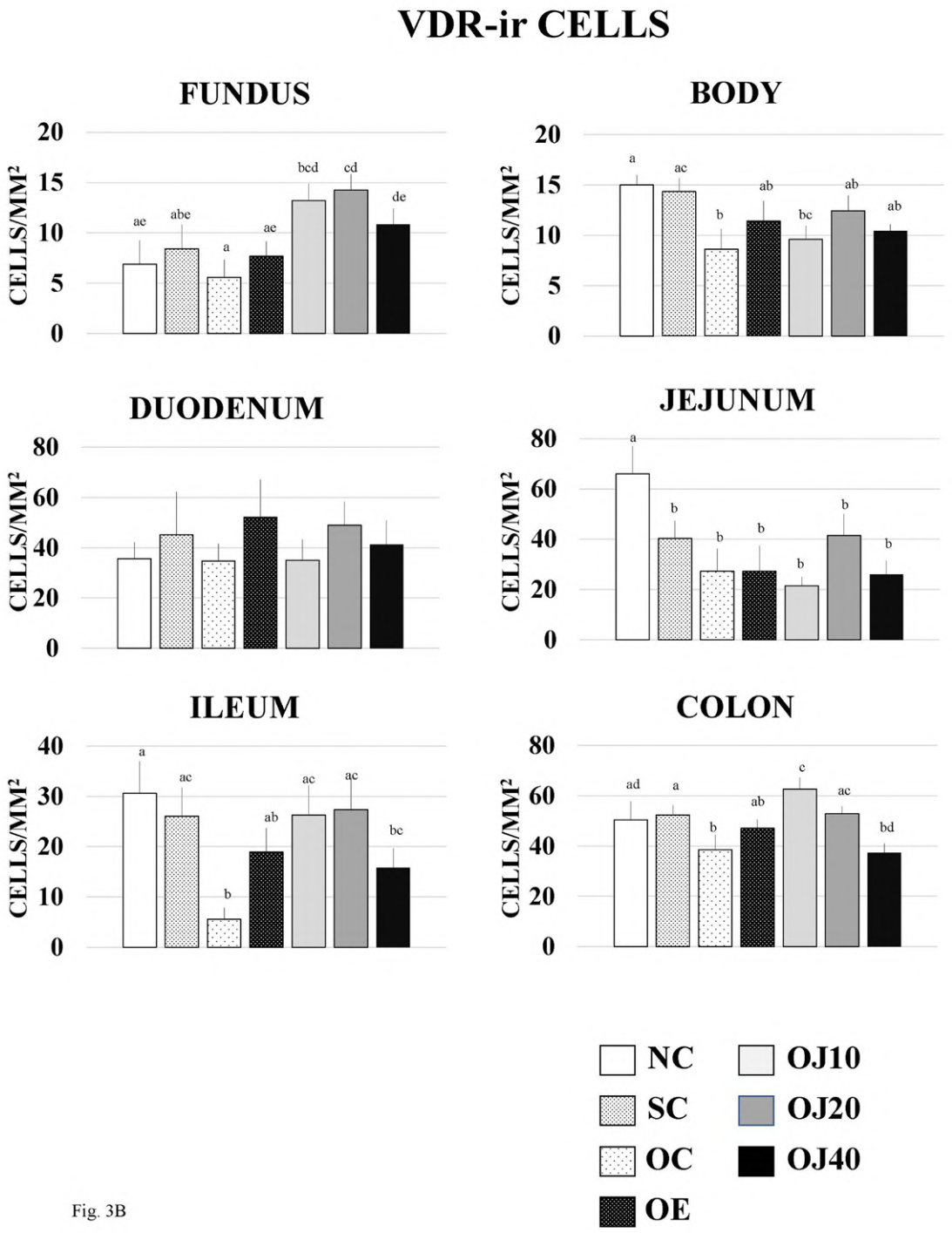

Fig. 3B

Fig. 3.- 3B) Number of VDR-immunoreactive cells from the fundus, body, duodenum, jejunum, ileum, and colon. Columns superscript with different letters are significantly different at $p < 0.05$.

dose-related manner. The OJ10 group showed the highest ERα-ir cell number in almost all regions understudies, while the OC group had the lowest number in all six regions examined. Surprisingly, there was no significant difference between the number of ERα-ir cells in the body of the stomach and the jejunum of OJ groups and control groups, neither when the groups were compared to each other. In summary, the total number of ERα-ir per mm^2 in the six regions examined was highest in the ileum (760.92±133.64), and the lowest in the fundus of the stomach (166.73±23.08) (Table 2b).

Table 2b shows that the number of ERβ-ir was higher than ERα-ir in all six regions of the GI tract examined in this study but was comparable to a number of ERα-ir cells in the control and the YCJ treatment groups. Fig. 3D shows that, following orchidectomy, the number of ERβ-ir significantly dropped in all six regions examined except in the

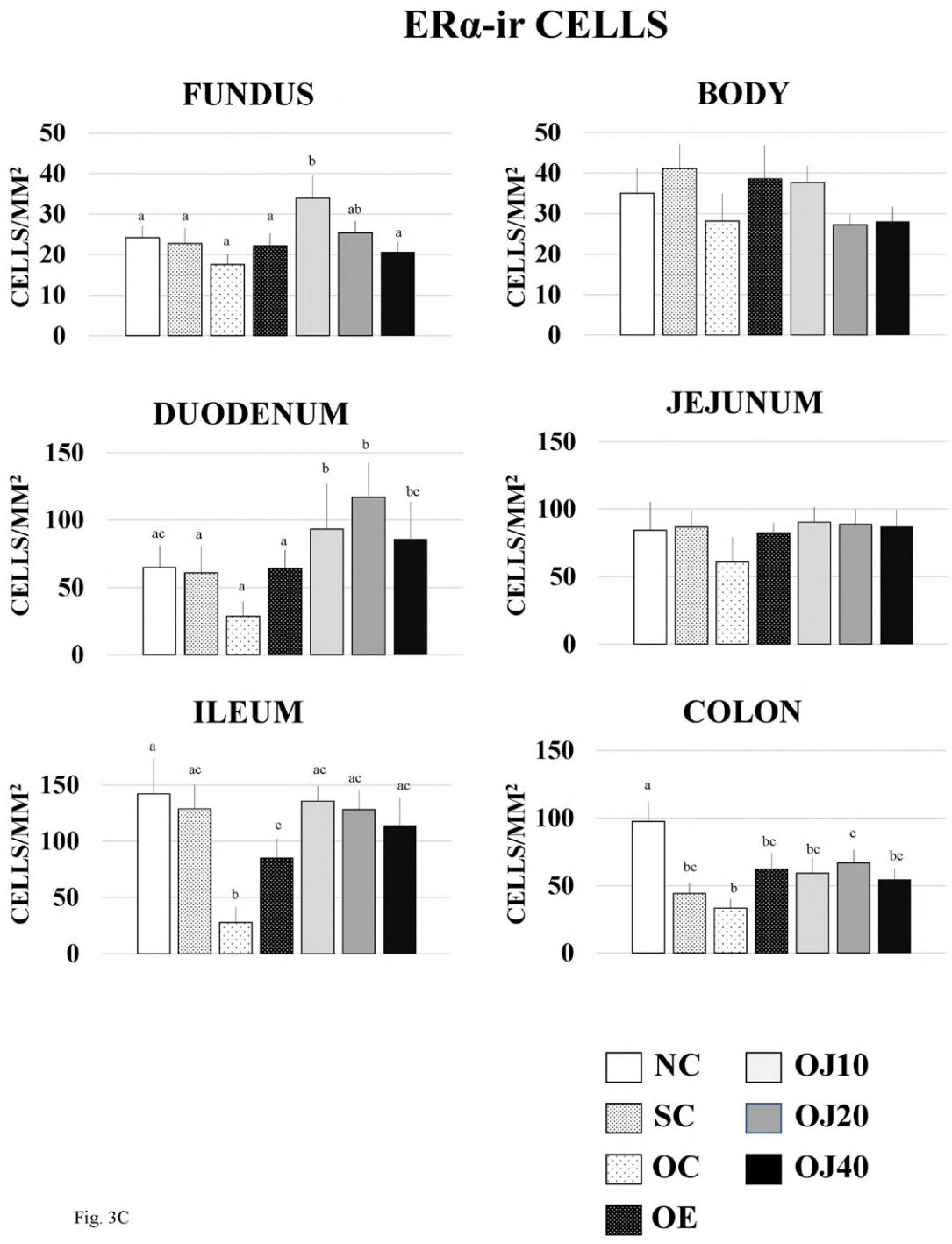

Fig. 3C

Fig. 3.- 3C) Numbers of ERα-immunoreactive cells from the fundus, body, duodenum, jejunum, ileum, and colon. Columns superscript with different letters are significantly different at $p < 0.05$.

body of the stomach, then increased when the ORx rats were treated with EB or YCJ treatments. With YCJ treatments, the numbers of the immunoreactive cells increased comparably with the control groups (NC and SC). In addition, in the body of the stomach, there was an insignificant difference between the OJ groups and the control groups, neither when each group was compared to the other. On the contrary to the other three antibodies, CB, VDR, and ERα, the total number of ERβ-ir per mm^2 in the six regions examined were highest in the body of the stomach (718.89±70.65) and the lowest in the duodenum (239.26±34.84) (Table 2b).

To find out if the numbers of CB-ir, VDR-ir were correlated to each other and with the numbers of ERα- and ERβ-ir cells, the number of CB-ir cells were plotted against those of VDR-, ERα- and ERβ-ir cells in the same animals, regardless of groups

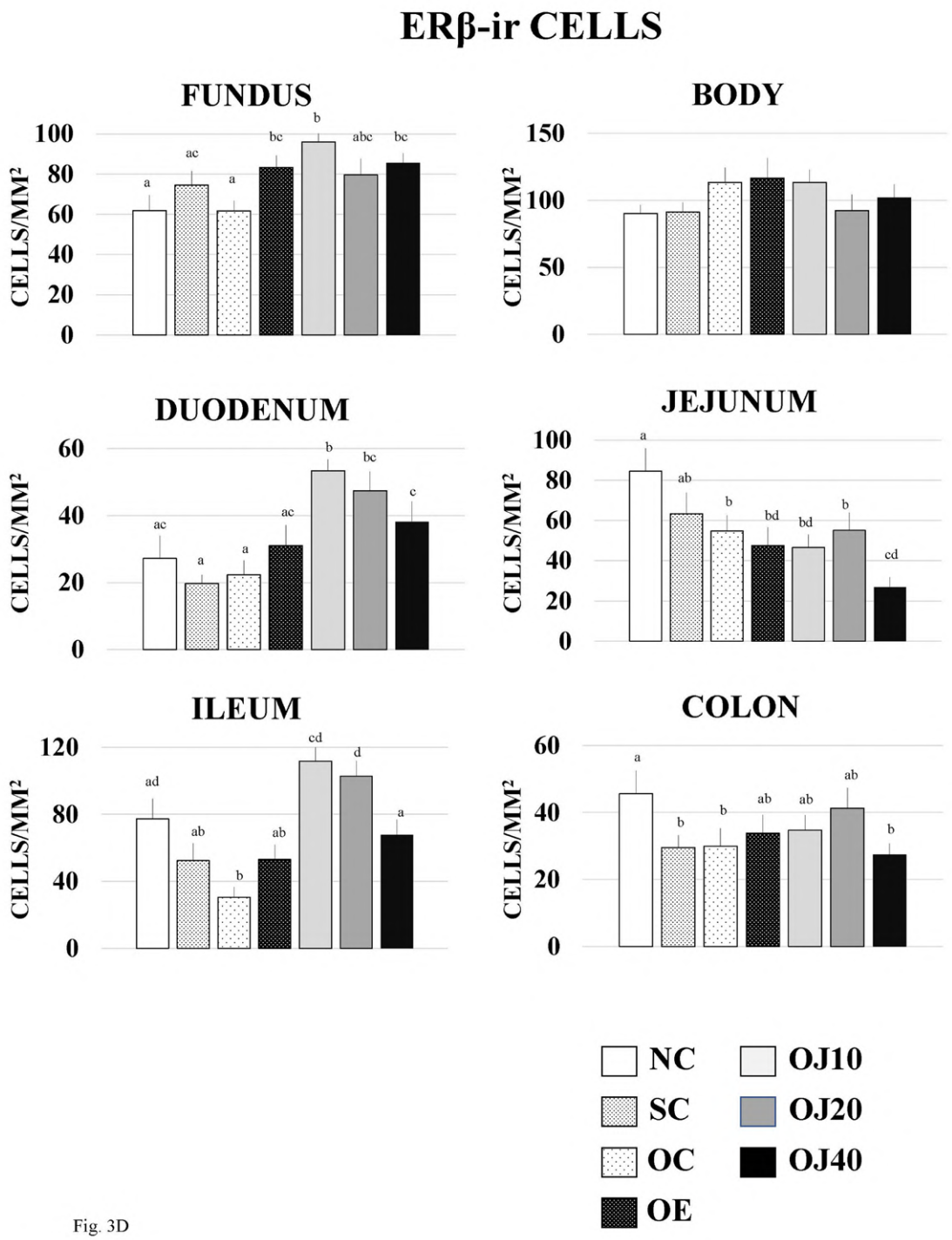

Fig. 3D

Fig. 3.- 3D) Number of ERβ-immunoreactive cells from the fundus, body, duodenum, jejunum, ileum, and colon. Columns superscript with different letters are significantly different at $p < 0.05$.

(Fig. 4). Likewise, the number of VDR-ir cells was plotted against those of ERα- and ERβ-ir cells.

The results revealed that the number of CB-ir cells was positively correlated with the number of VDR-ir cells in all regions of the GI tract (stomach, small intestine, and colon). The number of CB-ir cells were correlated positively with the numbers of ERα- and ERβ-ir cells, except in the ileum. The numbers of CB-ir correlated negatively with ERα-ir cells. The number of VDR-ir positively correlated with that of ERα- and ERβ-ir in all regions of the GI tract.

DISCUSSION

For centuries, YCJ has been used for various therapeutic purposes, but not for the prevention of

Fig. 4

(a)

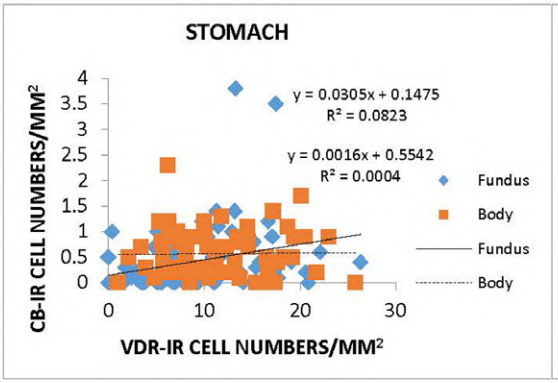

Fundus (R^2 = 0.0823, p = 0.016073)

Body (R^2 = 0.0004, p = 0.875328)

(b)

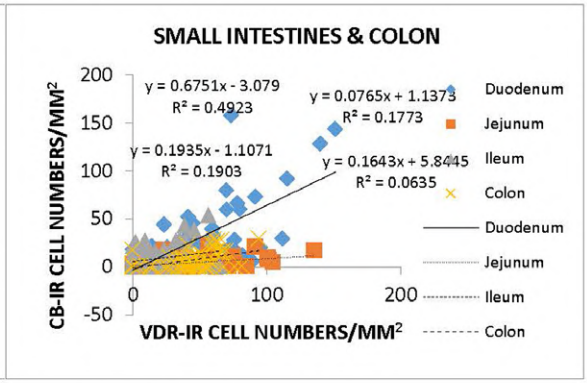

Duodenum (R^2= 0.4923, p = 1.32x10^{-11})

Jejunum(R^2= 0.1773, p = 0.000284)

Ileum(R^2= 0.0635, p = 0.035321335)

Colon(R^2 = 0.1903, p = 0.00016)

(c)

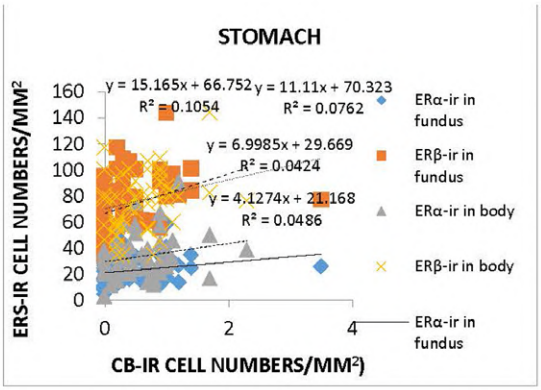

Fundus (CB vs ERα) (R^2 = 0.0486, p = 0.09048)

Fundus (CB vs ERβ) (R^2= 0.0762, p = 0.032729)

Body (CB vs ERα) (R^2 = 0.0424, p = 0.127793)

Body (CB vs ERβ)(R^2= 0.1054, p = 0.014646)

(d)

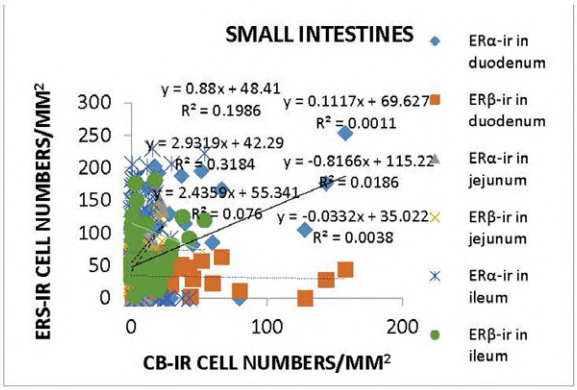

Duodenum (CB vs ERα)(R^2 = 0.1986, p = 0.000577)

Duodenum (CB vs ERβ) (R^2= 0.0038, p = 0.653447)

Jejunum (CB vs ERα) (R^2 = 0.076, p = 0.039799)

Jejunum (CB vs ERβ) (R^2= 0.3184, p = 5.92 x 10^{-6})

Ileum (CB vs ERα) (R^2 = 0.0186, p = 0.3155753)

Ileum (CB vs ERβ) (R^2= 0.0011, p = 0.80560674)

Fig. 4.- Plot of numbers of the CB-immunoreactive cells against the numbers of ERα-and ERβ-ir cells of the stomach **(a)**, of the small intestines and colon **(b)**; the CB-immunoreactive cells against the numbers of ERα- and ERβ-ir cells of the stomach **(c)**, of the small intestines **(d)** from the same rats and from all animal groups.

(e)

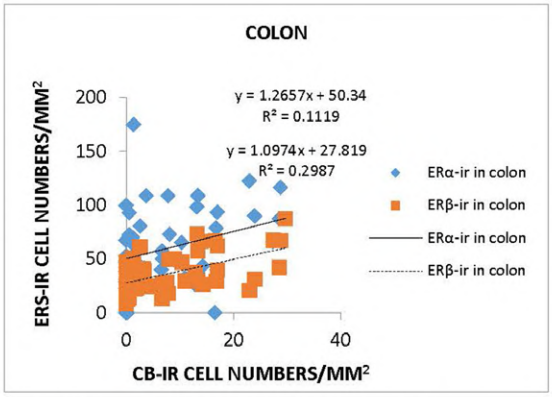

(f)

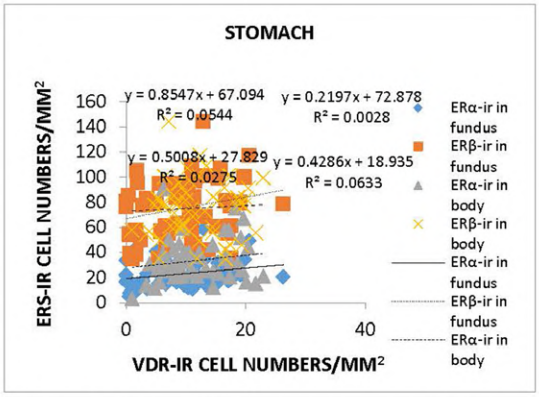

Colon (CB vs ERα)(R^2 = 0.1119, p = 0.0117366)

Colon (CB vs ERβ)(R^2= 0.2987, p = 1.31 x 10^{-5})

Fundus (VDR vs ERα)(R^2 = 0.0633, p = 0.052576)

Fundus (VDR vs ERβ)(R^2= 0.0544, p = 0.072767)

Body (VDR vs ERα)(R2 = 0.0275, p = 0.221759)

Body (VDR vs ERβ) (R^2= 0.0028, p = 0.698397)

(g)

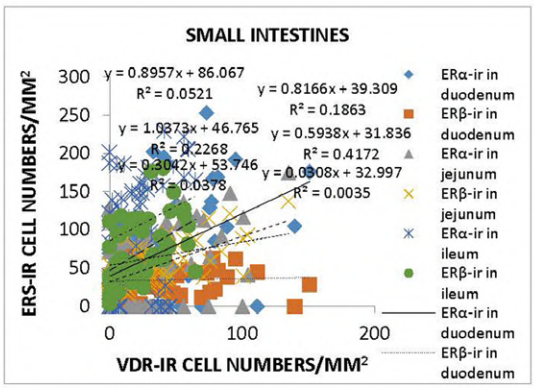

(h)

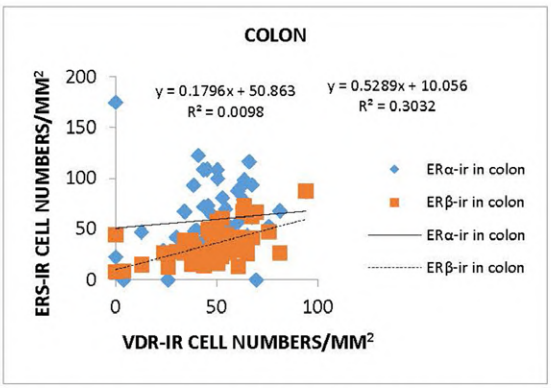

Duodenum (VDR vs ERα) (R^2 = 0.1863, p = 0.000896)

Duodenum (VDR vs ERβ) (R^2= 0.0035, p = 0.664124)

Jejunum (VDR vs ERα) (R^2 = 0.0378, p = 0.150797)

Jejunum (VDR vs ERβ) (R^2= 0.4172, p = 7.62 x 10^{-8})

Ileum (VDR vs ERα) (R^2 = 0.0521, p = 0.090592)

Ileum (VDR vs ERβ)(R^2= 0.2268, p = 0.000207125)

Colon (VDR vs ERα)(R^2 = 0.0098, p = 0.466974)

Colon (VDR vs ERβ)(R^2= 0.3032, p = 1.097 x 10^{-5})

Fig. 4.- Plot of numbers of the CB-immunoreactive cells against the numbers of ERα-and ERβ-ir cells of the colon **(e)**; the VDR-immunoreactive cells against the numbers of ERα- and ERβ-ir cells of the stomach **(f)**, of the small intestines **(g)**, of the colon **(h)** from the same rats and from all animal groups.

osteoporosis. We were the first research group to report back in 2014 that ORx/sham rats receiving YCJ at 100 mL/kg BW had a significantly higher number of argyrophilic endocrine cells in the GI tract as compared to controls (Radenahmad et al., 2014). Argyrophil endocrine cells are involved in GI functions, e.g., calcium absorption and GI motility, which might influence osteoporosis. These observations, nevertheless, were merely based on special staining, the Gremelius staining used in our study. To take one step further, we conducted the current study to investigate the microscopic changes inside the mucosa, including the epithelium and glands, using an immunohistochemical technique to detect the involvement of calbindin and vitamin D receptors in calcium absorption. Estrogen acts via estrogen receptors (ERs), currently known as ERα and Erβ. Therefore, anti-ERα and anti-ERβ antibodies were used in order to explore the possibility of phytoestrogenic properties of YCJ.

These results confirmed the thesis in our previous study, namely that argyrophilic cells detected by the Gremelius staining and CB-ir, a calcium-binding protein, and VDR-ir cells were mostly restored to normal level after feeding with YCJ in most regions of the GI tract of ORx rats.

The fact that calcitriol exerts its effect on calcium uptake by epithelial cells or other reactions rapidly raises some speculations about the possibility of a second VDR in the plasma membrane, associated with caveolae and a second calbindin protein in the cytoplasm (Norman, 2006). It has been reported that extra-nuclear estrogen receptors associated with the plasma membrane and or cytoplasmic organelles facilitate acute effects of estrogen on neuronal signaling (Hart et al., 2007).

Earlier, calbindin (CaBP-9k) mRNA expression was not detected by Northern blot analysis before in dairy cattle (Yamaguchi et al., 2002). However, a Ca^{2+}-sensing receptor (CaSR) has been identified on the basolateral membrane of rat parietal cells (Caroppo et al., 2001; Cheng et al., 1999). Studies in both rat and human stomachs found that CaSR plays an important regulatory role in acid secretion and mucosal repair (Kirchhoff and Geibel, 2006). We are the first group that identified the presence of calbindin in parietal cells and hypothesized that these cells are involved in calcium absorption. In the stomach, the number of CB-ir cells positively correlated with the numbers of ERα- and ERβ-ir cells, except for CB-ir with ERα-ir in the body of the stomach, implicating the possibility that phytoestrogen of YCJ might have influenced on CB-ir cell production in the stomach. Whether the acid secretion is involved in calcium absorption needs clarification. Nevertheless, the number of CB-ir cells in the stomach was much less than in small and large intestines. This agrees with a report by Lee et al. (2003), using Northern blot that CB-ir cells in the stomach were shown to be much less than that of the duodenum.

The expression of CB was detected primarily in the enterocytes of the duodenal villi. CB functions to regulate the amount of intracellular calcium to prevent cell death from the toxicity of free calcium (Hong and Jeung, 2013). Delorme et al. (1983) reported that the CaBP-9k gene is expressed in rat intestine due to its vitamin D-responsive DNA element (VDRE). However, in humans, this gene is only active in the duodenal mucosa epithelial cells, and its expression progressively decreases downstream from the duodenum, and it is scarcely found in the ileum and large intestine (Walters et al., 1999).

In the present study, very few CB-ir cells were found in the fundus and body of the stomach, and its expression level did not decrease downstream like in humans. The highest number was found in the duodenum, lowest in the jejunum, and increased distally from the ileum toward the colon. However, the highest number was found in the duodenum, as in the previous research reports, e.g., Yamagishi et al. (2002) and Sidler-Lauff et al. (2010). Factors such as the residence time and the absorption rate in a particular intestinal segment determine the amount of calcium absorbed (Wesserman, 1997). This phenomenon could be due to species variation. The number increases once again in the colon, implicating the calcium absorption function of this organ, since it was found that the incidence of osteoporosis increases in IBS (inflammatory bowel diseases) patients (Targownik et al., 2013).

It has been reported that estrogen may play a determinant physiological role in the amount of calcium absorbed from the intestine, where the presence of estrogen receptors has consistently been indicated in the mucosa of the alimentary tract (Fernandez et al., 1996; Francavilla et al., 1987; Hendrickse et al., 1993; Meggouh et al., 1991), which might include post-orchidectomy, as in the present study. The present study found that reduction of testosterone in ORx rats decreased CB production, but EB and YCJ treatments increased its production by cells in many regions of the GI tract, e.g., the fundus of the stomach, the jejunum, and the colon. In this study, YCJ treatment increased the number of CB-ir cells in OJ groups compared with the OE group. This agrees with the report by Patisaul and Jefferson (2010), which stated that soy phytoestrogen has health benefits with fewer adverse effects compared with synthetic (exogenous) estrogen.

Furthermore, the number of CB-ir cells correlated positively with the numbers of ERα- and ERβ-ir cells, except in the ileum. Using Micro-

CT and immunohistochemistry techniques, we found that exogenous estrogen (EB) and YCJ prevent osteoporosis in lumbar (L5) and femur bones (Yooprasert et al., 2015; Asae et al., 2017). Therefore, estrogen/phytoestrogen might influence CB production not only in the stomach but also in small and large intestines that influence bone calcium deposition. Further investigation is needed to clarify whether calcium uptake by parietal cells in the stomach or calcium uptake by enterocytes in the small and large intestine is also regulated by sex steroid hormones, e.g., estrogen, or phytoestrogen, e.g., YCJ, by increasing CB.

Physiologic interactions among various mechanisms of the PTH-vitamin D-endocrine system structured in a multilevel negative feedback loop determine the rate of active intestinal calcium absorption. Active calcium absorption from the intestine occurs in two primary mechanisms. One, through passive diffusion, when the luminal calcium is high, and two, through a more complex active absorption mediated by $1,25(OH)_2D_3$ when the luminal calcium is low (Bringhurst, 1995). Under the stimulation of parathyroid hormone (PTH), the kidney produces $1,25(OH)_2D_3$, where PTH secretion itself is influenced by the extracellular free calcium concentration detected by the calcium-sensing-receptors located in the membranes of parathyroid cells (Chattopadhyay et al., 1996).

With age, there is a decline in intestinal calcium absorption in humans (Avioli et al., 1965; Bullamore et al., 1970) and in rats (Russell et al., 1986). It has been suggested that, besides the PTH and vitamin D, estrogen also has specific physiological functions in the alimentary canal as indicated by the presence of its receptor (Fernandez et al., 1996; Francavilla et al., 1987; Meggouh et al., 1991; Hendrickse et al., 1993), the estrogen-receptor-associated proteins (Theisinger et al., 1993; Luqmani et al., 1992; Welter et al., 1994) and ER-D5 (Takeda et al., 1992) in this organ. Whether this is true with the function of estrogen in the stomach needs further investigation.

We were the first group to discover vitamin D receptors in parietal cells and enterocytes all along small and large intestines. The highest number of VDR-ir cells was found in the duodenum, agreeing with Sidler-Lauff et al. (2010), but in contrast with other reports. Christakos (2011) found that the highest levels of VDR were in the cecum and the colon, implicating the calcium absorption function of this organ and maybe acting together with CB-ir cells. Colonic calcium absorption is vitamin D-responsive, and it becomes important in conditions such as short bowel syndrome (Wada et al., 2009; Wali et al., 1990).

The findings reported by Teerapornpuntakit et al. (2009) and Zhang et al. (2010) reveal that TRPV6 protein and CB are detectable in all intestinal segments, in mice and rats, and the strongest immunoreactivity expression of TRPV6 is in the cecum and the colon. These reports also indicate that, in addition to the duodenum, the intestinal distal segment plays an important function in $1,25(OH)_2D_3$-mediated calcium homeostasis (Christakos et al., 2011).

Following orchidectomy, VDR-ir cells significantly dropped in all six regions examined. The number increased when the ORx rats were treated with EB or YCJ, indicating that estrogen and YCJ administration effectively restored the normal responsiveness of the GI to vitamin D. The finding agrees with reports by Gennari (1990), Civitelli (1988), and Heaney (1978) that estrogen administration was shown to effectively restore the normal responsiveness of the intestine to $1,25(OH)_2D_3$ in ovariectomized premenopausal women (Gennari et al., 1990) and postmenopausal women (Civitelli et al., 1988; Heaney et al., 1978). The number of immunoreactive cells in the OJ groups was higher than that of the OE group, even though the difference was not significant. This phenomenon shows that EB dose injection in this study was sufficient to restore the number of the immunoreactive cells, but phytoestrogen derived of YCJ was more potent than exogenous estrogen (EB) in increasing these cells in almost all regions of the GI tract.

Many reports indicate that CB is not required for vitamin D-dependent intestinal calcium absorption (Perez et al., 2008), and increased intestinal calcium transport has been observed in vitamin D deficient pregnant and lactating rats (Halloron and Deluca 1980; Boass et al.,1981,

Brommage et al., 1990). Krisinger (1991) reported that CB alone could not facilitate 1,25-dihydroxy vitamin D3–mediated increases in intestinal calcium absorption in rats.

In contrast, the results in this study revealed that the number of CB-ir cells positively correlated with VDR-ir in all regions of the GI tract (stomach, small intestine, and colon). Our results agreed with Choi and Jeung (2008), who concluded that intestinal CB is clearly regulated by vitamin D.

A positive correlation (except CB-ir with ERα-cells in the ileum) between CB-ir cells with either ERα- and ERβ-ir may suggest that the active ingredient(s) of YCJ acted through the binding with either ERα or ERβ. It needs to be further investigated if the same cells that were positive for the estrogen receptors were also positive for CB. If co-localization of ERα or ERβ with CB in the same cells exists, it probably means that the expression of CB was due to the binding of YCJ active ingredient(s) with the estrogen receptors. This phenomenon was also found with VDR-ir cells. The number of VDR-ir positively correlated with either ERα- and ERβ-ir cells, suggesting that the active ingredient(s) of YCJ acted through the binding with either ERα or ERβ that caused calcium absorption via CB-ir cells in the "transcellular pathway" along the alimentary tract of ORx rats treated with YCJ.

Estrogenic compounds show different affinities to ERα and ERβ. ERα dominates in several specific tissues in comparison with ERβ that is expressed in other tissues, including bone and the GI tract (Gustafsson, 1999). It is known that endogenous or exogenous estrogens are specific to ERα rather than ERβ. In contrast, containing the phytoestrogen, β-sitosterol, YCJ reacts specifically with ERβ rather than ERα (Kuiper et al., 1998; Sayoh et al., 2008).

It has been indicated by this study that ERβ-ir was found to be much more positively stained than ERα-ir in all six regions of the GI tract examined, particularly in the stomach, where its fundus and body bind stronger to ERβ than ERα. It was reported that both mRNA and enzyme activity of aromatase (P450arom) and estrogen synthetase (Simpson et al., 1994) were detected in the gastric mucosa of rats at levels comparable with that of the ovary, and a high concentration of 17β-estradiol was detected in the portal vein arising from the stomach (Ueyama et al., 2002).

According to Devlin (2011), the two forms of ER have co-expression activity in neurons but different physiological functions, as indicated by the study on knock-out mice. It was reported that ERα is linked to synaptic plasticity, while ERβ to neural cell differentiation. More investigations are required to know the mechanism(s) activated by estrogen/phytoestrogen in the GI tract of male rats.

Researchers hypothesize that a diet rich in isoflavones has a protective effect on the bones (Tham et al., 1998). Even though we found that the YCJ component is primarily beta-sitosterol, since YCJ has a wound-healing effect and almost all isoflavone has a wound-healing effect, phytoestrogen of YCJ could likely be categorized as a member of the isoflavone group. Almost all proteins (antibodies) detected in the present study showed a higher number of immunoreactive cells when ORx rats were treated with lower YCJ treatments (OJ10 and OJ20) than with a higher dose of YCJ treatment (OJ40). Vincent and Fitzpatrick (2000) found that genistein, a kind of isoflavone in ovariectomized rats, has a biphasic effect. Lower doses improved bone mineral as opposed to high doses on bone mineral density. Therefore, YCJ could act as a kind of selective estrogen receptor moderator.

The possibility of the skeletal effects of testosterone is believed to be mediated by the aromatization of androgen to estrogens, as confirmed by findings of the presence of osteoporosis in men with mutations in aromatase gene (Carani et al., 1997) or estrogen receptor gene (Smith et al., 1994). Furthermore, Khosla et al. (1998), Slemenda et al. (1997), and Darko Kastelan et al. (2006) reported that estrogen rather than testosterone levels are more closely correlated with bone mineral density in older adults.

CONCLUSION

We were the first research team that found that there were CB-ir and VDR-ir in parietal cells of the stomach and the enterocytes of intestinal villi

of the small intestine and the colonocytes of the colon. The results of this study revealed that: (1) EB injection at 2.5 µg/kg BW/day for three days per week is enough to restore all immunoreactive cells detected by anti-CB-, anti-VDR-, anti-ERα- and anti-ERβ-ir antibodies. (2) The various doses of YCJ treatment restored the decreased numbers of CB-, VDR-, ERα- and ERβ-ir caused by orchidectomy to normal or close-to-normal levels; (3) the effects of YCJ were comparable to those of EB treatment. In most cases, the doses of YCJ at 10 mL/kg BW/d were the best. (4) This study indicates that not only CB and VDR but also estrogen/phytoestrogen is important in calcium absorption involved in the maintenance of calcium homeostasis. These findings indicate that feeding YCJ could account for, at least in part, the protective role of estrogen replacement against osteoporosis in older adults or men with hypogonadism.

ACKNOWLEDGEMENTS

Prince of Songkla University supported this study, grant no. SCI591097S. The authors would like to thank Professor Boonsirm Withyachumnarnkul, who put lots of input and kind suggestions in writing this manuscript.

REFERENCES

ASAE A, SAETAN J, RADENAHMAD N (2017) Beneficial effects of young coconut juice on reduced bone loss in orchidectomized rats. The 40th Annual conference of the Anatomy Association of Thailand. Chonburi, Thailand 17-19 May.

AVIOLI LV, MCDONALD JE, LEE SIN (1965) The influence of age on the intestinal absorption of ^{47}Ca in women and its relation to ^{47}Ca absorption in postmenopausal osteoporosis. *J Clin Invest,* 44: 1960-1967.

BARBOZA GD, GUIZZARDI S, TALAMONI NT (2015) Molecular aspects of intestinal calcium absorption. *World J Gastroent,* 21(23): 7142-7154.

BITZER J, KENEMANS P, MUECKC AO (2008) Breast cancer risk in postmenopausal women using testosterone in combination with hormone replacement therapy. *Maturitas,* 59: 209-218.

BOASS A, TOVERUD SU, PIKE JW, HAUSSLER MR (1981) Calcium metabolism during lactation: enhanced intestinal calcium absorption in vitamin D-deprived, hypocalcemic rats. *Endocrinology,* 109: 900-907.

BRINGHURST RF (1995) Calcium and phosphate distribution, turnover, and metabolic action. In: DeGroot LI (ed). *Endocrinology*. Saunders Company, Philadelphia, pp 1015-1043.

BROMMAGE R, BAXTER DC, GIERKE LW (1990) Vitamin D-independent intestinal calcium and phosphorus absorption during reproduction. *Am J Physiol,* 259: G631-638.

BULLAMORE JR, GALLAGHER JC, WILKINSON R, NORDIN BEC, MARSHALL DH (1970) Effect of age on calcium absorption. *Lancet,* 2: 535-537.

CARANI C, QIN K, SIMONI M, FAUSTINI-FUSTINI M, SERPENTE S, BOYD J, KORACH KS, SIMPSON ER (1997) Effects of testosterone and estradiol in a man with aromatase deficiency. *N Engl J Med,* 337: m 91-95.

CAROPPO R, GERBINO A, DEBELLIS L, KIFOR O, SOYBEL DI, BROWN EM, HOFER AM, CURCI S (2001) Asymmetrical, agonist-induced fluctuations in local extracellular [$Ca(2^+)$] in intact polarized epithelia. *Embo J,* 20: 6316-6326.

CHATTOPADHYAY N, MITHAL A, BROWN EM (1996) The calcium-sensing receptor: a window into the physiology and pathophysiology of mineral ion metabolism. *Endocr Rev,* 17: 289-307.

CHEN Z, WANG O, NIE M, ELISON K, ZHOU D, LI M, JIANG Y, XIA W, MENG X, CHEN S, XING X (2015) Aromatase deficiency in a Chinese adult man caused by aromatase deficiency in a Chinese adult man caused by novel compound heterozygous CYP19A1 mutations: Effects of estrogen replacement therapy on the bone, lipid, liver and glucose metabolism. *Mol Cell Endocrinol,* 399: 32-42.

CHENG I, QURESHI I, CHATTOPADHYAY N, QURESHI A, BUTTERS RR, HALL AE, CIMA RR, ROGERS KV, HEBERT SC, GEIBEL JP, BROWN EM, SOYBEL DI (1999) Expression of an extracellular calcium-sensing receptor in rat stomach. *Gastroenterology,* 116: 118-126.

CHOI KC, JEUNG EB (2008) Molecular mechanism of regulation of the calcium-binding protein calbindin-D_{9k}, and its physiological role(s) in mammals: a review of current research. *J Cell Mol Med,* 12(2): 409-420.

CHRISTAKOS S, DHAWAN P, PORTA A, MADY LJ, SETH T (2011) Vitamin D and intestinal calcium absorption. *Mol Cell Endocrinol,* 347(1-2): 25-29.

CIVITELLI R, AGNUSDEI D, NARDI P, ZACCHEI F, AVIOLI LV, GENNARI C (1988) Effects of one-year treatment with estrogens on bone mass, intestinal calcium absorption, and 25-hydroxyvitamin D-1 alpha-hydroxylase reserve in postmenopausal osteoporosis. *Calci Tissue Int*, 42: 77-86.

DELORME AC, DANAN JL, ACKER MG, RIPOCHE MA, MATHIEU H (1983) In rat uterus 17 beta-estradiol stimulates a calcium-binding protein similar to the duodenal vitamin D-dependent calcium-binding protein. *Endocrinology,* 113: 1340-1347.

DEVLIN TM (2011) *Textbook of Biochemistry with Clinical Correlation.* 7th ed. John Wiley and Sons, Inc. Philadelphia, USA, pp 928-930.

FERNANDEZ E, LAVECCHIA C, DAVANZO B, FRANCESCHI S, NEGRI E, PARAZZINI F (1996) Oral contraceptives, hormone replacement therapy and the risk of colorectal cancer. *Br J Cancer,* 73: 1431-1435.

FRANCAVILLA A, DI LEO A, POLIMENO L, CONTE D, BARONE M, FANITTA G, CHIUMARULO, RIZZO G, RUBINO M (1987) Nuclear and cytosolic estrogen receptors in human colon carcinoma and in surrounding noncancerous colonic tissue. *Gastroenterology*, 93: 1301-1306.

GALLAGHER JC, RIGGS BL, EISMAN J, HAMSTRA A, ARNOUD SB, DELUCA HF (1979) Intestinal calcium absorption and serum vitamin D metabolites in normal subjects and osteoporotic patients. *J Clin Invest,* 64: 729-736.

GENNARI C, AGNUSDEI D, NARDI P, CIVITELLI R (1990) Estrogen preserves a normal intestinal responsiveness to 1,25-dihydroxyvitamin D_3 in oophorectomized women. *J Clin Endocrinol Metab,* 71: 1288-1293.

GUSTAFSSON JA (1999) Review: estrogen receptor-**β** a new dimension in estrogen mechanism of action. *J Endocrin*, 163: 379-383.

HALLORAN BP, DELUCA HF (1980) Calcium transport in small intestine during pregnancy and lactation. *Am J Physiol,* 239: E64-68.

HART SA, SNYDER MA, SMEJKALOVA T, WOOLEY CS (2007) Estrogen mobilizes a subset of estrogen receptor-**α**-immunoreactive vesicles in inhibitory presynaptic boutons in hippocampal CA1. *J Neurosci,* 27: 2102-2111.

HEANEY RP, RECKER RR, SAVILLE PD (1978) Menopausal changes in calcium balance performance. *J Lab Clin Med*, 92: 953-963.

HENDRICKSE CW, JONES CE, DONOVAN IA, NEOPTOLEMOS JP, BAKER PR (1993) Oestrogen and progesterone receptors in colorectal cancer and human colonic cancer cell lines. *Br J Surg*, 80: 636-640.

HONG EJ, JEUNG EB (2013) Biological significance of calbinding-D_{9k} withing duodenal epithelium. *Int J Mol,* 14: 23330-23340.

JIANGSAKUL J, RADENAHMAD N, WONGSUWANLERT M (2015) Effects of young coconut juice on calcium-absorbing cells and vitamin D receptors in stomach of ovariectomized rats. The 36th National Graduate Research Conference. Chiangmai, Thailand, October 29-31.

KHOSLA S, MELTON LJ III, ATKINSON EJ, O'FALLON WM, KLEE GG, RIGGS BL (1998) Relationship of serum sex steroid levels and bone turnover markers with bone mineral density in men and women: a key role for bioavailable estrogen. *J Clin Endocrinol Metab,* 83: 2266-2274.

KIRCHHOFF P, GEIBEL JP (2006) Role of calcium and other trace elements in the gastrointestinal physiology. *World Gastroenterol*, 12(20): 3229-3236.

KRISINGER J, STROM M, DARWISH HD, PERIMAN K, SMITH C, DELUCA HF (1991) Induction of calbindin-D_{9k} mRNA but not calcium transport in rat intestine by 1,25-dihydroxyvitamin D_3 24-momologs. *J Biol Chem,* 266: 1910-1913.

KUIPER G, LEMMEN JG, GARLSSON B, CORTON JC, SAFE SH, VAN DER SAAG PT, VAN DER BURG B, GUSTAFSSON JA (1998) Interaction of estrogenic chemicals and phytoestrogens with estrogen receptor **β**. *Endocrinology*, 139: 4252-4263.

LEE GS. CHOIKC, PARK SM, AN BS, CHO MC, JEUNG EG (2003) Expression of human calbindin-D_{9k} correlated with age, vitamin D receptor and blood calcium level in the gastrointestinal tissues. *Clin Biochem*, 36: 255-261.

LUQMANI YA, RYALL G, SHOUSHA S, COOMBES RC (1992) An immunohistochemical survey of pS2 expression in human epithelial cancers. *Int J Cancer,* 50: 302-304.

MEGGOUHF, LOINTIER P, SAEZ S (1991) Sex steroid and 1,25-dihydroxyvitamin D_3 receptors in human colorectal adenocarcinoma and normal mucosa. *Cancer Res,* 51: 1227-1233.

NORMAN AW (2006) Minireview: vitamin D receptor: new assignments for an already busy receptor. *Endocrinology,* 147: 5542-5548.

PATISAUL HB, JEFFERSON W (2010) The pros and cons of phytoestrogen. Frontiers in *Neuroendocrinology,* 31(4): 400-419.

PEREZ AV, PICOTTO G, CARPENTIERI AR, RIVOIRA MA, PERALTA LOPEZ ME, TOLOSADETALAMONI NG (2008) Minireview on regulation of intestinal calcium absorption. *Digestion,* 77: 22-34.

RADENAHMAD N, BOONYOUNG P, KAMKAEW K, CHANCHULA K, KIRIRATP (2014) Effects of young coconut juice on the number of argyrophil cells in gastrointestinal tract of male rats. Novel preliminary finding. *Songklanagarin J Sci Technol,* 36(6): 599-606.

RADENAHMAD N, SALEH F, SAWANGJAROEN K, RUNDORN W, WITHYACHUMNARNKUL B, CONNOR RJ (2009) Young coconut juice reduces histopathological changes in the brain that is induced by hormonal imbalance. A possible implication to postmenopausal women. *Histol Histopathol Cell Mol Biol,* 24(6): 667-674.

RADENAHMAD N, SAYOH I, SALEH F, SAWANGJAROEN K, SUBHATHIRASAKUL P, BOONYOUNG P, RUNDORN W, MITRANUN W (2012) Young coconut juice can accelerate the healing process of cutaneous wounds. *BMC Compl Altern Med,* 12(1): 1-10.

RADENAHMADN**,**VONGVATCHARANONU,WITHYACHUMNARNKUL B, CONNOR RJ (2006) Serum levels of 17β-estradiol in ovariectomized rats fed young-coconut juice and its effect on wound healing. *Songklanagarin J Sci Technol,* 28(5): 897-910.

RUSSELL JE, MORIMOTO S, BRIGE SJ, FAUSTO A, AVIOLI LV (1986) Effects of age and estrogen on calcium absorption in the rat. *J Bone Miner Res,* 1: 185-189.

SAYOH I, RADENAHMAD N, KIRIRAT P, BOONYOUNG P, CHUNCHULA K, MITRANUN W (2008) Changes of argyrophil cells in gastrointestinal tract of ovariectomized rats fed with young coconut juice. *Malaysian J Microsc,* 4: 237-245.

SIDLER-LAUFF K, BOOS A, KRAENZLIN M, LIESEGANG A (2010) Influence of different calcium supplies and a single vitamin D injection on vitamin D receptor and calbindin D9k immunoreactivities in the gastrointestinal tract of goat kids. *J Anim Sci*, 88: 3598-3610.

SIMPSON ER, MAHENDROO MS, MEANS GD, KILGORE MW, HINSHELWOOD MM, GRAHAM-LORENCE S, AMARNEH B, ITO Y, FISHER CR, MICHAEL MD, MENDELSON CR (1994) Aromatase cytochrome P450, the enzyme responsible for estrogen biosynthesis. *Endocr Rev,* 15: 342-355.

SLEMENDA CW, LONGCOPE C, ZHOU L, HUI SL, PEACOCK M, JOHNSTON CC (1997) Sex steroids and bone mass in older men. *J Clin Invest,* 100: 1755-1759.

SMITH EP, BOYD J, FRANK GR, TAKAHASHI H, COHEN RM, SPECKER B, WILLIAMS TC, LUBAHN DB, KORACH KS (1994) Estrogen resistance caused by mutation in the estrogen-receptor gene in a man. *N Engl J Med,* 331: 1056-1061.

SUWANPAL P, RADENAHMAD N, YUSUH M, EKSOMTRAMATE M, RUANGSRI P, CHANTANASUKSILPA A (2011) Effects of young coconut juice on increasing mandibular cancellous bone in orchidectomized rats: Novel preliminary findings. *Songklanagarind J Sci Technol,* 33(6): 617-623.

TAKEDA H, YAMAKAWA M, TAKAHASHI T, IMAI Y, ISHIKAWA M (1992) An immuno-histochemical study with an estrogen receptor-related protein (ER-D5) in human colorectal cancer. *Cancer,* 69: 907-912.

TARGOWNIK LE, BERNSTEIN CN, LESLIE WD (2013) Inflammatory Bowel disease and the risk of osteoporosis and fracture. *Maturitas,* 76: 315-319.

THAM DM, GARDNER CD, HASKELL WL (1998) Clinical Review 97: potential benefits of dietary phytoestrogens: a review of the clinical, epidemiological, and mechanistic evidence. *J Clin Endocrinol Metab*, 83: 2223-2235.

THEISINGER B, GUTHKE R, BLIN N, WELTER C, SEITZ G (1993) Influence of steroid hormones on pS2//BCEI gene expression in xenografted colon tumors. *In Vivo,* 7: 411-414.

TEERAPORNPUNTAKIT J, DORKKAM N, WONGDEE K, KRISHNAMRA N, CHAROENPHANDHU N (2009) Swimming stimulates transepithelial calcium transport and alters the expression of gene related to calcium absorption in the intestine of rats. *Am J Physiol Endocrinol Metab,* 296: E775-786.

UEYAMA T, SHIRASAWA N, NUMASAWA M, YAMADA K, SHELANGOUSKI M, ITO T, TSURUO Y (2002) Gastric parietal cells: potent endocrine role in secreting estrogen as a possible regulator of gastro-hepatic axis. *Endocrinology,* 143: 3162-3170.

UEYAMA T, SHIRASAWA N, ITO S, TSURUO Y (2004) Estrogen-producing steroidogenic pathways in parietal cells of the rat gastric mucosa. *Life Sci*, 74: 2327-2337.

VINCENT A, FITZPATRICK LA (2000) Soya isoflavones: are they useful in menopause? *Mayo Clin Proc,* 75: 1174-1184.

WADA K, TANAKA H, MAEDA K, INOUE T, NODA E, AMANO R, KUBO N, MUGURUMA K, YAMADA N, YASHIRO M, SAWADA T, NAKATA B, OHIRA M, HIRAKAWA K (2009) Vitamin D receptor expression is associated with colon cancer in ulcerative colitis. *Oncology Reports,* 22: 1021-1025.

WALI RK, BAUM CL, SITRIN MD, BRASITUS TA (1990) 1,25$(OH)_2$ vitamin D_3 stimulates membrane phosphoinositide turnover, activates protein kinase C, and increases cytosolic calcium in rat colonic epithelium. *J Clin Invest*, 85: 1296-1303.

WALTERS JR, HOWARD A, LOWERY LJ, MAWER EB, LEGON S (1999) Expression of genes involved in calcium absorption in human duodenum. *Eur J Clin Invest,* 29: 214-219.

WESSERMAN RH (1997) Vitamin D and the intestinal absorption of calcium and phosphorus. In: Feldman D, Glorieus FH, Pike JW (eds). *Vitamin D*. Academic Press, San Diego, pp 259-273.

WELTER C, THEISINGER B, RIO MC, SEITZ G, SCHUDER G, BLIN N (1994) Expression pattern of breast-cancer-associated protein pS2/ BCEI in colorectal tumors. *Int J Cancer,* 56: 52-55.

YAMAGISHI N, YUKAWA YA, ISHIGURO N, SOETA S, LEE IH, OBOSHI K, YAMADA H (2002) Expression of calbindin-D9k messenger ribonucleic acid in the gastrointestinal tract of dairy cattle. *J Vet Med,* 49: 461-465.

YAMAGUCHI T, YAMAUCHI M, SUGIMOTO T, CHAUHAN D, ANDERSON KC, BROWN EM, CHIHARA K (2002) The extracellular calcium Ca^{2+}o-sensing receptor is expressed in myeloma cells and modulates cell proliferation. *Biochem Biophys Res Commun,* 299: 532-538.

YOOPRASERT P, BOONYOUNG P, CHANCHULA K, NUANPLAB S, RADENAHMAD N **(**2015) Young coconut juice reduces bone loss in ovariectomized rats by reducing osteoclast activity via estrogen receptors. Proceedings of the 38th Annual Conference of the Anatomy Association of Thailand, Pattaya, Chonburi, Thailand, June 24-26.

YUSUH M, PHOCHANUKOON N, RADENAHMAD N, EKSOMTRAMATE M, RUANGSRI P, CHANTANASUKSILPA A, REUNGCHAUMRATKUL A (2010) Changes of condyle cartilage in orchidectomized rats fed with young coconut juice: Novel preliminary findings. *Songklanagarin J Sci Technol*, 32(4): 333-339.

ZHANG W, NA T, WU G, JING H, PENG JB (2010) Down-regulation of intestinal apical calcium entry channel TRPV6 by ubiquitin E3 ligase Nedd4-2. *J Biol Chem,* 285: 36586-36596.

Neuroprotective effect of beta-D-glucan polysaccharide on hyperglycaemia-induced cerebral injury in diabetic animal model

C.A. Agbor, C.E. Fischer, E.A. Agaba, W.A. Nnenna

Department of Anatomy, Faculty of Basic Medical Sciences, University of Calabar, Nigeria

SUMMARY

An edible mushroom, *Aricularia polytricha* is used by local Nigerians in managing diabetes-related complications including infertility and diabetic neuropathy, but this age-long practice has been going on without the corresponding clinical trial and acceptable experimentation. β-D-Glucan polysaccharide is a bioactive fractionate of *Auricularia polytricha*, an edible mushroom with nutritional and therapeutic property. This study was intended to investigate the neuroprotective effect of β-D-Glucan polysaccharide on hyperglycaemia-induced cerebral injury in diabetic Wistar rats. Experimental animals were grouped into four: Group A served as normal control and was placed on distilled water, while groups B, C and D were induced with diabetes using 65 mg/kg bw of streptozotocin (STZ). Diabetic animals in Groups C and D were treated with 120 mg/kg bw and 200 mg/kg bw of β-D-Glucan polysaccharide respectively. Group B served as diabetic control animals. An analysis of oxidative stress markers (superoxide dismutase, catalase and melondialdehyde) was done to estimate serum levels of the markers; histopathological examination was done to determine micro-structural alteration of brain cells; cell quantification was also done to assess the degree of hypertrophy and proliferation of neurons. Statistical analysis was carried out using Analysis of Variance at $p<0.05$. Results showed that hyperglycaemic ambience induced a significant increase in serum level of oxidative stress markers with a concomitant increase in cell count, volume and mean size. Increase in glial cells aggregation in the cerebral cortex are indicators of cerebral damage in diabetic control animals. However, levels of oxidative stress markers were significantly downgraded following β-D-Glucan polysaccharide administration. Glial cell aggregation and inflammatory infiltrates were also decreased in diabetic models placed on β-D-Glucan polysaccharide when compared to diabetic control animals, indicating reversal in cerebral damage. The present study suggests that β-D-Glucan polysaccharide has neuroprotective effect in diabetes-induced cerebral damage in Wistar rat.

Key words: β-*D-Glucan polysaccharide* – Diabetic neuropathy – Cerebrum – Oxidative stress

INTRODUCTION

Diabetes mellitus (DM) is one of the leading causes of mortality and morbidity among chronic

Corresponding author:
C. A. Agbor. University of Calabar, PMB 1115, Nigeria. E-mail: agbor_cyril@yahoo.com - Orcid No.: 0000-0002-7343-5326

Submitted: November 8, 2021. **Accepted:** January 13, 2022
https://doi.org/10.52083/WCXG2854

diseases across the world (Bhatia et al., 2010). In Sub-Saharan Africa, it is estimated that among 20 million people are living with diabetes, about 62% are not diagnosed and the number is expected to reach 41.1 million by 2035 (Dahiru et al., 2016). Nigeria had a highest number of people with diabetes in Sub-Saharan Africa, with an estimated 4.7 million people of the adult population aged 20-79 (Ugwu et al., 2020).

A good number of diabetic-related outcomes such as generation of oxidative stress and lipid peroxidation will negatively affect individuals with both type 1 and type 2 diabetes Mellitus (Bhatia et al., 2010). Numerous biochemical pathways are being triggered by high hyperglycemic ambience resulting in cerebrovascular insult. Hyperglycemia is also capable of increasing levels of Reactive Oxygen Species (ROS), thereby resulting in cellular dysfunction and mutations (Nishikawa et al., 2000).

Oxidative stress has been indirectly connected to the clinical consequences of microvascular and macrovascular injury (Baker et al., 2004). Oxidative DNA damage can occur through either oxidation of DNA bases, primarily by direct attack on the purine and pyrimidine bases or through strand breaks and cross-linking in DNA (Chabory et al., 2009). In a study by Maker et al. (2009), experimentally induced oxidative stress in vitro significantly resulted in an increase in fragmentation, modification in base structure, deletions, clustering and frame shifts in chromatin. Furthermore, mitochondrial exposure to ROS provokes apoptotic process through release of Apoptosis Inducing Factor (AIF) resulting in apoptosis. This can further aggravate fragmentation in DNA strand (Agbor and Anyanwu, 2020). Reactive Oxygen Species (ROS) is required in little amount for maintenance of homeostasis. However, excessive generation will overrun the internal antioxidant defense system, thereby causing various degrees of damage (Agbor and Anyanwu, 2020).

Management and treatment of diabetes-related complications such as neuropathy have been of great concern, especially in developing countries where availability, cost implication and danger of adulteration associated with drugs pose a great challenge. β-D-glucan polysaccharide is a fractionate of *Auricularia polytricha*, an edible mushroom known for its nutritive and therapeutic properties (Chang et al., 2011), and is used by local Nigerian communities in management of diabetes-related complications without the required scientific and clinical proof of efficacy.

Additionally, β-D-glucan polysaccharide has been found to be a good exogenous source of antioxidants, as they always exist as conjugates with other biomolecules such as amino acid, protein, lipid, and nucleic acid residue (Nie et al., 2011). As the gradual shift to herbal therapy with its attendant increasing acceptance, even among the elite, confirm the claim that herbal remedies can provide cure for several diseases (Anthony et al., 2006), this study is therefore intended to investigate the neuroprotective effect of β-D-glucan polysaccharide fractionate of *Auricularia polytricha* on hyperglycaemia-induced cerebral injury in diabetic Wistar rat models.

MATERIALS AND METHODS

Preparation of extract

Auricularia Polytricha was obtained from a central market located in Etung Local Government Area of Cross River State, Nigeria. It was authenticated in the Department of Biological Sciences, University of Nigeria. The fungi were dried at room temperature for one week and ground to powder. 200g of *A. polytricha* was soaked in 1000ml of ethanol, labelled and covered for 72 hours, after which a clean filter paper (Watman No 1) was used to filter extracts. The filtrate was evaporated to dryness at 40^{o}C in a vacuum using a rotatory evaporator. The extract was then weighed and kept at 4^{o}C in refrigerator until further use. (Agbor and Anyanwu, 2020).

Fractionation of β-D-glucan polysaccharide

β-D-glucan polysaccharide was experimentally separated from *A. polytricha* using acetyl trimethyl ammonium bromide to form a precipitated complex with the acidic polysaccharide. It was further purified through a combination of fractional precipitation with acetic acid using ion-exchange chromatography (Zhang et al., 2007).

Experimental animals

Ethical clearance for this research was obtained from the Ethical Committee, Faculty of Basic Medical Sciences, University of Calabar, Nigeria. Twenty-eight (28) adult male Wistar rats (six months old) with weight range of 150-220 g were used for this research. The rats were divided into four groups and kept in four clean cages designated A, B, C and D, with seven rats in each group. The rats were allowed to acclimatize for two weeks in the animal house, Department of Anatomy, Faculty of Medicine, University of Nigeria, Enugu Campus, and allowed unrestricted access to commercially available chow (livestock feed) and water.

Experimental design

The experimental grouping, treatment and dosage is as shown in Table 1.

Induction of hyperglycaemia

After fasting for twelve hours, hyperglycaemia was induced by administering streptozotocin (STZ) intra-peritoneally, reconstituted in 0.5M Sodium citrate and administered at a dose of 65 mg/kg.bw (Ugochukwu and Babady, 2003).

Confirmation of diabetes

Diabetes was confirmed three days after administration of STZ using Accu-Check glucometer (Roche diagnostic, Germany) with blood samples obtained from tails of Wistar rats. Blood glucose levels at 80-120 mg/dl were considered normal, while animals with hyperglycaemic levels above 120 mg/dl were considered diabetic. (Anyanwu and Agbor, 2020, 2021).

Administration of extract

β-D-glucan polysaccharide administration commenced two weeks after induction of hyperglycaemia by oral gastric intubation and lasted for ten weeks.

Histopathological studies

At termination, the animals were sacrificed, and the brain tissue collected, weighed using an electronic weighing balance (Mettler Instrument AG, Switzerland), and suspended in buffered neutral formaldehyde for further processes with conventional histological techniques. Sections were cut at 5.0 µm, stained in Heamatoxylin and Eosin (H&E) and examined under a light microscope. Image J Software was used for estimating cell count and volume (Oyesolape et al., 2020).

Evaluation of oxidative stress markers

Oxidative stress markers were analyzed using blood obtained by cardiac puncture. Samples were transported to the laboratory for biochemical study. Oxidative stress marker kit (Sigma-Aldrich Products, Germany) was used to demonstrate for Soperoxide Dimutase (SOD), Catalase and Melondialdehyde (MDA) (Agbor and Anyanwu, 2020).

Statistical analysis

Data obtained from this study were recorded and analyzed using one way analysis of variance (ANOVA) with SPSS program (version 20). Post-hoc test was conducted using Fischer's Least Significant Difference (LSD) to determine statistical significance among groups. Probability level of $P<0.05$ was considered significant.

Table 1. Experimental animals were divided into four (4) groups and treated as follows.

GROUP	DESIGNATION	TREATMENT	DOSE
A	Normal control	Distilled water	3 ml
B	Diabetic control	Streptozotocin (STZ)	65 mg/kg.bw of STZ
C	STZ + AP (Low Dose)	STZ + β-D-glucan polysaccharide	65 mg/kg.bw of STZ + 120 mg/kg.bw of β-D-glucan polysaccharide
D	STZ + AP (High Dose)	STZ + β-D-glucan polysaccharide	65 mg/kg.bw of STZ + 200 mg/kg.bw of β-D-glucan polysaccharide

RESULTS

Blood glucose levels

As shown in Fig. 1, blood glucose levels recorded by diabetic control group (184.11±4.5) were remarkably higher when compared to the normal control (82.32±1.7) at p<0.05. However, animals in group C (147.94±3.1) and D (144.02±2.1) had glucose levels slightly lower than diabetic control animals following administration of β-D-glucan polysaccharide. Glucose concentration in groups B, C and D confirms hyperglycemic states of the experimental animals.

Biochemical analysis

Serum levels of SOD (DC: 8.11±0.4 vs NC: 2.43±1.2), catalase (DC: 3.09±2.1 vs NC: 1.49±1.0) and melondialdehyde (DC: 2.91±3.4 vs NC: 0.87±1.4) show that all oxidative stress markers in diabetic control animals were significantly higher at p<0.05 when compared to normal control. However, diabetic animals treated with 120 mg/kg bw and 200 mg/kg bw of β-D-glucan polysaccharide had significantly (p<0.05) reduced activities of SOD (Group C: 4.04±2.3; Group D: 3.19±4.0), catalase (Group C: 2.07±1.6; Group D: 1.51±4.1) and melondialdehyde (Group C: 2.23±1.3; Group D: 1.27±2.0) when compared with diabetic control (Figs. 2 and 3).

Cell quantification and size

As shown in Table 2, cerebral cell count (DC: 3986±3.3 vs NC: 2027±4.0), total area (DC: 80,344±2.8 vs NC: 51,621±3.3) and average area (DC: 77.88±0.2 vs NC: 26.07±2.1) in diabetic control animals increased significantly P<0.05 when compared to normal control (Group A). However, groups C and D (Diabetic animals placed on 120 mg/kg bw and 200 mg/kg bw of β-D-glucan polysaccharides respectively) had reduced cell count (C: 3062±4.2; D: 2633±1.6), total area (C: 73,636±2.2; D: 65,221±5.1) and mean size (C: 22.17±2.0; D: 19.72±1.1). These values were significantly lower (at p<0.05) when compared to diabetic control animals.

Histological observations (Figs. 4a-4d)

Histopathological sections of different experimental groups are shown in Figs. 4a to 4d. Section of cerebrum in group A (Normal

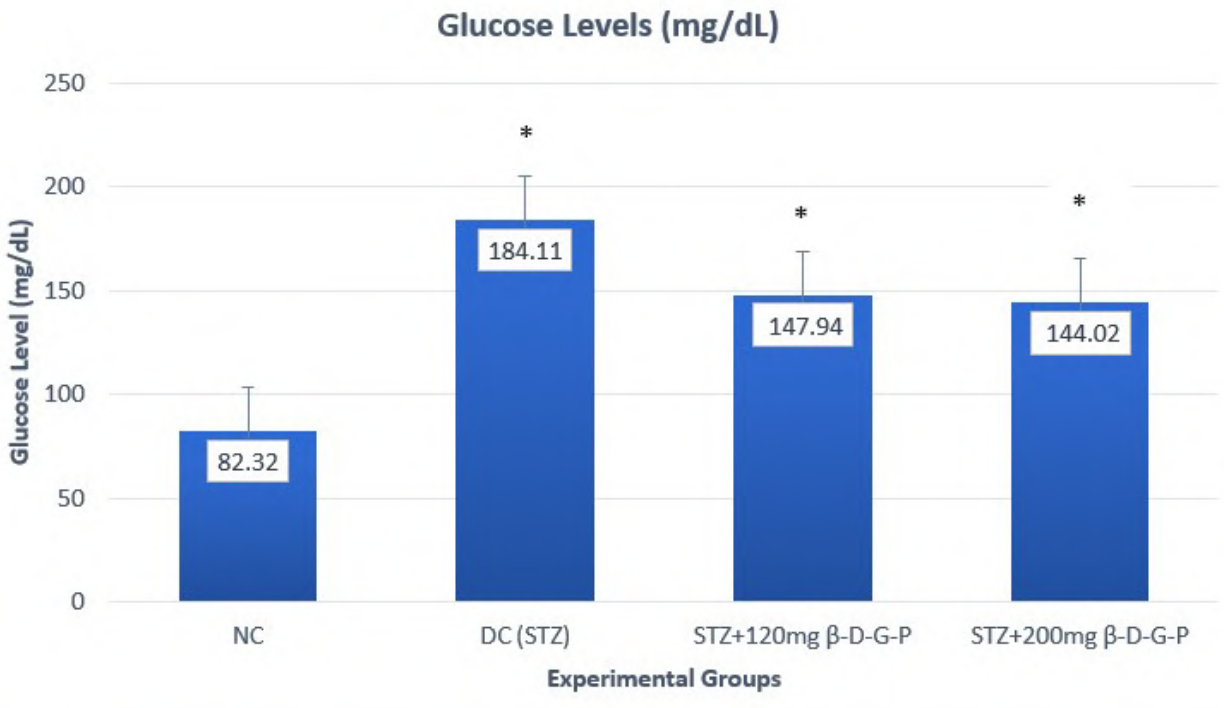

Fig 1.- Comparison of blood glucose levels of different experimental groups. Values are expressed as mean ± SEM. N = 5. * = Values are remarkably decreased when compared to normal control at p<0.05. NC – Normal Control, DC – Diabetic Control, STZ – Streptozotocin, β-D-G-P – Beta-D-Glucan Polysaccharide.

control) showed normal histology with no glial cells aggregation (Fig. 4a). In Fig. 4b, Section of cerebral cortex in group B (Diabetic control) showed cytoarchitectural alterations; the cells were mildly swollen with both intra-cytoplasm and nuclei vacuolation, aggregation of glial cell was extensive. Microglia cells were also noted with extensive inflammatory infiltrates.

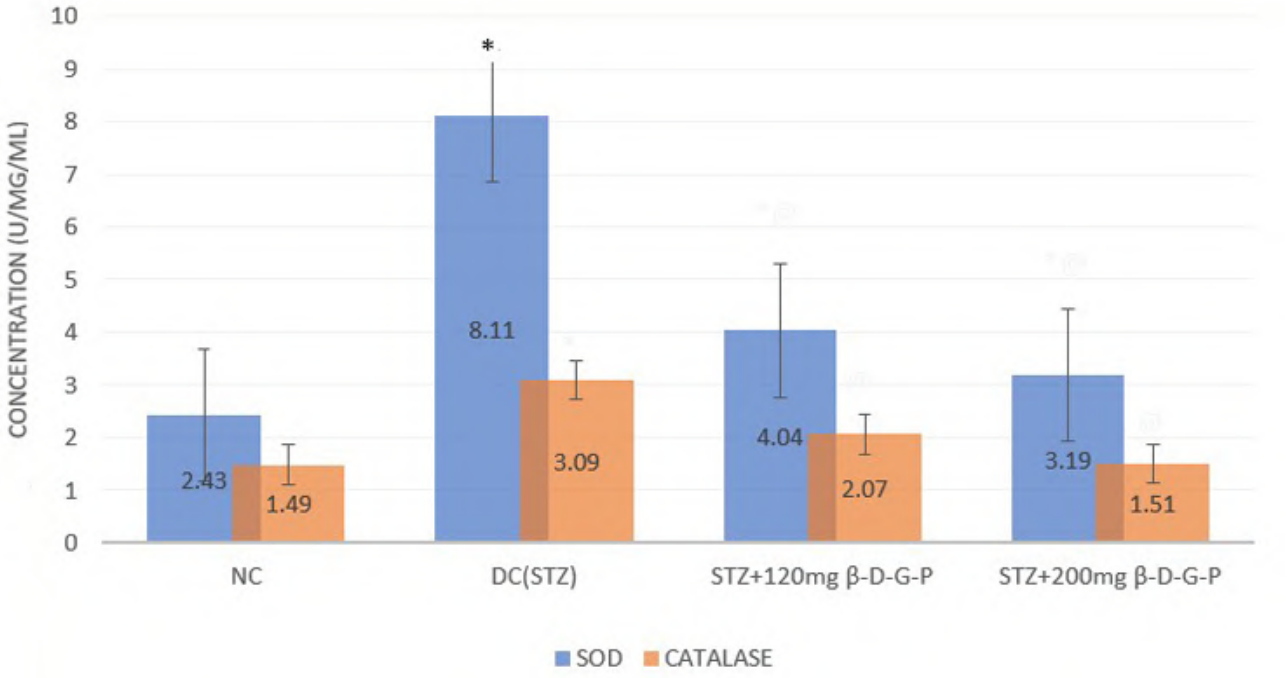

Fig. 2.- Comparison of superoxide dismutase (SOD) and catalase in the different experimental groups. Values are expressed as mean ± SEM. N = 5. * = Values are significantly decreased when compared to normal control at p<0.05. @ = Values are significantly increased when compared to diabetic control at p<0.05. NC – Normal Control, DC – Diabetic Control, STZ – Streptozotocin, β-D-G-P – Beta-D-Glucan Polysaccharide.

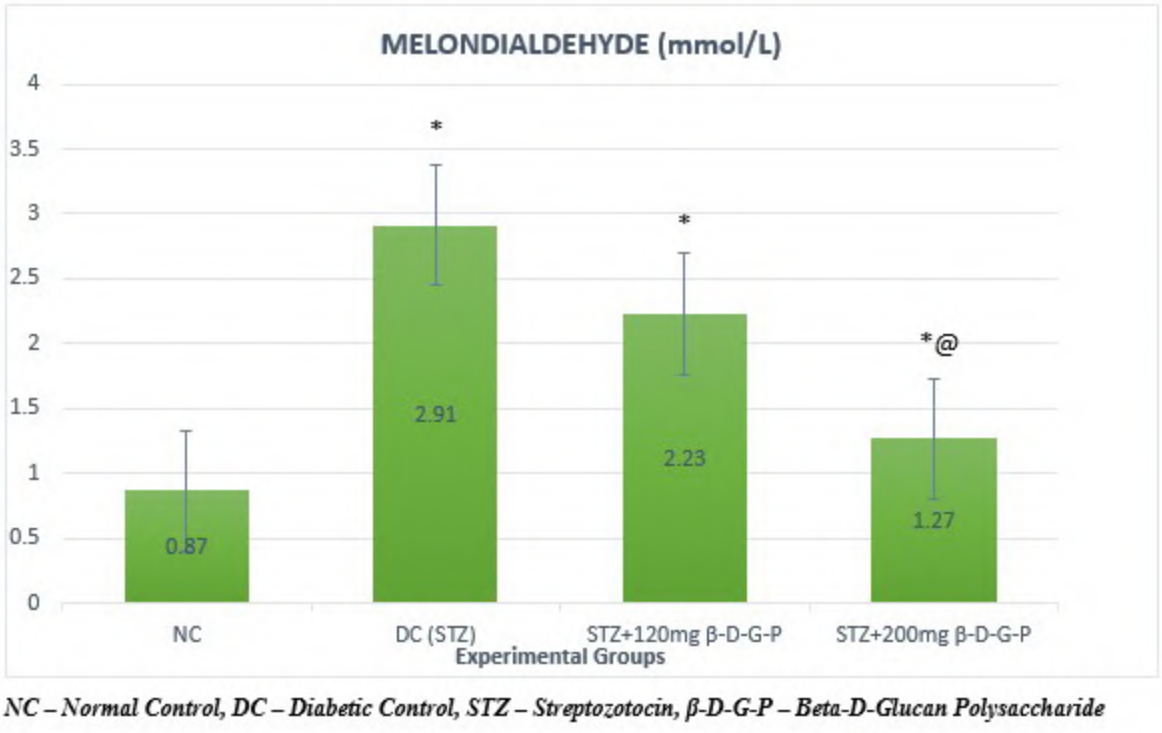

Fig. 3.- Comparison of melondialdehyde in the different experimental groups. Values are expressed as Mean ± SEM. N = 5. * = Values are significantly decreased when compared to normal control at p<0.05. @ = Values are significantly increased when compared to diabetic control at p<0.05.

Table 2. Cell quantification and size in different experimental groups.

GROUP	CELL COUNT	TOTAL AREA	AVERAGE SIZE
A	2027	51,621	17.88
B	3986*	80,344*	26.07*
C	3062*	73,636*	22.17*
D	2633*@	65,221*@	19.72*@

Values are expressed as mean ± SEM. N = 7. ***** = Values are significantly increased when compared to Normal Control at p<0.05. **@** = Values are significantly decreased when compared to Diabetic Control at p<0.05.

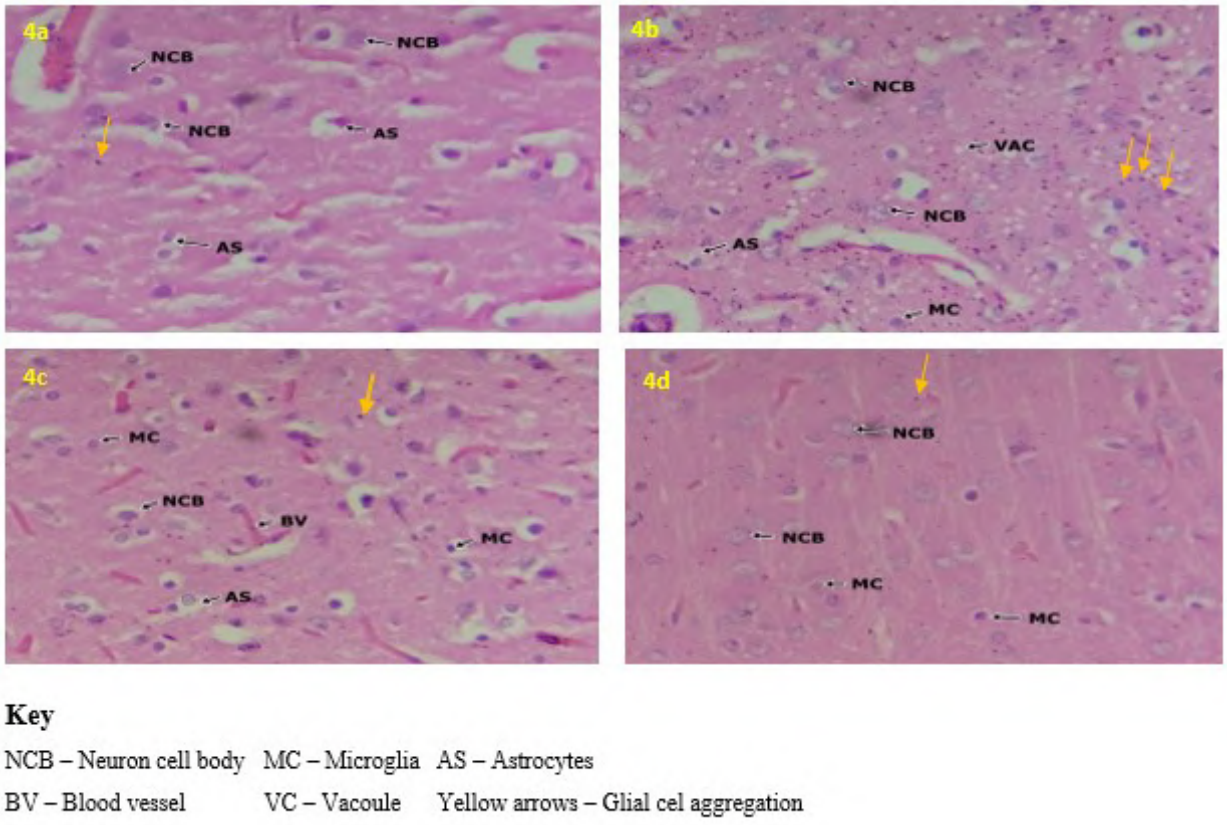

Fig. 4.- Sections of the cerebral cortex in all groups studied. **4a:** Section of cerebrum in group A (Normal control) showing normal histology with no glial cell aggregation. **4b:** Section of cerebral cortex in group B (Diabetic control) showing alterations, the cells were mildly swollen with both intracytoplasmic and nuclei vacuolation, aggregation of glial cells was extensive. Microglial cells were also noted with extensive inflammatory infiltrates. **4c:** Section of cerebral cortex in group C (STZ+120 mg/kg bw β-D-Glucan polysaccharide) showing mild alterations, the cells were mildly swollen with aggregation of glial cell was almost absent and inflammatory infiltrates very mild. **4d:** Section of cerebral cortex in group C (STZ+200 mg/kg bw β-D-Glucan polysaccharide) showing no alterations. Aggregation of glial cell was absent with no inflammatory infiltrates. NCB – neuron cell body; MC – Microglia; AS – Astrocytes; BV – Blood vessel; VC – Vacoule; Yellow arrows – Glial cell aggregation.

Section of cerebral cortex in group C (STZ + 120 mg/kg bw β-D-Glucan polysaccharide) as revealed in Fig. 4c showed mild cytoarchitectural alterations; the cells were mildly swollen, aggregation of glial cell was almost absent and inflammatory infiltrates were very mild. No distortions in histological sections were observed in Fig. 4d (section of cerebrum in group C placed on STZ+200 mg/kg bw β-D-Glucan polysaccharide). Aggregation of glial cell was absent with no inflammatory infiltrates.

DISCUSSION

This study was intended to investigate the neuroprotective effect of β-D-Glucan polysaccharide on hyperglycaemia-induces cerebral injury in diabetic Wistar rats. Observation from this research has revealed that β-D-glucan polysaccharide improved antioxidant capacity and cerebral function in hyperglycemia-induced cerebral injury. From the observation, oxidative stress markers, which significantly increased in the diabetic control, were lowered slightly following β-D-glu-

can polysaccharide treatment. Peptide moiety in polysaccharide has been found to be responsible for free radical scavenging activity of β-D-glucan polysaccharide and lipid peroxidation inhibitory effect on superoxide and hydroxyl radicals (Lee et al., 2003). More so, polysaccharide-protein complexes are linked to amino acids such as lysine, tyrosine, methionine, histidine and tryptophan, which are capable of donating a proton to the electron-deficient reactive oxygen species (ROS). Even though a comprehensive investigation into the mechanism of action of β-D-Glucan polysaccharide is still lacking, it has been documented that its low molecular weight and existence in conjugate forms may trigger an interaction with certain receptors that may result in some specific therapeutic signaling pathway to benefit host organ (cerebrum). Furthermore, β-D-Glucan polysaccharide is found to possess lipid peroxidation inhibitory effect, the reasons being that polysaccharide-polyphenol conjugates are known to be mediated by hydrophobic interactions in the cell membranes; as a consequence, hydrophobic cavities and crevasses may exist for these conjugates, thereby preventing damage of the cell membrane. Renard et al. (2001) reported similar findings.

This study has also demonstrated that brain damage in the diabetic control group (DC) is evident in aggregation of glial cells, presence of inflammatory infiltrates and severe neuronal loss in the cerebral cortex. Very critical histopathological activities have been reported in the brain during hyperglycemic injury given to the glucose utilization. Cerebral inflammation and its vascular complications have been documented in diabetes-induced brain injury (Drake et al., 2011). Aggregation of glial cells is a first line biomarker indicating neural damage, and is activated by inflammatory pathways and cytotoxic product such as ROS and interleukin. Consequently, glial cells are activated in response to brain injury and increase in aggregation of these cells is a consequence of the severity of inflammation (Drake et al., 2011).

A significantly higher cell count, sizes and volume cerebral cells of diabetic control animals when compared to normal control are indicative of brain damage. This is consistent with findings from Selim and Selim (2013), who reported that hypertrophy and proliferation of neurons is in response to chemical and mechanical insult meant to enhance structural and functional changes occasioned by hyperglycemia-induced cerebral injury. This forms the basis for pathogenesis of neurodegenerative diseases. However, groups C and D, diabetic animals placed on 120 mg/kg bw and 200mg/kg bw of β-D-glucan polysaccharides respectively, had progressively reduced cell count, volume and mean size accompanied by lower degree of glial cell aggregation and reduced inflammatory infiltrates accompanied by neuronal loss indicating reversal in cerebral damage.

CONCLUSION

β-D-glucan polysaccharide has been shown from this research to regulate diabetes-induced oxidative stress generation, suppress glial cells aggregation and decrease cell count, sizes and volume in cerebrum of hyperglycemic rat. The underlying mechanism of this neuroprotective effect can be traced to its strong antioxidant capacity. This study may have suggested that β-D-glucan polysaccharide fractionized from edible fungus *A. polytricha* is a potential antioxidant, anti-inflammatory and neuroprotective agent capable of ameliorating diabetes-induced cerebral injury.

ACKNOWLEDGEMENTS

We acknowledge the technical support from Department of Histopathology, University of Calabar Teaching Hospital, Nigeria and Endocrinology Laboratory in the department of Biochemistry, University of Calabar Nigeria.

AUTHORS' CONTRIBUTIONS

All authors gave equal contribution to this research.

REFERENCES

ANYANWU GE, AGBOR CA (2020) Assessment of testicular histomorphometric parameters and reticular fibres density on testicular tissue of diabetic Wistar rat placed on *Auricularia Polytricha*. *Jordan J Biol Sci*, 13 (Supplement): 709-714.

ANYANWU GE, AGBOR CA (2021) Correlation between oxidative stress generation, reticular fiber density and testicular histomorphometric parameters of streptozotocin-induced diabetic Wistar rat. *J Bio-Science*, 29(2): 1-8.

AGBOR CA, ANYANWU GE, AUDU SJ (2020) *Auricularia polytricha* restores altered reproductive parameters in streptozotocin induced diabetic Wistar rat. *J Basic Appl Zool*, 81: 29.

ANTHONY BO, OLADIPO AL, ADEDOYIN KL, TAJUDIN IA (2006) Phytochemistry and spermatogenic potential of aqueous extracts of *Cissus Populnear*. *Sci World J*, 6: 2140-2146.

BAKER MA, KRUTSKIKH A, CURRY BJ, MCLAUGHLIN EA, AITKEN RJ (2004) Identification of cytochrome P450-reductase as the enzyme responsible for NADPH-dependent lucigenin and tetrazolium salt reduction in rat epididymal sperm preparations. *Boil Reprod,* 71: 307-318.

BHATIA DK, SHARMA AK, PATHANIA PC, KHAUDURI NC (2010) Antifertility effect of crude extract of *Adiantum Lunulatum* on reproductive organs of male Wistar rats. *Int J Biol Forum,* 2(2): 88-93.

CHABORY E, DAMON C, LENOIR A, HENRY-BERGER J (2009) Epididymis seleno-independent glutathione peroxidase 5 maintain sperm DNA integrity in mice. *J Clin Invest,* 119: 2074-2085.

CHANG JS, KIM HJ, BAE JT, PARK SH, KIM SE, KIM OM (2011) Inhibition effects of *Auricularia auricula-judae* methanol extract on lipid peroxidation and liver damage in benzo(a)pyrene-treated mice. *J Korean Soc Food Sci Nutrit,* 27: 712-717.

DAHIRU T, ALIYU A, SHEHU A (2016) A review of population-based studies on diabetes mellitus in Nigeria. *Sub-Saharan Afr J Med,* 3: 59-64.

DRAKE C, BOUTIN H, JONES MS, ADAM D, MCCOLL BW, SELVARAJAH JR, HULME S, GEORGIOU RF, HINZ R, GERHARD A, VAIL A, PRENANT C, JULYAN P, MAROY R, BROWN G, SMIGOVA A, HERHOLZ K, KASSIOU M, CROSSMAN D, FRANCIS S, PROCTOR SD, RUSSELL JC, HOPKINS SJ, TYRRELL PJ, ROTHWELL NJ, ALLAN SM (2011) Brain inflammation is induced by co-morbidities and risk factors for stroke. *Brain Behav Immun*, 25: 1113-1122.

LEE HB, YU MI-RA, YANG Y, JIANG Z, HA H (2003) Reactive oxygen species-regulated signaling pathways in diabetic nephropathy. *J Am Soc Nephrol,* 14: S241-S245.

MAKER K, AGARWAL A, SHARMA R (2009) Oxidative stress and male infertility. *Ind J Med Res,* 129: 357-367.

NIE SP, XIE MY (2011) A review on the isolation and structure of tea polysaccharides and their bioactivities. *Food Hydrocolloids*, 25(2): 144-149.

NISHIKAWA T, EDELSTEIN D. BROWNLEE M (2000) The missing link: a single unifying mechanism for diabetes complication. *Kidney J*, 77: 526-530.

OYESOLAPE BO, ENOCK OD, DEEPSHIKHA PK (2020) Protective role of diosgenin against hyperglycaemia-mediated cerebral ischemic brain injury in zebrafish model of type II diabetes mellitus. *Heliyon,* 6(1): e03296.

RENARD CM, BARON A, GUYOT S, DRILLEAU JF (2001) Interactions between apple cell walls and native apple polyphenols: quantification and some consequences. *Int J Biol Macromol,* 29(2):115-125.

SELIM AS, SELIM AO (2013) Effect of streptozotocin-induced diabetes mellitus on the cerebellar cortex of adult male albino rats: histological and immunohistochemical study. *Egypt J Histol,* 36: 103-113.

UGOCHUKWU NH, BABADY NE (2003) Antihyperglycaemic effect of aqueous and ethanolic extracts of *Gongronema latifolium* leaves on glucose and glycogen metabolism in livers of normal and streptozotocin induced diabetic rat. *Life Sci*, 73(150): 1925-1938.

UGWU E, YOUNG E, NKPOZI M (2020) Diabetes care knowledge and practice among primary care physicians in Southeast Nigeria: a cross sectional study. *BMC Fam Pract*, 21: 128.

ZHANG H, WANG ZY, YANG L, YANG X, WANG X, ZHANG Z (2007) *In vitro* antioxidant activities of sulfated derivatives of polysaccharides extracted from *Auricularia auricular*. *Int J Mol Sci,* 12: 3288-3302.

Formaldehyde and anti-fertility: correlation between testicular cytoarchitecture and semen analysis

Olugbenga O. Eweoya[1], A.O. Oyewopo[2], O.T. Olaniyan[3], Babatunde J. Dare[4]

[1] Department of Anatomical Sciences, University of Abuja, Abuja, Nigeria

[2] Department of Anatomy, University of Ilorin, Ilorin, Kwara State, Nigeria

[3] Laboratory for Reproductive Biology and Developmental Programming, Department of Physiology, Edo State University, Uzairue, Iyamho, Edo State, Nigeria

[4] Department of Anatomy, Osun State University, Oshogbo, Osun State, Nigeria

SUMMARY

The anti-fertility effect of formaldehyde was investigated on the testicular cytoarchitecture and semen of Sprague-Dawley rats exposed to formaldehyde by inhalation. Thirty adult male rats were randomly selected into three (3) groups of ten (10) rats each. The treatment group 2 and group 3 were exposed to 40% stock concentration of formaldehyde for 1 min/m^2 and 2 min/m^2 respectively daily for four (4) weeks of experimental period. The control group (group 1) was allowed free access to natural air throughout the experimental period. Testis was dissected out following cervical dislocation and fixed in Bouins fluid for histological processing. Caudal Epididymis was also dissected out and suspended in 1ml of Hams F- 10 solution for estimation of sperm concentration and motility.

Semen analysis revealed a significant reduction in sperm concentration and sperm motility in the treated groups. Histological alterations in the seminiferous tubule and degeneration of spermatogenic cells were observed in the treated groups compared with the control. Reduction in sperm concentration and motility and histological alteration of the testes in the treated rats showed that formaldehyde might have toxicity on the reproductive organ.

Key words: Formaldehyde – Testis – Semen – Anti-fertility – Cyto-architecture, - Spermatogenesis

INTRODUCTION

Infertility is one of the major health problems among married couples (Agarwal and Prabakaran, 2005). Approximately 20-30% of couples with infertility can be traced to combined female and male factors (Oyewopo et al., 2018). Several conditions and factors can interfere with sperm development and reduce sperm quality and quantity. Such factors may include: drug treatment, toxin, infectious organisms, air pollution and malnutrition (Fujii et al., 2003, Olaniyan et al., 2021a, Olaniyan et al., 2021c).

In each testis are 200 to 300 lobules, and within each lobule are 1 to 4 convoluted lobules

Corresponding author:
Babatunde J. Dare. Department of Anatomy, Osun State University, Oshogbo, Osun State, Nigeria. Phone: +2348077805474. E-mail: babatunde.dare@uniosun.edu.ng

Submitted: December 6, 2021. **Accepted:** January 16, 2022

https://doi.org/10.52083/ARBR9022

composed of germinal epithelia cell, called seminiferous tubules, and between the tubules are groups of interstitial cells (of Leydig) that secrete the hormone testosterone after puberty (Sheweita et al., 2005; Olaniyan et al., 2021d). Successful spermatogenesis take place at a temperature of about 3^{o}C below normal body temperature and require hormonal regulation such as Follicle Stimulating Hormone (FSH), Luteinizing Hormone (LH) and Testosterone (Sheweita et al., 2005).

Formaldehyde is a chemical primarily used for preservation of tissues in research and in manufacturing industry where resin, particle board, plywood, leather, paper and pharmaceutical products are produced (Wong et al., 2006). It is also a flammable, choking, colorless, and reactive gas. Exposure to formaldehyde can be from both direct environmental source and from metabolism of xenobiotics (Wong et al., 2006). However, it has been shown that the level of exposure to formaldehyde in occupational environment is relatively high as compared to other sources (Wong et al, 2006). There are various sources of formaldehyde; the major anthropogenic sources that grossly affect human and others animals are the indoor, environment or long-term outdoor pollution, which poses a significant threat to public health (Yu et al., 2005; Tang et al., 2009). Formaldehyde is a volatile, highly soluble compound in water which can rapidly diffuse into many tissues and cause distortion of cells (Metz et al., 2004).

Emerging evidence supports an association between formaldehyde exposure and multiple adverse health effects (Tang et al., 2009).

It was reported that long-term exposure to formaldehyde negatively affects the hematological parameters and respiratory system; it also causes irritation of the eyes and nasal pathway in animals (Yu et al., 2005).

The reproductive and developmental toxicity associated with formaldehyde exposure remains inconclusive (Duong et al., 2011), and this prompted us to investigate the formaldehyde action on the testicular cytoarchitecture and semen analysis of adult male Sprague Dawley rats.

MATERIALS AND METHODS

Experimental Animal

A total of 30 male adult Sprague-Dawley rats weighing between 160-200 g were obtained from the animal house Department of Physiology, Ladoke Akintola University, Ogbomosho, Oyo State. The rats were allowed to acclimatize for 2 weeks at photo periodic condition of 12hrs light and 12 hrs darkness natural cycles, and were fed with a standard Pfizer diet obtained from Bendel Feeds Ilorin and water *ad libitum.* T experiment was carried out in the Department of Anatomy University of Ilorin, in accordance with the Animal Experimentation Committee Regulation.

Experiment design

The animals were randomly selected into three (3) groups, each comprising ten (10) Wistar rats. 40% stock concentrations of formaldehyde were soaked in Cotton wool and the animals were exposed to the 40% stock concentration by inhalation at varying time per meter square area. Group 1 (control) were exposed to natural fresh air throughout the experimental period. Group 2 and Group 3 were exposed to 40% concentration of formaldehyde by inhalation for a period of 1 minutes/m^2 and 2 minutes/m^2 area of exposure respectively daily for the 4 weeks of experimental period between 0900 and 1000 hours. Animals were sacrificed by cervical dislocation at the end of 4th week.

Sample collection and processing

The animals were euthanized by cervical dislocation twenty-four hours after last administration and the testes tissue were excised. The testis from each rat was fixed in Bouin's fluid for routine histological haematoxylin & eosin (H/E), while the caudal epididymis used in sperm analysis.

Histological Analysis

Testes were carefully excised, cut in slabs of 0.5 cm thick, fixed in Bouins fluid and processed routinely for paraffin embedding. 5µ sections were obtained with rotatory microtome and processed for Heamatoxylin and Eosin Stain (H&E). Sections

were observed with light microscope and photomicrographs were taken for further analysis (Bustos-Obregon et al., 2003).

Sperm analysis

The caudal epididymis was dissected out, several incisions (1 mm) were made in the caudal epididymis, which was suspended in 1ml of Ham's f-10 solution after 3-5 minutes of incubation at 37°C. The sperm swim up and the concentration and motility were determined by using new improved Neubauer Haemocytometer (Tang et al., 2003; Olaniyan et al., 2021b).

RESULTS

Semen analysis revealed a significant reduction ($p<0.05$) in sperm concentration and motility in the treated group as compared with the control group table 1. Spermatocyte concentration significantly decrease in relation to the time of exposure to 40% stock solution of formaldehydes. Animals exposed for 2 minutes per meter square area demonstrated marked reduction in the sperm concentration associated with loss of motility integrity when compared with the control animals without restriction to the normal air exhalation and inhalation. Formaldehyde exposure for the period for 1 minute per area square demonstrated mild impact on the sperm characteristics and quality.

There was significant histological alteration in the testes of group 2 and group 3 rats that were exposed to the formaldehyde as compared with the control. There was disruption of the seminiferous tubule and degeneration of spermatogenic cells. There was also edema of the interstitial connective tissue in the treated groups compared to the control (Fig. 1). Animals in the control group expressed the histological architecture of the testes, presenting the three types of the cells: the spermatogonia population, the Sertoli and the interstitial Leydig cells in the interstitial spaces. All stages of spermatogonia cells were expressed across the seminiferous tubules and the mature Spermatocytes in the ad-luminal compartment. Abnormal widening of the interstitial spaces, de-arrangement in the lining basal membranes and seminiferous tubules shrinkage were observed in the animals exposed for a period of 1 minute per square area. Complete loss of spermatogonia cells across the tubules was observed in the group with the long period of exposure per unit area, loss of the basal membrane integrity and complete breakdown of the interstitial spaces as evident in the loss of quality in the sperm characteristics.

DISCUSSION

The anti-fertility effect of formaldehyde was investigated on the testicular cytoarchitecture and on semen analysis in Sprague-Dawley rats treated with formaldehyde. The usual quantity of semen ejaculated at each coitus averages 3.5 million in man, and varies according to species (Fujii et al., 2003). When the number of sperm per each milliliter falls below normal, the animal is likely to be infertile. Even though only a single sperm is necessary for fertilization, the ejaculate usually must contain a tremendous number of sperm from which only one sperm will fertilize the ovum (Fujii et al., 2003). Whenever the majority of sperms are morphologically abnormal or are found to be non motile, the condition is likely to be infertile, even though the remaining sperms may appear to be normal (Fujii et al., 2003).

The present study revealed that there was decreased sperm concentration and reduction in motility of sperm of the treated rats as compared with the control, which is in tandem with the previous study conducted by Zhou et al. (2006) in male humans, and this is further supported by

Table 1. Sperm concentration and motility of the treated rats compared with controls.

	No. of rats	Sperm concentration× 10^6	Sperm Motility%
Group 1	10	60.14 ± 0.70	75.25 ± 6.26
Group 2	10	56.20 ± 0.52	62.15 ± 3.17
Group 3	10	22.13 ± 0.68*	40.15 ±3.12*

Values are mean ± SEM. (n): * indicates significant different when compared with the control group ($p<0.05$)

another study on adult male rats with large dose formaldehyde exposure (Zhou et al., 2011).

The decrease in sperm concentration and reduction in sperm motility caused by the action of formaldehyde showed that formaldehyde may cause infertility in animals depending on the length of exposure, but not with low-dose exposure (Zhou et al., 2011). Study by Collins et al. (2001) in both humans and animals contradicts this report, even though other routes apart from inhalation were disregarded.

Histological observation of the testicular cytoarchitecture showed disarrangement of seminiferous tubules and destruction of spermatogenic cells in the treated group, which was worst in the group 3 animals. This histological alteration of the testes may alter the initiation and maintenance of spermatogenesis in the rats according to Dare et al. (2021), who report a decrease in the number of Spermatogonia and differentiating cells in the testes of rats treated with cadmium chloride, a free-radical-generating agent similar to the effect of exposure to formaldehyde on the sperm characteristics and the histological architecture observed in this study.

CONCLUSION

This study has shown that formaldehyde affects the cytoarchitecture and sperm characteristics of adult male Sprague-Dawley rats, and can be reasonably concluded to have toxic effects on the reproductive organs of the male rats and, by extension, humans.

REFERENCES

AGARWAL A, PRABAKARAN SA (2005) Oxidative stress and antioxidants in male infertility: a difficult balance. *Iran J Reprod Med*, 3: 1-8.

BUSTOS-OBREGON E, GONZALEZ-HORMAZABAL P (2003) Effect of a single dose of malathion on spermatogenesis in mice. *Asian J Androl*, 5: 105-107.

COLLINS JJ, NESS R, TYL RW, KRIVANEK N, ESMEN NA, HALL TA (2001) A review of adverse pregnancy outcomes and formaldehyde exposure in human and animal studies. *Regul Toxicol Pharmacol*, 34: 17-34.

DARE BJ, OPEYEMI MK, ADEGOKE AA, OLAFUSI OO (2021) Protective role of *Dracaena Arborea* aqueous extract on cadmium induced testicular toxicity in adult Wistar rats (*Rattus Novergicus*). *J Basic Appl Med Sci*, 1(3): 16-28.

DUONG A, STEINMAUS C, MCHALE CM, VAUGHAN CP, ZHANG L (2011) Reproductive and developmental toxicity of formaldehyde: a systematic review. *Mutat Res*, 728(3): 118-138.

FUJII J, LUCHI Y, MATSUKI S, ISHIL T (2003) Cooperative function of antioxidant and redox system against oxidative stress in male reproductive tissue. *Asian J Androl*, 5: 231-242.

METZ B, KERSTEN GF, HOOGERHOUT P, BRUGGHE HF, TIMMERMANS HA, DE JONG A (2004) Identification of formaldehyde-induced modifications in protein: reactions with model peptides. *J Biol Chem*, 279: 6235-6243.

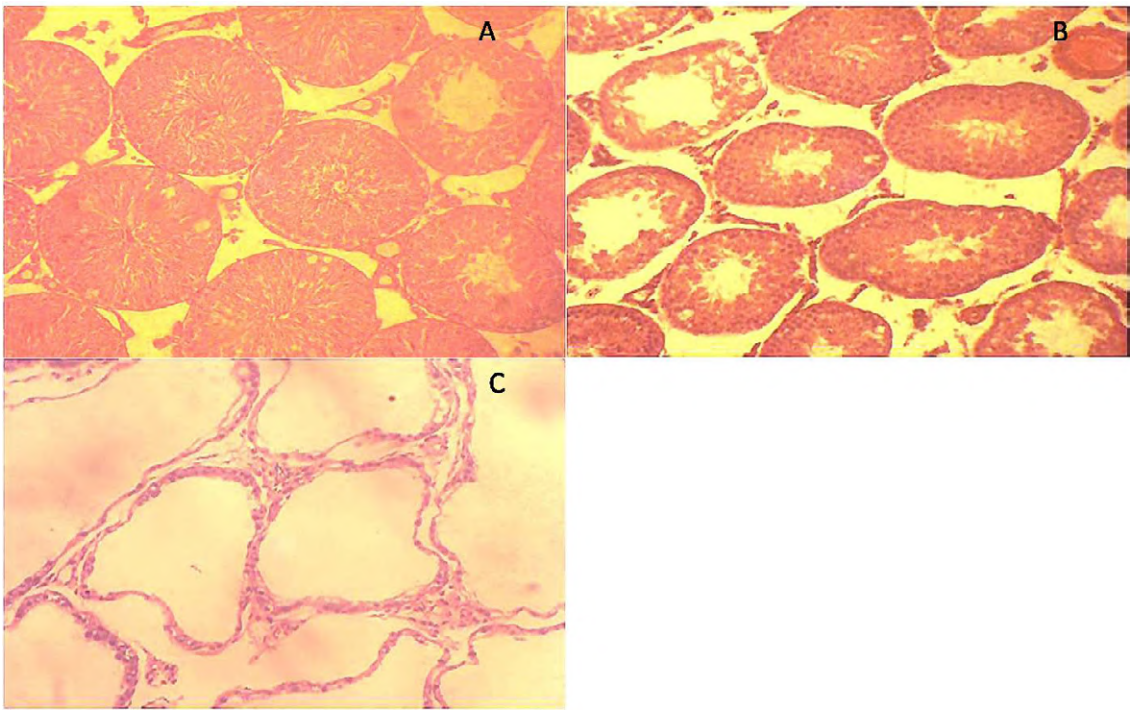

Fig. 1.- A: Cross section of the testes of control rats showing the normal architecture of the testis. **B:** Cross section of the seminiferous tubules of rat treated with 40% FA for 1 min/m^2 showing disruption in the spermatogenic cell. **C:** Cross section of seminiferous tubules of rat treated with 40% FA for 2 min/m^2 showing degeneration of spermatogenic cell. H&E staining, x400.

OLANIYAN OT, DARE A, OKOLI B, ADETUNJI CO, IBITOYE BO, OKOTIE GE, EWEOYA O (2021a) Increase in SARS-CoV-2 infected biomedical waste among low middle-income countries: Environmental sustainability and impact with health implications. *J Basic Clin Physiol Pharmacol*, doi: 10.1515/jbcpp-2020-0533.

OLANIYAN OT, OJEWALE OA, DARE A, ADEBAYO O, ENYOJO JE, OKOTIE GE, ADETUNJI CO, MADA BS, OKOLI BJ, EWEOYA OO (2021b) *Cocos nucifera L.* oil alleviates lead acetate-induced reproductive toxicity in sexually-matured male Wistar rats. *J Basic Clin Physiol Pharmacol*, doi: 10.1515/jbcpp-2020-0281.

OLANIYAN OT, ABDULFATAI OO, OLUGBENGA O, EWEOYA O, ADETOLA AA, OLAMIDE AA, AZEEZ O, ADEOYE OO (2021c) Modulatory role of vitamin E on proton pump (ATPase) activity of cadmium chloride-induced testicular damage in Wistar rats. *Biomed Res Int*, 2021: 4615384. doi: 10.1155/2021/4615384.

OLANIYAN OT, DARE A, OKOTIE GE, ADETUNJI CO, IBITOYE BO, EWEOYA O, DARE JB, OKOLI BJ (2021d) Ovarian odorant-like biomolecules in promoting chemotaxis behavior of spermatozoa olfactory receptors during migration, maturation, and fertilization. *Middle East Fertil Soc J*, 26: 3. https://doi.org/10.1186/s43043-020-00049-w.

OYEWOPO AO, OLAWUMI J, ADELEKE O, OYEWOPO C (2018) Review on the role of glutathione on oxidative stress and infertility. *JBRA Assist Reprod*, 22(1): 61-66. doi: 10.5935/1518-0557.20180003

SHEWEITA SA, TILMISANY AM, AL-SAWAF H (2005) Mechanism of male infertility: role of anti oxidants. *Curr Drug Metab.* 6: 495-501.

TANG M, XIE Y, YI Y (2003) Effects of formaldehydes on the germ cells of male mice. *Wei Sheng Jiu*, 32: 544-548.

TANG X, BAI Y, DUONG A, SMITH MT, LI L, ZHANG L (2009) Formaldehyde in China: production, consumption, exposure levels, and health effects. *Environ Int*, 35: 1210-1224.

WONG EY, RAY R, GAO DL, WERNLI KJ, LI W, FITZGIBBONS EO (2006) Reproductive history, occupational exposure and thyroid cancer risk among women textile workers in Shanghai, China. *Int Arch Occup Environ Health,* 79(3): 251-258.

YU ZQ, JIANG SF, LENG SG, HE FS, ZHENG YX (2005) Early genetic effects on workers occupationally exposed to formaldehyde. *Zhonghus YU, Fang YX, Za Zhi*, 39: 392-395.

ZHOU DX, QIU SD, ZHANG J, WANG ZY (2006) Reproductive toxicity of formaldehyde to adult male rats and the functional mechanism concerned. *Sichuan Da Xue Xue Bao Yi Xue Ban*, 37(4): 566-569.

ZHOU D, ZHANG J, WANG H (2011) Assessment of the potential reproductive toxicity of long-term exposure of adult male rats to low-dose formaldehyde. *Toxicol Ind Health*, 27(7): 591-598.

Human unilateral bifid coronoid process – Report of a rare accidental radiographic finding

Karthikeya Patil, C.J. Sanjay, V.G. Mahima, Lakshminarayana Kaiyoor Surya

Department of Oral Medicine and Radiology, JSS Dental College and Hospital, JSS Academy of Higher Education and Research, Mysore - 570 015, India

SUMMARY

Routine panoramic radiographic evaluations reveal morphological differences in the maxillofacial structures, particularly the mandible. Although bifid condyle variants are prevalent, bifid coronoid processes are rarely reported. Here a regular digital Orthopantomograph (OPG) was advised for the patient's routine dental care, which revealed the presence of a unilateral bifid coronoid process on the right side of the jaw, which was confirmed with Cone Beam Computed Tomography (CBCT). This is notable, because it is only the second incidence of its kind to be documented.

Key words: Coronoid process – Anatomical variation – Radiography

INTRODUCTION

The human mandible is the largest, strongest, and only long bone in the skull that has the capacity for separate movement except for the tympanic ossicles and it is anatomically and symmetrically divided into body, ramus, coronoid, and condylar processes bilaterally (Schafer and Thane, 1890). The mandible has a bowed body, which is convex anteriorly, and has two rami that rise posteriorly and have condylar and coronoid processes on both sides (Desai et al., 2014). The coronoid is a thin triangular beak-like process placed anterosuperiorly of the ramus and gives attachment to two important muscles of mastication, the temporalis and masseter, thus emphasizing the morpho-functional dependence. The coronoid process is a membranous type of bone subjected to minimum resorption which can be harvested for local graft, causing less morbidity, no apparent functional limitation, and no cutaneous scarring (Hamilton, 1960). Anatomical and morphological variations have been reported with regard to the shape, length, and width of the coronoid process, and only a few reports mention the bifurcation, or bifid coronoid process. In their letter to the editor, Kansu et al. (1994) mentioned the first instance of the bifid coronoid process in which a detailed description was not given. This article reports a rare instance of an accidental finding of the unilateral bifid coronoid process. Our case may be the second well-documented instance reported in the English literature.

Corresponding author:
Dr Sanjay CJ MDS. Department of Oral Medicine and Radiology, JSS Dental College and Hospital, JSS Academy of Higher Education and Research, Mysore - 570 015, India. Phone: +91 9742565566. E-mail: drsanjaycj_dch@jssuni.edu.in

Submitted: December 16, 2021. **Accepted:** December 29, 2021

https://doi.org/10.52083/MZCM9500

CASE REPORT

A 58-year-old male patient reported to our outpatient department with a fractured lower back tooth. He had been hypertensive for 15 years, and was on regular medication. He had no other comorbidities. The initial physical examination was within normal limits. His intraoral examination revealed deep caries of 27, 28, with grade 1 mobility and root stumps of 26, 35, 36. He had generalized gingival inflammation with recession and shallow periodontal pockets and exhibited partially edentulous upper and lower arches. A panoramic radiograph (Orthopantomograph, OPG) revealed an interesting anatomical peculiarity in the coronoid process apart from the dental and periodontal pathologies (Fig. 1, showing the bifid coronoid process in the OPG). A CBCT examination confirmed the bifid nature of the coronoid process (Fig. 2 showing the 2-D representation and Fig. 3 showing the 3-D representation of the bifid coronoid process).

DISCUSSION

The mandible, or submaxilla, is a "U"-shaped bone that forms the lower jawline and articulates with the temporal bone on either side. It has a curved body shape with two rami. Each ramus consists of two processes: coronoid and condylar. The coronoid process (from Greek korone, "like a crown") is formed by the extension of the ascending ramus into a thin triangular eminence which is flattened from side to side and varies in shape and size (Nayak et al., 2015). The mandible, thus being strategically located, is commonly affected during inflammation, infections, and trauma. Thus, it is the most commonly radiographed bone in the face.

Recent advancements in trauma imaging, such as CBCT, have paved the way for the detection of variations in the mandible's structural anatomy. Our patient's CBCT image revealed a triangular coronoid process with a bifurcation, consistent with a bifid coronoid presentation, which is defined as "the division of the coronoid process, either antero-posteriorly or medio-laterally, by a cleft/groove/notch that provides attachment to the temporalis muscle". In this instance, the term "bifid" refers to the presence of a bifurcation or groove that divides the coronoid process antero-posteriorly into two parts.

Numerous variations in the shape of the coronoid process have been documented, but few on the double or bifid coronoid process.

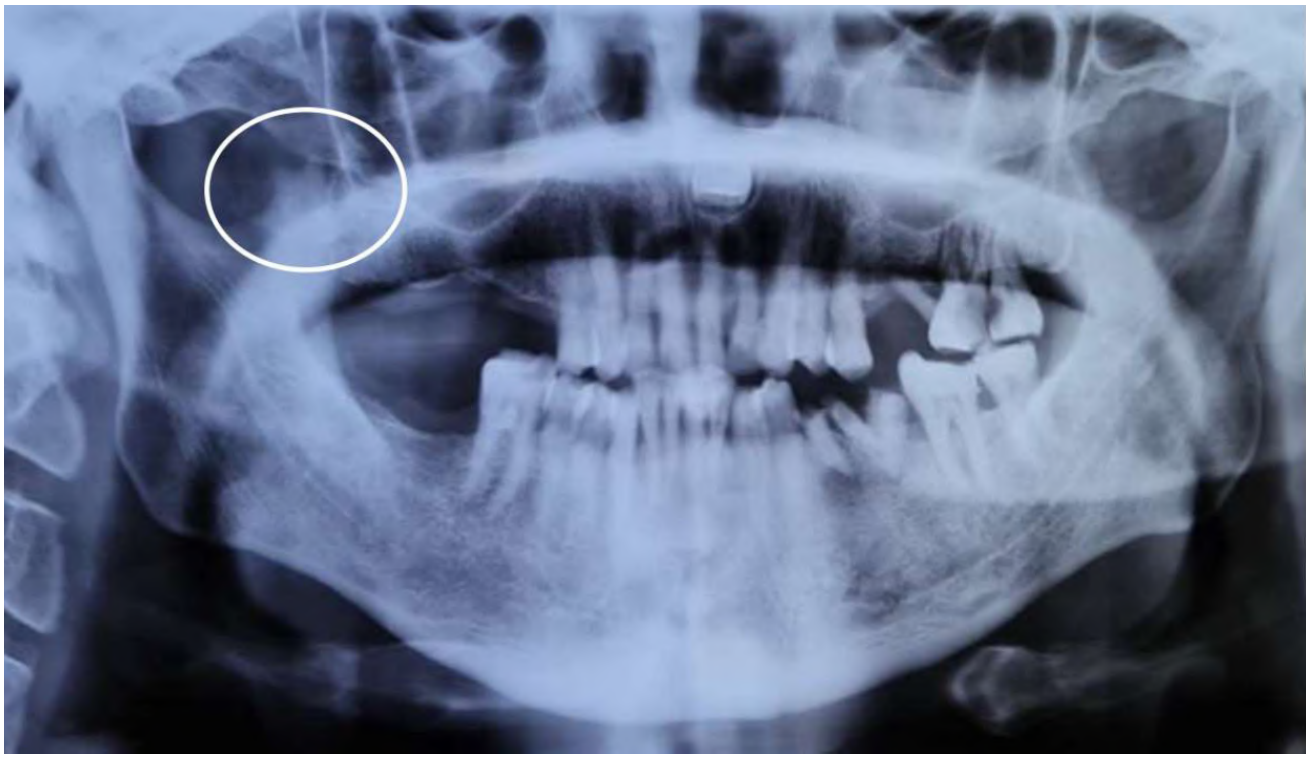

Fig. 1.- The bifid coronoid process in the Orthopantomograph (OPG).

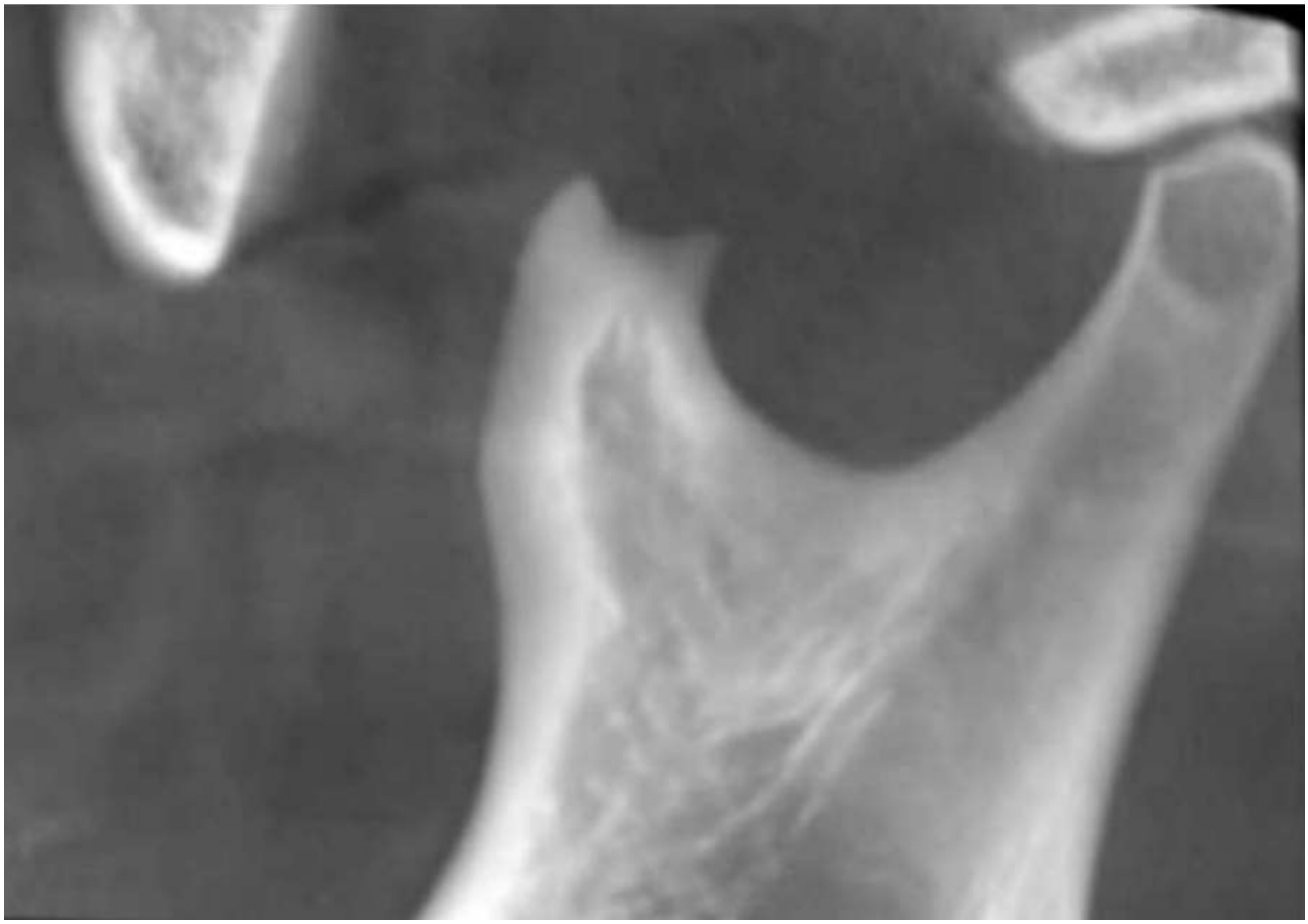

Fig. 2.- 2-D representation of the bifid coronoid process.

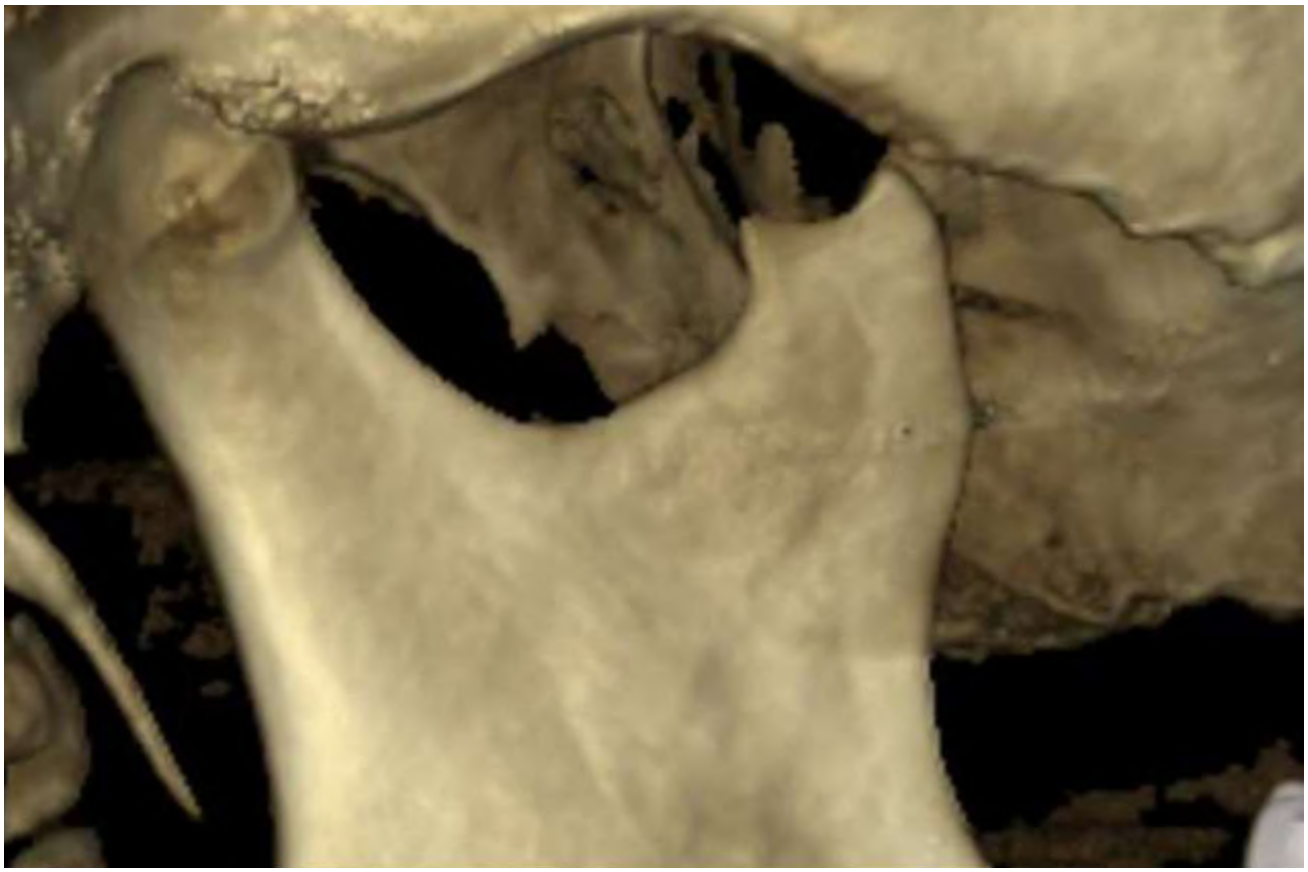

Fig. 3.- 3-D representation of the bifid coronoid process.

The present case is a novice's account of such an occurrence. Earlier, Schafer and Thane (1890) described it as a beak-shaped process in 1915, while Schulz (Subbaramaiah et al., 2015) described it as an S-shaped, undulant, and low-symmetrical process in 1933. The process's sabre-like curvature was attributed to ageing. As a result, a number of authors, including Hamilton and Williams et al (1960) and Basmajian and Slonecker (1989), have referred to it as a triangular process. Additionally, the presence of a double or second coronoid process has been mentioned. According to Isaac and Holla (2001), the coronoid process is triangular, hook-shaped, and rounded. Based on the literature, the following shapes are classified and are described as follows (Fig. 4 shows the schematic representation of various forms of the coronoid process):

Triangular-pointed apex, straight anterior and posterior borders, notch

Hook shaped—pointed apex, convex anterior border, concave posterior border, notch

Rounded – blunt apex, anterior and posterior borders straight, notch absent

Miscellaneous – which doesn't fit into any of them (Subbaramaiah et al., 2015).

Kasat and Bhuiyan (2016), identified hook-shaped coronoid processes (54.5%) as the most common in their analysis of 109 dried mandibles, followed by triangular (23.5%) and rounded processes (17.0 percent). This corroborates the findings by Subbaramaiah et al. (2015). But this was in contrast to other researches, the majority of which were conducted in various parts of India. The triangular shape of the coronoid process was most frequently observed in research by Isaac and Holla (2001) and Desai et al. (2014). According to Pradhan et al. (2014), the coronoid process is most commonly hook-shaped. In their study of 157 mandibles, Isaac and Holla (2001) found that hook-shaped mandibles were 27.4%, triangular mandibles were 49.6%, and rounded mandibles were 23.6%. The author discovered that the rounded type was almost equally prevalent in male and female mandibles, the triangular type was slightly more prevalent in females, and the hook type was more prevalent in male mandibles. Our finding of unilateral bifid coronoid process may be the first well-documented case report following Kansu et al. (1994), who did not include a thorough description in their letter to the editor.

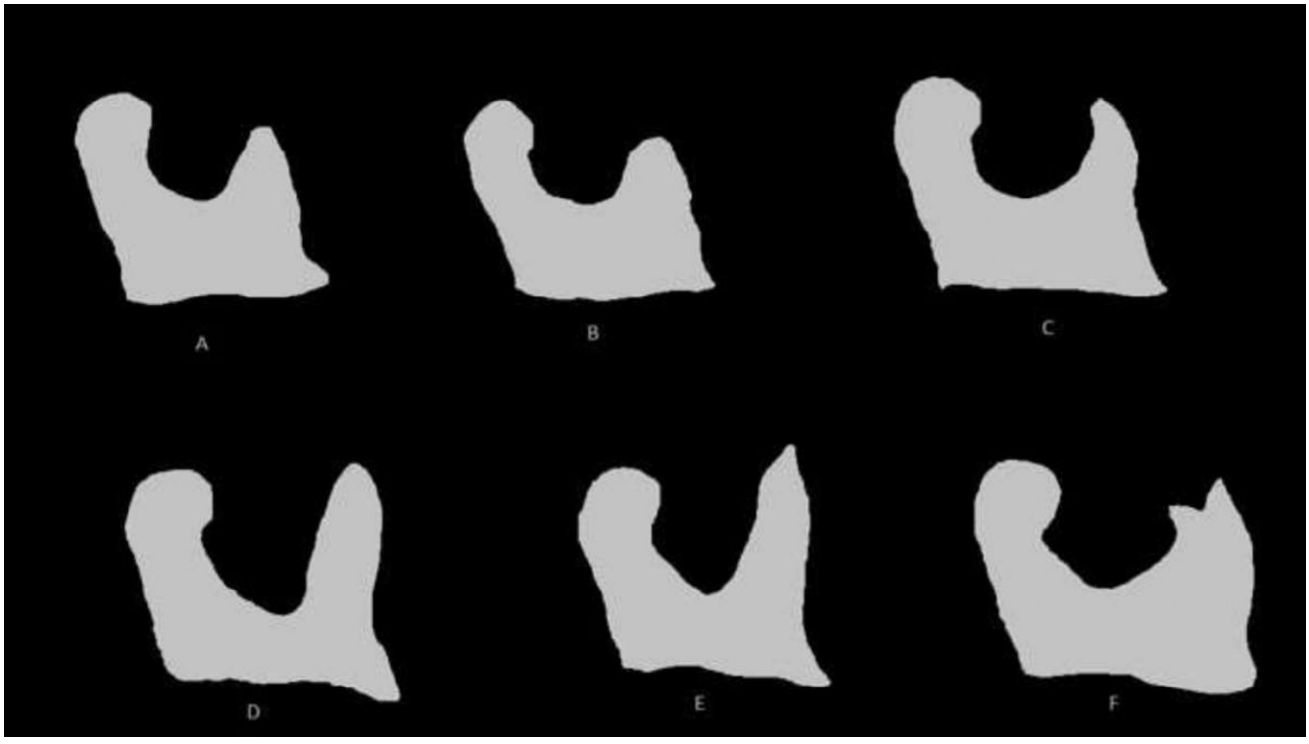

Fig. 4.- Schematic representation of various forms of the coronoid process.

The development of the craniofacial region is a complex process. This requires the integration of multiple specialized tissues, including the ectoderm of the surface, the neural crest, the mesoderm, and the pharyngeal endoderm. The lower jaw develops primarily between the fourth and eighth weeks of gestation, beginning with the paired mandibular prominences. All of these prominences are formed during the fourth week of gestation by the proliferation of neural crest cells that migrate into the arches from the neural crest. The mandibular primordia's neural crest cells originate primarily in the anterior rhombencephalon region and give rise to connective tissue components such as cartilage, bone, and ligaments in the facial and oral regions (Liu et al., 2010). Diet has a significant effect on the muscular pull on the bony process, and can significantly alter the shape of the coronoid process. Occupation and hormones have an effect as well (Jadhav and Vedpathak, 2017). For example, basket makers who frequently weave with their mouths have a larger coronoid process as a result of functional overactivity of the temporalis. Factors disrupting the formation of the lower jaw can alter the mandible's morphology. For instance, hyperactivity of the temporalis muscle results in reactive coronoid process elongation. Additionally, temporomandibular joint dysfunction caused by chronic disc displacement is associated with unilateral hyperplasia. It is mentioned as a factor in the development of Jacob's disease (Jimenez Alvarez and Valdes Reyes, 2020). Additionally, trauma, genetic, and familial factors may play a role. Ankylosing spondylosis has also been linked to mandibular elongation (Bechterew disease) in one study (Wenghoefer et al., 2008). In our patient, there was no previous history, clinical and/or radiological evidence of trauma, hence the cause of this unusual variation could be attributed to the developmental remodeling of the mandible. The cause of this rare variation is elusive, and extensive studies are required in this direction.

The coronoid process is gaining importance as a graft material in all aspects of reconstructive cranial maxillofacial surgeries like orbital floor reconstruction, paranasal augmentation, and temporomandibular joint ankylosis (Mintz et al., 1998). In this regard, there is a need for an understanding of the detailed anatomy and development of the coronoid process. Imaging studies of the coronoid will be a routine, which will report the occurrence of rare variations in the morphology of the coronoid. Different techniques can be used to obtain autologous, allograft, or synthetic bone grafts. Autologous bone grafts are harvested from one area of the patient's body and used in another area of the same person. Because the risks of infection, bleeding, and tissue damage are lower than with allografts, surgeons prefer this method.

Typically, graft bone is obtained from the iliac crest, rib, or calvarium. When the injury is minor, the coronoid process can be used as a graft material. As previously stated, the coronoid process graft has a number of advantages. It is critical to determine that the dimensions of the issued bone are adequate prior to performing grafting operations. In the present case, having a bifid or double coronoid process can be more useful, as one of the two can be spared for its functional adequacy and the other cultured as a graft.

CONCLUSION

The coronoid process is a vital structure in the mandible and exhibits diverse variations in its morphology. Significant differences might lead to difficulty in mastication and a decreased range of movement of the temporomandibular joint. Increased utilization of various imaging modalities will reveal unusual variations of coronoid that have to be reported. This is a prompt report of the incidence under this consideration. The maxillofacial surgeon can benefit from knowledge of the coronoid process's morphological shapes. It is an excellent donor graft site for reconstructive purposes, because it is used to repair osseous defects in the oral and faciomaxillary regions such as alveolar defects, orbital floor repair, maxillary augmentation, and correction of mandibular non-union fractures.

REFERENCES

BASMAJIAN JV, SLONECKER CE (1989) Grant's method of Anatomy. In: *Side of skull, temporal and infratemporal regions*. 11th ed. Williams and Wilkins, Baltimore, pp 615-616.

DESAI VC, DESAI SD, SHAIK HS (2014) Morphological study of the mandible. *J Pharm Sci Res*, 6(4): 175-177.

HAMILTON WJ (1960) Textbook of human anatomy and locomotion system, 2nd edition. McMillan, pp 60-62.

ISAAC B, HOLLA SJ (2001) Variations in the shape of the coronoid process in the adult human mandible. *J Anat Soc India*, 50: 137-910.

JADHAV DS, VEDPATHAK SB (2017) Variations in the shape of the coronoid process of adult human mandible in Marathwada and Western Maharashtrian region. *Int J Anat*, 4(2): 17-19.

JIMENEZ ALVAREZ JA, VALDÉS REYES JM (2020) Jacob´s disease, a rare disease of the coronoid process of the mandible. *SVOA Dentistry*, 1: 22-26.

KANSU H, KANSAS O, AKGUNLU F (1994) Bifid coronoid process. *Oral Surg Oral Med Oral Pathol*, 78(2): 136.

KASAT PA, BHUIYAN PS (2016) A study on coronoid process of the dry adult human mandibles. J Anat Soc India, 65(1): 9-14.

LIU YP, BEHRENTS RH, BUSCHANG PH (2010) Mandibular growth, remodeling and maturation during infancy and childhood. *Angle Orthodontist*, 80(1): 97-100.

MINTZ SM, ETTINGER A, SCHANKEL T, GLEASON M (1998) Contralateral coronoid process bone grafts for orbital floor reconstruction – an anatomical and clinical study. *J Oral Maxillofac Surg*, 56(10): 1140-1144.

NAYAK S, PATRA S, SINGH G (2015) Study of the size of coronoid process of mandible. *ISOR J Dent Med Sci*, 14(6): 66-69.

PRADHAN S, BARA DP, PATRA S, NAYAK S, MOHAPATRA C (2014) Anatomical study of various forms of mandibular coronoid process in relation to gender and age. *IOSR J Dent Med Sci*, 13(8): 9-14.

SCHAFER EA, THANE GD (1890) Elements of Anatomy in the bones of the head. Longman Green Co., London, pp 60-61.

SUBBARAMAIAH M, BAJPE R, JAGANNATHA SR, JAYANTI KS (2015) A study of various forms of coronoid process in determination of sex. *Ind J Clin Anat Physiol*, 2(4): 199-203.

WENGHOEFER M, MARTINI M, ALLAM JP, NOVAK N, REICH R, BERGE SJ (2008) Hyperplasia of the coronoid process in patients with ankylosing spondylitis (Bechterew disease). *J Craniofac Surg*, 19: 1114-1118.

The orobasal organ of Ackerknecht in a male body donor: A case report

Moritz Staeber, Sven Schumann

Institute for Microscopic Anatomy and Neurobiology, University Medical Center, Johannes Gutenberg-University, Mainz, Germany

SUMMARY

During histological evaluation of the oral cavity of a 61-year-old West-European male body donor, we observed a bizarre epithelial formation at the border between gingiva and oral mucosa, which most likely was an orobasal organ (of Ackerknecht). Although the orobasal organ probably does not have a functional significance, it is of clinical interest, because it must not be confused with a pathological condition like oral precancerous lesions or oral cancer.

Key words: Oral cavity – Gingiva – Oral mucosa – Vestigial organ – Evolutionary anatomy

INTRODUCTION

Vestigial anatomical structures are considered to have lost much or all of their function through evolution. These structures (e.g., leg bones in whales, external ear muscles in humans) can give insights into the phylogenetic history of species, since homologous structures indicate common ancestry. Additionally, vestigial structures can be of clinical importance, since these structures might be involved in pathological conditions (e.g., inflammation of Meckel's diverticulum), or be confused with pathologies. For example, the juxtaoral organ (of Chevitz or Zenker) in the cheek histologically mimics perineural invasion of cancer cells (Danforth and Baughman, 1979; Sancheti et al., 2015). While some of these rudiments are widely known, there are several structures which are widely neglected in medical literature, like the orobasal organ (of Ackerknecht).

The orobasal organ was discovered by and named after the veterinary anatomist Eberhard Ackerknecht in 1912 (Ackerknecht, 1912). He described morphologically highly variable epithelial invaginations (often two) behind the lower medial dentes incisivi in different mammalian species. The orobasal organ is considered to be a rudimentary structure without physiological function. Some authors hypothesize that this organ represents a remnant of the anterior sublingual gland, a salivary gland which is present in reptiles (Keller, 1922), but this interpretation did not go unchallenged. Therefore, the evolutionary history of the orobasal organ remains unknown, so far.

CASE REPORT

In the oral cavity of a 61-year-old West-European male who died of colon cancer, we observed a bizarre epithelial formation at the border between gingiva and oral mucosa, which most likely represents an orobasal organ (of Ackerknecht). This man

Corresponding author:
Sven Schumann, MD. Institute for Microscopic Anatomy and Neurobiology, University Medical Center, Johannes Gutenberg-University, Johann-Joachim-Becher-Weg 13, D-55128 Mainz, Germany. Phone: +49 173 2473997. E-mail: sven.schumann@uni-mainz.de

Submitted: December 30, 2021. **Accepted:** February 1, 2022

https://doi.org/10.52083/PWMD5478

was part of the body donation program of the Anatomical Institutes of the Johannes Gutenberg-University, Mainz, Germany. He donated his body voluntarily for medical education and research in accordance with common donation procedures for anatomical bequests in Germany. The body had been preserved via arterial perfusion with a formaldehyde solution and subsequent formaldehyde immersion within a humidity chamber. For histological examination, oral tissue was dissected and embedded in paraffin. Serial sections were stained with hematoxylin and eosin. No earlier oral pathologies were known in this patient.

In the present case, we observed an approximately 1.5 mm high (from luminal to basal) and 0.6 mm long bell-shaped epithelial body which pierced into the lamina propria at the border between the lingual gingiva (LG) behind the lower medial incisors and the oral mucosa (OM) of the floor of the mouth (Fig. 1). The estimated thickness of the epithelial body in serial sections was 0.5 mm. The epithelial body consisted out of non-keratinized stratified squamous cells. No signs of epithelial cell degeneration, keratinization or secretion were visible. We observed an intact basement membrane around this structure. Serial sections did not show a lumen within this structure, but on the mucosal surface a small pit was formed. Within the lamina propria, we did not observe greater nerve fibers or sensory bodies in direct vicinity of this structure.

COMMENTS

Because of its special morphology and localization, this structure most likely is a case

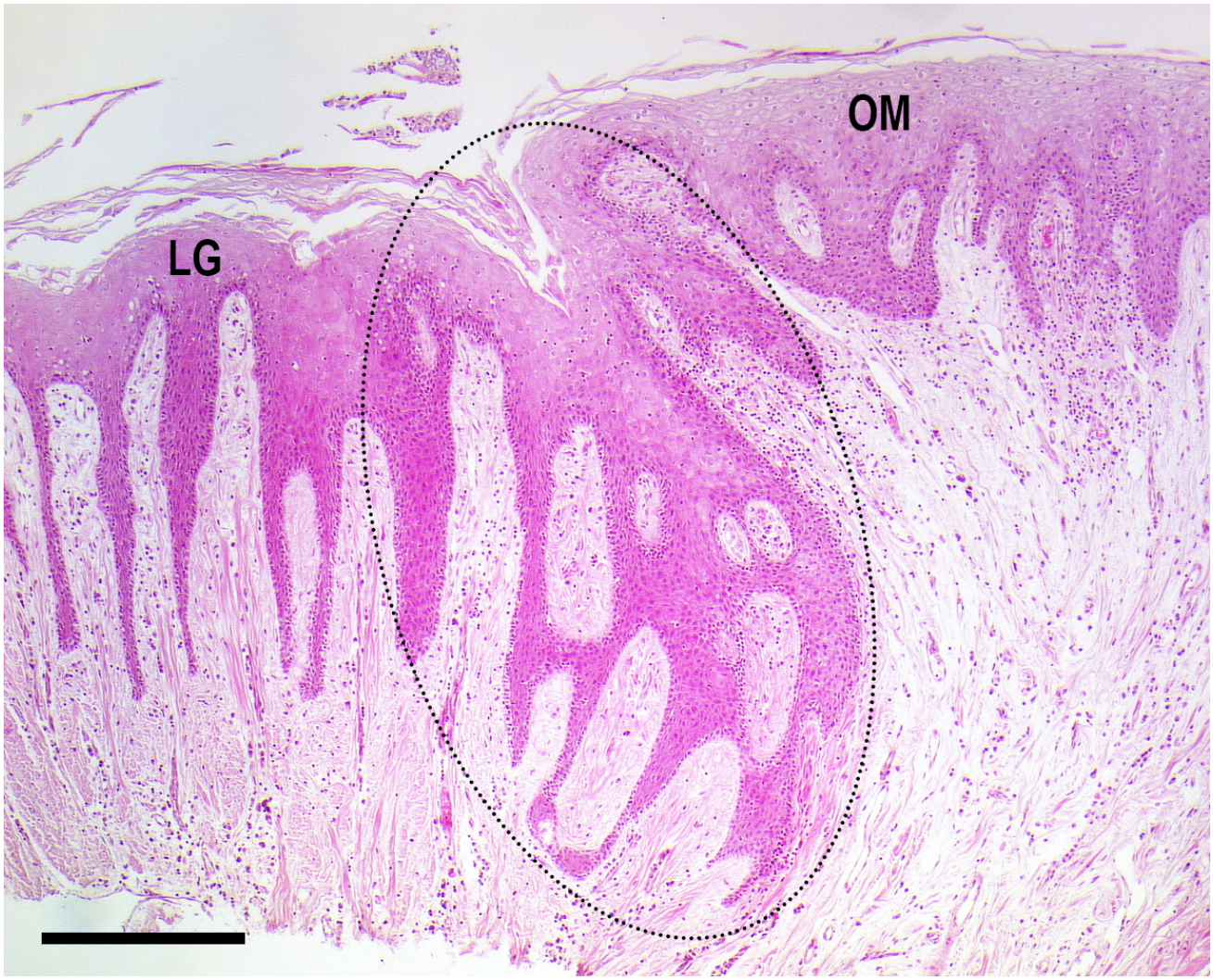

Fig. 1.- Hematoxylin-eosin-stained section of the putative orobasal organ (of Ackerknecht) (within the ellipse) at the border between the lingual gingiva (LG) and the oral mucosa (OM). Bar = 250 µm.

of an orobasal organ, also known as the organ of Ackerknecht, a highly neglected structure in anatomical literature. The existence of the orobasal organ in human embryos, fetuses and children was shown in multiple studies (Eberle, 1925-26; Schückher, 1937; Zorzoli, 1954; Kagawa, 1956), but, to our knowledge, until now there is only one publication which proves the existence of the orobasal organ in human adults (De Risky, 1954). In this publication, De Risky histologically identified 13 orobasal organs in a dissection case series of 15 adult humans. In contrast to other oral or perioral structures like the juxtaoral organ or oral neuroepithelial bodies (Cheng et al., 2016), the histological features of the orobasal organ do not give any hints to a secretory or receptor function of this structure (Malinovsky et al., 1996). Due to its location at the border between gingiva and oral mucosa, mechanical stress of this region might influence the development of this organ. Ungerecht (1951) hypothesized that the orobasal organ might be involved in the development of oral dermoid cysts but experimental or clinical data are missing.

Although the orobasal organ most likely does not have a functional significance, it is of clinical interest, because it must not be confused with a pathological condition like oral precancerous lesions or oral cancer. We hope that this report will increase awareness of this obscure but obviously physiological anatomical structure, and thereby decrease the chance of a misdiagnosis and unnecessary therapeutic intervention. Additionally, further investigation in comparative anatomy of this structure both in human and animals might give new insights into the evolution of oral structures.

ACKNOWLEDGEMENTS

The authors sincerely thank those who donated their bodies to science so that anatomical research and teaching could be performed. Results from such research can potentially increase scientific knowledge and can improve patient care. Therefore, these donors and their families deserve our highest respect.

REFERENCES

ACKERKNECHT E (1912) Ein eigenartiges Organ im Mundhöhlenboden der Säugetiere. *Anat Anz*, 41: 434-449.

CHENG E, COHEN MA, SCOGNAMIGLIO T (2016) Neuroepithelial structure resembling the juxtaoral organ of Chievitz: usual morphology in an unusual location. *Int J Surg Pathol*, 24(8): 721-722.

DANFORTH RA, BAUGHMAN RA (1979) Chievitz's organ: a potential pitfall in oral cancer diagnosis. *Oral Surg Oral Med Oral Pathol*, 48(3): 231-236.

DE RISKY S (1954) The organ of Ackerknecht in humans. *Rass Odontotec*, 35(1): 61-67.

EBERLE W (1925-26). Zur Entwicklung des Ackerknecht'schen Organs. *Anat Anz*, 60: 263-279.

KAGAWA G (1956) Über das früheste Stadium der Entwicklung der Zähne des Menschen. *Arch Histol Jpn*, 10: 483-523.

KELLER E (1922) Über ein rudimentäres Epithelialorgan im präfrenularen Mundboden der Säugetiere. *Anat Anz*, 55: 265-285.

MALINOVSKY L, UMLAUF R, CAVALLOTTI C, MALINOVSKA V, HEES H, VEGA JA, D'ANDREA V (1996) Sensory systems around cavum oris in man. *Dtsch Zschr Akup*, 39(6): 136-139.

SANCHETI SM, SAWAIMOON S, ZAMEER MAL (2015) Juxtaoral organ of Chievitz, an obscure anatomical structure masquerading as perineural invasion of mucoepidermoid carcinoma: case report and review of literature. *Int J Surg Pathol*, 23(6): 461-463.

SCHUECKHER R (1937) Embryologische Untersuchungen über das Ackerknechtsche Organ bei Ratte und Mensch. *Z Mikrosk Anat Forsch*, 41: 558-568.

UNGERECHT K (1951) Zur Genese der Dermoidcysten am Mundboden. *Arch Ohr- usw Heilk u Z Hals- usw Heilk*, 160: 316-327.

ZORZOLI E (1954) Ackerknecht's organ in animals and man. *Biol Lat*, 7(3): 585-597.

First detailed musculoskeletal study of a fetus with scoliosis and review of current literature

Andrew E. Barra[1], Herman Chadha[2], Rui Diogo[1]

[1] *Department of Anatomy, Howard University College of Medicine, Washington DC, USA*
[2] *Saint George's University Medical School, West Indies, Grenada*

SUMMARY

No papers have described, so far, the muscular anomalies present in human fetuses with scoliosis. This paper provides a detailed report along with images on the musculoskeletal structures of a fetus with scoliosis, focusing in particular on the musculature of the posterior thoracic region. The dissections reveal several anomalies in different muscle groups secondary to the severe curvature of the spine. This study, which is part of a broader attempt to describe and collect knowledge about human musculoskeletal abnormalities occurring in congenital scoliosis, as well as in a plethora of other conditions and syndromes, will likely lead not only to a greater understanding of congenital scoliosis in particular and human congenital malformations in general, but also to wider discussions on developmental and evolutionary biology. Such studies are crucial to help in the diagnosis and management options to improve quality of life in patients diagnosed with congenital scoliosis in particular.

Key words: Congenital scoliosis – Muscles – Fetuses – Birth defects – Comparative anatomy – Human anatomy

INTRODUCTION

Scoliosis is defined as an abnormal curvature of the spine, specifically at least 10 degrees in the lateral aspect, and can be characterized as congenital, idiopathic or syndromic (Altaf et al., 2013). Congenital scoliosis can be caused by either an embryological defect of vertebrae formation or a defect in vertebral segmentation (Kose and Campbell, 2004). Congenital scoliosis is yet to be linked to a known cause. Environmental factors (hypoxia, vitamin A deficiency, exposure to alcohol, valproic acid, boric acid, and hyperthermia) (Li et al., 2015), genetics, vitamin deficiencies, hormones, and drugs, have all been linked to the occurrence of vertebral defects, either individually or in combination (Hensinger, 2009). The physiologic damage develops early in the embryologic cycle, well before cartilage and bone growth, and the resultant defects can involve complete or partial fusion of the vertebrae, as well as a lack of development of the vertebrae, which can result in a curvature that can progress with time (Hensinger, 2009).

Somites are the precursors of the vertebral bodies. As the somites are formed, the development process of fetal vertebral growth in

Corresponding author:
Rui Diogo. Dept. of Anatomy, Howard University College Medicine, Numa Adams Building, room 1101, 520 W St. NW, 20059 Washington, DC, USA. Phone: 202-6400982; Fax: 202-5367839. E-mail: rui.diogo@howard.edu

Submitted: January 4, 2022. **Accepted:** February 2, 2022

https://doi.org/10.52083/AFND5066

the human fetus starts at about 3 to 5 weeks (Erol et al., 2002; Larsen, 1997). Somitogenesis is the mechanism by which the precursor spine tissue is segmented; formation of somitogenesis happens between 20 and 30 days after conception, in the first month of pregnancy (Erol et al., 2002; Larsen, 1997). However, at 6 to 8 weeks, the somites begin to segment, and therefore congenital defects can arise long before chondrification and ossification in this process. Even earlier, during the development of the vertebral mesenchymal anlage in weeks 4 to 5, a vertebral defect can be seen for the first time (Erol et al., 2002; Larsen, 1997). The intersegmental artery and a differential in nutritional blood flow are thought to be closely linked to the development of the definitive vertebral body, as cells closest to the artery tend to divide more quickly (Tanaka and Uhthoff, 1981a, b). The problem does not seem to be caused by the notochord; however, it tends to be caused by the intersegmental arteries during resegmentation: e.g., the cartilaginous anlage of the vertebral body has been shown to have malformations, allowing for certain theories regarding the pathogenesis of congenital scoliosis (Tanaka and Uhthoff, 1981a, b). Importantly, the changes occur early in the pregnancy; no vertebral changes have been observed in fetuses older than 16 weeks (Tanaka and Uhthoff, 1981a, b). Vertebral deformities may thus be caused by a lack of vertebral development and structures, such as hemivertebra, or a failure of segmentation, causing defects of the intervertebral disk, which involves unilateral and segmented bars on the anterior and posterior sides of the spine, or a mixture of the two. Since various sections of the vertebral body and posterior elements may be involved to differing degrees, many classification schemes have been created (Tanaka and Uhthoff, 1981a, b).

So far, no papers have described the muscular anomalies present in human fetuses with scoliosis, as is also the case for many other conditions and syndromes occurring in humans. In order to reduce this key lack of knowledge, which is critical medical knowledge, in the last years Diogo and his colleagues have been actively working on the normal and 'abnormal' phenotypic embryonic and fetal development of human muscles (Alghamdi et al. 2017, 2018; Boyle et al., 2020; Crowley et al., 2019; Diogo et al., 2015a, b; 2019a, b; Gondre-Lewis et al., 2016; Karauda et al., 2021; Olewnik et al., 2018; Yurasakponget al., 2020). The present work is therefore done in the context of this wider comparative project. Namely, this paper provides the first detailed description of –including several anatomical images showing– the musculoskeletal structures of a human fetus with scoliosis, focusing in particular on the musculature of the posterior thoracic region. Due to the rarity of human fetuses with scoliosis that are available for dissection, information about a single individual is indeed a crucial contribution to comparative and pathological human anatomy. Specifically, this paper compares the results obtained with the very scarce anatomical information available in the literature about this condition, and discusses the data gathered, taking into account previous observations by the authors concerning other medical conditions and broader current evolutionary and developmental discussions.

MATERIALS AND METHODS

A male fetus with scoliosis –approximately between 16 to 20 gestational weeks– was dissected at Rui Diogo's lab, Department of Anatomy, Howard University College of Medicine (Fig. 1). The fetus is part of a collection obtained in the 1980s by Professor Aziz, which was donated to Diogo's lab for research. It was preserved in alcohol. Standard microdissection instruments were used for the dissections. The microdissections were bilateral and mostly focused on muscles, with nerves and major blood vessels maintained wherever possible. The deeper muscles were observed after the superficial muscles were cut close to their attachment. Complete detachment was avoided in order to maintain the muscle's integrity for future research. The following characteristics of each muscle were observed: 1) presence/absence, 2) origin, 3) insertion, 4) variation in number of bellies and/or tendons, and 5) overall muscular configuration. Muscles were compared to those of 'normal' human adults as well as 'normal' fetuses, based on descriptions based on works by Diogo and colleagues (see above). At each point of the

dissection, images were taken as a guide using a professional Nikon D90 camera with an AF-S Micro NIKON 60 mm lens to record various anatomical regions. To highlight a particular muscle, close images were taken and labeled accordingly. For size comparison, each photograph included a regular centimeter scale.

RESULTS

External features

Upon inspection of the posterior thorax, severe curvature of the spine is appreciated with overall appearance of the fetus leaning to the left side (Figs. 1-2). There is also evidence of tilted, uneven shoulders, with the left shoulder blade protruding more than the right, prominence of the ribs on the left side, and uneven waistline with the left hip higher than the contralateral side.

Posterior thoracic Musculature

Upon reflecting the left trapezius, measurements revealed that the left trapezius was approximately 0.5 cm greater than the right side. Apart from this, the trapezius of both sides has a normal configuration, attaching to the spinous processes of the vertebrae C7-T12, the spine of the scapula, and the superior nuchal line (Fig. 3). A thin muscle layer of the latissimus dorsi was appreciated bilaterally, of approximately equal measurements, and a normal configuration, attaching to the vertebral spines from T7 to the sacrum and inferior angle of the scapula (Fig. 4). The levator scapulae also has a normal overall configuration, originating from the transverse processes of C1-C4 vertebrae, but was abnormally fused with the trapezius muscle (Fig. 5). The splenius capitis has a normal configuration, attaching to the ligamentum nuchae and spines of C7-T6 vertebrae (Fig. 6). The

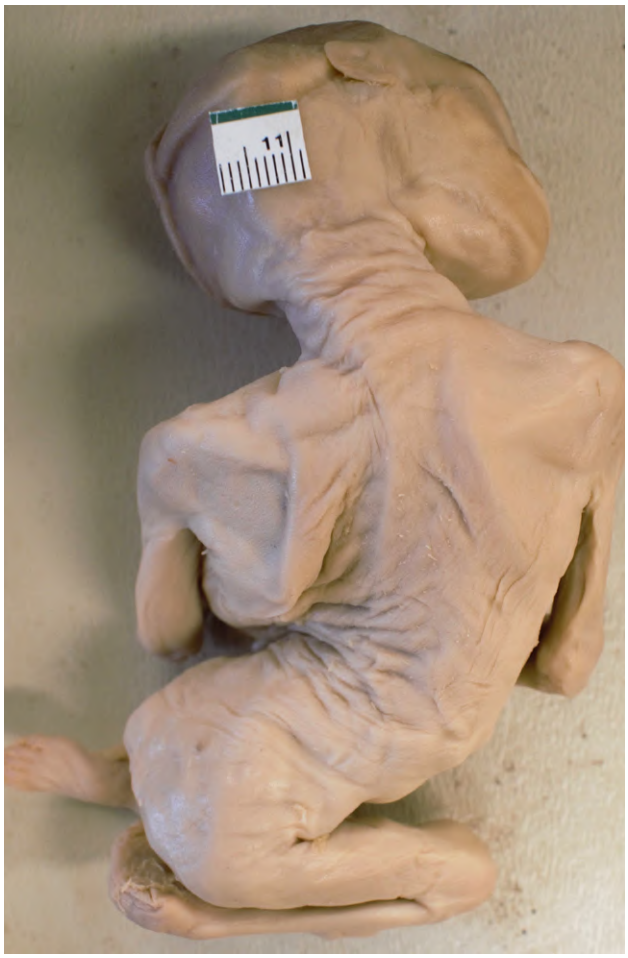

Fig. 1.- Posterior view of the fetus, showing a prominent left sided curvature of the spine.

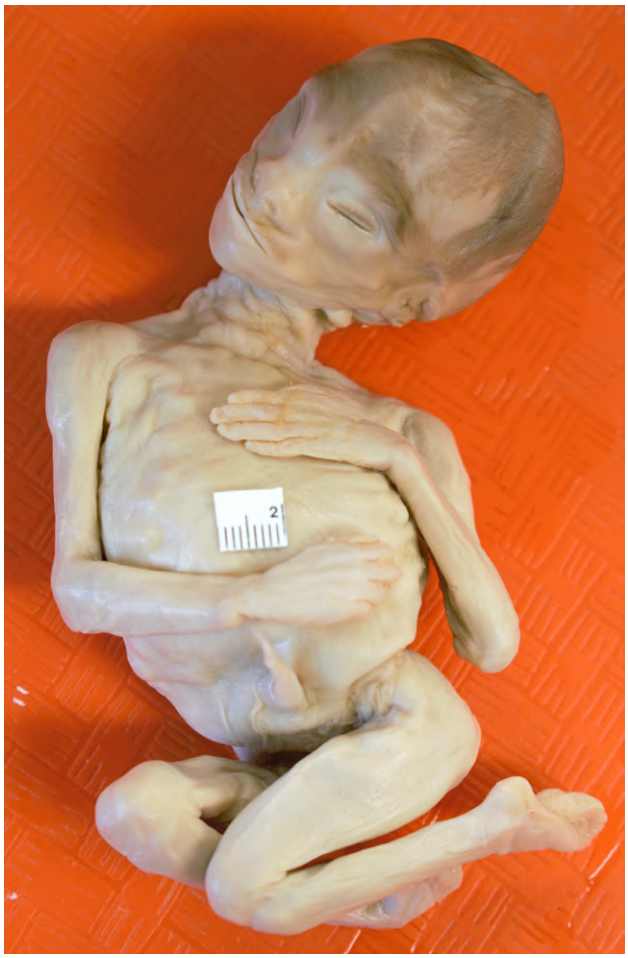

Fig. 2.- Anterior view of the fetus, showing a prominent left sided curvature of the spine.

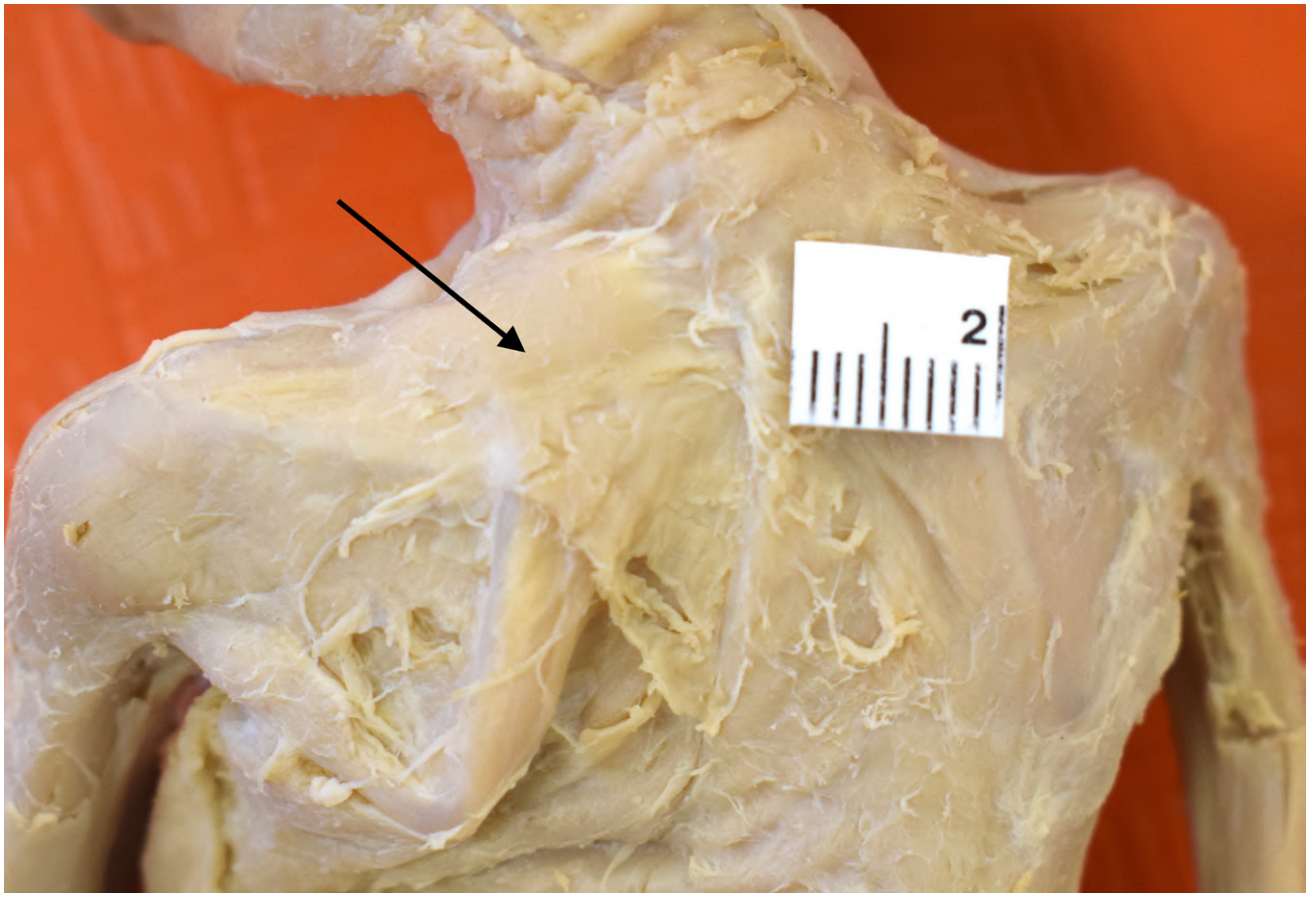

Fig. 3.- This image shows the trapezius muscle properly attached to the spinous processes C7-C12, spine of the scapula and the superior nuchal line.

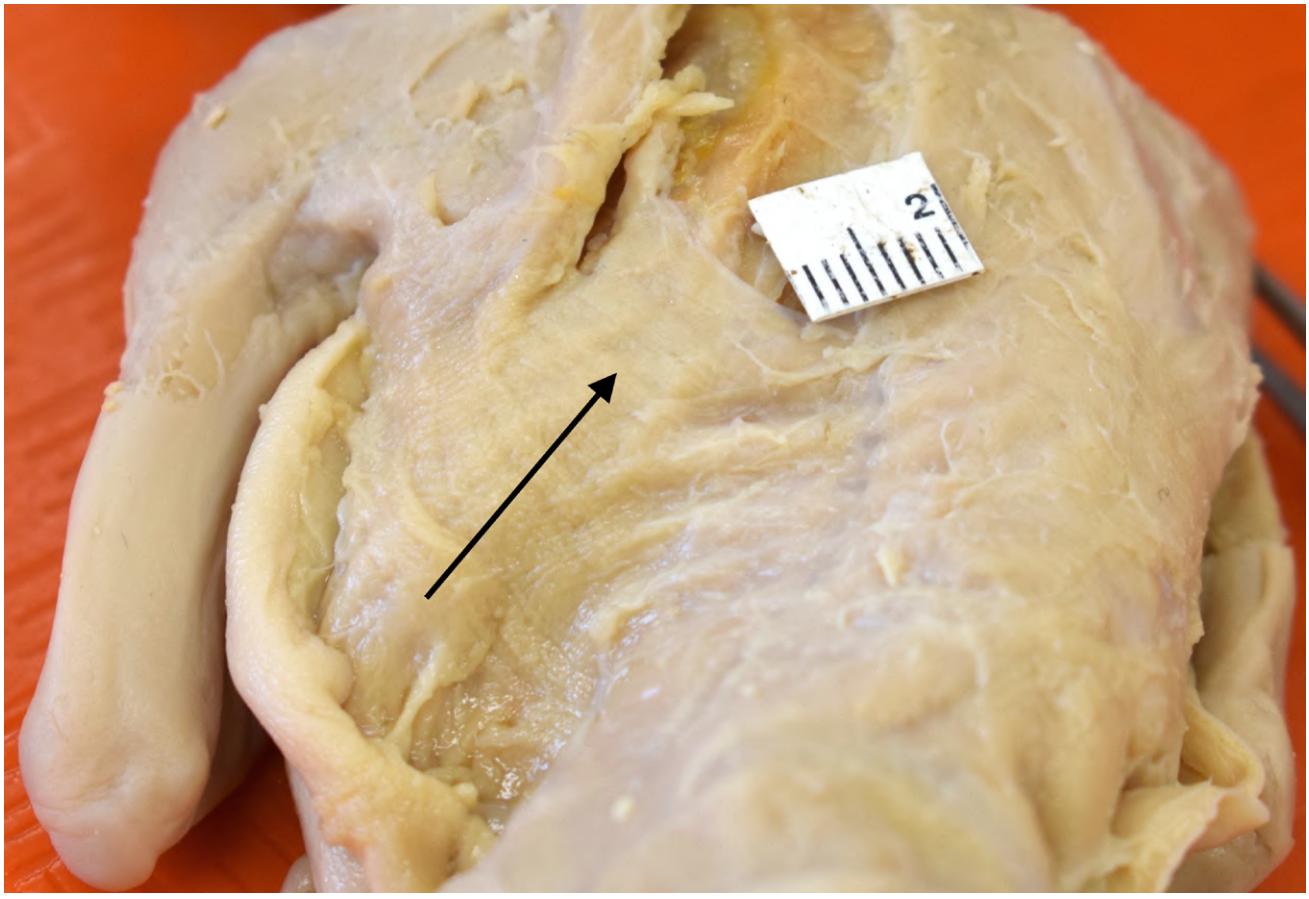

Fig. 4.- View showing of the latissimus dorsi.

supraspinatus, infraspinatus, and teres minor had mainly normal attachments (Fig. 7): distally to the superior, middle, inferior facets on the greater tubercle of the humerus, respectively. There was a thin layer of short muscle fibers between the medial border of the scapula and the neural tissues in the back, which seemed to correspond to a very underdeveloped rhomboid major and minor. Erector spinae muscles were fused and difficult to distinguish (Fig. 8). The other muscles of the body seemed to have the typical configuration for a male fetus of this age. In Table 1 we summarize the muscular anomalies we found in this fetus.

Table 1. Normal musculature vs. anomalous musculature observed in a fetus with congenital scoliosis.

Normal musculature	Anomalous musculature
Trapezius muscle approximately equal lengths bilaterally	Trapezius muscle 0.5 cm greater on left than right
Levator scapulae separated from trapezius	Levator scapulae fused with trapezius
Erector spinae muscles separate into spinalis, Longissimus, and iliocostalis	Erector spinae muscle fused

DISCUSSION

Since small spinal deformities frequently go undetected, the true incidence of congenital scoliosis in the general community remains unknown. Congenital intervertebral or vertebral body defects cause an imbalance in the trunk's longitudinal development in around 10% of cases of structural scoliosis (Burnei et al., 2015; Hedequist and Emans, 2004, 2007; Oestreich et al., 1998). Girls have a 2.5:1 chance of developing congenital scoliosis compared to boys (Jaskwhich et al., 2000; Konieczny et al., 2013). Curves appear equally often to the left and right. The incidence of the curve varies by degree of the spine: upper thoracic: 33%, lower thoracic: 31%, thoracolumbar: 20%, lumbar: 11%, and lumbosacral: 5% (Terminology Committee, 1976). The affected fetus in our case was a male, which is not consistent with the recorded higher frequency of females relative to males.

In the male fetus analyzed for this study, it was observed that various anomalies occur in the musculoskeletal system (Figs. 1-8; Table 1). Other studies have shown that patients with

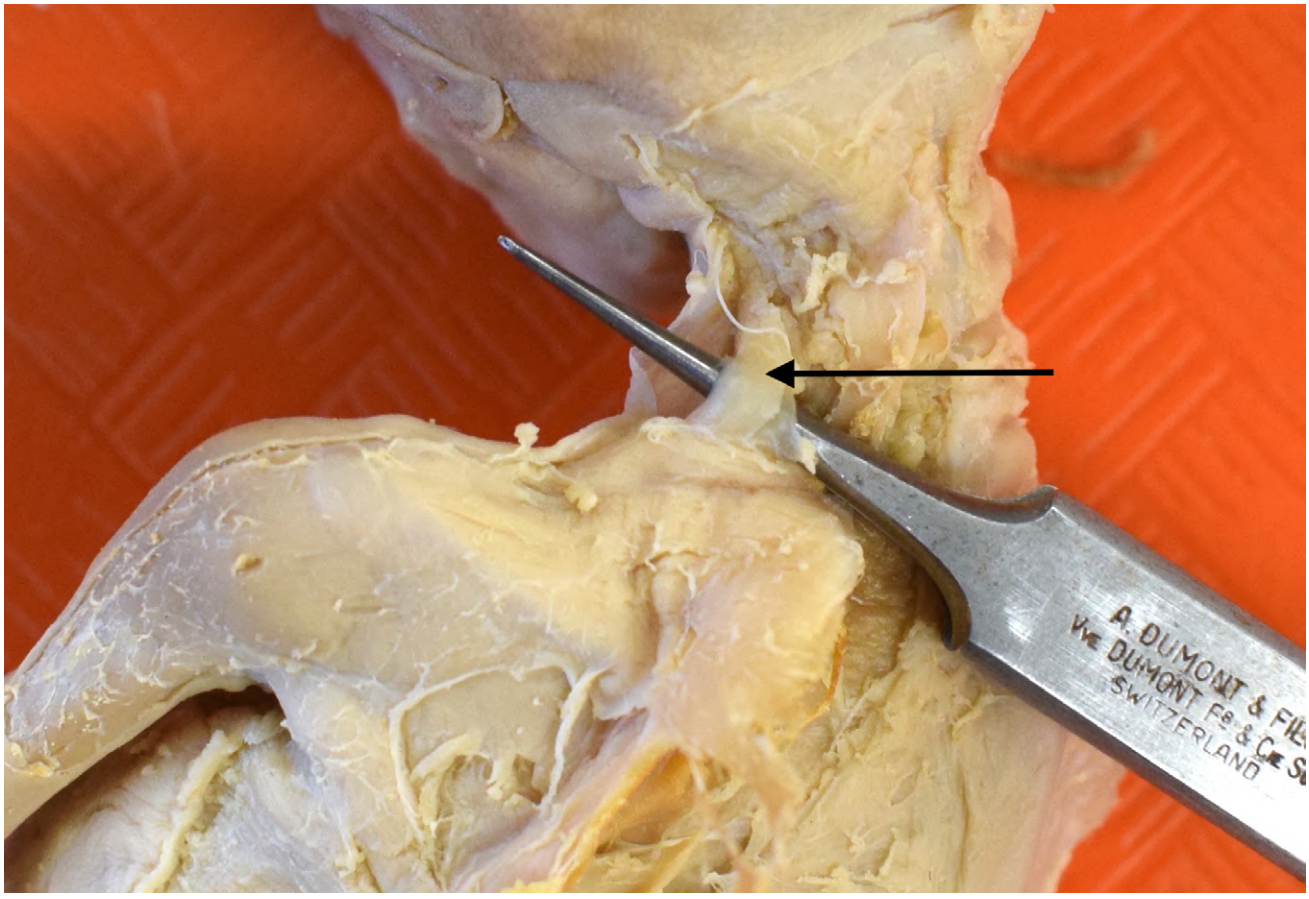

Fig. 5.- View showing the left levator scapulae abnormally fused to the trapezius muscle.

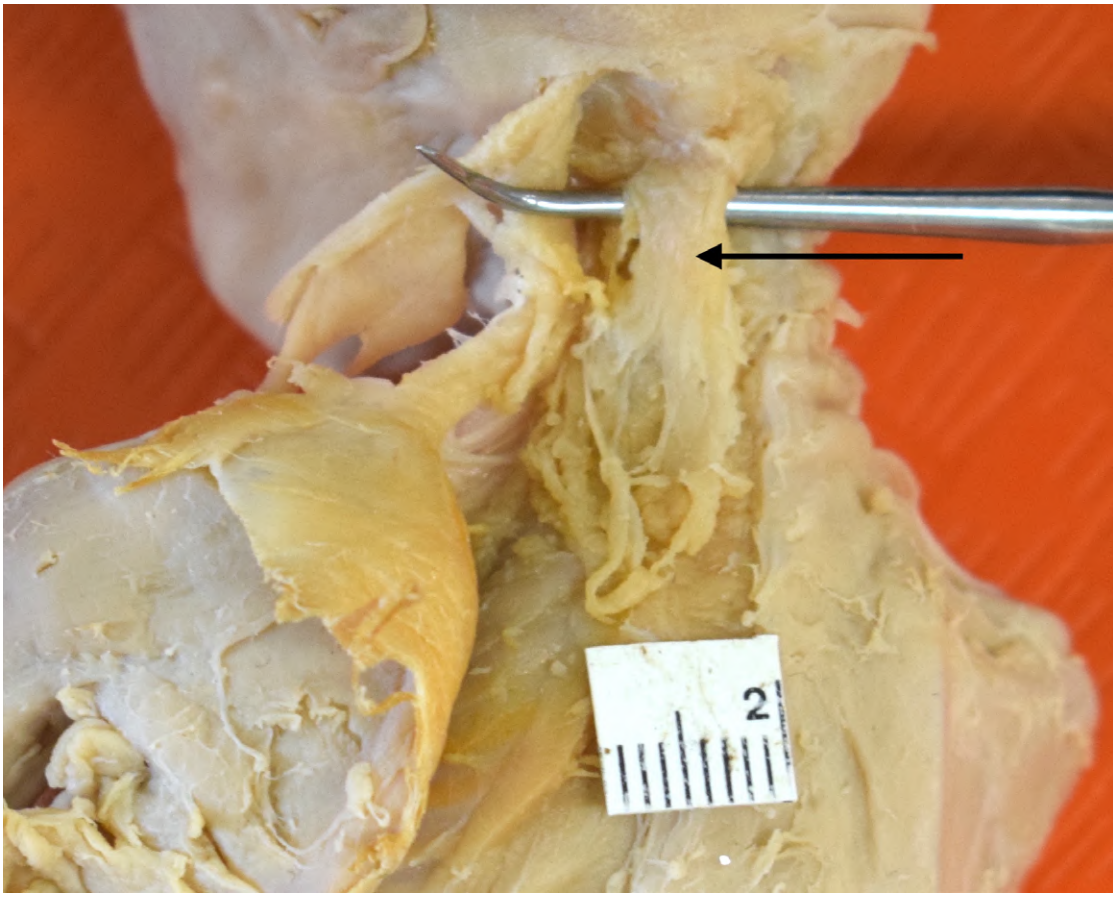

Fig. 6.- View showing the splenius capitis attached to the ligamentum nuchae and spines of C7-T6 vertebrae.

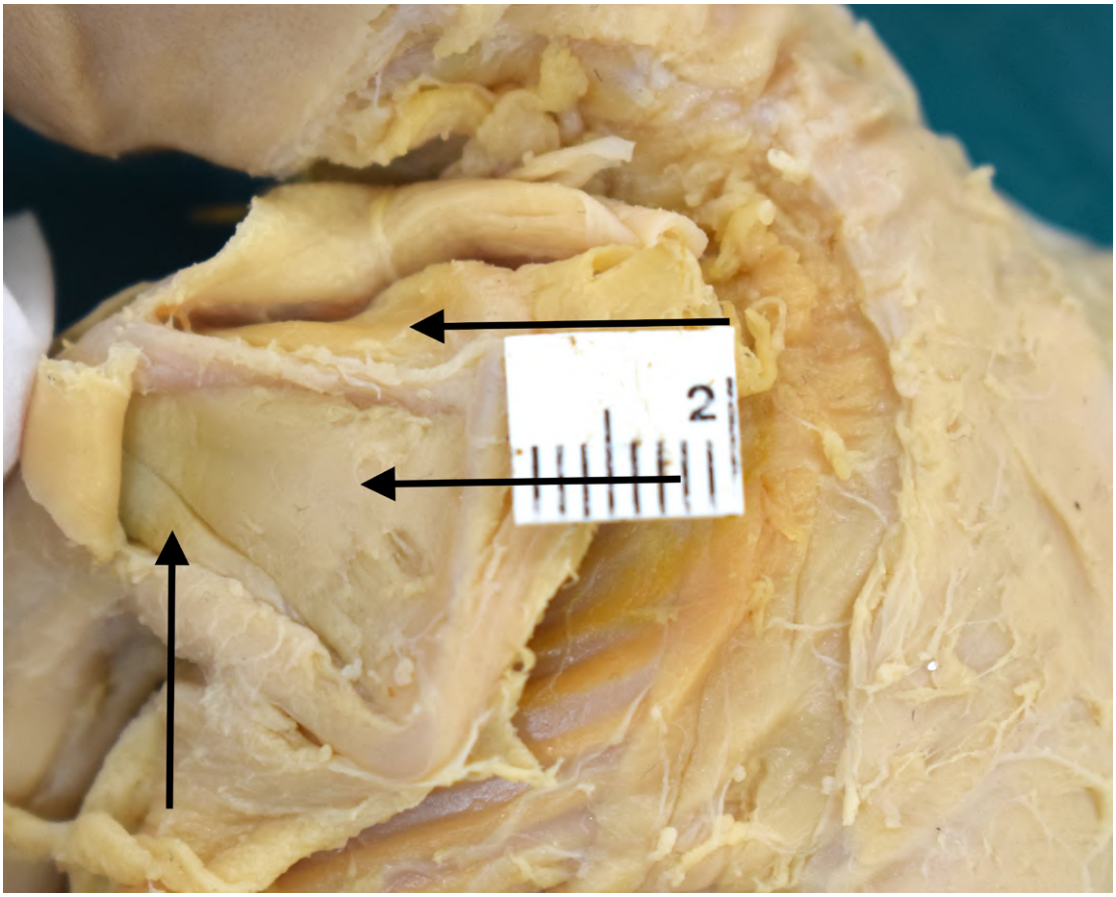

Fig. 7.- View showing the supraspinatus, infraspinatus and teres minor attached distally to the superior, middle, inferior facets on the greater tubercle of the humerus, respectively.

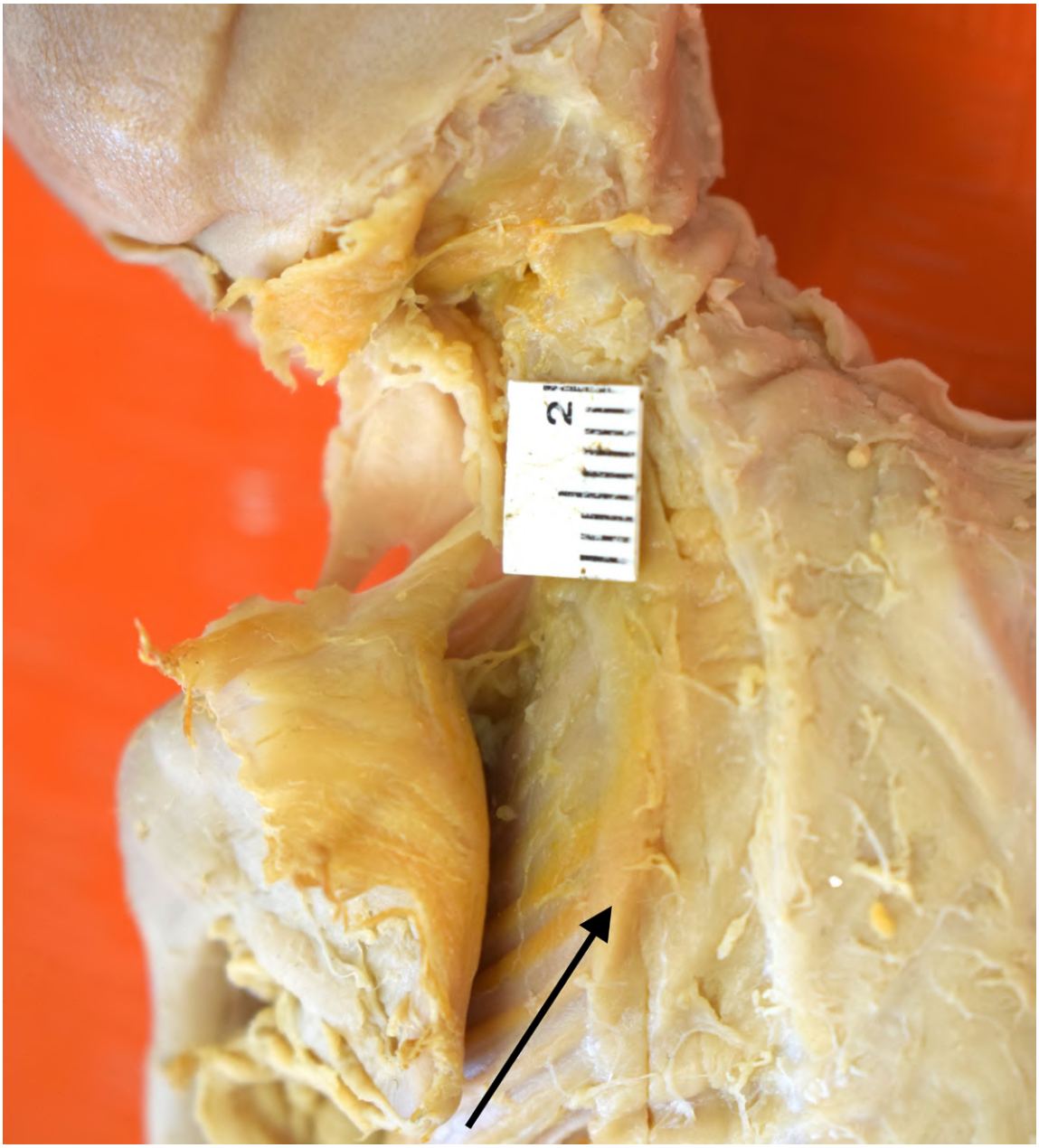

Fig. 8.- View showing of the erector spinae muscles which were fused together.

congenital scoliosis may have anomalies in other organ systems in as many as 61 percent of cases (Beals et al., 1993; Shen et al., 2013). Since the spine, genitourinary tract, musculoskeletal system, and cardiovascular system all develop during similar times, an embryonic insult to one or more of these systems may occur. Therefore, defects of one system should prompt evaluation of the other related systems to be evaluated as well. For instance, congenital spinal deformity is also linked to clubfoot, developmental dysplasia of the shoulder, limb hypoplasia, and Sprengel's deformity (Hensinger, 2009). Overall, the patient must be evaluated extensively for musculoskeletal abnormalities, as these are the most prominent organ system anomalies involved with congenital scoliosis (Hedequist and Emans, 2004, 2007). Since congenital abnormalities are linked to congenital scoliosis in the thoracic and lumbar spine, the entire spine, including the cervical spine, must be examined (Arlet et al., 2003; Beals et al., 1993).

However, as noted above, not only such correlational studies are missing in the literature, but even detailed studies of soft tissue anomalies seen in specific conditions, such as scoliosis, are also missing in the literature, which prevents a deep knowledge and understanding of birth

defects in general. In this study, the first detailed one of a fetus with scoliosis, did reveal a series of muscle anomalies, including abnormal muscle lengths and fused muscles (Table 1). However, further studies are needed to determine if these anomalies are consistently present in other fetuses having this condition, as well as in other organ systems. It is absolutely crucial to study correlational features and associated syndromes in detail, because the detection of less apparent defects can have a significant impact on the patient's overall well-being, maybe even more so than the discovery of more obvious defects. Additionally, the best management of these complex spine deformities would require a complete knowledge of the natural history of the deformity, as well as treatment principles. New imaging techniques such as three-dimensional computed tomography (CT) and magnetic resonance imaging (MRI) are useful for studying the underlying deformity and learning how dynamic deformities evolve (Van Goethem et al., 2007). Careful monitoring with radiographic assistance aids in determining if surgical intervention is needed (Van Goethem et al., 2007).

However, it should be pointed out that, at this point, current techniques, including MRI, often do not allow to mirror the fine details that can be detected in microdissections, such as the very tiny abnormal bundles of fibers connecting muscles such as trapezius and the levator scapulae in the fetus dissected by us. Therefore, studies such as this one are crucially needed for a greater understanding of congenital scoliosis in particular, but also of human congenital malformations in general, as well as to help in the diagnosis and management options to improve quality of life in patients diagnosed with congenital scoliosis in particular.

REFERENCES

ALGHAMDI, MA, ZIERMANN JM, GREGG L, DIOGO R (2017) A detailed musculoskeletal study of a fetus with anencephaly and spina bifida (craniorachischisis), and comparison with other cases of human congenital malformations. *J Anat*, 230: 842-858.

ALGHAMDI M, DIOGO R, IZQUIERDO R, PASTOR FJ, DE PAZ F, ZIERMANN J (2018) Detailed musculoskeletal study of a fetus with trisomy 18 (Edwards syndrome) with Langer's axillary arch, and comparison with other cases of human congenital malformations. *J Anat Sci Res*, 1: 1-8.

ALTAF F, GIBSON A, DANNAWI Z, NOORDEEN H (2013) Adolescent idiopathic scoliosis. *BMJ*, 2013: 346.

ARLET V, ODENT T, AEBI M (2003) Congenital scoliosis. *Eur Spine J*, 12: 456-463.

BEALS RK, ROBBINS JR, ROLFE B (1993) Anomalies associated with vertebral malformations. *Spine*, 18: 1329-1332.

BOYLE EK, MAHON V, DIOGO R (2020) Muscles lost in our adult primate ancestors still imprint in US: on muscle evolution, development, variations, and pathologies. *Curr Mol Biol Rep*, 6: 32-50.

BURNEI G, GAVRILIU S, VLAD C, GEORGESCU I, GHITA RA, DUGHILĂ C, ONILĂ A (2015) Congenital scoliosis: an up-to-date. *J Med Life*, 8: 388.

CROWLEY B, STEVENSON S, DIOGO R (2019) Radial polydactyly: putting together evolution, development and clinical anatomy. *J Hand Sur*, 44: 51-58.

DIOGO R, ESTEVE-ALTAVA B, SMITH C, BOUGHNER JC, RASSKIN-GUTMAN D (2015a) Anatomical network comparison of human upper and lower, newborn and adult, and normal and abnormal limbs, with notes on development, pathology and limb serial homology vs. homoplasy. *PloS One*, 10: e0140030.

DIOGO R, SMITH CM, ZIERMANN JM (2015b) Evolutionary developmental pathology and anthropology: A new field linking development, comparative anatomy, human evolution, morphological variations and defects, and medicine. *Dev Dyn*, 244: 1357-1374.

DIOGO R, SIOMAVA N, GITTON Y (2019a) Development of human limb muscles based on whole-mount immunostaining and the links between ontogeny and evolution. *Development*, 146: 131-150.

DIOGO R, ZIERMANN JM, SMITH C, ALGHAMDI M, FUENTES JS, DUERINCKX A (2019b) First use of anatomical networks to study modularity and integration of heads, forelimbs and hindlimbs in abnormal anencephalic and cyclopic vs normal human development. *Sci Rep*, 9: 1-25.

EROL B, KUSUMI K, LOU J, DORMANS JP (2002) Etiology of congenital scoliosis. *Uni Penn Orthop* J, 15: 37-42.

GONDRÉ LEWIS MC, GBOLUAJE T, REID SN, LIN S, WANG P, GREEN W, HERMAN MM (2015) The human brain and face: mechanisms of cranial, neurological and facial development revealed through malformations of holoprosencephaly, cyclopia and aberrations in chromosome 18. *J Anat*, 227: 255-267.

HEDEQUIST D, EMANS J (2004) Congenital scoliosis. *JAAOS*, 12: 266-275.

HEDEQUIST D, EMANS J (2007) Congenital scoliosis: a review and update. *J Pediat Orthop*, 27: 106-116.

HENSINGER RN (2009) Congenital scoliosis: etiology and associations. *Spine*, 3: 1745-1750.

HENSINGER RN, LANG JE, MACEWEN GD (1974) Klippel-Feil syndrome; a constellation of associated anomalies. *J Bone Joint Surg*, 56: 1246-1253.

JASKWHICH D, ALI RM, PATEL TC, GREEN DW (2000) Congenital scoliosis. *Curr Opinion Pediatr*, 12: 61-66.

KARAUDA P, PAULSEN F, POLGUJ M, DIOGO R, OLEWNIK L (2021) Morphological variability of the fibularis tertius tendon in human fetuses. *Folia Morphol (Warsz)*, 2021: doi: 10.5603/FM.a2021.0039.

KONIECZNY MR, SENYURT H, KRAUSPE R (2013) Epidemiology of adolescent idiopathic scoliosis. *J Children's Orthop*, 7: 3-9.

KOSE N, CAMPBELL RM (2004) Congenital scoliosis. *Med Sci Monitor*, 10: RA104-RA110.

LARSEN W (1997) Differentiation of the somites and the nervous system: segmental development and integration. *Human Embryol*, 1997: 73-104.

LI Z, YU X, SHEN J (2015) Environmental aspects of congenital scoliosis. *Environm Sci Pollution Res*, 22: 5751-5755.

OESTREICH AE, YOUNG LW, POUSSAINT TY (1998) Scoliosis circa 2000: radiologic imaging perspective. *Skeletal Radiol*, 27: 591-605.

OLEWNIK Ł, WAŚNIEWSKA A, POLGUJ M, PODGÓRSKI M, ŁABĘTOWICZ P, RUZIK K, TOPOL M (2018) Morphological variability of the palmaris longus muscle in human fetuses. *Surg Radiol Anat*, 40: 1283-1291.

SHEN J, WANG Z, LIU J, XUE X, QIU G (2013) Abnormalities associated with congenital scoliosis: a retrospective study of 226 Chinese surgical cases. *Spine*, 38: 814-818.

TANAKA T, UHTHOFF HK (1981a) Significance of resegmentation in the pathogenesis of vertebral body malformation. *Acta Orthop Scand*, 52: 331-338.

TANAKA T, UHTHOFF HK (1981b) The pathogenesis of congenital vertebral malformations: a study based on observations made in 11 human embryos and fetuses. *Acta Orthop Scand,* 52: 413-425.

TERMINOLOGY COMMITTEE (1976) Scoliosis Research Society. A glossary of scoliosis terms. *Spine*, 1: 57.

VAN GOETHEM J, VAN CAMPENHOUT A, VAN DEN HAUWE L, PARIZEL PM (2007) Scoliosis. *Neuroimaging Clin North Am*, 17: 105-115.

YURASAKPONG L, DIOGO R, CHAIYAMOON A, MEEMON K, SUWANNAKHAN A (2020) Extensor indicis radialis and extensor medii proprius associated with an unknown fibromuscular slip: a case report. *SN Comprehensive Clin Med*, 2: 2456-2459.

Median nerve entrapment by variant anatomical structures

Manasi Telang[1], Boycho Landzhov[1], Łukasz Olewnik[2], R. Shane Tubbs[3-7], Georgi P. Georgiev[8]

[1]Department of Anatomy, Histology and Embryology, Medical University of Sofia, Sofia, Bulgaria
[2]Department of Anatomical Dissection and Donation, Chair of Anatomy and Histology, Medical University of Lodz
[3]Department of Anatomical Sciences, St. George's University, Grenada
[4]Department of Neurosurgery, Tulane University School of Medicine, New Orleans, Louisiana, USA
[5]Department of Neurology, Tulane University School of Medicine, New Orleans, Louisiana, USA
[6]Department of Structural and Cellular Biology, Tulane University School of Medicine, New Orleans, Louisiana, USA
[7]Department of Surgery, Tulane University School of Medicine, New Orleans, Louisiana, USA
[8]Department of Orthopedics and Traumatology, University Hospital Queen Giovanna-ISUL, Medical University of Sofia, Sofia, Bulgaria

SUMMARY

Entrapment neuropathies are common and are frequently encountered by physicians in clinical practice. Median nerve entrapment, being one of the most common neuropathies in the upper extremity, must be studied in detail if the extent of injury it can cause is to be understood fully. Various anatomical variations are discovered frequently and reviewing these will advance medical practice in the search for suitable treatments. A broad understanding of the symptoms of median nerve entrapment, motor as well as sensory, is essential, along with its effects on surrounding structures.

Key words: Median nerve – Compression – Anatomical variations – Clinical significance

INTRODUCTION

Nerves are highly susceptible to injury and often become vulnerable, leading to entrapment, which causes swelling and focal flattening (Jarvik et al., 2000). Any nerve is prone to injury and to entrapment between structures close to it. Entrapment or compression occurs when variant structures pinch or pressure the nerve (Miller and Reinus, 2010). Some peripheral neuropathies, which are typical clinical disorders, can be classified one of two ways: compressive entrapment and non-compressive entrapment (Spinner and Amadio, 2003).

To explain the clinical findings of nerve entrapment, it is essential to understand the broad range of neuropathies usually presenting as sensory abnormalities, including pain, paresthesia, and loss of sensation or numbness. Another possibility is motor weakness in the muscles innervated by that particular nerve (Georgiev and Jelev, 2009a; Slavchev and Georgiev, 2013).

Corresponding author:
Georgi P. Georgiev, MD, PhD. Department of Orthopaedics and Traumatology, University Hospital Queen Giovanna – ISUL, Medical University of Sofia, 8, Bialo More Str., BG 1527 Sofia, Bulgaria. Phone: +359884 493523. E-mail: georgievgp@yahoo.com - Orcid No.: 0000-0001-8343-0337

Submitted: December 2, 2021. **Accepted:** December 14, 2021

https://doi.org/10.52083/ZBDM6965

Entrapment neuropathies are common and are frequently encountered by physicians in their clinical practice (Hobson-Webb and Juel, 2017). They can be mononeuropathic or polyneuropathic. A classic example of a condition causing neuropathy is diabetes (Rota and Morelli, 2016). While most mononeuropathies are superimposed on a polyneuropathic background, they require knowledge of neuroanatomy and clinical diagnosis (Hobson-Webb and Juel, 2017).

The aim of this study is to summarize for clinicians the different anatomical variations that can provoke median nerve (MN) compression.

THE MEDIAN NERVE

The MN is one of the most substantial nerves of the upper limb. It contains fibres from all the nerve roots of the brachial plexus (C5 to Th1). It innervates the flexor muscles of the anterior compartment of the forearm (except for the flexor carpi ulnaris and the medial part of the flexor digitorum profundus (FDP), since these two are innervated by the ulnar nerve) (Spinner, 2003). Within the hand, it innervates the thenar muscles and the two lateral lumbricals. The sensory function of the median nerve is quite easy to deduce considering its location. It has a palmar cutaneous branch, which supplies the lateral part of the palm, and a digital cutaneous branch, which supplies the skin over the first two and half fingers and the thumb (Meyer et al., 2018).

Because of its location in the arm, the nerve sits ventral to the brachial artery. As it descends further proximally, it crosses over to become more medial and then enters the elbow at the cubital fossa. This is where it passes into the anterior "superficial" compartment of the forearm. Within the forearm, it travels between the FDP and the flexor digitorum superficialis muscle (FDS), and two major branches emerge. The proximal branch is the anterior interosseous nerve (AIN), which supplies the deep flexor muscles of the anterior compartment of the arm. These muscles include the pronator quadrates, flexor pollicis longus (FPL) and the lateral half of the FDP. The superficial and intermediate layers are directly innervated by the MN. The pronator teres (PT), flexor carpi radialis (FCR) and palmaris longus (PL) are muscles of the superficial layer supplied by the MN. The flexor carpi ulnaris is innervated by the ulnar nerve.

The distal branch of the MN, called the palmar cutaneous nerve, passes over the flexor retinaculum. It innervates the skin of the lateral palm. It enters the hand and divides into a recurrent and a common palmar digital branch. The recurrent branch supplies the thenar muscles and passes between the flexor pollicis brevis and abductor pollicis brevis and then supplies the opponens pollicis. The palmar digital nerves supply the lateral two lumbricals of the hand. The common palmar digital nerves divide into two to form the proper palmar digital nerves and supply the lateral three and a half digits (Clemente, 1985).

MEDIAN NERVE ENTRAPMENT

An insight into the location and course of the MN makes it easier to locate the regions where the nerve can become entrapped. Much research on this topic has established that there are several regions in the upper limb where the MN can suffer compression (Andreisek et al., 2006; De Smet, 2002).

Coracobrachialis and brachialis muscles

Different variations of the coracobrachialis muscle (CB) that pass over the MN can be involved in MN neuropathy: four-headed CB, CB longus and coracoepitrochlearis muscle (El-Naggar and Saggaf, 2004; Georgiev et al., 2017; 2018a, b; Olewnik et al., 2020). Other possible causes of MN compression are accessory slips from the brachialis muscle that cross over the nerve (Bilecenoglu et al., 2005). George and Nayak (2009) presented a case in which the MN and brachial artery appeared normal in the upper part of their course in the arm, but in the lower 1/3rd they both lay deep to the accessory slip of the brachialis instead of passing superficial to brachialis as normal.

A cause of this kind could have greater clinical significance, but as Georgiev et al. (2017) point out, the lack of clinical reports could be explained, on the one hand, by the rarity of these variations and lack of knowledge of them, and, on the other, by the limited skin incision performed during

decompression. The coracobrachialis longus can compress the median nerve at a different level (Olewnik et al., 2020).

Ligament of Struthers and supracondylar process

The ligament of Struthers and the supracondylar process (Fig. 1a) are found in the distal 1/3 of the medial aspect of the arm. The presence of these in humans is a rare legacy from earlier species. They are reported to interfere with the course of the MN (Pratt, 2005).

Supracondylar process syndrome

The rarest of all compression neuropathies of the MN is supracondylar process syndrome. Among all compression neuropathy cases, only about 0.5% are attributable to this syndrome (Meyer et al., 2018; Georgiev and Tubbs, 2020).

Struthers described the supracondylar process and its associated ligament in 1848. It is a beak-shaped bone spur arising in the distal anteromedial portion of the humerus. Congenitally, this variation is seen in 0.1% to 2.7% of people and is usually asymptomatic. It is sometimes possible for the CB to attach to the supracondylar process. The process is said to be easily visible on oblique radiographs but is often missed on anteroposterior and lateral images (Opanova et al., 2014).

Following a fracture, the MN can be compressed by the osteofibrous structures lying in this space. Symptoms appear on dynamic examination of the elbow (Wertsch and Melvin, 1982). Compression occurs at the level of the distal humerus as the MN passes under the bony curvature, continuing to the median epicondyle. Muscle hypertrophy or strenuous use can aggravate the irritant effect of this structure (Spinner et al., 1991). A supracon-

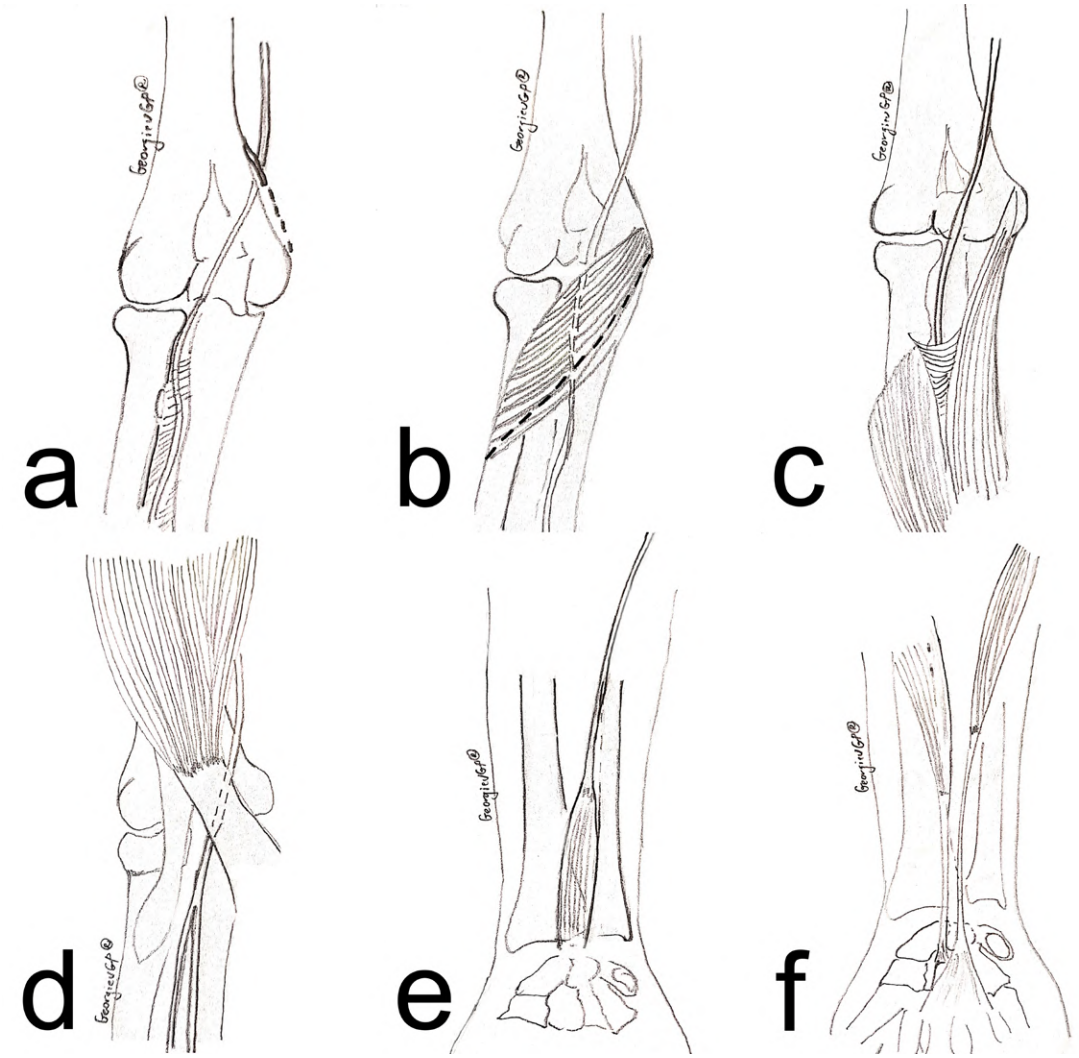

Fig. 1.- Possible sites of compression of median nerve. **a)** Supracondylar process and Ligament of Struthers; **b)** Pronator teres; **c)** Fibrous arcade at the proximal margin of the flexor digitorum superficialis; **d)** Lacertus fibrosus; **e)** Reversed palmaris longus; **f)** Palmaris profundus.

dylar process can be found by X-ray (Shon et al., 2018).

Ligament of Struthers

The MN is rarely entrapped by the Struthers' ligament, which connects supracondylar process to the medial epicondyle. The MN and the brachial artery pass through a small arch. Electromyography is useful in such cases to confirm compression (Sener et al., 1998).

It is usually asymptomatic but is known to produce symptoms post-trauma (Shon et al., 2018). The patient's history often includes avoiding activities that typically involve forearm, wrist and/or finger extension. On examination, discomfort during forearm supination and elbow extension is aggravated. The radial pulse can also be attenuated. Muscle weakness has been noted in the pronator teres and this is the hallmark of pronator syndrome (Shon et al., 2018). Sener et al. (1998) presented a case of a 35-year-old woman with a two-year history of pain and paresthesia involving her right elbow. Symptoms seemed to be worsening during elevation of the hand upwards or active extension of the elbow and pronation of the forearm. Direct radiograms led to a clear diagnosis of supracondylar process without Struthers' ligament on MRI. However, surgical exploration revealed both a supracondylar process and a Struthers' ligament.

Bicipital aponeurosis (lacertus fibrosus)

The bicipital aponeurosis (lacertus fibrosus) (Fig. 1d) is described accurately as a ligamentous sheet just past the elbow joint. It originates from the tendon of the biceps muscle and the flexor-pronator fascia. Along with the MN, the brachial artery passes through the cubital fossa under the lacertus fibrosus (Bilecenoglu et al., 2005).

The most common presenting symptoms are loss of key and tip pinch strength accompanied by loss of fine motor skills and a sense of clumsiness. It causes dropping of objects and, rarely, transient paresthesia in the MN-innervated region of the hand (Lalonde, 2014). There is decreased power in the FPL, FDP and FCR and, rarely, a positive Tinel's sign. In most cases the main complaint is loss of motor function, seldom loss of sensory function. The initial treatment consists of bivalve cast splinting. If this treatment fails, the patient is indicated for surgery to release the tight lacertus fibrosus that is compressing the MN (Swiggett and Ruby, 1986).

There are rare causes of MN compression due to the lacertus fibrosus, possibly involving hemorrhage in the cubital fossa (Johnson and Melvin, 1967). Caetano et al. (2017) presented a study analyzing anatomical variations of the lacertus fibrosus and their implications for MN compression. They dissected sixty upper limbs of 30 cadavers, 26 male and four female. Fifteen of them had been preserved in formalin and glycerol; 15 were fresh. The results revealed that in 55 limbs, the short and long heads of the biceps brachii muscle contributed to the formation of the lacertus fibrosus. There was a significant contribution from the short head. In 42 limbs there was a thickened lacertus fibrosus, suggesting this could be a potential factor in compression and entrapment.

Pronator Syndrome

This is a comparatively rare syndrome resulting from entrapment of the MN between the humeral and ulnar heads of the PT (Lee, 2014; Eversmann, 1983). Spinner (1991) called it a controversial disorder because the symptoms are vague; discomfort in the forearm with occasional radiation into the arm, often described as fatigue-like pain. Secondary symptoms include numbness in the hand. Women are at a greater risk than men of developing symptoms such as little finger numbness, especially if they are exposed to repetitive industrial movements. The imaging commonly used for diagnosis is electromyography (Spinner, 1991).

Pronator syndrome can be caused by hypertrophy of the PT muscle or by congenital abnormalities (Fig. 1b). A high origin of the PT from the humerus is a rare variation. Commonly, this muscle starts from an existing supracondylar process and from a fibrous band extending between the supracondylar process and the medial epicondyle, the ligament of Struthers. Between this ligament and the distal part of the humerus an arch is formed through which the MN and brachial artery pass distally; in rare variants, the ulnar artery or nerve also passes though it (Jelev and Georgiev, 2009).

Clinical presentations are pain and tingling in the volar aspect of the elbow, forearm and wrist as the prime symptoms, all without muscle weakness. The wrist flexion test, called the Phalen test, shows negative results (Wertsch and Melvin, 1982). Either a Struthers' ligament or lacertus fibrosus level compression can be suspected if the symptoms of pain or weakness are aggravated by flexion of the elbow against resistance, usually between 120 and 135 degrees. Pronator syndrome is suspected only when the symptoms are aggravated by resistance to pronation of the wrist. Another scenario common in this context is irritation due to resisted flexion of the FDS of the middle finger. The arch of the FDS must be examined carefully (Eversmann, 1983; Hagert, 2013).

If pronator syndrome is diagnosed, the MN is thoroughly examined. There are four possible sites of compression of the MN at the pronator teres muscle: (1) around 4 cm above the medial epicondyle of the humerus, a small hook-shaped bony process called the supracondylar process, which acts as accessory origin of the pronator teres. This is the ligament of Struthers; (2) the fascia of the lacertus fibrosus, which courses from the bicipital tendon over the mass of proximal forearm flexor muscles; (3) reflections of muscle fascia forming fibrous bands that form the deep head of the PT, which has a sharp aponeurotic edge, or just simple hypertrophy of the muscle itself; (4) the tendinous aponeurotic arch of the radial attachment of the FDS (Fig. 1c) under which the MN nerve can be compressed (Eversmann, 1983).

The MN can be compressed because of morphological variability of the pronator teres (humeral and ulnar heads). If only the humeral head is present, the nerve passes underneath it. If there are two heads, the nerve passes between them, which predisposes it to compression. Sometimes a PT has two heads and the nerve passes behind them (Olewnik et al., 2018).

Anterior interosseous nerve syndrome

Another syndrome that is common owing to entrapment of a branch of the MN is anterior interosseous nerve syndrome (AINS). It is also referred to as Kiloh-Nevin syndrome. It occurs when the nerve is compressed in the proximal forearm. There could be direct nerve trauma or compression caused by a hematoma or a mass or tumor. The manifestation of this syndrome is vague pain in the proximal part of the forearm, typically triggered by exercise and subsiding on rest (Eversmann, 1983; Miller and Reinus, 2010). AINS has no characteristic sensory signs and symptoms. There is weakness of the FDP and pronator quadratus, sometimes even paralysis upon clinical examination. Common initial symptoms include a deep, unrelenting pain in the proximal forearm, which then leads to a lack of dexterity or weak pinching ability. This syndrome is often confused with Parsonage-Turner syndrome. EMG reveals fibrillations in the affected muscles and MRI studies are informative (Spinner, 1991).

Much research related to surgical procedures and exploration of the course of the MN indicates that reflecting the superficial head of the pronator teres and even the deep head at the radius enables the distal portion of the MN to be visualized. The FDS can also be reflected. In such cases, the origin of the FDS is separated, enabling us to view the entire MN. It is superficial to the anterior interosseous nerve. The potentially aberrant muscles that have been identified as causing compression neuropathy of the anterior interosseous nerve are: (1) the accessory head of the flexor pollicis longus, also called Gantzer's muscle; (2) the flexor carpi radialis brevis (Eversmann, 1983).

Flexor pollicis longus (FPL)

Gantzer's muscle originates from the medial epicondyle or the coronoid process, lying on the ulnar side of the FPL. In supination, the anterior interosseous nerve is compressed (Bilecenoglu et al., 2005). Gantzer identified two different variant muscle bellies in 1813. These are parts of the deep flexor region of the forearm and insert into either the FDP or the FPL. They were named after Gantzer himself. Atavism in action; the accessory heads of the FDP and FPL show incomplete division of the deep layers of the muscles (Saxena et al., 2013).

Al Qattan (1996) studied 25 right upper limbs and documented the incidence, origin, insertion, nerve supply and relationships of Gantzer's

muscle. The said muscle was present in 13 of the 25 cadavers. The anterior interosseous nerve supplied it in all of the specimens. It originated from the medial humeral epicondyle in 11 of the cadavers. In the other two, there was a dual origin from medial epicondyle and the coronoid process of the ulna. Insertion was into the FPL in the ulnar part. Although there was no close relationship to Gantzer's muscle, the MN passed between the superficial and deep heads of the pronator teres in 11 of the 13 specimens. In the remaining two, the MN was closely related to Gantzer's muscle because it passed deep to the deep head of the PT in one of the cadavers (Al Qattan, 1996).

Flexor carpi radialis brevis (FCRB)

There is a growing trend towards treating distal radius fractures with volar plating, so it is useful to have somewhat deeper knowledge of the FCRB. This muscle has been described in the Japanese literature in multiple cadaver studies. Its reported incidence is 2.6% to 7.5%. Insertion of the FCRB is variable; it can insert into any metacarpal base except the first or fifth or the carpal bones on the radial side such as the scaphoid, trapezium, trapezoid and capitate. The FCRB could potentially compress the anterior interosseous nerve, but since the site of compression is very distal to its branches supplying the FPL and FDP, it rarely becomes clinically significant enough to show symptoms (Eversmann, 1983).

Carpal Tunnel Syndrome

The most frequently encountered MN compression syndrome is carpal tunnel syndrome (CTS). Most cases are idiopathic, with a range of etiologies that include trauma, conditions associated with imbalance of hormones, or metabolism. Other physiological causes of CTS are hemodialysis, obesity, lupus erythematosus, scleroderma, thyroid disorders and amyloidosis. The syndrome can possibly be caused by the direct influence of external forces, either vibration or direct pressure (De Smet, 2005; Meyer et al., 2018).

Aberrant muscles can cause syndromes of MN entrapment (Georgiev, 2020; Georgiev, 2021a; Georgiev, 2021b). The usual symptoms include restricted movement of the hand accompanied by burning pain in the distal part of the forearm. Such anatomical variations can also cause painful compartment syndrome owing to lack of space (Agarwal et al., 2014).

On reviewing the literature, three muscle variations emerge: (1) 1st or 2nd lumbrical; (2) PL and its anatomical variants; (3) superficial flexor of the index finger (Miller, 2010).

1st or 2nd lumbrical

Since the MN supplies motor innervation to the 1st and 2nd lumbricals, any variation in these could affect the MN and cause compression or entrapment.

1st lumbrical: Different variations of this muscle can be summarized: an accessory slip can arise from the FPL tendon, the FDS tendon, the first metacarpal opponens pollicis or the palmar carpal ligament. Cases have been reported where a fasciculus arose from muscular belly of the superficial or deep flexor and joined the 1st lumbrical. The 1st lumbrical can also be doubled, one being normal while the second arises from the FDS. A slip from the FPL giving a tendon to the 1st lumbrical has also been described. A supplementary head for the 1st lumbrical originating from the 1st palmar interosseous has also been found (Bergman et al., 2021).

2nd lumbrical: It is possible for the second lumbrical to arise from the two tendons between which it is present. A doubling of the second lumbrical has been reported, one slip sent to the radial side of the middle finger and one to the ulnar side of the index (Bergman et al., 2021).

Redondo et al. (2011) presented a case of a 52-year-old woman with pain and paresthesia in the left MN several months after a carpal tunnel release. Surgical revision after follow-ups of the echogram revealed an aberrant muscle with proximal origin from the forearm and muscular belly passing under the carpal tunnel inserting into the first lumbrical. Bhandari and Palazzo (2017) also presented a case of an accessory lumbrical muscle found during carpal tunnel decompression. A muscle in the carpal tunnel was discovered superior to the FDS. Pulling this muscle led to flexion at the proximal interphalangeal joint of the index

finger. Sbai et al. (2019) described a 35-year-old left-handed woman who developed numbness, tingling, pain and weakness in the left hand affecting the thumb, index finger and middle finger; she had no prior history of such symptoms, which were aggravated by exercise. Surgical exploration immediately revealed an abnormal lumbrical tendon, which was easily exposed on opening the mid-palmar fascia and flexor retinaculum. The MN looked flattened by the tendon.

Variations of the palmaris longus muscle (PL)

There are many potential changes or variations in the regular anatomy of the PL. There can be reversed PL (Fig. 1e), bifid, trifid reversed and RPL coexisting with ADM. A digastric PLM or a PLM with intermediate muscle belly are also possible. Absence, duplication, and triplication are all tangible possibilities. There are accessory slips to the hypothenar muscles and PLM profundus (Fig. 1f). The latter is one cause of entrapment and congestion of the MN (Georgiev et al., 2009a, b; Kotov et al., 2017; Georgiev et al., 2017).

Surgical exploration infrequently reveals variant muscles in the carpal tunnel. It can be challenging to identify or classify them and they can cause confusion as they usually obscure the anatomy that is considered normal, posing a dilemma to the surgeon. Acknowledging that they can be present removes the doubts (Bhandari and Palazzo, 2017). A case study by Park (2019) revealed statistics on how many people could develop muscular anatomical variations of the volar aspect of the wrist because of CTS. Among 973 wrists in 644 patients, eight wrists in eight patients presented with variant muscles. They were presumed to be PL tendon variants or accessory ADM muscles. Early recognition of these anatomical variations can help to avoid unnecessary surgery and ensure better recovery among patients (Park, 2019).

Ninković et al. (1995) presented a case of a 28-year-old right-handed male lumberjack admitted to hospital for pain, tingling and numbness of the right thumb, index and middle fingers. Several days earlier, while using a power saw, the patient experienced sudden pain in the right wrist and noticed a concomitant swelling along the right forearm. Treatment provided temporary relief but the symptoms continued, leading to further exploration of the swelling. A hypertrophic RPL was discovered as the cause of acute MN compression.

Bhandari and Palazzo (2017) presented a case of a palmaris profundus found during surgery on a 24-year-old male for a crush injury to the hand. The tendon to his right ring finger was injured as well as the MN. This variant muscle originated from the distal end of the radius, passing through the carpal tunnel and fusing its tendon with the FDS tendon to the little finger. The patient had no symptoms so the muscle was not resected. Sbai et al. (2019) presented another case of a palmaris profundus tendon in a 25-year-old female who for many years had experienced paresthesia and numbness in the territory of the MN of the left hand. Investigation revealed an aberrant tendon on the anterior surface of the MN. The tendon had a deep insertion into the palmar aponeurosis (Sbai et al., 2019). These authors pointed out that a variant muscle can be supposed to cause compression neuropathy in a patient in the "usual" age group, with symptoms aggravated by physical activity.

Variant muscle belly of flexor digitorum superficialis

The kind of variant discussed here is not very rare and is usually accompanied by such symptoms as hand tremors. The most common variant muscle belly arises from and inserts into the FDS tendon, and the action is typically on the index finger (Vichare, 1970; Smith, 1971; Das and Brown, 1975, Elias and Schulter-Ellis, 1995).

Another not so common muscle belly variant originates from the transverse carpal ligament and inserts into the tendon of the FDS of the index finger (Wesser et al., 1969; Still and Kleinert, 1973). Tanzer (1959) found that the muscular part of the FDS occasionally extends distally into the carpal tunnel and can only be seen once the tunnel is decompressed (Figueiredo and Hooper, 1980). Baruch and Hass (1977) discovered that the muscle belly passing through the carpal tunnel traveled deep to the other FDS tendons in the forearm and was crossed by the MN.

Kono (2003) presented a case of a transscaphoid perilunate dislocation. The patient complained of

mild numbness in the three radial fingers. He was treated with closed reduction of dislocation and the symptoms cleared. He underwent surgery to fix the scaphoid and luno-triquetral and capitolunate joints. Two hours after surgery he complained of severe paresthesia of the radial three fingers and difficulty in flexing them. Another exploratory surgery showed the MN to be severely compressed between the transverse carpal ligament and the swollen muscle bellies of the FDS of the long and ring fingers within the carpal tunnel. A release was performed and the pain and paresthesia disappeared post-op. Sbai et al. (2019) presented a 65-year-old female suffering from paresthesia and numbness in the MN territory of the right hand, accompanied by a positive Tinel's sign and Phalen test. There were no signs of thenar atrophy. A hypertrophic FDS of the middle finger engaged with the carpal tunnel was identified. The MN was congested and release resolved all the symptoms. Boutasta et al. (2012) presented a case of a 38-year-old housewife with severe pain and paresthesia at the right wrist, worsening after activity. A variant long muscle belly arising from the FDS of the index finger was observed. It extended proximally into the carpal tunnel and the MN was compressed.

There are five types of FDS variants as proposed by Elliot (1999). Type I entails a belly that arises at the carpal level, inserting into the same FDS from which it arose. Type II has a variant muscle arising from the palmar fascia and the distal border of the transverse carpal ligament. In this case, it terminates with the normal tendon and the muscle is entirely in the palm. Type III was described as digastric and appearing in the palm, interrupted and even replaced by a fleshy muscle belly. Type IV originated in the forearm and passed under the flexor retinaculum. It then extended into the carpal tunnel. Type V is less common. It is considered to represent anatomical variations in the superficial muscle layer in the distal part of the forearm (Elliot et al., 1999; Boutasta et al., 2012).

The sublime bridge

A potential site for compression of the MN is the sublime bridge, described by Tubbs et al. (2010). Despite the scattered incidence, this possibility must be considered. The sublime bridge is tendinous in most specimens and is intimately related to the MN and the anterior branch of the MN, which arises proximally to it. Usually, the history of a patient with this syndrome involves constant repetitive pronation and supination of the forearm along with pain and paraesthesia over the anterior part of the forearm (Tubbs et al., 2010).

Role of median artery in CTS

The median artery (MA) is found between the anterior surface of the MN and the deep surface of the FDS. In adults, it is always close to the MN and it usually ends before reaching the wrist. This is called a. comitans nervi mediani, meaning it is an MA of the antebrachial type. In other cases, the artery reaches the hand to contribute to the blood supply to the fingers. This is the palmar type of MA (Jelev and Georgiev, 2011). Rarely, an MA originates at the elbow and courses anteriorly to the antebrachial flexor muscles. This is called a 'superficial' MA. Even though its development is not fully understood, the MA is believed to be a transitory vessel that depicts the arterial axis of the forearm during early embryonic life (Jelev and Georgiev, 2011)

Multiple clinical disorders can result from the presence of a well-developed MA; in turn, it can affect closely related structures such as the MN. In the carpal tunnel, if the MA is the palmar type, it could have an external diameter more than 2.0 mm, causing increased pressure on the MN and therefore potentially causing CTS. Even MA injuries such as thrombosis, aneurysm, traumatic rupture or calcification can cause CTS. According to Jelev and Georgiev (2011), confirming the presence of a sufficient anastomotic blood supply is crucial in such cases as the MN can be injured by ischemia.

Lisanti et al. (1995) presented a case where the patient exhibited no systemic pathological evidence, but had a history of neurolysis of the MN at both wrists. Symptoms resolved on the right side, while those on the left persisted. Surgical exploration revealed a persistent MA. Sometimes, a distal thrombosis of the MA also manifests as MN compression. Salter et al. (2011) presented a case of CTS due to thromboses of the MA detected by

high resolution ultrasound and Doppler. The MA was also associated with a bifurcated MN. This thrombus was resolved by anticoagulant treatment. Akgun et al. (2017) presented a similar case in which there was a bifurcated MN with an MA lying between the divisions. Doppler examination was used to confirm the diagnosis.

Transverse carpal muscle (TCM)

Tuncali et al. (2005) described three cases of TCM found during routine decompression for CTS. A rare variant of the hand that can cause compression of the MN leading to CTS is a unilateral accessory transverse carpal muscle located palmar to the transverse carpal ligament. The TCM, though an aberrant muscle, is important during surgical exploration of the carpal tunnel as it can be accompanied by a recurrent motor branch and there is an evident risk of iatrogenic injury to it. It is very useful to study and interpret the variables, especially during surgery. Nastis et al. (2020) presented a case of a 38-year-old right-handed male with CTS symptoms in the right hand. The MN was compressed according to a nerve conduction study, with sensory and motor delay. Surgical exploration revealed a transverse muscle overlapping the transverse carpal ligament and flexor retinaculum, which was named the TCM. It was suggested that the TCM could result from aberrant migration of epiblastic cells from the muscle pronator quadratus. It could be accompanied by a recurrent motor branch and could potentially be an iatrogenic injury risk. The MN motor branch is at high risk during operations on the transverse carpal ligament, particularly if there is flexor retinaculum division. If there is a wide TCM, it could also cause the MN motor branch to follow an abnormal course.

Role of Imaging Studies

For any sort of diagnosis suspected clinically, imaging is the main method of confirmation. This is true for MN entrapment. The usual types of imaging used for such cases are MRI and sonographies. Sometimes, imaging leads to an alternate diagnosis that could have been proposed as a differential (Miller and Reinus, 2010). Diagnostic imaging such as cross-sectional imaging, typically ultrasound or MRI, reveals the anatomical intricacies of nerves and the changes that can occur during compression (Spratt et al, 2002). Even though MRI should be reserved for cases that are inconclusive on clinical and electrodiagnostic findings, or where the symptoms are unusually severe, it is an extremely useful technique for compressive neuropathies (Bordalo-Rodrigues and Rosenberg, 2004).

Axial views are the most useful images for demonstrating CTS changes in MRI features. Even a hyperintense signal of the nerve is seen on T2-weighted or STIR images. Specificity and sensitivity of MR findings for CTS are low but MRI findings are useful for detecting a space-occupying lesion, inflammatory arthritis or anatomical variations as causes of CTS (Dong et al., 2012).

In pronator syndrome, there is a noted pattern of muscle denervation that indicates edema on fluid-sensitive sequences on MRI, unless there is a mass or hematoma as secondary cause (Dong et al., 2012). Usually, because the perifascial fat is minimal, the MN is depicted poorly at the elbow. In axial images, the MN is visible between the pronator teres and brachialis muscles. It can even appear normal at the site of entrapment.

In some cases of nerve injury, thickening or signal abnormalities have been reported. On MRI, the anatomical basis of pronator syndrome is inconspicuous unless a mass or osseous fracture is close to the nerve. The pronator teres or other muscles innervated by the MN distal to the site of the lesion can give an abnormally high signal. This is on T2-weighted fat-suppressed, STIR, or T1-weighted images (Andreisek et al., 2006).

In Kilon-Nevin syndrome or AINS, patients can show signal intensity changes related to muscle denervation involving the FDP, FPL and pronator quadratus (Dong et al., 2012). The AI nerve is usually visible between the FDS and FDP muscles on MRI. In patients who have this syndrome with an acute or subacute onset, STIR images depict increased signals in the FDP, FPL and pronator quadratus. MR signal intensity corresponding to the fourth and fifth fingers is normal as they are not involved in Kilon-Nevin syndrome (Andreisek et al., 2006).

Most of the anatomical constraints causing this syndrome are not visible on MRI. However, if a focal entrapment or compression of the nerve is observed in MRI, it can alert surgeons to avoid a long incision crossing the cubital fossa. If there is an additional development of T1-weighted MRI signal abnormalities, it could indicate worsening of the syndrome; but if there is normalization of T2-weighted muscle signal intensity, there is recovery of nerve function (Andreisek et al., 2006).

The MRI features of patients with supracondylar process syndrome are not well established but we can draw conclusions from conventional radiographs. Apart from the supracondylar process, MRI can show the Struthers' ligament and its relationship to the MN. This can be useful for detecting occult fractures of the supracondylar process radiographically (Andreisek et al., 2006).

The MN appears ovoid in axial cross-sectional views in the proximal part of the carpal tunnel and has a flatter appearance at the pisiform bone level and distally in the carpal tunnel. The findings in patients with CTS are not always directly linked to the nerve but can involve other contents of the carpal tunnel. The best way to evaluate the syndrome is to note the flattening of the MN, comparing the nerve diameter at the levels of the hook of the hamate and the distal radius. MRI can also show increased signal intensity on T2-weighted fat-suppressed or STIR images. It can show bowing of the flexor retinaculum at the level of the hook of the hamate. If the sensitivity and specificity are low for CTS, it has no role in the clinical assessment of this condition. Nor does it have clinical value if the CTS is caused by a neoplasm, arthritis or anatomical variations (Bordalo-Rodrigues et al., 2004; Dong et al., 2012).

Sonography

A method being used widely for evaluating structures within the carpal tunnel is musculoskeletal sonography. Bifurcated MNs and persistent MAs have been documented and multiple examples of sonographic appearances of the FDS and lumbrical muscle bellies extending into the carpal tunnel have been provided, but dynamic imaging makes it easier to describe and work with such cases as we can recognize specific muscle bellies. Several potential differential diagnoses can be made such as persistent MA, lipoma, masses and cysts, or even inflammation around the tendons of the carpal tunnel. Along with investigations of the structures in the longitudinal plane, isolated finger movements can be used to identify specific muscles (Takata and Roll, 2019). Moreover, ultrasound-guided minimally invasive release of the cubital tunnel and carpal tunnel has also been performed (Gruber et al., 2021; Loizides et al., 2021).

Theoretical causes for muscle anatomical variations

Anatomical variations can be divided into anatomical variations of nerves, tendons, vessels and muscles. Exact causes of muscle anatomical variations are not yet known, but according to many authors and researchers, they were formerly attributed to the "ontogeny recapitulates phylogeny" conjecture. Even though this conjecture has been discredited, muscles are known to originate by myocytes migrating into the muscle anlage by the tendon primordium. These anatomical variations are likely to be due to aberrations in embryological signaling (Elliot et al., 1999; Laxminarayan and Michelle, 2017).

CONCLUSION

MN entrapment neuropathies can affect people for a wide range of reasons. There are multiple common causes while others are considered rare. Usually, they are discovered upon surgical intervention or exploration or during imaging studies, but awareness of these anatomical variations that can potentially trap the MN help in achieving better outcomes of recovery and patient care. Surgery has countless adverse effects on the body. The first rule of medicine is "Do no harm", and if treatment can be made suitable to patients, long-term wellbeing can be promoted.

AUTHORS' CONTRIBUTIONS

Manasi Telang — student/assistant — project development, data collection and management, data analysis and manuscript writing.

Boycho Landzhov (MD, PhD) — professor — data analysis and manuscript editing.

Łukasz Olewnik (D.P.T., PhD) — professor — data analysis and manuscript editing.

Richard Shane Tubbs (MD, PhD) — professor — data analysis and manuscript editing.

Georgi P. Georgiev (MD, PhD) — assistant professor — data collection, data analysis and manuscript editing.

All authors have read and approved the manuscript.

REFERENCES

AGARWAL P, GUPTA S, YADAV P, SHARMA D (2014) Cadaveric study of anatomical variations of the median nerve and persistent median artery at wrist. *Indian J Plast Surg*, 47: 95-101.

AKGUN AS, ERTAN G, ULUS S (2017) Acute carpal tunnel syndrome caused by thrombosed persistent median artery associated with bifurcated median nerve in a pregnant woman. *BMJ Case Rep*, 17: bcr2017221446.

AL-QATTAN MM (1996) Gantzer's muscle - an anatomical study of the accessory head of the flexor pollicis longus muscle. *J Hand Surg Br*, 21: 269-270.

ANDREISEK G, CROOK DW, BURG D, MARINCEK B, WEISHAUPT D (2006) Peripheral neuropathies of the median, radial, and ulnar nerves: MR imaging features. *Radiographics*, 26: 1267-1287.

BARUCH A, HASS A (1977) Anomaly of the median nerve. *J Hand Surg Am*, 2: 331-232.

BERGMAN RA, AFIFI AK, MIYAUCHI R (2017) Illustrated encyclopedia of human anatomic variations. Available via DIALOG. https://www.anatomyatlases.org/AnatomicVariants/MuscularSystem/Text/L/19Lumbricales.shtml

BHANDARI L, PALAZZO M (2017) Anomalous muscles encountered in carpal tunnel: A report of two cases. *J Clin Diagn Res*, 11: PD03-PD04.

BILECENOGLU B, UZ A, KARALEZLI N (2005) Possible anatomic structures causing entrapment neuropathies of the median nerve: an anatomic study. *Acta Orthop Belg*, 71: 169-176.

BORDALO-RODRIGUES M, ROSENBERG ZS (2004) MR imaging of entrapment neuropathies at the elbow. *Magn Reson Imaging Clin N Am*, 12: 247-263.

BORDALO-RODRIGUES M, AMIN P, ROSENBERG ZS (2004) MR imaging of common entrapment neuropathies at the wrist. *Magn Reson Imaging Clin N Am*, 12: 265-279.

BOUTASTA T, HAMICHE M, OUARET MY (2012) Carpal tunnel syndrome and trigger finger at the wrist caused by an anomalous flexor digitorum superficialis of the index: a case report and review of literature. *Eur Orthop Traumatol*, 3: 85-87.

CAETANO EB, VIEIRA LA, ALMEIDA TA, GONZALES LAM, BONA JE, SIMONATTO TM (2017) Bicipital aponeurosis. Anatomical study and clinical implications. *Rev Bras Ortop*, 53: 75-81.

CLEMENTE CD (1985) Anatomy of the Human Body. Lea and Febiger, Philadelphia.

DAS SK, BROWN HG (1975) An anomalous flexor digitorum sublinis to index finger with absent lumbrical. *Br J Plast Surg*, 28: 299-300.

DE SMET L (2002) Median and ulnar nerve compression at the wrist caused by anomalous muscles. *Acta Orthop Belg*, 68: 431-438.

DE SMET L, STEENWERCKX A, VAN DEN BOGAERT G, CNUDDE P, FABRY G (1995) Value of clinical provocative tests in carpal tunnel syndrome. *Acta Orthop Belg*, 61: 177-182.

DONG Q, JACOBSON JA, JAMADAR DA, GANDIKOTA G, BRANDON C, MORAG Y, FESSELL DP, KIM SM (2012) Entrapment neuropathies in the upper and lower limbs: anatomy and MRI features. *Radiol Res Pract*, 2012: 230679.

ELIAS LS, SCHULTER-ELLIS FP (1985) Anomalous flexor superficialis indicis: two case reports and literature review. *J Hand Surg Am*, 10: 296-299.

ELLIOT D, KHANDWALA AR, KULKARNI M (1999) Anomalies of the flexor digitorum superficialis muscle. *J Hand Surg Br*, 24: 570-574.

EL-NAGGAR MM, AL-SAGGAF S (2004) Variant of the coracobrachialis muscle with a tunnel for the median nerve and brachial artery. *Clin Anat*, 17: 139-143.

EVERSMANN WW JR (1983) Compression and entrapment neuropathies of the upper extremity. *J Hand Surg Am*, 8: 759-766.

FIGUEIREDO UM, HOOPER G (1980) Abnormal course of the median nerve associated with an anomalous belly of flexor digitorum superficialis. *Hand*, 12: 273-274.

GEORGE BM, NAYAK SB (2008) Median nerve and brachial artery entrapment in the abnormal brachialis muscle – a case report. *Neuroanatomy*, 7: 41-42.

GEORGIEV GP (2020) Reversed palmaris longus muscle: a popular object of anatomical and surgical studies and some misdescriptions. *Surg Radiol Anat*, 42: 297-298.

GEORGIEV GP (2021a) Nerve entrapment vs. possible nerve entrapment in terms of meticulous description of potential possibility of nerve compression by variant anatomical structures in cadaver cases. *Morphologie,* 10: S1286-0115(21)00021-7.

GEORGIEV GP (2021b) Re: Wang CK, Ng CY. Accessory flexor carpi ulnaris: a rare cause of distal ulnar nerve compression. J Hand Surg Eur. 2021, 46: 197-199. *J Hand Surg Eur*, 46: 1014-1015.

GEORGIEV GP, JELEV L (2009) Unusual coexistence of a variant abductor digiti minimi and reversed palmaris longus and their possible relation to median and ulnar nerves entrapment at the wrist. *Rom J Morphol Embryol*, 50: 725-727.

GEORGIEV GP, JELEV L, OVTSCHAROFF WA (2009a) Unusual combination of muscular and arterial variations in the upper extremity: a case report of a variant palmaris longus and an additional tendinous portion of the flexor carpi ulnaris together with a persistent median artery. *Anatomy*, 3: 58-61.

GEORGIEV GP, JELEV L, SURCHEV L (2009b) Presence of palmaris longus related variations in three members of a family. *J Hand Surg Eur Vol*, 34: 277-278.

GEORGIEV GP, ILIEV AA, DIMITROVA IN, KOTOV GN, MALINOVA LG, LANDZHOV BV (2017) Palmaris longus muscle variations: clinical significance and proposal of new classifications. *Folia Med (Plovdiv)*, 59: 289-297.

GEORGIEV GP, LANDZHOV B, TUBBS R (2018a) A novel type of coracobrachialis muscle variation and a proposed new classification. *Cureus*, 9: e1466.

GEORGIEV GP, TUBBS R, LANDZHOV B (2018b) Coracobrachialis longus muscle: humeroepitrochlearis. *Cureus*, 10: e2615.

GEORGIEV GP, ILIEV A, KOTOV G, KARABINOV V, APOSTOLOV M, LANDZHOV B (2019) Surgical anatomy of the carpal tunnel. The Bulgarian contribution. *Med Pregl*, 55: 22-27.

GEORGIEV GP, TUBBS RS (2020) Variant pronator teres muscle and supracondylar process: interesting for anatomists and surgeons but a well-known variation. *Surg Radiol Anat*, 42: 909.

GRUBER H, HONOLD S, SKALLA E, KONSCHAKE M, LOIZIDES A (2021) Novel minimally invasive ultrasound-guided cubital tunnel release: extending the scope? *Ultraschall Med*, 2021, doi: 10.1055/a-1511-8359.

HAGERT E (2013) Clinical diagnosis and wide-awake surgical treatment of proximal median nerve entrapment at the elbow: a prospective study. *Hand (NY)*, 8: 41-46.

HOBSON-WEBB LD, JUEL VC (2017) Common entrapment neuropathies. *Continuum (Minneap Minn)*, 23: 487-511.

JARVIK JG, KLIOT M, MARAVILLA KR (2000) MR nerve imaging of the wrist and hand. *Hand Clin*, 16: 13-24.

JELEV L, GEORGIEV GP (2009) Unusual high-origin of the pronator teres muscle from a Struthers' ligament coexisting with a variation of the musculocutaneous nerve. *Rom J Morphol Embryol*, 50: 497-499.

JELEV L, GEORGIEV GP (2011) A rare case of superficial median artery of high brachial origin: anatomical and clinical considerations of the superficial brachiomedian artery. *Anatomy*, 5: 39-43.

JOHNSON EW, MELVIN JL (1967) Sensory conduction studies of median and ulnar nerves. *Arch Phys Med Rehabil*, 48: 25-30.

KONO H (2003) Acute carpal tunnel syndrome caused by anomalous muscle bellies: a case report. *Hand Surg*, 8: 141-143.

KOTOV G, ILIEV A, GEORGIEV GP, KARABINOV V, LANDZHOV B (2017) Clinical significance of anatomical variations in the carpal tunnel: literature review. *Acta Morphol Anthropol*, 24: 109-113.

LALONDE D (2015) Lacertus syndrome: a commonly missed and misdiagnosed median nerve entrapment syndrome. *BMC Proc*, 9: A74.

LEE YM, SONG SW, SUR YJ, AHN CY (2014) Flexor carpi radialis brevis: an unusual anomalous muscle of the wrist. *Clin Orthop Surg,* 6: 361-364.

LISANTI M, ROSATI M, PARDI A (1995) Persistent median artery in carpal tunnel syndrome. *Acta Orthop Belg*, 61: 315-318.

LOIZIDES A, HONOLD S, SKALLA-OBERHERBER E, GRUBER L, LÖSCHER W, MORIGGL B, KONSCHAKE M, GRUBER H (2021) Ultrasound-guided minimal invasive carpal tunnel release: an optimized algorithm. *Cardiovasc Intervent Radiol*, 44: 976-981.

MEYER P, LINTINGRE PF, PESQUER L, POUSSANGE N, SILVESTRE A, DALLAUDIÈRE B (2018) The median nerve at the carpal tunnel and elsewhere. *J Belg Soc Radiol*, 102: 17.

MILLER TT, REINUS WR (2010) Nerve entrapment syndromes of the elbow, forearm, and wrist. *AJR Am J Roentgenol*, 195: 585-594.

NATSIS K, PIAGKOU M, KOIMTZIS G, ZIBIS AH (2020) A transverse carpal muscle causing carpal tunnel syndrome. *Cureus*, 12: e7275.

NINKOVIĆ M, HEFEL L. OHLER K (1995) Acute median nerve compression produced by reversed palmaris longus muscle. *Eur J Plast Surg*, 18: 129-130.

OLEWNIK Ł, PODGÓRSKI M, POLGUJ M, WYSIADECKI G, TOPOL M (2018) Anatomical variations of the pronator teres muscle in a Central European population and its clinical significance. *Anat Sci Int*, 93: 299-306.

OLEWNIK Ł, ZIELINSKA N, KARAUDA P, DUPARC F, GEORGIEV GP, POLGUJ M (2021) The co-occurrence of a four-headed coracobrachialis muscle, split coracoid process and tunnel for the median and musculocutaneous nerves: the potential clinical relevance of a very rare variation. *Surg Radiol Anat*, 43: 661-669.

OPANOVA MI, ATKINSON RE (2014) Supracondylar process syndrome: case report and literature review. *J Hand Surg Am*, 39: 1130-1135.

PARK SH (2019) Anomalous muscles of the wrist encountered during endoscopic carpal tunnel surgery. *J Korean Neurosurg Soc*, 62: 90-95.

PRATT N (2005) Anatomy of nerve entrapment sites in the upper quarter. *J Hand Ther*, 18: 216-229.

REDONDO MG, GARCÍA-GUILARTE RF, DE CASTRO AB, PEREZ CC (2011) Carpal tunnel syndrome caused by an anomalous muscle belly of the index finger lumbrical. *Eur J Plast Surg*, 34: 61-63.

ROTA E, MORELLI N (2016) Entrapment neuropathies in diabetes mellitus. *World J Diabetes*, 7: 342-353.

SALTER M, SINHA NR, SZMIGIELSKI W (2011) Thrombosed persistent median artery causing carpal tunnel syndrome associated with bifurcated median nerve: A case report. *Pol J Radiol*, 76: 46-48.

SAXENA A, AGARWAL KK, PARSHURAM V, DAS AR (2013) Gantzer muscles and their applied aspects: an exceptional finding. *Singapore Med J*, 54: e102-104.

SBAI M, ARAB R, ESSID L, GALLAS A, KHELIL K, BOUSSEN M, MAALA R (2019) Carpal tunnel syndrome caused by anatomic anomalies muscles: A three cases report. *Asian J Res Surg*, 2: 1-6.

SENER E, TAKKA S, CILA E (1998) Supracondylar process syndrome. *Arch Orthop Trauma Surg*, 117: 418-419.

SHON HC, PARK JK, KIM DS, KANG SW, KIM KJ, HONG SH (2018) Supracondylar process syndrome: two cases of median nerve neuropathy due to compression by the ligament of Struthers. *J Pain Res*, 11: 803-807.

SLAVCHEV SA, GEORGIEV GP (2013) Aberrant abductor digiti minimi muscle found during open surgical decompression of the carpal tunnel: case report. *Rev Arg Anat Clín*, 5: 88-91.

SMITH RJ (1971) Anomalous muscle belly of the flexor digitorum superficialis causing carpal-tunnel syndrome. Report of a case. *J Bone Joint Surg Am*, 53: 1215-1216.

SPINNER RJ, AMADIO PC (2003) Compressive neuropathies of the upper extremity. *Clin Plast Surg*, 30: 155-173.

SPINNER RJ, CARMICHAEL SW, SPINNER M (1991) Partial median nerve entrapment in the distal arm because of an accessory bicipital aponeurosis. *J Hand Surg Am*, 16: 236-244.

SPRATT JD, STANLEY AJ, GRAINGER AJ, HIDE IG, CAMPBELL RS (2002) The role of diagnostic radiology in compressive and entrapment neuropathies. *Eur Radiol*, 12: 2352-2364.

STILL JM JR, KLEINERT HE (1973) Anomalous muscles and nerve entrapment in the wrist and hand. *Plast Reconstr Surg*, 52: 394-400.

SWIGGETT R, RUBY LK (1986) Median nerve compression neuropathy by the lacertus fibrosus: report of three cases. *J Hand Surg Am*, 1: 700-793.

TAKATA SC, ROLL SC (2019) Identification of Aberrant Muscle Bellies in the Carpal Tunnel using Sonography. *J Diagn Med Sonogr*, 35: 62-68.

TANZER RC (1959) The carpal-tunnel syndrome; a clinical and anatomical study. *J Bone Joint Surg Am*, 41: 626-634.

TUBBS RS, MARSHALL T, LOUKAS M, SHOJA MM, COHEN-GADOL AA (2010) The sublime bridge: anatomy and implications in median nerve entrapment. *J Neurosurg*, 113: 110-112.

TUNCALI D, BARUTCU AY, TERZIOGLU A, ASLAN G (2005) Transverse carpal muscle in association with carpal tunnel syndrome: report of three cases. *Clin Anat*, 18: 308-312.

VICHARE NA (1970) Anomalous muscle belly of the flexor digitorum superficialis. Report of a case. *J Bone Joint Surg Br*, 52: 757-759.

WERTSCH JJ, MELVIN J (1982) Median nerve anatomy and entrapment syndromes: a review. *Arch Phys Med Rehabil*, 63: 623-627.

WESSER DR, CALOSTYPIS F, HOFFMAN S (1969) The evolutionary significance of an aberrant flexor superficialis muscle in the human palm. *J Bone Joint Surg Am*, 51: 396-398.